PHYSICOCHEMICAL STUDIES OF THE INCLUSION OF SELECTED AGROCHEMICALS IN CYCLODEXTRINS

DYANNE LOUISE CRUICKSHANK

Thesis presented for the degree of

DOCTOR OF PHILOSOPHY

in the Department of Chemistry

UNIVERSITY OF CAPE TOWN

August 2011

ACKNOWLEDGEMENTS

My special thanks to:

- Professors Mino R. Caira and Susan A. Bourne for their excellent supervision, encouragement and the many opportunities they afforded me.

- Professor Luigi R. Nassimbeni for his many suggestions and for continually challenging me with new ideas.

- Drs. Hong Su and Clive Oliver for assistance on the single crystal X-ray diffractometers.

- The past and present members of the Centre for Supramolecular Chemistry Research, especially Kate Davies, Vincent Smith, Emile Engel and Jinjing Li for their friendship and support over the last few years.

- Professors Elba I. Buján and Rita H. de Rossi as well as Raquel V. Vico at the National University of Córdoba for their supervision and assistance with all the work performed on fenitrothion in solution.

- Natalia M. Rougier (PhD student at the National University of Córdoba) for her assistance in the laboratory both in South Africa and in Argentina, her encouragement, enthusiasm, guidance and for being an exceptional friend.

- Drs. Mircea Bogdan and Sorin Fărcaş at the National Institute for Research and Development of Isotopic and Molecular Technologies, Cluj-Napoca, Romania for assistance with the ^{1}H NMR and ITC analyses.

- The National Research Foundation, the Equity Development Program (UCT Chemistry Department) and the University of Cape Town for financial support.

- And finally my friends and family for their endless support and encouragement.

PUBLICATIONS AND CONFERENCES

Parts of this thesis have been presented at the following conferences:

- Oral presentation: *Inclusion of agrochemicals in cyclodextrins: X-ray structural and thermoanalytical studies*, M. R. Caira, D. L. Cruickshank and S. A. Bourne, 25th National Chemistry Congress with International Participation, Erzurum, Turkey, 27 Jun-2 Jul **2011**.
- Poster presentation: *Inclusion del insecticida fenitrothion en ciclodextrinas metiladas: Estudios en estado sólido y de reactividad*, N. M. Rougier, D. L. Cruickshank, R. H. de Rossi, E. I. Buján, S. A. Bourne and M. R. Caira, XVII Congreso Argentino de Fisicoquímica y Química Inorgánica, Córdoba, Argentina, 3-6 May, **2011**.
- Poster presentation: *The inclusion of an agrochemical in cyclodextrins: An X-ray structural investigation and the effect of cyclodextrins on the reactivity*, D. L. Cruickshank, N. M. Rougier, R. V. Vico, R. H. de Rossi, E. I. Buján, S. A. Bourne and M. R. Caira, 40th South African Chemical Institute (SACI) Convention, Johannesburg, South Africa, 16-21 Jan, **2011**.
- Poster presentation: *Inclusion of agrochemicals in cyclodextrins*, D. L. Cruickshank, N. M. Rougier, R. V. Vico, R. H. de Rossi, E. I. Buján, S. A. Bourne, M. R. Caira, 1st Argentinean Workshop in Environmental Science, Rosario, Argentina, 23-25 Nov, **2009**.
- Poster presentation: *Inclusion of fenitrothion in TRIMEB: Effect on the guest reactivity in solution*, N. M. Rougier, R. V. Vico, R. H. de Rossi, E. I. Buján, D. L. Cruickshank, M. R. Caira and S. A. Bourne, XVII Simposio Nacional de Química Orgánica, Guaymallen, Mendoza, Argentina, 15-18 Nov, **2009**.
- Poster presentation: *The inclusion of an agrochemical in native and derivatised cyclodextrins*, D. L. Cruickshank, M. R. Caira and S. A. Bourne, 12th International Seminar on Inclusion Compounds, Stellenbosch, South Africa, 4-9 April, **2009**.
- Poster presentation: *The inclusion of agrochemicals in cyclodextrins*, D. L. Cruickshank, M. R. Caira and S. A. Bourne, 39th South African Chemical Institute (SACI) Convention, Stellenbosch, South Africa, 30 Nov-5 Dec, **2008**.

Parts of this thesis have been published:

- D. L. Cruickshank, S. A. Bourne and M. R. Caira, Solid-state structures and thermal properties of inclusion complexes of the phenylurea herbicide cycluron with permethylated cyclodextrins, *Arkivoc*, **2011**, 7, 103-115.
- N. M. Rougier, D. L. Cruickshank, R. V. Vico, S. A. Bourne, M. R. Caira, E. I. Buján and R. H. de Rossi, Effect of cyclodextrins on the reactivity of fenitrothion, *Carbohydrate Research*, **2011**, 346, 322-327.
- D. Cruickshank, N. M. Rougier, R. V. Vico, R. H. de Rossi, E. I. Buján, S. A. Bourne and M. R. Caira, Solid-state structures and thermal properties of inclusion complexes of the organophosphate insecticide fenitrothion with permethylated cyclodextrins, *Carbohydrate Research*, **2010**, 345, 141-147.
- M. Mic, D. Cruickshank and I. Turcu, Assessment of molecular interactions in a cycluron-cyclodextrin inclusion complex, *Journal of Physics: Conference Series,* **2009**, 182, 012011, 1-4.

Abstract

DYANNE LOUISE CRUICKSHANK ***AUGUST 2011***

PHYSICOCHEMICAL STUDIES OF THE INCLUSION OF SELECTED AGROCHEMICALS IN CYCLODEXTRINS

Pesticides frequently display adverse properties such as low aqueous solubility, low stability, and high toxicity that limit their applications and render them environmentally hazardous. The possibility of improving these physical properties has been attempted by complexing four pesticides with native and derivatised cyclodextrins (CDs). The pesticides studied included: the phenylurea herbicide, cycluron; an organochlorine insecticide, endosulfan; an organophosphorus insecticide, fenitrothion; and the chloroacetanilide herbicide, acetochlor. A study of CD complexation with these pesticides in solution as well as in the solid state was undertaken.

In the solid state, complexes were prepared via the methods of kneading and co-precipitation and then characterised using thermogravimetry (TG), differential scanning calorimetry (DSC) and hot stage microscopy. The host-guest ratios of the inclusion complexes were determined using either ^{1}H NMR spectroscopy or elemental analysis, or from the weight loss percentage associated with guest desolvation from the TG trace. Single crystal X-ray analysis allowed complete structural elucidation, while powder X-ray diffraction was used to confirm that the single crystal was representative of the bulk sample and to determine whether or not the complex diffractogram matched that of an existing reference diffractogram of a known isostructural CD complex series. Many of the single crystal X-ray structures displayed excessive guest disorder but also presented interesting and novel packing arrangements.

Evidence of complex formation between cycluron and the native CDs in solution was achieved using ^{1}H NMR spectroscopy and isothermal titration calorimetry (ITC). From the ^{1}H NMR chemical shifts the stoichiometries and association constants for the complexes were determined, while ITC provided the thermodynamic parameter of enthalpy change in addition to the stoichiometry and binding constant, which allowed the Gibbs free energy change and entropy change to be calculated. A different type of solution-state investigation was carried out with fenitrothion. As fenitrothion readily hydrolyses in basic media, the rate of hydrolysis was studied in the presence and absence of various CD molecules. In the presence of derivatised CDs, the rate of inhibition of fenitrothion hydrolysis was found to be significantly greater than in the presence of native CDs, a result that was correlated with the mode of inclusion of the insecticide molecule in the different host molecules. A second technique, induced circular dichroism, was used to investigate the relative orientation that the molecule of fenitrothion adopts within the CD molecules in solution. In several cases the results obtained in solution corresponded with the crystal structures.

A further set of experiments was conducted, whereby the thermal stabilities of three isostructural inclusion complexes were evaluated using thermogravimetric analysis. Activation energies for guest loss were evaluated by solid-state kinetic experiments and mechanistic models were derived.

This is a fundamental study illustrating the ability of pesticides from different classes to form inclusion complexes with native and derivatised CDs. Characterisation of these complexes both in the solid state and in solution was performed using a wide variety of analytical techniques. Data derived from these studies have value in the context of applying CD technology to the safe and efficient use of pesticides, examples including the remediation of contaminated soils and the use of CD-pesticide inclusion compounds as ingredients for novel agrochemical formulations.

TABLE OF CONTENTS

CHAPTER 1: INTRODUCTION

CHAPTER 2: EXPERIMENTAL

CHAPTER 3: CYCLURON

CHAPTER 4: ENDOSULFAN

CHAPTER 5: FENITROTHION

CHAPTER 7: CONCLUSION

Chapter 1: Introduction

In this chapter the physical and structural properties of native and derivatised cyclodextrins are presented. Various parameters are defined and an introduction to the analytical techniques used to study cyclodextrin complexation in solution and in the solid state will be discussed. This will be followed by a review of agrochemical-cyclodextrin complexes and finally, the aims and objectives will be stated based on the pesticides selected for study as potential guests.

CYCLODEXTRINS

Cyclodextrins (CDs) are a group of structurally related natural products formed during bacterial digestion of cellulose.[1] The common native CDs are composed of six, seven or eight glucopyranose units linked to one another by an α-(1,4) glycosidic bond and referred to as α-CD (cyclohexaamylose), β-CD (cycloheptaamylose) and γ-CD (cyclooctaamylose), respectively (Figures 1 (a) and (b)). The $^4C_1$ chair conformation of each glucopyranose unit and the rotational flexibility around the glycosidic linkage result in a truncated cone-shaped macrocyclic molecule rather than a cyclindrically shaped molecule.[2] The central cavities of CDs are lined with the ethereal oxygen atoms (O4) and the backbone carbon atoms of each glucopyranose unit, resulting in a hydrophobic interior cavity. Hydroxyl groups are present at both rims of a CD cavity, imposing a hydrophilic character to the exterior of a CD molecule. The narrower rim contains one primary hydroxyl group (O6-H) per glucose unit and the wider secondary rim has two hydroxyl groups (O2-H and O3-H) per glucose unit (Figure 1(c)). A series of intramolecular hydrogen bonds (O2•••H-O3') between the secondary hydroxyl groups exist, which stabilises the CD molecule and reduces the aqueous solubility of cyclodextrins to a certain degree.[2,3,4] The solubilities of α-, β- and γ-CD are 14.5, 1.85 and 23.2 g dm^{-3} at 25 °C, respectively.[5,6] Native CDs are capable of forming inclusion complexes with hydrophobic molecules both in solution and in the solid state, with guests that are partly or completely hydrophobic.[1,3]

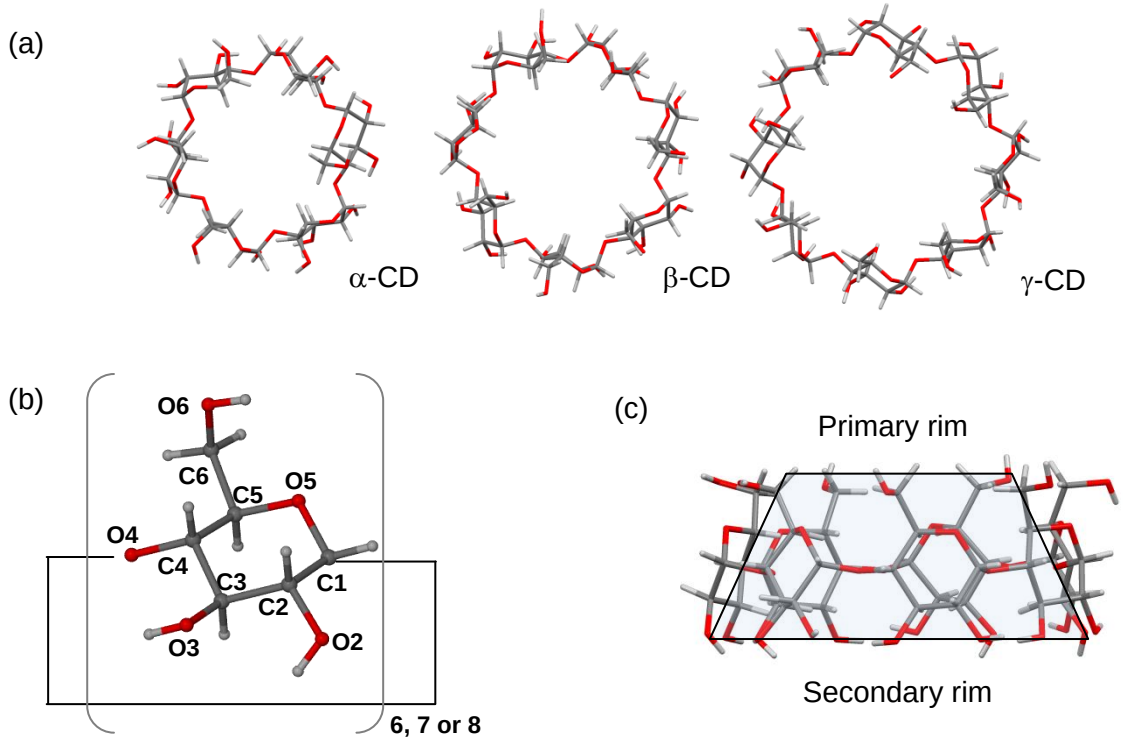

Figure 1. *(a)The macrocyclic rings of α-, β- and γ-CD, (b) an α D-glucopyranose unit and (c) the truncated cone-shape of a CD molecule illustrating the narrow primary rim and wider secondary rim.*

DERIVATISED CYCLODEXTRINS

Derivatising a CD involves substituting the hydroxy groups with methoxy groups or other functional groups. Methylation of the hydroxyl groups can cause significant changes in the physical and chemical properties of CD molecules. A particularly peculiar property of these CDs is the negative temperature coefficient of their aqueous solubilities.[7] As a result their aqueous solubilities are significantly higher at room temperature when compared to the native CDs but lower at higher temperatures. Methylation of the native CDs increases the depth of a CD cavity by *ca.* 2 Å which creates a larger hydrophobic environment in which guest molecules can position themselves.[8] In this particular study three crystalline derivatised CDs and two common industrially produced non-crystalline derivatised CDs were used.

Hexakis(2,3,6-tri-*O*-methyl)-α-cyclodextrin (TRIMEA) and heptakis(2,3,6-tri-*O*-methyl)-β-cyclodextrin (TRIMEB) are two trimethylated CD derivatives that are modified at the C2-OH, C3-OH and C6-OH hydroxyl position of α- and β-CD respectively (Figure 2). Full methylation of these CDs leads to marked distortion of the CD ring and individual glucose units as the intramolecular O2•••H-O3' hydrogen bond network is lost. The third crystalline CD derivative used in this study is heptakis(2,6-di-*O*-methyl)-β-cyclodextrin (DIMEB) which is selectively methylated at the C2-OH and C6-OH hydroxyl positions of β-CD. DIMEB retains the interconnecting O2•••H-O3' hydrogen bonds and thus has a very similar conformation and geometry to that of the native β-CD molecule.

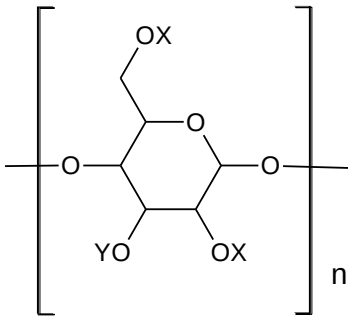

TRIMEA: X = CH_3, Y = CH_3, n = 6

TRIMEB: X = CH_3, Y = CH_3, n = 7

DIMEB: X = CH_3, Y = H, n = 7

Figure 2. *Schematic representation of the derivatised CD molecules.*

Randomly methylated β-CD (RAMEB) and 2-hydroxypropyl-β-CD (HP-β-CD) are amorphous materials, the latter being used widely in the pharmaceutical industry in order to increase the solubility of particular drug molecules. RAMEB is produced on an industrial scale and its application as a substitute for DIMEB in the pharmaceutical, cosmetic and agrochemical industry has been of interest lately.[3,9,10]

CYCLODEXTRIN INCLUSION COMPLEXATION

No covalent bonds are formed between a cyclodextrin and guest molecule during complexation, and in aqueous solutions the guest molecule can readily dissociate from the CD (Equation 1). The most common mode of binding between a CD and guest molecule involves the insertion of the less polar part of a guest molecule into the CD cavity, while the more hydrophilic part either protrudes from the CD cavity and is in contact with the solvent or it is included in the CD cavity and located near the more polar primary or secondary rim.

$$CD + G \underset{}{\overset{K}{\rightleftharpoons}} CD{\cdot}G \qquad (1)$$

Possible driving forces leading to host-guest complexation include electrostatic interactions, van der Waals interactions, hydrophobic interactions and hydrogen bonding between the host and guest molecules, the release of high energy water molecules from the hydrophobic interior cavity of the CD molecules and the release of strain energy in the macromolecular ring of the CD.[11,12] Which of these effects make a greater contribution to the overall formation of an inclusion complex is still not fully understood. According to Liu *et al,*[12] who published a review based on the various forces mentioned above, all the forces, except those involved in the release of conformational strain and the release of cavity-bound high-energy water molecules from the CD cavity, are important in complex formation. It is difficult to determine the role of water upon formation of an inclusion complex owing to the enthalpy-entropy compensation effects. Todorova *et al*[13] studied a well-characterised system in order to establish how the binding affinity of a drug molecule is dependent not only on the structure of the drug but also on the involvement of water in the binding reaction. By comparing the entropy and enthalpy contributions and determining the heat capacity changes for a β-CD and γ-CD complex with three drugs, they concluded that the β-CD binding reactions are enthalpically-driven while the γ-CD binding reactions are entropically-driven. This can be interpreted as less reorganisation of the water molecules occurring when the drug molecules bind to γ-CD than when they bind to β-CD, implying that the original bulk water is retained when the drug molecule binds to the larger γ-CD cavity. The size of the CD cavity therefore demonstrates one of many factors to be considered when evaluating the role of water in the complexation process. With regard to the energy associated with the relief of conformational strain upon guest inclusion, it has been shown that CD molecules usually undergo a significant conformational change upon complex formation; however, this conformational change does not necessarily drive the formation of a CD complex but is rather a result of CD complexation.[12]

CRYSTALLOGRAPHIC STUDY OF CYCLODEXTRIN INCLUSION COMPLEXES

Structural features of cyclodextrins

The pyranose rings of each glucose unit for the native CDs and the derivatised CDs (TRIMEA, TRIMEB and DIMEB) are relatively rigid and generally adopt the $^4C_1$-chair conformation.[14] There is limited conformational freedom for the native CDs while the derivatised CDs are somewhat more flexible due to the methoxyl groups at the primary and secondary rims which promote greater tilting and flexibility around the C1-O4′-C4′ glycosidic link (primed numbers refer to the adjacent glucose unit).[8,15]

Intramolecular hydrogen bonding

At the secondary rims of the native CDs strong intramolecular hydrogen bonds form between adjacent glucose units. The hydroxyl groups at position 2 and 3 of every glucose residue either act as hydrogen bond donors or acceptors to the hydroxyl groups on adjacent glucose units (O2–H•••O3′ or O2•••H–O3′). A study by Saenger *et al*[16,17,18] described this particular hydrogen bonding occurrence with the term 'flip-flop hydrogen bonds'. This term was coined by Saenger after performing neutron diffraction studies and discovering the dynamic disorder of the hydrogen atoms for a β-CD hydrate crystal structure. The hydrogen atoms on the hydroxyl groups were shown to be present in two positions with varying populations. The average O2•••O3′ hydrogen bond distances decrease as the number of glucose units increases (3.05, 2.92 and 2.84 Å for α-, β- and γ-CD respectively), which corresponds to an increase in the hydrogen bond strength.[19] DIMEB also contains a network of intramolecular hydrogen bonds; however, they are only of the type O2•••H–O3' and have a similar average O2•••O3' distance (2.91 Å) to that of β-CD.[19] Complete methylation of α- and β-CD (yielding TRIMEA and TRIMEB respectively) results in loss of this intramolecular hydrogen bonding network.

The primary hydroxyl groups

For all CDs, there is a high degree of conformational flexibility at the narrow primary rim of a CD molecule where the primary hydroxyl/methoxyl groups have rotational freedom around the C6-O6 bond (refer to Figure 1 for key to numbering). The rotation around this bond relative to the CD cavity is described by the torsion angle ω (O5-C5-C6-O6). A value of approximately -60° for the ω torsion angle indicates that the primary hydroxyl groups have a *(-)-gauche* conformation and that the C6-O6 bonds are directed away from the cavity. A

positive value of ~60° implies that the hydroxyl groups are in a *(+)-gauche* conformation and the C6-O6 bonds are directed towards the interior of the CD cavity.

Parameters describing the conformations of cyclodextrins

By comparing the macrocyclic conformation of an uncomplexed host with that of a complexed host one can make certain statements regarding the effect that the various guests have on the host's conformation. Harata and Saenger have defined certain parameters for describing the macrocyclic symmetry of CD molecules.[8,20] These parameters are based on the O4 atoms which are used to construct polygons from which certain distances and angles can be measured and compared (Figure 3). More specifically, these parameters include the O4 distance to the polygon centroid (c) (*l*), the glycosidic O4•••O4′ distance (*D*), the O4•••O4′•••O4″ angle (ϕ) and the O4•••O4′•••O4″•••O4‴ torsion angle (*d*). Another parameter not directly defined by the polygon is the possible O2•••O3′ intramolecular hydrogen bond distance, denoted D_3.

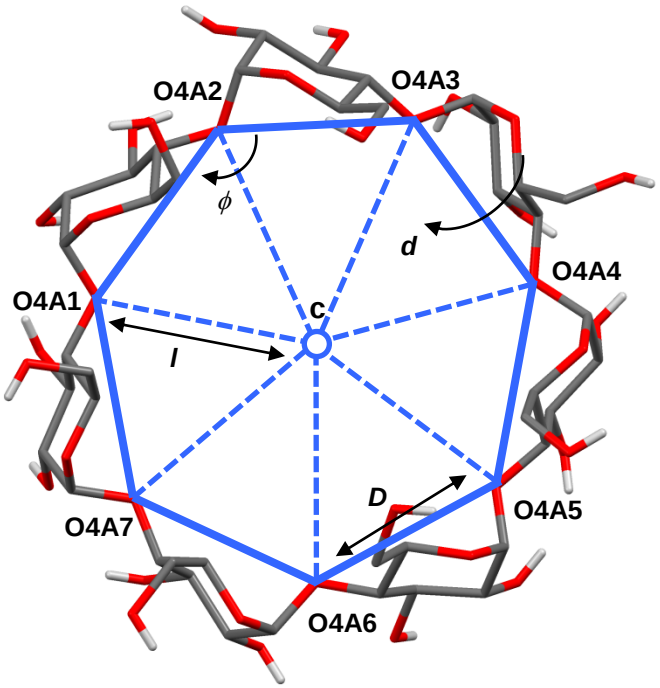

Figure 3. *Principal geometric parameters of the O4-polygon used to describe the geometry of each host molecule.*

For an undistorted CD molecule the mean O4 plane (Figure 4 (a)) would pass through all O4 atoms and the torsion angles (*d*) would be zero. One measure of the deviation from coplanarity of the O4 atoms is the deviation (α) of each O4 atom from the O4 mean plane. In addition, the tilt angles τ_1 and τ_2 evaluate the relative inclinations of each glucose unit relative to the O4 mean plane. Tilt angle τ_1[21] is the angle that the mean plane through six

atoms of the glucopyranose ring (C1, C2, C3, C4, C5 and O5) makes with the line orthogonal to the O4 mean plane (Figure 4 (b)), whilst tilt angle τ_2[22] is defined as the angle between the O4 plane and the mean plane through atoms O4, C4, C1 and O4′ of a given glucose ring (Figure 4 (c)). Ideally both definitions should yield the same result but due to the slight distortions of the glucopyranose units this is not always the case. Positive values are normally seen for all glucose units of the native CDs, indicating an inward tilt of the primary rim towards the centre of the CD cavity. Negative values indicate that the glucose units on the primary side tilt away from the CD cavity.

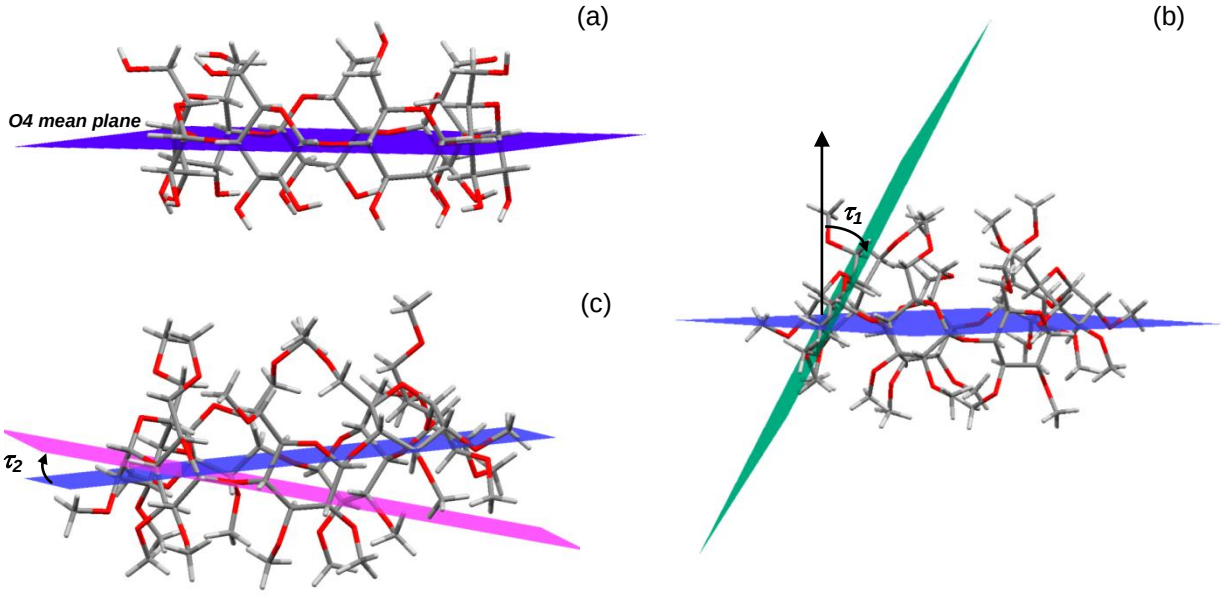

Figure 4. *(a) The O4 mean plane through a β-CD host molecule. (b) and (c) illustrate the relevant planes involved in calculating the τ_2 and τ_1 tilt angles for a single glucose unit. A TRIMEB host molecule has been used to define the dihedral angles in (b) and (c).*

The mean values for the parameters previously discussed are shown in Table 1. These were individually calculated from the hydrated host forms (uncomplexed host crystal structures) which were obtained from the Cambridge Structural Database.[23] It is obvious that the O4•••O4′•••O4″•••O4‴ (*d*) torsion angles, the deviation of atoms from the O4 mean plane (α) and the O2•••O3′ bond distances (D_3) are considerably larger for TRIMEA and TRIMEB when compared to the other host molecules. DIMEB has very similar geometrical features to those of β-CD while γ-CD, which has one extra glucose unit, has slightly greater *I*, *D* and ϕ values. These parameters are important when describing the geometry and symmetry of a CD macrocycle. Upon guest inclusion, changes in the values of these

parameters may give one an indication of the extent to which a guest molecule has altered the shape of the CD macrocycle and the conformation of the individual glucose units.

Table 1. *Geometrical parameters describing the macrocyclic conformation of five crystalline host molecules.*[a]

Parameters	*β-CD*	*γ-CD*	*TRIMEA*	*TRIMEB*	*DIMEB*
l (Å)	5.0	5.9	4.2	4.9	5.0
D (Å)	4.4	4.5	4.2	4.4	4.4
ϕ (°)	128	135	118	126	128
d (°)[b]	6	6	17	22	7
α (Å)[b]	0.15	0.09	0.32	0.44	0.13
D_3 (Å)	2.84	2.82	3.44	3.72	2.88
τ_1 (°)	+12.6	+13.9	+17.4	27.7[c]	+13.3
τ_2 (°)	+13.9	+14.4	+21.5	31.6[c]	+14.6

[a] Calculated using the published crystal forms of each CD from the CSD. The refcodes for the respective host names were as follows: β-CD, POBRON; γ-CD CIWMIE10; TRIMEA, TEVCEC; TRIMEB, average of HEZWAK01, WAGLUM and WAGLOG; DIMEB, average of QIYKEO, BOYFOK04 and CEQCUW). [b] The absolute values were used to calculate the mean values. [c] One residue in both WAGLUM and WAGLOG had a negative tilt angle and two residues in the HEZWAK01 were negative. The absolute values were used when calculating the mean values.

Parameter used to describe the relative shifts of the macrocycles

For a better understanding of the relative positions of the CD molecules comprising a dimeric unit of certain CD complexes it is necessary to quantify the lateral shift of one macrocycle relative to the other. This lateral shift can be defined by the distances R_A and R_B in Figure 5. The O4 mean planes for two CD macrocycles are represented in blue and their respective centroids in pink. Symbol n_A refers to the normal distance between the centroid of macrocycle A and the O4 mean plane of macrocycle B (*vice versa* for n_B). Symbol *h* represents the distance between the two centroids. With the n_A and *h* distances one can determine the relative shift between the centroids and thus the lateral shift between two macrocycles. The same procedure can be used to determine the intermolecular shift between two CD dimers. R_A and R_B may differ significantly depending on the angle between the two O4 mean planes.

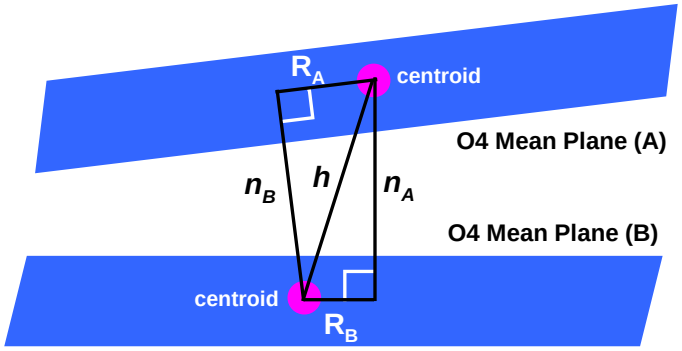

Figure 5. *Schematic diagram used to describe the relative lateral shift between two CD molecules.*

Packing arrangements of cyclodextrin complexes

Caira reviewed the phenomenon of isostructurality of CD inclusion complexes in 2001.[24] This review describes the common packing features of CD inclusion complexes containing organic guest molecules and their characteristic PXRD patterns. The term 'isostructurality' is used to describe two or more crystalline phases having identical or quasi-identical packing motifs;[25] thus, these phases have similar unit cell dimensions and a similar internal arrangement of molecules. For CD complexes, which are ternary systems consisting of a CD host, guest and water molecules, the larger relatively inflexible CD host molecules are responsible for whether or not two CD complexes can be termed isostructural.

CD inclusion complexes can exist in the monomeric or dimeric form. The packing motifs for both the monomeric and dimeric CD inclusion structures can be broadly categorised into one of two packing modes, which are the cage-type and channel-type modes. Channel-type structures are formed by cavity-to-cavity alignment of the cyclodextrin macrocycles, either in a head-to-head or head-to-tail fashion (or a combination of both), thus forming infinite columns (Figure 6 (a)). Cage-type structures are formed when the cavity of the cyclodextrin is blocked on both sides by adjacent cyclodextrin molecules (Figures 6 (b)-(d)). The cage-type structures can either have a herringbone or brickwork-type packing arrangement depending on whether the CD molecules are tilted with respect to one another in their particular layer or not. Figures 6 (c) and (d) display only the monomeric versions of these two packing motifs but dimeric complexes pack in this way as well. There are several other well-classified packing arrangements for CD molecules and their complexes, but they will not be discussed here and the pertinent packing motifs will be presented in the relevant sections of this thesis.

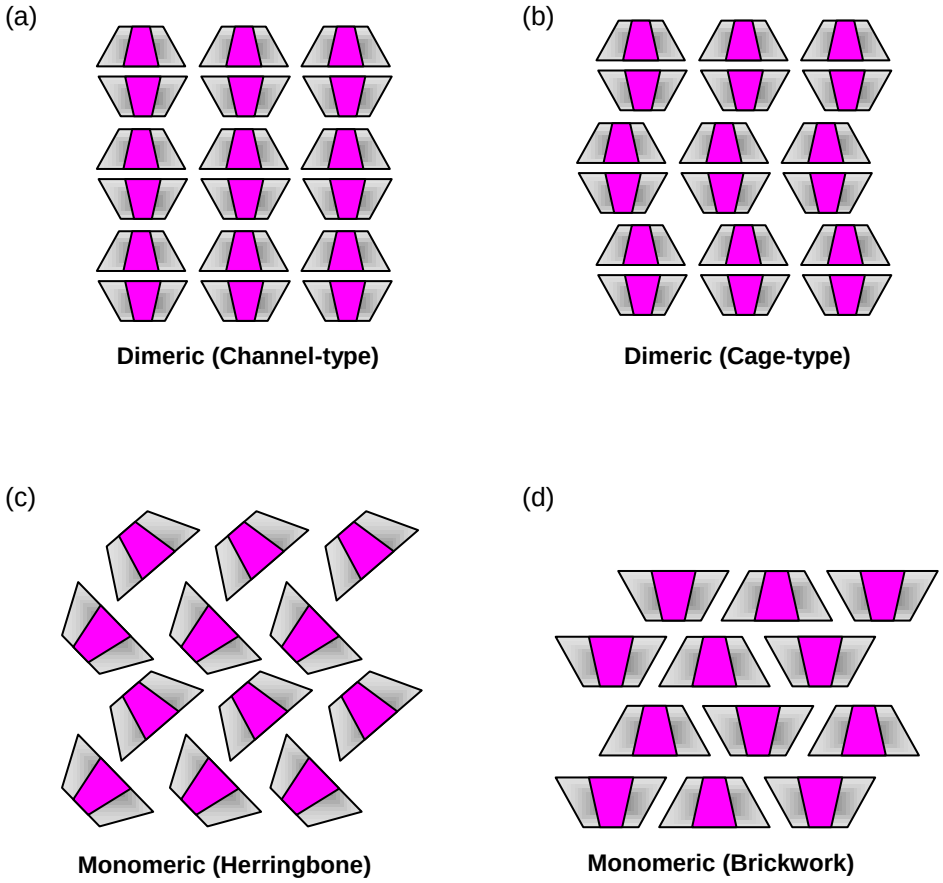

Figure 6. *Selected examples of the dimeric and monomeric packing arrangements of CD complexes showing the broad classification of channel-type (a) and cage-type (b) packing arrangements. The cage-type motifs can be further subdivided into the herringbone (c) and brickwork packing motif (d).*

β-CD complexes are commonly found to be either monomeric or dimeric and crystallise in the channel-type and cage-type packing arrangements with slight variations. The structures of many β-CD inclusion complexes have been elucidated; thus, several isostructural series have been established for these complexes, each with its own characteristic PXRD pattern.[24] All γ-CD complexes have been found to crystallise in the same tetragonal space group $P4_12$, which displays a trimeric channel-type packing motif.

A handful of single crystal X-ray structures of TRIMEA complexes with small organic guest molecules have been elucidated. These complexes are monomeric and pack in a head-to-tail channel-type arrangement.[26,27] The larger guest molecules form complexes with TRIMEA that crystallise in a 'layer' arrangement whereby the host molecules are arranged with alternating orientations within the same plane.[28] Three other dimeric TRIMEA complexes have been published, two of which are described in this thesis and one other which packs in

a unique bimodal head-to-tail fashion [$(TRIMEA)_2$·metoprolol]. [29] This particular complex does not pack in infinite columns as the complex units are laterally offset from one another.

Various packing modes are observed for DIMEB complexes. These include the head-to-tail channel-type arrangements, modified brickwork and modified herringbone-type packing arrangements. There are also DIMEB complexes in which the guest molecules are positioned in the intermolecular spaces between the CD molecules.[30] The TRIMEB complexes, of which there are several, pack mainly in the screw channel-type packing arrangement in a head-to-tail fashion. The guest molecules are rarely fully included in the TRIMEB cavities, a portion of the guest molecule typically protruding from the secondary rim into the interstitial spaces between the CD molecules.[8]

CHARACTERISATION METHODS: SOLID-STATE COMPLEXES

X-ray diffraction methods

Single crystal X-ray diffraction is an exceptionally valuable technique from which one can obtain three-dimensional structural information for CD host molecules and their complexes. More specifically, one can obtain detail regarding the mode of guest inclusion in the CD cavity, the conformation of the guest molecule included, the nature of the host-guest interactions (e.g. hydrogen bonding/hydrophobic contacts) and the structural role of water. The technique of single crystal X-ray diffraction has contributed more to the field of CD inclusion complexes than any other method.[31]

Another useful diffraction method is that of powder X-ray diffraction (PXRD), which is a fast and relatively simple technique employed for complex identification and characterisation. It does not require the expertise, extensive data-capture and computational effort as that involved in single crystal X-ray analysis. PXRD is an excellent screening method from which the packing arrangement of an inclusion complex can be deduced (refer to the concept of isostructurality on pg. 9) before single crystals of the sample are prepared.[24]

Thermal analytical methods

Thermal methods such as differential scanning calorimetry (DSC) and thermogravimetry (TG) represent a very popular and widespread analytical approach to the characterisation of multicomponent systems such as CD inclusion complexes in the solid state.[32] A thermal analytical technique such as DSC can be used for preliminary qualitative investigations of CD inclusion complexes where a comparison of the thermal behaviour of single components,

their physical mixtures and the inclusion compound is made. The disappearance of a melting peak for a crystalline guest molecule or a significant change in the thermal profile of an inclusion complex (e.g. onset temperatures) may suggest complex formation. On the other hand, TG may be used to evaluate water content, host-guest stoichiometry, the onset of decomposition as well as to determine the energy associated with various solid-state processes.

Solid-state reaction kinetics

The aim of most solid-state kinetic studies is to elucidate the molecular details of a solid-state reaction.[33] The field of solid-state kinetics is a controversial one as the rate equation (Equation 2) and the Arrhenius equation (Equation 3), which are normally applicable to homogeneous systems, are applied to heterogeneous systems. The Maxwell-Boltzmann energy distribution function provides the starting point for a theoretical explanation of Arrhenius behaviour in homogeneous reactions. Galwey *et al* [34] have considered the application of the Arrhenius equation to solid-state systems and found that the energy distribution functions for both electronic energy and phonon energy approximate to the same form as that in the Maxwell-Boltzmann distribution and hence these functions are capable of explaining the fit of *k* and T data to an Arrhenius-type equation.

$$\frac{d\alpha}{dt} = f(\alpha)\, k(T) \tag{2}$$

$$k(T) = A\, e^{-E_a/RT} \tag{3}$$

Certain models have been derived for solid-state reactions and have been mechanistically classified as nucleation, geometrical contraction, diffusion and reaction order models.[33] Nucleation-based reactions have a rate-limiting step which involves the formation and growth of nuclei normally at sites that are imperfect within the reactant crystal. The geometrical contraction models assume that nucleation occurs rapidly on the surface of the crystal and the reaction interface then moves towards the centre of the crystal. Reactions which require the transport of reactants to, or products away from, the site of a chemical change may be controlled by a diffusion process and thus diffusion models have been derived to describe these processes. Finally, reaction order models are the simplest models as they are similar to those used in homogeneous kinetics but instead of the reaction rate being proportional to concentration it is primarily dependent on the amount or fraction of remaining reactant. Solid-state processes, however, more often than not, show complex rate behaviour that cannot always be attributed to a single kinetic model.

Typical solid-state reactions studied include phase transformations, desolvation of hydrates and other solvates, and thermal decompositions. These reactions can be studied with thermal analytical methods by measuring a sample property as it is heated or held at a constant temperature. If a reaction involves weight loss, then the kinetics of the reaction can be studied using TG, while if heat is evolved or consumed during a reaction, a kinetic evaluation can be made using DSC or differential thermal analysis (DTA). The type of reaction studied in this thesis involves the release of a guest molecule from a CD cavity. No covalent bonds are formed or broken in this process and the host molecules remain chemically unchanged.

CHARACTERISATION METHODS: COMPLEXATION IN SOLUTION

X-ray studies yield precise information on the CD complex structure in the solid state. It is, however, important to understand the dynamics of these complexes in solution since most CD applications take place in this state. Nuclear magnetic resonance studies can give proof of complex formation in the form of small chemically induced shifts, occurring upon host-guest interaction. Calorimetric measurements performed using instrumentation such as an isothermal titration calorimeter can provide certain thermodynamic parameters and give greater insight into the driving forces associated with host-guest complexation in solution, while spectroscopic techniques such as circular dichroism yield information on the relative positions of guest molecules in the CD cavities.

Solution ^{1}H NMR spectroscopy and binding constants

Nuclear magnetic resonance (NMR) spectroscopy is an indirect method that is frequently used to determine the binding constants between a CD molecule and various guest molecules. Demarco and Thakkar published the first paper in 1970 in which they discuss evidence of complexation between β-CD and aromatic guest molecules using NMR spectroscopy.[35] Since then, the procedure of measuring a change in the chemical shift values of CD and guest protons as a function of concentration has been important in determining the stoichiometry, possible host-guest conformations and association constants for a host-guest system.

Each glucopyranose unit of a CD molecule contains two methine protons (H_3 and H_5) that are directed towards the interior of the CD cavity (Figure 7) and three which are located on the exterior of the CD cavity (H_1, H_2 and H_4). The methylene protons (H_{6a} and H_{6b}) of a CD molecule are located at the narrow primary rim of the CD cavity. If inclusion of a guest

molecule into a CD does occur one would expect protons H_3 and H_5 to undergo measurable ^{1}H NMR chemical shift changes, whereas protons H_1, H_2 and H_4 should remain relatively unaffected. Depending on the guest and size of the CD cavity the methylene protons of the CD may also show measurable changes in chemical shift. A similar treatment can be applied to the protons of an included guest molecule. It has been well documented that protons H_3 and H_5 shift upfield on inclusion of aromatic guests and that aromatic protons shift downfield upon increasing CD concentrations.[36,37,38,39]

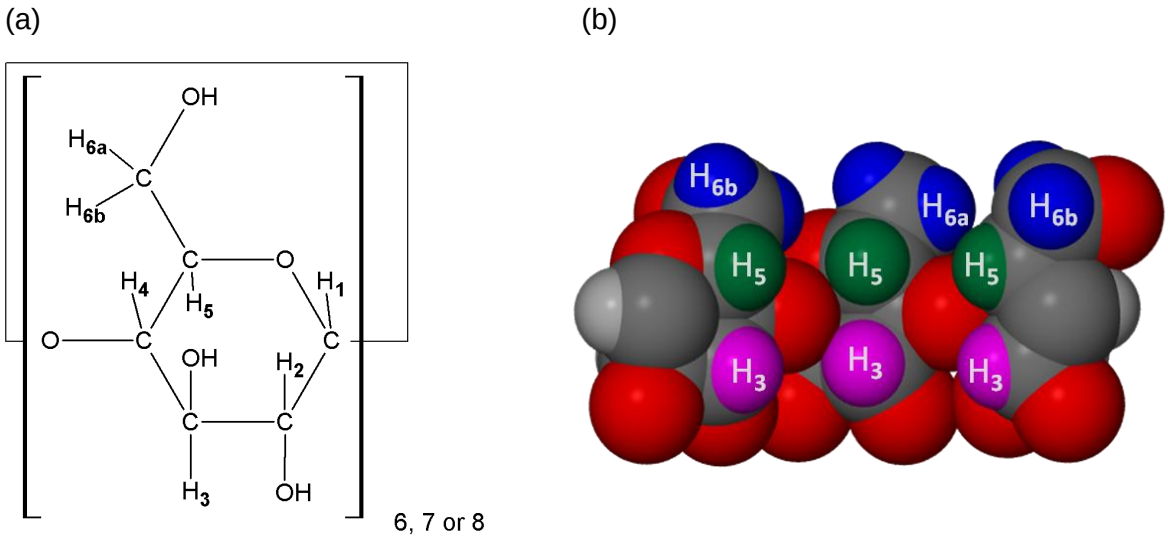

Figure 7. *(a) The glucopyranose unit of α-CD (6), β-CD (7) and γ-CD (8) with the proton numbering scheme employed. (b) A cross-sectional view of a cyclodextrin molecule illustrating how protons H_3 and H_5 line the cavity and protons $H_{6a,b}$ are situated at the narrow primary rim of the CD cavity (the hydroxyl protons are omitted for clarity).*

The complexation-induced shifts (CISs) one observes in ^{1}H NMR spectra for host-guest complexes are dependent on the exchange rate of the associated and dissociated form of the complex relative to the timescale of the NMR experiment. If the host-guest complexation equilibrium is slower than that of the NMR timescale two sets of signals would be observed, one for the complexed host and guest and one for the uncomplexed host and guest. If the exchange rate is similar to the timescale of the NMR experiment, the NMR peaks broaden and/or disappear making it impossible to measure the CIS values.[40] For the NMR study presented in this thesis the exchange rate between the complexed and uncomplexed form was much faster than the NMR timescale, resulting in an NMR spectrum with peaks that appeared at a weighted average chemical shift value of the complexed host and free host. The method of continuous variation is used to determine the stoichiometry in the form of a Job plot. With the stoichiometry of the complex confirmed and using the CIS values it is

possible to determine the association constant for complex formation between a CD and a guest molecule.

Isothermal titration calorimetry

The understanding of host-guest interactions between cyclodextrins and guest molecules requires a complete characterisation of the binding energetics and thermodynamic parameters involved between two interacting molecules. Isothermal titration calorimetry (ITC) is the only direct method that can measure the heat change during complex formation at a constant temperature.[41] Accurate measurement of this heat flow allows determination of binding constants, reaction stoichiometry, enthalpy changes and entropy changes for a particular host-guest system being studied. Recent developments in the instrumentation for calorimetry allow detection of very weak interactions involving low heats of binding thus making it suitable to evaluate weaker interactions such as cyclodextrin complexation.[42,43]

The Gibbs free energy change for a particular process is given by Equation 4. The spontaneous association of two molecules is characterised by a negative ΔG value which means that negative ΔH values and positive $T\Delta S$ (and thus positive ΔS) values promote complex formation. This being said, depending on the relative values of ΔH and ΔS it is possible to determine whether a reaction is enthalpically- or entropically-driven. A common effect known as enthalpy-entropy compensation occurs where an enthalpic gain from changing the structure of a compound to increase the number of bonding interactions is offset by a negative entropy change due to more order being created within the system, thus reducing the magnitude of change in ΔG.[41,44,45]

$$\Delta G = \Delta H - T\Delta S \qquad (4)$$

Non-covalent interactions such as electrostatic, van der Waals, hydrophobic, hydrogen bonding, charge transfer, π-π stacking and steric effects are all weak interactions that can be responsible for the process of cyclodextrin complexation.[11] One can make certain assumptions and logical explanations based on the entropy and enthalpy values obtained from a single ITC experiment, but by combining these data with structural information one can have a better idea of the intermolecular interactions and driving forces involved.[46]

Circular dichroism

Circular dichroism is a spectroscopic technique that detects the differential absorption of left and right circularly polarised light passing through a chiral substance.[47] A circular dichroism spectrum essentially contains an absorption signal with a positive and/or negative sign.

Cyclodextrins themselves to do not absorb light in the UV-vis region (200-1000 nm) and therefore do not display a circular dichroism signal. However, upon complexation of an achiral guest molecule with a CD it is possible to induce a circular dichroism signal and this phenomenon is known as induced circular dichroism (ICD) (Figure 8).

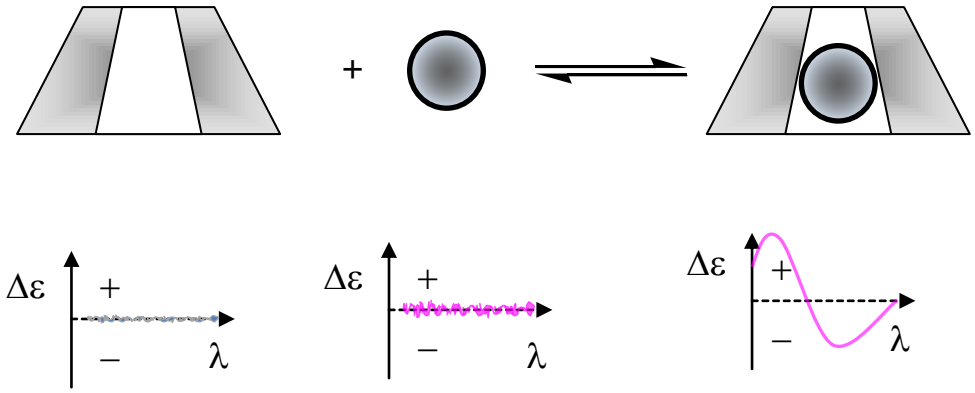

Figure 8. *Schematic representation of an ICD signal for a host molecule and an achiral, chromophoric guest molecule and the resulting ICD spectrum when complexation occurs in solution (Δε is defined as the difference between the molar extinction coefficients of the left and right circularly polarised light passing through a particular sample).*

The sign, shape and intensity of ICD signals for CD complexes are structure-dependent and can thus be used to identify possible arrangements of the host and guest molecules. A qualitative interpretation of the relative host-guest geometry can be made, using proposed rules based on the Kirkwood-Tinco theory of polarisabilities.[48] These rules, which will be discussed in the relevant section, were derived specifically for aromatic chromophores interacting with CD molecules. Induced circular dichroism can also be used to estimate association constants in a similar way that NMR spectroscopy and UV-vis spectroscopy are used.

APPLICATION OF CYCLODEXTRINS IN AGROCHEMISTRY

CDs have been studied extensively within the last few decades especially within the pharmaceutical industry, food and cosmetic industry, biotechnology industry and in the field of analytical chemistry.[49] CDs which have been used in drug formulations have been shown to improve the bioavailability, chemical stability, absorption and controlled release of some drugs.[2] In 1985 Szejtli reviewed the subject of cyclodextrins and pesticides, stating that within the next decade, there would be a rapid development in the application of CDs in pesticide formulations.[50] This has in fact been realised as the price of CDs has decreased

considerably since 1973 when 1 kg of β-CD cost ~2000 USD. Today the price of β-CD is ~1 USD/kg and the rate of CD production has significantly increased, thus making the large quantities required for use in the agrochemical industry possible. Certain derivatised CDs are also produced on an industrial scale (e.g. RAMEB and HP-β-CD) and show unique and practically important properties, such as their exceptionally high solubilising ability, thus rendering them effective in this industry.[49,51]

The undesirable physicochemical properties associated with agrochemicals include their poor aqueous solubility, chemical, thermal and physical instability, high volatility, high soil mobility and poor wettability. These poor physicochemical properties result in an excess quantity of the agrochemical being applied to crops as the majority of the material is not in a suitable form for the target to ingest or absorb. The excess material is then susceptible to photodegradation or decomposition through various biochemical processes which render the material ineffective.[52] The high-mobility toxic byproducts or intact sample may then become part of the water drainage areas via agricultural runoff and leaching, affecting the residing farming communities which depend on that particular water source. Alternatively, the agrochemicals or toxic byproducts bind to soils, eventually rendering the crops and soil unusable due to the high levels of dispersed pesticide residues.

The poor physical properties of agrochemicals can be addressed for the better through their inclusion in cyclodextrins.[53] The complexes formed between cyclodextrins and agrochemicals are new entities and have properties which are in many instances superior to those of the uncomplexed materials. CD complexation can increase the aqueous solubility and thus improve the absorption of these chemicals, which may reduce the quantity of the material applied to the crop fields. An enhancement in the chemical stability of the pesticide can be achieved through CD complexation, which will reduce the quantity of ineffective and toxic byproducts. Volatile liquids or sublimable crystalline pesticides can be transformed into stable, solid powders which are safer to handle and transport before being transformed into a suitable liquid formulation. Furthermore, cyclodextrin inclusion can improve the wettability and bioavailability of selected agrochemicals.[50,53]

Numerous studies have been published demonstrating unequivocally the physical and chemical stabilisation effects that CD complexation may have on agrochemicals. For example, fenitrothion-, malathion- and chlorpyrifos-β-CD solid-formulation complexes were stored over a nine-year period with no significant change in the overall content of the insecticides, while the physical mixtures showed a decrease in the insecticide content over

the same time frame.[54] Kinetic studies of the alkaline hydrolysis of chlorpyrifos, methyl parathion, parathion and fenitrothion have shown a decrease in the rate of reaction in the presence of CDs relative to that in their absence, proving that CD complexation confers chemical stability on these agrochemicals.[55,56] However, for paraoxon which is also an organophosphorus insecticide, analogous hydrolysis experiments showed an increase in the rate of hydrolysis in the presence of CDs. This was explained on the basis of the guest functional group that is susceptible to hydrolysis being located outside the CD cavity.[57] Photostability effects have also been observed for certain CD-pesticide formulations; however, in several cases, CDs have increased the photodegradation rate of some pesticides, an effect which may be useful in other areas such as soil remediation.[58,59,60]

Villaverde *et al* have performed numerous studies on the interaction between CDs and the pyridazinone herbicide norflurazon. These researchers have prepared and characterised complexes between norflurazon and the native CDs both in solution and the solid state.[61,62] In addition to confirming the existence of these complexes in both phases, Villaverde *et al* explored a useful application of the CDs that relates to the remediation of pesticide-contaminated soils. They found that at low β-CD concentrations there is a high prevalence for both the CD and the herbicide to adhere to the soil particles, retarding the mobility of the herbicide, whereas at high β-CD concentrations norflurazon tends to complex with β-CD which acts as a solubilising agent.[63,64] In a separate study they performed desorption experiments of norflurazon in the presence of α-CD and γ-CD, observing an enhanced solubilisation effect induced by these CD molecules which increased the removal of previously adsorbed norflurazon material from the soil.[61]

Solubility enhancement is one of the major advantages of CD inclusion since an improvement in the solubility of pesticides has a direct impact on the bioavailability of these compounds for their respective targets. Methylated CDs have been shown to improve the solubility of several pesticides to a larger extent than the native CDs. For example, complexation of the herbicide 2,4-D with α-CD, HP-β-CD and RAMEB yielded 3-, 9- and 17-fold increases in the solubility of the herbicide, respectively, relative to the solubility of the uncomplexed material.[65,66,67]

Furthermore, pesticides can be complexed with CDs to reduce their volatility. Solid-formulations of selected volatile pesticides and CDs have been shown to exhibit negligible vapour pressures as CDs produce higher energy barriers for vaporisation. Sulfluramid, which is an expensive insecticide with a relatively high vapour pressure, showed a reduction

in volatility through complexation with β-CD;[68] in addition, this particular CD-insecticide complex displayed a very high thermal stability. Several other instances where CDs have reduced the volatility of pesticides in solid formulations have been reported.[69] Finally, CD-pesticide solid formulations can also be effective in masking the unpleasant smell of some pesticides.

From the examples mentioned above it is obvious that CDs can beneficiate pesticide formulations substantially; however, the primary advantage of CD inclusion derives from the ability of pesticides to dissociate from CD molecules to act upon their targets. The association constant is a measure of the strength of this interaction and if it is too large the pesticide will be ineffective as it remains encapsulated in the CD. It is difficult to determine the value at which the association constant would be considered too large. The pharmaceutical industry uses a reference value of 10 000;[70] thus, if the association constant exceeds this value, the complex will not dissociate in solution and the drug is ultimately rendered ineffective. If the association constant is less than 10 000, there will be a sufficient quantity of the guest uncomplexed in order for it to perform its specific function.

MOTIVATION AND OBJECTIVES

Agrochemicals are used throughout the world and their application has become essential in the agricultural industry as one has to maintain the high demand and high standard of farming production expected from consumers. These chemicals, however, have the ability to cause substantial environmental and ecological damage, greatly reducing their benefits.

Agrochemicals

The term agrochemical refers to all chemical products used in the agricultural industry to help manage an agricultural ecosystem. These chemical products include pesticides, synthetic fertilisers, soil conditioners and plant growth regulators. The class of pesticides can be further subdivided into insecticides, herbicides, fungicides and acaricides. In this study two insecticides and two herbicides were investigated and their chemical structures, aqueous solubilities and melting points are shown in Table 2.

Table 2. *Chemical structures and physical properties of the pesticides chosen for study.*

Pesticide **(phase at 25 °C)**	**Chemical Structure**	**Molecular formula and weight**	**Solubility (mg dm^{-3}) at 25 °C**	**Melting point (°C)**
Cycluron (solid)	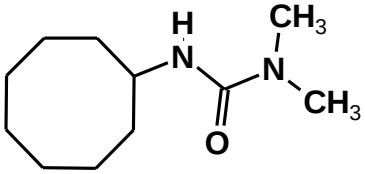	$C_{11}H_{22}N_2O$ 198.3	1200[71]	134-138[71]
Endosulfan (solid)	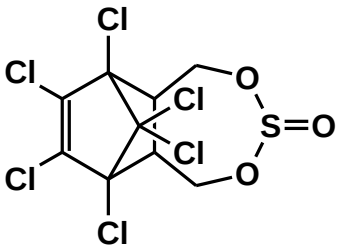	$C_9H_6Cl_6O_3S$ 406.9	0.33[71]	70-100[71]
Fenitrothion (liquid)	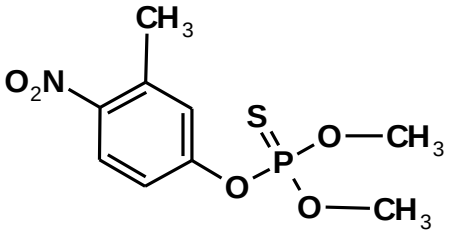	$C_9H_{12}NO_5PS$ 277.2	30[72]	3.4[73]
Acetochlor (liquid)	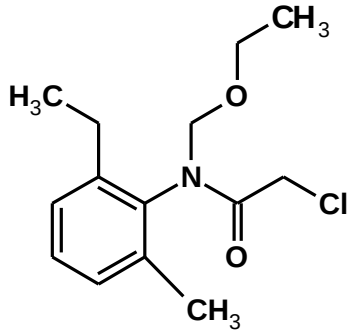	$C_{14}H_{20}ClNO_2$ 269.8	40[74]	<0.0[74]

Cycluron

Cycluron (3-cyclooctyl-1,1-dimethylurea) is a substituted urea that was introduced for herbicidal purposes in 1958.[71] It is generally used in combination with other chemicals as a pre-emergence herbicide for the control of annual weeds in sugar beet and a number of vegetable crops. Cycluron is one of many urea herbicides which are not highly toxic to animals but upon exposure to UV light their toxicity may increase significantly. The photodegradation products of urea-type herbicides have been identified by capillary gas chromatography and it has been suggested that radical processes are mainly responsible for the decomposition of these molecules.[75] Furthermore, the toxicity of certain urea herbicides

has been found to increase dramatically in aerobic conditions through elimination of a methyl group of the urea moiety and the formation of a formylated derivative (Figure 9).[76]

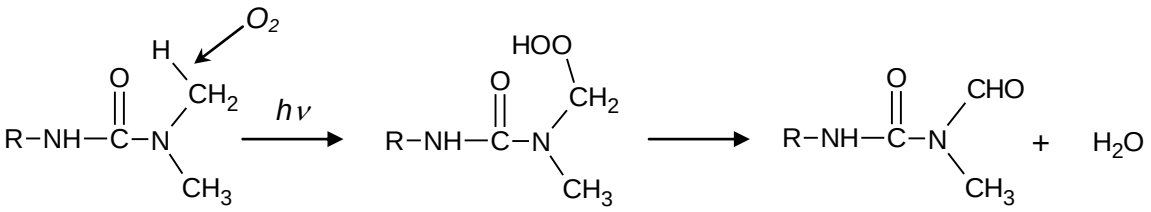

Figure 9. *The reaction scheme illustrating the removal of a methyl group through the formation of a formylated derivative.*

CDs have the ability to protect these molecules from UV radiation and thus CD inclusion of urea herbicides is particularly relevant in this context. This herbicide has a high aqueous solubility in comparison to the other pesticides dealt with in this thesis. This permitted accurate CD-cycluron solution-state studies to be performed using techniques such as ^{1}H NMR spectroscopy and ITC.

Endosulfan

The organochlorine insecticide endosulfan (6,7,8,9,10,10-hexachloro-1,5,5a,6,9,9a-hexahydro-6,9-methano-2,4,3-benzodioxathiepine-3-oxide) is a broad spectrum pesticide typically applied as a 7:3 (α:β) isomeric mixture to cereals, fruits, vegetables and cotton crops.[77] Many countries have already banned the use of endosulfan due to its acute toxicity and role as an endocrine disruptor. A global ban on the manufacture and use of endosulfan was recently negotiated at a convention on Persistent Organic Pollutants in April 2011.[78] India is the world's largest producer and consumer of endosulfan and as a result of this ban, that country now needs to source other insecticides which are most likely to be more costly and less effective. In the meantime, the excessive use of this agrochemical, its semi-volatile nature and relative persistence in the air, soil and water,[79,80] continue to have detrimental effects on aquatic organisms and the human population. When we commenced with this project in 2008, endosulfan was still being used in excessively large quantities and our primary focus was to complex endosulfan with CDs to improve the endosulfan formulations and prevent the atmospheric transport and deposition of this insecticide. The work on endosulfan presented here is nonetheless relevant, as CDs can be used to remove this insecticide from the environment through remediation of soils and aquatic ecosystems.

Fenitrothion

Fenitrothion [*O,O*-dimethyl *O*-(3-methyl-4-nitrophenyl) phosphorothioate)] is a broad spectrum organophosphorus insecticide and acaricide used for pest control in rice paddies, vegetable, cereal and cotton crops. More specifically, in South Africa, fenitrothion is commonly used for post-harvest storage of wheat crops.[81] Fenitrothion acts by irreversibly inhibiting the enzyme acetylcholinesterase which is essential for the function of the central nervous system of insects.[82] Organophosphorus insecticides were specifically developed to replace the organochlorine pesticides as they are less persistent in the environment and thus pose less long-term health risks to non-target aquatic organisms and humans.[83]

The stability of fenitrothion has been extensively studied with the primary aim of understanding the fate of fenitrothion in the environment.[84,85] The O-P functionality of all organophosphate pesticides is susceptible to nucleophilic attack and thus the efficacy and bioavailability of these insecticides is compromised. Stabilising these molecules and preventing rapid chemical and photolytic decomposition of the molecules is possible via complexation with CDs. Furthermore, fenitrothion being an oil at ambient temperature, can be transformed into a solid material on complexation, which will enable safer handling and transport of the chemical before being dissolved in a suitable solvent for application.

An investigation of the chemical stability of fenitrothion has been conducted, leading to the conclusion that the rate of hydrolysis of the insecticide is retarded in the presence of β-CD.[86] This inhibitory effect was attributed to the formation of an inclusion complex in solution. In addition to the stability studies, the possible orientation of the fenitrothion molecule in the β-CD cavity in solution has also been explored using circular dichroism.[87]

Acetochlor

Acetochlor [2-chloro-*N*-(ethoxymethyl)-*N*-(2-ethyl-6-methylphenyl) acetamide] is a selective systemic chloroacetanilide herbicide used for the pre-emergence and early post-emergence of annual grasses and selected broad-leaved weeds in maize. Numerous physiological processes such as lipid and protein synthesis are affected by treatment with acetochlor.[88]

An extensive amount of research has been carried out on the chloracetanilide herbicides alachlor and metolachlor, as they are amongst the most popular pesticides in the United States and have been in use for more than 30 years, while acetochlor has only been in use since 1994.[89] Several literature articles focus on the methods used to identify the parent herbicide as well as its metabolites that form through various chemical, biological and physical degradation processes.[90,91,92] No fundamental work on acetochlor and its

complexation with CDs has been published. Owing to the poor solubility and oil-like consistency of acetochlor, CDs are ideal carrier molecules that can improve these properties through formation of CD inclusion complexes.

Objectives

The primary objective of this project is to study the inclusion of four selected agrochemicals in both native and derivatised CDs in the solid state and in solution. For the solid-state inclusion complexes, this investigation focuses on the i) preparation, ii) determination of chemical composition, iii) analysis of thermal behaviour and iv) elucidation of the crystal structure. The objectives are achieved using spectroscopic techniques such as ^{1}H NMR spectroscopy, X-ray diffraction methods (PXRD and single crystal XRD) and thermal methods. Thermal techniques include TG, DSC and hot stage microscopy. Using these methods information about the thermal stability of each inclusion complex is obtained. The nature of the host-guest interactions (hydrogen bonding, hydrophobic contacts) and the position of the pesticide molecule within the CD cavity are also established.

In solution, complexation between the CD molecules and pesticides are investigated using ^{1}H NMR spectroscopy, isothermal titration calorimetry, induced circular dichroism and chemical reaction kinetics. These analytical techniques allow the determination of fundamental quantities, which include the association constants, host-guest stoichiometries and thermodynamic parameters for each host-guest system studied. The relative positions of a given guest molecule in various cyclodextrins are investigated in addition to the stabilising effect that CDs impose on labile insecticides.

REFERENCES

1. J. Szejtli, *Chem. Rev*., **1998**, 98, 1743-1753.
2. K. H. Frömming and J. Szejtli, in *Topics in Inclusion Science - Cyclodextrins in Pharmacy*, Kluwer Academic Publishers, Dordrecht, The Netherlands, **1993**, vol. 5, ch. 1.
3. E. M. Martin Del Valle, *Process Biochem.*, **2004**, 39, 1033-1046.
4. J. Szejtli, *Pure Appl. Chem*., **2004**, 76, 1825-1845.
5. W. Saenger, J. Jacob, K. Gessler, T. Steiner, D. Hoffman, H. Sanbe, K. Koizumi, S. M. Smith and T. Takaha, *Chem. Rev*., **1998**, 98, 1787-1802.
6. J. Szejtli, in *Comprehensive Supramolecular Chemistry, Cyclodextrins,* eds. J. L. Atwood, J. E. D. Davies, D. D. MacNicol and F. Vögtle, Pergamon, UK, **1996**, vol. 3, ch. 2.
7. A. Kusmin, R. E. Lechner, M. Kammel and W. Saenger, *J. Phys. Chem. B*, **2008**, 112, 12888-12898.
8. K. Harata, *Chem. Rev*., **1998**, 98, 1803-1827.
9. G. Jozefaciuk, A. Muranyi and E. Fenyvesi, *Environ. Sci. Technol*., **2003**, 37, 3012-3017.
10. A. Hazekamp and R. Verpoorte, *Eur. J. Pharm. Sci*., **2006**, 29, 340-347.
11. M. V. Rekharsky and Y. Inoue, *Chem. Rev.*, **1998**, 98, 1875-1918.
12. L. Liu and Q.-X. Guo, *J. Inclusion Phenom. Macrocyclic Chem.*, **2002**, 42, 1-14.
13. N. A. Todorova and F. P. Schwarz, *J. Chem. Thermodynamics*, **2007**, 39, 1038-1048.
14. M. L. Bender and M. Komiyama, in *Cyclodextrin Chemistry*, Springer-Verlag, Berlin, **1978**.
15. K. Harata, in *Cyclodextrins and their complexes*, ed. H. Dodziuk, Wiley-VCH Verlag GmbH & Co. KGaA, Weinheim, **2006**, ch. 7, 147-198.
16. W. Saenger, C. Betzel, B. E. Hingerty and G. M. Brown, *Nature*, **1982**, 296, 581-583.
17. W. Saenger, C. Betzel, B. E. Hingerty and G. M. Brown, *Angew. Chem., Int. Ed. Engl*., **1983**, 22, 883-884.
18. V. Zabel, W. Saenger and S. A. Mason, *J. Am. Chem. Soc*., **1986**, 108, 3664-3673.
19. K. Harata, in *Inclusion Compounds*, eds. J. L. Atwood, J. E. D. Davies and D. D. MacNicol, Oxford University Press, London, **1984**, vol. 5, ch. 9.
20. W. Saenger, in *Inclusion compounds*, eds. J. L. Atwood, J. E. D. Davies and D. D. MacNicol, Oxford University Press, London, **1984**, vol. 2, ch. 8.
21. F. W. Lichtenthaler and S. Immel, *Liebigs Ann*., **1996**, 27-37.
22. K. Harata, *Bull. Chem. Soc. Jpn.*, **1979**, 52, 2451- 2459.

23. Cambridge Structural Database and Cambridge Structural Database system, Version 5.32, Cambridge Crystallographic Data Centre, University Chemical Laboratory, Cambridge England, February **2011**.
24. M. R. Caira, *Rev. Roum. Chim.*, **2001**, 46, 371-386.
25. A. Kálmán and L. Párkányi, in *Advances in Molecular Structure Research*, JAI Press Inc., Greenwich, USA, **1997**,189-226.
26. K. Harata, *J. Chem. Soc., Perkin Trans. 2*, **1990**, 799-804.
27. K. Harata, K. Uekama, M. Otagiri, F. Hirayama and Y. Sugiyama, *Bull. Chem. Soc. Jpn.*, **1982**, 55, 3386-3389.
28. S. Makedonopoulou, K. Yannakopoulou, D. Mentzafos, V. Lamzin, A. Poppov and I. M. Mavridis, *Acta Crystallogr., Sect. B: Struct. Sci*., **2001**, 57, 399-409.
29. M. R. Caira, W. T. Mhlongo and J. Li, *J. Optoelectron. Adv. M.*, **2008**, 10, 2255-2260.
30. K. Harata, *Bull. Chem. Soc. Jpn.*, **1988**, 282, 53-63.
31. K. Harata, in *Comprehensive Supramolecular Chemistry*, *Cyclodextrins*, eds. J. L. Atwood, J. E. D. Davies, D. D. MacNicol and F. Vögtle, Pergamon, UK, **1996**, vol. 3, ch. 9.
32. F. Giordano, C. Novak and J. R. Moyano, *Thermochim. Acta*, **2001**, 380, 123-151.
33. A. K. Galwey and M. E. Brown, in *Handbook of Thermal Analysis and Calorimetry,* ed. M. E. Brown, Elsevier Science B. V., The Netherlands, **1998**, vol. 1, ch. 3.
34. A. K. Galwey and M. E. Brown, *Thermochimica Acta*, **2002**,386, 91-98.
35. P. V. Demarco and A. L. Thakkar, *J. Chem. Soc., Chem. Commun*., **1970**, 2-4.
36. C.-S. Lu, C.-J. Hu, Y. Yu and Q.-J. Meng, *Chem. Pharm. Bull.,* **2000**, 48, 56-59.
37. N. Dupuy, D. Barby, M. Bria, S. Marquis, L. Vrielynck and J. Kister, *Spectrochim. Acta A*, **2005**, 61, 1051-1057.
38. S. K. Upadhyay and G. Kumar, *Chem. Central J*., **2009**, 3, 9-19.
39. V. J. Smith, D. Bogdan, M. R. Caira, S. A. Bourne and S. I. Fărcaş, *Supramol. Chem*., **2010**, 22, 172-177.
40. K. Hirose, *J. Inclusion Phenom. Macrocyclic Chem*., **2001**, 39, 193-209.
41. G. A. Holdgate, *Biotechniques*, **2001**, 31, 164-184.
42. A. C. Illapakurthy, C. M. Wyandt and S. P. Stodghill, *Eur. J. Pharm. Biopharm*., **2005**, 59, 325-332.
43. E. Freire, O. L. Mayorga and M. Straume, *Anal. Chem*., **1990**, 62, 950A-959A.
44. W. H. J. Ward, *Drug Discov. Today*, **2005**, 10, 1543-1550.
45. H. Fisher and N. Singh, *Methods Enzymol*., **1995**, 259, 194-221.
46. T. Davies, R. E. Hubbard and J. R. H. Tame, *Protein Sci*., **1999**, 8, 1432-1444.

47. D. Krois and U. H. Brinker, in *Cyclodextrins and their complexes*, ed. H. Dodziuk, Wiley-VCH Verlag GmbH & Co. KGaA, Weinheim, **2006**, ch. 10.
48. E. Charney, in *The molecular basis of optical activity: optical rotary dispersion and circular dichroism*, J. Wiley and Sons, New York, **1979**.
49. J. Szejtli, *Pure Appl. Chem*., **2004**, 76, 1825-1845.
50. J. Szejtli, *Starch*, **1985**, 37, 382-386.
51. R. Saikosin, T. Limpaseni and P. Pongsawasdi, *J. Inclusion Phenom. Macrocyclic Chem*., **2002**, 44, 191-196.
52. N. L. Wolfe, U. Mingelgrin and G. C. Miller, in *Pesticides in the soil environment: processes, impacts and modelling*, ed. H. H. Cheng, Soil Science of America, Inc., Madison, Wisconsin, USA, **1990**, ch. 5.
53. E. Morillo, in *Cyclodextrins and their complexes*, ed. H. Dodziuk, Wiley-VCH Verlag GmbH & Co. KGaA, Weinheim, **2006**, ch. 16.
54. L. Szente and J. Szejtli, in *Comprehensive Supramolecular Chemistry, Cyclodextrins*, eds. J. L. Atwood, J. E. D. Davies, D. D. MacNicol and F. Vögtle, Pergamon, UK, **1996**, vol. 3, ch. 17.
55. R. V. Vico, R. H. de Rossi and E. I. Buján, *J. Phys. Org. Chem*, **2009**, 22, 691-702.
56. M. Kamiya, K. Nakamura and C. Sasaki, *Chemosphere*, **1995**, 30, 653-660.
57. M. Kamiya, S. Mitsuhashi and M. Makino, *Chemosphere*, **1992**, 25, 783-796.
58. M. Kamiya, K. Nakamura and C. Sasaki, *Chemosphere*, **1994**, 28, 1961-1966.
59. J. Villaverde, C. Maqueda, T. Undabeytia and E. Morillo, *Chemosphere*, **2007**, 69, 575-584.
60. M. Kamiya, K. Nakamura and C. Sasaki, *Chemosphere*, **2001**, 42, 251-255.
61. J. Villaverde, J. I. Pérez-Martínez, C. Maqueda, J. M. Ginés and E. Morillo, *Chemosphere*, **2005**, 60, 656-664.
62. J. Villaverde, E. Morillo, J. I. Pérez-Martínez, J. M. Ginés and C. Maqueda, *J. Agric. Food Chem.*, **2004**, 52, 864-869.
63. J. Villaverde, C. Maqueda and E. Morillo, *J. Agric. Food Chem.*, **2006**, 54, 4766-4772.
64. J. Villaverde, *J. Hazard Mater.*, **2007**, 142, 184-190.
65. J. I. Pérez-Martínez, J. M. Ginés, E. Morillo, M. L. Rodríguez and J. R. Moyano, *Pest Manag. Sci.*, **2000**, 56, 425-430.
66. J. I. Pérez-Martínez, M. J. Arias, J. M. Ginés, J. R. Moyano, E. Morillo, P. J. Sanchez-Soto and C. Novak, *J. Thermal Anal*., **1998**, 51, 965-972.
67. J. I. Pérez-Martínez, J. M. Ginés, E. Morillo, M. L. Rodríguez and J. R. Moyano, *Environ. Technol*., **2000**, 21, 209-216.

68. R. C. Bergamasco, G. M. Zanin and F. F. de Moraes, *J. Agric. Food Chem*., **2005**, 53, 1139-1143.
69. L. Szente, *J. Thermal Anal*., **1998**, 51, 957-963.
70. L. A. Miller, R. L. Carrier and I. Ahmed, *J. Pharm. Sci*., **2007**, 96, 1691-1707.
71. *The Pesticide Manual*, eds. C. R. Worthing and R. J. Hance, British Crop Protection Council: Lavenham, Suffolk, England, 8th edn., **1987**.
72. S. Lacorte and D. Barcelo, *Environ. Sci. Technol*., **1994**, 28, 1159-1163.
73. *Farm chemicals handbook*, Meister Publishing Co., Willoughby, Ohio, **1999**, C 177.
74. *The Merck Index: An Encyclopedia of Chemicals, Drugs, and Biologicals*, eds. M. J. O'Neil, P. E. Heckelman, C. B. Koch, K. J. Roman, C. M. Kenny and M. R. D'Arecca, Merck & Co., Inc., Whitehouse Station, NJ, USA, 14th edn., **2006**.
75. K. Lányi, *Chromatographia*, **2003**, 57, S235-S241.
76. C. Tixier, L. Meunier, F. Bonnemoy and P. Boule, *Int. J. Photoenergy*, **2000**, 2, 1-8.
77. W. F. Schmidt, S. Bilboulian, C. P. Rice, J. C. Fettinger, L. l. McConnell and C. J. Hapeman, *J. Agric. Food Chem.*, **2001**, 49, 5372-5376.
78. N. Stafford, *Endosulfan banned as agreement is reached with India*, 6 May **2011**, RSC, Chemistry World, http://www.rsc.org/chemistryworld/News/2011/May/06051102.asp, accessed on 05/07/2011.
79. J. Weber, C. J. Halsall, D. Muir, C. Teixeira, J. Small, K. Solomon, M. Hermanson, H. Hung and T. Bidleman, *Sci. Total Environ*., **2010**, 408, 2966-2984.
80. T. George, N. S. Beevi and G. Priya, *Pestic. Res. J*., **2009**, 21, 109-111.
81 . M. A. Dalvie and L. London, *Crop Protection*, **2009**, 28, 864-869.
82. T. Wu, Q. Gan and U. Jans, *Environ. Sci. Technol*., **2006**, 40, 5428-5434.
83. B. Liu, L. L. McConnell and A. Torrents, *Chemosphere*, **2001**, 44, 1315-1323.
84. T. Matsushita, Y. Matsui, S. Taniwaki and K. Ikeba, *Water Sci. Technol*., **2008**, 53, 741-747.
85. B. Druzina and M. Stegu, *Int. J. Environ. Anal. Chem*., **2007**, 87, 1079-1093.
86. R. V. Vico, E. I. Bujan and R. H. de Rossi, *J. Phys. Org. Chem*., **2002**, 15, 858-862.
87. M. Kamiya and K. Nakamura, *Pestic. Sci*., **1994**, 41, 305-309.
88. *Metabolic pathways of agrochemicals, Herbicides and Plant Growth Regulators*, eds. T. R. Roberts and D. H. Hutson, Royal Society of Chemistry, Great Britain, **1998**.
89. D. W. Kolpin, E. M. Thurman and D. A. Goolsby, *Environ. Sci. Technol*., **1996**, 30, 335-340.
90. A. Munoz, W. C. Koskinen, L. Cox and M. J. Sadowsky, *J. Agric. Food Chem*., **2011**, 59, 619-627.

91. K. A. Hostetler and E. M. Thurman, *Sci. Total Environ*., **2000**, 248, 147-155.
92. H.-R. Buser and M. D. Müller, *Environ. Sci. Technol*., **1995**, 29, 2023-2030.

Chapter 2: Experimental

In this chapter the selected agrochemicals and cyclodextrin host molecules are identified. The chapter is then divided into two parts. Part 1 discusses the experimental procedures, techniques and apparatus used for characterisation of all the solid-state complexes prepared. Part 2 describes the methods and apparatus used to study complexation between the cyclodextrins and agrochemicals in solution. The kinetic procedures adopted to study the degradation kinetics of a particular agrochemical are also discussed.

MATERIALS

Host compounds

α-Cyclodextrin, β-cyclodextrin, γ-cyclodextrin, TRIMEA [hexakis-(2,3,6-tri-*O*-methyl-α-CD)], TRIMEB [heptakis-(2,3,6-tri-*O*-methyl-β-CD)], DIMEB [heptakis-(2,6-di-*O*-methyl-β-CD)] and hydroxypropyl-β-cyclodextrin (HP-β-CD) were obtained from Cyclolab (Budapest, Hungary) and used as received. These hosts had a purity > 98%. Randomly methylated β-cyclodextrin (RAMEB) was obtained from the Druggists Group Research, South Africa.

Guest compounds

The agrochemicals, cycluron and fenthion, were obtained from Sigma Aldrich (Germany). Fenitrothion was isolated from a commercial sample of Sumithion (Sumitomo Chemical) by column chromotography. ^{1}H NMR spectroscopy, ^{31}P NMR spectroscopy and GC-MS confirmed the purity of fenitrothion. Acetochlor with a purity > 98% was purchased from ChemService (USA) and Dr. Ehrenstorfer Laboratories (Germany). The commercial sample of endosulfan (purity > 99.9%) was purchased from Riedel-de Haën, Sigma Aldrich (Germany) while the individual isomers of endosulfan (purity > 98.5%) were obtained from Dr. Ehrenstorfer Laboratories (Germany).

PART 1: SOLID-STATE METHODOLOGY

COMPLEX PREPARATION AND CRYSTAL GROWTH

All complexes were initially prepared in a 1:1 molar ratio of the guest and CD. The two main complexation methods used were the kneading and co-precipitation methods. In Chapter 6 the method of co-grinding was used which ensured homogeneous samples in bulk quantity. Specific details such as the masses, volumes, temperatures and times for the preparation of all solid-state complexes are discussed in detail prior to further discussion of the complexes in each chapter.

Kneading method

The agrochemical and CD were ground together in a mortar for 45 min with water being added dropwise so as to maintain a paste-like consistency. If there was proof of complexation using PXRD the material was recrystallised and further analyses were performed.

Co-precipitation method

In general the native CD complexes were prepared by first dissolving the host compound in water at an elevated temperature. The agrochemical was then added to this solution which was stirred for prolonged periods. The latter was then filtered through a 0.45 µm filter into a clean vial and left to evaporate at room temperature or placed in a Dewar flask which allowed the solutions to cool from 60° C to room temperature over a few days. For the TRIMEA, TRIMEB and DIMEB complexes the CD-guest solutions were prepared at lower temperatures (~20 °C) and then left to crystallise in an oven set to 60 °C.

Co-grinding method

A similar procedure was followed to that of the kneading method, but no water was added. This method was only successful in producing inclusion complexes between TRIMEB and the three guests which are oils at room temperature (fenitrothion, fenthion and acetochlor).

THERMAL ANALYSIS

Three thermal analytical techniques were used, namely thermogravimetry (TG), differential scanning calorimetry (DSC) and hot stage microscopy (HSM). All three techniques measure a change in the physical properties of a sample as a function of temperature.

Thermogravimetric analysis and differential scanning calorimetry

Thermogravimetric analysis (TGA) measures a change in the mass of a sample as a function of temperature under a controlled atmosphere. Mass losses were used to confirm the host-guest ratio for particular complexes that showed a one-step mass loss associated with the guest being released. The number of water molecules of crystallisation per host molecule for each complex was also determined through thermogravimetric (TG) experiments. The technique of differential scanning calorimetry (DSC) measures the difference in energy inputs between a reference pan and a sample pan in a controlled atmosphere as a function of temperature. The onset temperatures, temperature range and the enthalpy of various thermal events can be determined from the resulting endothermic and exothermic peaks.

Sample preparation for both TG and DSC experiments proceeded as follows. The crystals were removed from the mother liquor using a spatula and then placed directly on filter paper. The crystals were then surface-dried with filter paper and carefully transferred to an open alumina or aluminium crucible in the case of TG measurements and closed vented aluminium pans for DSC measurements. Sample masses were between 0.5 and 2.0 mg for DSC measurements and between 2 and 8 mg for all TG runs.

Two TG instruments were used, a Mettler Toledo TG/ SDTA851^e with STAR^e software (Version 6.10) and a TA-Q500 Thermogravimetric Analyzer, TA instruments, with Universal Anlaysis 2000 software. These two instruments differ significantly as the Mettler Toledo TG has a horizontal furnace design and the TA Q500 a vertical design. The two DSC instruments used were a Perkin-Elmer PC7-Series instrument and a DSC-Q200, TA instruments. The TA instruments both operate with dry nitrogen purge gas flowing at a rate of 50 ml min^{-1} whereas the other two instruments operated with a flow rate of 30 ml min^{-1}. A heating rate of 10 K min^{-1} was used for all standard TG and DSC experiments performed. However, the temperature range for each experiment differed due to the nature of the samples and their different decomposition/melting temperatures. All endothermic events on the DSC traces are depicted with a peak in the upward direction.

Non-isothermal and isothermal experiments were conducted with different experimental parameters. For the non-isothermal TG runs the samples were heated from 20 to 300 °C at different heating rates (1.0, 2.5, 5.0, 7.5 and 10.0 K min^{-1}). The isothermal TG runs were performed by heating the sample at a rate of 30 or 40 K min^{-1} to a specific temperature and then holding it there for 300 min. Further details regarding the isothermal and non-

isothermal kinetic experiments performed on the various samples will be discussed in Chapter 6.

Hot stage microscopy

Hot stage microscopy (HSM) was used to confirm the TG and DSC results as well as correlate the thermal events with observable physical changes. Events such as colour changes, opacity changes, the appearance of bubbles or even recrystallisation of the sample are not visible using TG and DSC; however, these events are easily captured by HSM. The temperatures recorded for the HSM images are slightly higher than the DSC and TG temperatures recorded for similar events and this is due to the differences in crystal size and the conditions under which the HSM, TG and DSC analyses were performed.

All samples were placed on a cover slip with silicone oil and viewed with a Nikon SMZ-10 stereoscopic microscope fitted with a Linkam THMS600 hot stage and a Linkam TP92 manual temperature control unit. Images were captured with a real-time Sony Digital Hyper HAD colour video camera and viewed with the Soft Imaging System program, analySIS.[1]

ELEMENTAL ANALYSIS

A Fisons EA1108 CHNS-O Elemental Analyser was used to determine the percentage of carbon, hydrogen, nitrogen and sulphur that was present in various samples. This was a useful instrument for determining the host-guest stoichiometry of CD inclusion complexes. The experimental C, H, N and S percentages were compared to the calculated percentages in each case.

POWDER X-RAY DIFFRACTION

Powder X-ray diffraction (PXRD) was used as a preliminary tool to determine whether complexes had been formed from the three methods described above (kneading, co-precipitation and mechanical co-grinding). The PXRD pattern of each putative complex was compared to a set of reference PXRD patterns for a known series of isostructural inclusion complexes.[2] If a match was obtained, complexation was confirmed and further structural information such as the approximate unit cell dimensions was deduced. If the pattern did not match that of a known isostructural series, the experimental pattern was examined to see whether it was similar to that of the native CDs or if the pattern had superimposed peaks of the agrochemical and CD, which would indicate no complexation between these components.

For each X-ray crystal structure determined in this study refined unit cell parameters, space group symmetry, atomic co-ordinates and thermal parameters were used as input for the program LAZY PULVERIX[3] in order to generate an idealised PXRD pattern. LAZY PULVERIX uses the formula $I_{hkl} = mLp|F(hkl)|^2$, where I(*hkl*) is the intensity of the reflection with indices *hkl*, *m* is the reflection multiplicity, L the Lorentz factor, *p* the polarisation factor, and *F(hkl)* the structure factor. By generating this calculated PXRD pattern using LAZY PULVERIX it is possible to see whether or not the single crystal is representative of the bulk material.

Powder X-ray diffraction (PXRD) patterns were recorded using a Huber Imaging Plate Guinier Camera 670 using nickel-filtered Cu$K\alpha_1$ radiation (λ = 1.5405981 Å) produced at 40 kV and 20 mA by a Philips PW1120/00 generator fitted with a Huber long fine-focus tube PW2273/20 and a Huber Guinier Monochromator Series 611/15. Kneaded samples were applied directly to the MYLAR® polyester film (Thin-Film Sample supports, West Chester, Pennsylvania, USA) and suspended in a flat sample holder. Some derivatised cyclodextrin complexes were gently ground in a mortar first to ensure uniform particle size and then placed either on the MYLAR® polyester film with a thin layer of Paratone N oil[4] or in a 1 mm Lindemann capillary which was then mounted vertically in a capillary holder. A 2θ range of 4-100° was used with a step size of 0.005° 2θ. The samples were exposed to the radiation for 30 min with 10 multiscans to collect the data. A Huber High-Temperature Controller HTC 9634 unit was used with the capillary holder in order to obtain PXRD patterns at elevated temperatures.

NMR SPECTROSCOPY

Nuclear Magnetic Resonance (NMR) spectroscopy was used in many instances throughout this study. Firstly it was used as a tool to determine the host to guest stoichiometry of the solid-state inclusion complexes that were prepared. The crystals were dissolved in an appropriate deuterated solvent and the ^{1}H NMR spectrum was recorded. By integrating the respective proton signals the host-guest ratio of the solid-state inclusion complexes was determined. The ^{1}H NMR spectra used to determine the host-guest stoichiometries can be found in Appendix A with their abbreviated complex names. These files have a .pdf file extension and can be viewed using Adobe Reader. ^{1}H NMR and ^{31}P NMR spectroscopy were also used to assess the integrity of unstable agrochemicals in the solid-state inclusion complexes.

A Varian-Unity 400 (400 MHz) or a Varian-VXR 300 (300 MHz) or a Bruker AMX 400 (400 MHz) spectrometer was used to investigate all solid-state crystals which had been dissolved in an appropriate deuterated solvent. Common solvents used for these experiments were $CDCl_3$ and $(CD_3)_2SO$ purchased from Sigma Aldrich (Germany). The data were analysed using the Bruker software TopSpin™.

CRYSTAL STRUCTURE DETERMINATION

A single crystal of adequate size, quality and optical uniformity was obtained for each complex chosen for single crystal X-ray analysis. Depending on the nature of the CD complex a slightly different procedure was followed before mounting the crystal on the goniometer head under a cold stream of nitrogen. For all native CD complexes the crystals were placed directly into paratone N oil4 to prevent loss of included crystalline water molecules. The derivatised CD complexes were maintained at a temperature of 60 °C in their mother liquor. A crystal was then quickly selected from the vial and surface-dried on filter paper before being placed in the paratone N oil. If the surface water is not removed, the crystals dissolve at room temperature.

Data-collection

Crystal intensity data were collected on one of two single crystal X-ray diffractometers; either a Nonius KappaCCD (Charge Coupled Device) single crystal X-ray diffractometer, using graphite-monochromated MoKα radiation (λ = 0.71069 Å) generated by a Nonius FR590 generator operated at 54 kV and 23 mA was used, or a Bruker KAPPA APEX II DUO single crystal X-ray diffractometer employing MoKα radiation (λ =0.71069 Å) generated by a Bruker K780 generator operated at 50 kV and 30 mA.[5] All single crystals were maintained at low temperatures between 100 and 173 K throughout the data-collections. These low temperatures were maintained by cooling the crystals with a constant stream of N_2 gas at a flow rate of 20 $cm^3\,min^{-1}$ with the aid of a Cryostream cooler (Oxford Cryostreams UK). Unit cell refinement and data reduction were performed using the programs DENZO and SCALEPACK[6] for all data-collections performed on the Nonius Kappa CCD diffractometer while data collected on the Bruker Apex II used the program SAINT[7] for unit cell refinement and data reduction. All intensity data were corrected for Lorentz-polarisation effects. The X-ray diffraction data obtained from a crystal containing heavy atoms such as sulphur, phosphorus and chlorine were corrected for absorption using the program SADABS.[8] Space group determinations were carried out by examining systematic absences and matching the observed conditions to a known space group. The space group was verified using the

program XPREP[9] which also prepares the SHELXS-97 input files required for structure solution.

Structure solution and refinement

Several structures were solved by the isomorphous replacement method, which involves using the co-ordinates from the non-hydrogen atoms of an isostructural inclusion complex as a trial model for refinement in the program SHELXH-97.[10] If the unit cell dimensions were not very similar to any of the known isostructrural CD inclusion complexes, SHELXD was used to solve the structure *ab initio*. Full-matrix least-squares refinements were performed using SHELXH-97 which was accessed through the X-seed interface.[11]

SHELXD

SHELXD[12] is specifically designed to solve larger structures by *ab initio* methods from native data when a solution with SHELXS-97 is not possible.[13] SHELXD is based on the dual-space strategy first introduced in the program *Shake and Bake* by Miller *et al.*[14,15,16] The shake and bake method alternates phase refinement in reciprocal space with density modification in real space until a global minimum of the *minimal function* derived by Miller *et al* is obtained.[17] For the program SHELXD, phases in reciprocal space are expanded from the 40% most reliable phases using the tangent formula devised by Karle and Hauptman in 1956.[18,19] This method leads to phase divergence away from a sensible arrangement of atoms which is why the alternated real-space cycles are used to constrain the number of expected *N* (unique atom) sites with approximately equal scattering power. SHELXD is an efficient and robust program that makes solving the substructure of cyclodextrin complexes easier when alternative methods such as isomorphous replacement are not adequate.

SHELXH-97

SHELXH-97 employs the full-matrix least-squares method by minimising the sum of the squares of the differences between the observed and calculated intensities ($\sum w (F_o^2 - F_c^2)^2$). The agreement between the observed (F_o) and calculated (F_c) structure factors is expressed by the residual index R_1, where a low R_1 value indicates a satisfactory model (Equation 1). A second residual index parameter, wR_2, indicates the agreement between the observed and calculated intensities for the refinement against F^2 (Equation 2). Refinement against F^2 tends to magnify the deviations of the goodness-of-fit, S (defined later), from unity compared with refinement against F and therefore these values are not directly comparable to structures refined against F.

$$R_1 = (\sum | |F_o| - |F_c| |) / \sum |F_o| \quad (1)$$

$$wR_2 = \left[(\sum w (F_o^2 - F_c^2)^2) / (\sum w (F_o^2)^2) \right]^{\frac{1}{2}} \quad (2)$$

The weighting scheme w in Equation 2 and the parameters a and b were refined for each structure using Equations 3 and 4 below. The terms a and b are chosen in the above weighting scheme to produce constant distributions of $\left[\sum w (F_o^2 - F_c^2)^2 \right]$ with $\sin\theta$ and $(F_o / F_{max})^{\frac{1}{2}}$. S is defined by Equation 5 where n is the number of reflections and p is the total number of parameters refined. A well-refined structure with good quality data will have an S value close to unity, and the ratio n/p equal to or greater than 8 for structures consisting of atoms with a $Z < 18$.[20]

$$w = 1 / \left[\sigma^2 (F_o^2) + (aP)^2 + bP \right] \quad (3)$$

$$P = [2 F_c^2 + Max (0, F_o^2)] / 3 \quad (4)$$

$$S = \left[\sum (w (F_o^2 - F_c^2)^2) / (n - p) \right]^{\frac{1}{2}} \quad (5)$$

ADDITIONAL RESOURCES

Atom co-ordinates of host molecules of isostructural cyclodextrin complexes were obtained from the Cambridge Structural Database (CSD)[21] in order to solve some of the CD structures using the method of isomorphous replacement. The CSD was also used to obtain averaged bond distances and angles from structures with similar motifs to those investigated in this thesis. Molecular parameters and geometrical data with their associated e.s.d.s and non-bonding distances were calculated using the program PLATON.[22] Molecular packing and stereo diagrams were created with POV-Ray for Windows.[23] Mercury Version 2.3 was also used to create various molecular diagrams.[24] LAYER was used for the graphic display of intensity data as simulated precession photographs.[25]

The final crystallographic data files for each crystal structure addressed in this thesis can be found in Appendix B under a folder with the abbreviated name of the complex. Table 1 lists the file types and information they contain.

***Table 1**. File types found in Appendix B.*

File extensions	Contents
.HKL	Reflection data
.RES	SHELX co-ordinate data
.CIF	Crystallographic information file
.FCF	Structure factor tables
.LIS	Platon output
.XL	SHELX output file
.SUP	Tabulated supplementary data

PART 2: SOLUTION-STATE METHODOLOGY

NMR SPECTROSCOPY

NMR spectroscopy was used to determine the complex stoichiometry, association constant and relative position of the herbicide, cycluron, within the CD cavity in solution. For this, the method of continuous variation (Job Plots) was used in conjunction with two non-linear least-squares regression programs, ConstEQ and ConstEQV (described below).

Method of continuous variation (Job plot)

In order to study the stoichiometry between a host and guest molecule in solution using the method of continuous variation, two equimolar stock solutions of both the guest (G) and host (H) were prepared in D_2O. A series of solutions were made so that a complete range ($0 < r < 1$) of ratios $r = [X] / ([H]_t + [G]_t)$ is sampled. [X] is equivalent to the concentration of the host or the guest for the sample and $[H]_t$ and $[G]_t$ are the total concentrations of the host and guest respectively. The total concentration for each sample is maintained constant ($[H]_t + [G]_t = M$, where M is the total concentration). Once these solutions were prepared they were left to equilibrate overnight. From the ^{1}H NMR spectra of each sample the quantity $\Delta\delta_{obs}$ was obtained by subtracting the observed shift value for a given sample from the chemical shift of the free X ($\Delta\delta_{obs} = \delta_{free} - \delta_{obs}$). $\Delta\delta_{obs}$•[X] was then plotted against r in a Job plot (Appendix C lists the chemical shifts for the complexes studied). The maximum point of the Job plot corresponds to the stoichiometry of the complex.[26]

The concentration of the stock solutions depended on the solubility of the guest and the cyclodextrin at 293 K.

Association constant

The association constants (K) can be determined using the same data ($\Delta\delta_{obs}$) as those used for the host-guest stoichiometry. There are two main methods that can be used to determine association constants based on spectrophotometric and NMR data. Graphical or linearisation methods rely on producing a linear relationship between the experimental data and K. This method requires approximations such as the global consideration of $[H]_i >> [G]_i$ (where i counts the sample number) which is not always possible or mathematically correct. The methods developed by Scatchard,[27] Benesi and Hildebrand,[28] and Scott[29] make use of this approximation and are often used even though it results in a different K value for each proton studied and does not provide an overall association constant for the particular inclusion complex being investigated.[30] The curve-fitting methods require no approximations

and make use of $\Delta\delta_i$ for all the observed protons in the determination of K. These programs include CALCK,[30] EMUL,[31,32] MULTIFIT,[31,33] and ConstEQ.[34]

The analysis of host-guest complexation is based on a simple equilibrium model in solution:

$$a{\cdot}H + b{\cdot}G \leftrightarrow H_aG_b, \text{ where } H_aG_b = C. \quad (6)$$

The association constant may be defined based on Equation (7) where H represents the host, G represents the guest, C represents the complex and a, b the stoichiometry. $[H]_t$ and $[G]_t$ represent the total concentrations of the host and guest and [H], [G] and [C] are the concentrations at equilibrium (Equations (8) and (9)). By substituting (8) and (9) into (7) we obtain Equation (10) and if a and b are equal to one (determined from a Job plot) the equation can be simplified to Equation (11).

$$K = \frac{[C]}{[H]^a\,[G]^b} \quad (7)$$

$$[H]_t = [H] + a{\cdot}[C] \quad (8)$$

$$[G]_t = [G] + b{\cdot}[C] \quad (9)$$

$$K = \frac{[C]}{([H]_t - a{\cdot}[C])^{\,a}\;([G]_t - b{\cdot}[C])^{\,b}} \quad (10)$$

$$K = \frac{[C]}{([H]_t - [C])\,([G]_t - [C])} \quad (11)$$

It is not possible to determine the concentration of the complex C directly from NMR spectroscopy due to the fast equilibrium between the complexed and uncomplexed forms in solution. A parameter known as the observed chemical shift value (δ_{obs}) is, however, directly proportional to the association constant and is thus measured. δ_{obs} is a weighted average chemical shift for the free, uncomplexed guest (δ_f) and the pure complexed state of the guest (δ_c) and can be represented by Equation (12) below. Further substitutions lead us to a simplified Equation (13).

$$\delta_{obs} = \frac{[G]\cdot\delta_f + [C]\cdot\delta_c}{[G]_t} \tag{12}$$

$$\delta_{obs} = \frac{[G]\cdot\delta_f + ([G]_t - [G])\cdot\delta_c}{[G]_t}, \qquad \text{since } [G]_t = [G]+[C]$$

$$\delta_{obs} = \left(\frac{[G]}{[G]_t}\right)\cdot\delta_f + \left(\frac{[G]_t - [G]}{[G]_t}\right)\cdot\delta_c ; \qquad \text{if } \frac{[G]}{[G]_t} = z \text{ then}$$

$$\delta_{obs} = z\cdot\delta_f + \delta_c\cdot(1-z) \tag{13}$$

As [G] approaches 0, z approaches 0, such that $\delta_{obs} \rightarrow \delta_c$, and when $[G] = [G]_t$ or $[G]_t >> [H]_t$, then z approaches 1 and $\delta_{obs} \rightarrow \delta_f$ (similarly proven for the host). If we observe that $\Delta\delta_{obs} = \delta_f - \delta_{obs}$ and that $\Delta\delta_c = \delta_f - \delta_c$ for the free components and the pure complex then we can derive Equation (14) where X = H or G for a 1:1 complex.

$$\Delta\delta_{obs}^{(X)} = \frac{[C]}{[X]_t}\cdot\Delta\delta_c^{(X)} \tag{14}$$

Substituting Equation (14) into Equation (10) we obtain Equation (15) where $[M] = [H]_t + [G]_t$. By solving Equation (15) we obtain the final Equation (16) for which only the negative solution is considered as the ratio $\Delta\delta_{obs}/\Delta\delta_c$ is always less than 1. Equation 16 correlates the total concentrations of the host and guest molecules with the observed difference in chemical shift values. $\Delta\delta_c$ and K are the two independent variables and are determined by using the experimental $\Delta\delta_{obs}$ values as initial reference values for a set of n equations where n refers to the number of samples studied.[34]

$$[X]_t^2\,(\Delta\delta_{obs}^{(X)})^2 - [X]_t\,\Delta\delta_{obs}^{(X)}\,\Delta\delta_c^{(X)}\left\{[M] + \frac{1}{K}\right\} + [H]_t\,[G]_t\left(\Delta\delta_c^{(X)}\right)^2 = 0 \tag{15}$$

$$\Delta\delta_{obs}^{(X)} = \frac{\Delta\delta_c^{(X)}}{2[X]_t}\times\left\{[M] + \frac{1}{K} \pm \left[\left([M]+\frac{1}{K}\right)^2 - 4\,[H]_t\,[G]_t\right]^{\frac{1}{2}}\right\} \tag{16}$$

Determination of the association constant, K

The association constants were calculated using two C^{++} programs known as ConstEQ and ConstEQV.[34] ConstEQV differs only slightly from that of ConstEQ and can be used when the data required from a Job plot do not suffice and a second set of NMR experiments is required where the concentration of the guest is kept constant and the concentration of the host is varied from 0 to a value at least ten times greater than that of the guest concentration. Both programs evaluate the data by a non-linear least-squares curve-fitting regression analysis of the observed chemical shift changes of the guest and CD NMR lines, as a function of concentration, according to Equation (16). The parameter [M] remains constant when using ConstEQ whereas it varies in the case of ConstEQV.

Equation 16 involves no approximations and correlates the total concentration of the host and guest molecules with the observed difference in the chemical shift, $\Delta\delta_{obs}$. ConstEQ and ConstEQV are based on an iterative procedure following specific algorithms in order to fit the experimental values of $\Delta\delta_{obs}$ to the appropriate equation. Each iteration step sets up a quadratic function to determine the direction of the search and calculates the loss error function E, defined as the sum of the squares of the deviations of the predicted values, until the search converges (Equation 17, where *i* counts the sample number and *j* the studied proton).

$$E = \sum_{i,j} \left(\Delta\delta_{obs}^{(i,j)} - \Delta\delta_{calc}^{(i,j)} \right)^2 \qquad (17)$$

In practice, convergence is obtained when the difference between two consecutive E values is less than 10^{-6}. The treatment of the entire set of protons studied produces one single K value for the whole process and a set of calculated $\Delta\delta_{calc}$ values. $\Delta\delta_{calc}$ represents the chemical shift difference (for a given proton) between the free molecule and the pure complex.[35] These two programs allow for both the host and guest protons to be observed for spectroscopic changes as a function of variable host and guest concentrations simultaneously, allowing up to 15 protons to be used in the fitting process. They are, however, limited to 1:1 host-guest stoichiometries.

Apparatus

A Bruker Avance III 500 (500 MHz) spectrometer was used to investigate CD complexation in solution. The ^1H NMR spectra were recorded in D_2O at 293.0 ± 0.1 K. Typical conditions were as follows: 32 K data points, sweep width 3500 Hz giving a digital resolution of 0.11

Hz/point. The 90° pulse width was 10 µs and the spectra were collected with 64 scans. The D_2O (deuterium content 99.7%) was purchased from INCD-ICSI (National R&D Institute for Cryogenics and Isotopic Technologies) Rm Valcea, Romania. The data were analysed using the Bruker software TopSpin™.

ISOTHERMAL TITRATION CALORIMETRY

Isothermal titration calorimetry (ITC) is a physical technique that allows the simultaneous determination of the association constant, enthalpy and stoichiometry for the interaction of two molecules in solution, thus providing a complete thermodynamic profile of a molecular interaction in a single experiment. An ITC measurement involves monitoring the transfer of heat between an analyte solution in a sample vessel and a reference solution in a reference vessel upon injection of a small aliquot of titrant solution into the sample vessel at a fixed operating temperature. In our case the sample vessel contained the agrochemical solution and the CD was injected into the agrochemical solution. Water was placed in the reference cell.

Determination of the association constant, K, the stoichiometry, n, and the change in enthalpy, ΔH.

The calorimetric data obtained from each ITC experiment are initially presented as the electrical power values required to maintain a constant temperature between the reference and sample vessel. Integration of the differential power signal with respect to time yields the heat change, Δq_i, between two consecutive additions *i* -1 and *i*. Plotting the heat change per mol of the total cyclodextrin concentration (Δq_i / $[CD]_{tot}$) against the ratio of the total cyclodextrin concentration to the total guest concentration ($[CD_i]_{tot}$ / $[G]_{tot}$) for each injection results in a typical titration curve from which the parameters K, n and ΔH can be determined through least-squares non-linear adjustment based on the Wiserman isotherm (Equation 18).[36,37,38] The parameter r is a composition variable, defined in Equation 19, V_0 refers to the effective volume of the solution in the titration cell and X_R is the absolute value of the guest to CD ratio ($[G]_t$ / $[CD]_t$). Using Equations 20 and 21 it was possible to calculate the free energy and entropy parameters.

$$\frac{dq}{d[CD]_T} = \Delta H\, V_0 \left[\frac{1}{2} + \frac{1 - X_R - r}{2\sqrt{(1 + X_R + r)^2 - 4X_R}} \right] \qquad (18)$$

$$r = \frac{1}{[CD]_T\ K} \quad (19)$$

$$\Delta G = -RT \ln K \quad (20)$$

$$\Delta G = \Delta H - T\Delta S \quad (21)$$

Apparatus

The heat flow resulting from the binding of the agrochemical to the cyclodextrin was measured at 298 K using a Nano ITC^{2G} (TA Instruments) which makes use of the NanoAnalyze software for data analysis. All solutions were degassed before measurements commenced. Injections were performed using a computer-controlled 250 µL Hamilton syringe. Depending on the volume injected (5 or 10 µL) a series of 20, 25 or 40 injections into the 1.4 ml sample cell was performed. The heat of dilution for the CD solutions into water was measured first and then subtracted from the heat of binding for each reaction before model-fitting. A stirring speed of 250 rpm was used throughout the experiment. Concentrations differed for each experiment and will be discussed in the following chapters.

INDUCED CIRCULAR DICHROISM

An induced circular dichroism experiment can be used to confirm that complexation is taking place in solution between a CD and an achiral, chromophoric guest molecule. It is also a useful tool to determine the relative orientation of a guest molecule in a CD molecule. Circular dichroism measurements were recorded on a JASCO Model J-810 spectropolarimeter. Each circular dichroism solution was prepared with filtered Mili-Q water. For every circular dichroism measurement performed a blank solution was also prepared. The blank solution contained the CD only and this spectrum was subtracted from the substrate-CD spectrum. A 1 cm path length cuvette was used and the following parameters were employed for each measurement to ensure the optimum spectrum: nitrogen flow rate = 15 $cm^3\ min^{-1}$; band width = 5 nm; response = 2 sec; scanning speed = 100 nm min^{-1}; range = 200 – 450 nm; accumulation = 4.

MATERIALS AND EXPERIMENTAL PROCEDURES USED TO STUDY THE DECOMPOSITION OF FENITROTHION

Materials

Aqueous solutions were prepared using water purified with a Millipore Milli-Q apparatus. 1,4-Dioxane was the co-solvent used and was purified by the Fieser method.[39] Before it was used to prepare the solutions for the kinetic reactions it was further distilled over $LiAlH_4$. All the inorganic reagents were of analytical grade and were used without further purification. NaOH was titrated against potassium phthalic acid (KHP), and HCl against borax to determine the accurate concentrations of the standard solutions prepared.

Kinetic procedures

The kinetic experiments were carried out under pseudo-first order conditions. The reactions were performed at a constant temperature of 298.0 ± 0.1 K and they were maintained in the dark in order to minimise photodegradation of fenitrothion, which is known to occur. The ionic strength for all reactions was maintained at 1 M and NaCl was used as the compensating electrolyte. The reactions were all followed by measuring the increase in absorbance of the reaction mixture at the wavelength maximum (λ_{max}) of the decomposition product. Cuvettes with an optical path length of 1 cm were used.

Equations used to fit the experimental data

For most reactions a simple exponential function was used to determine the k_{obs} values for each experiment (Equation 22). Here, Abs_t is the absorbance read at a specific wavelength at time t of the reaction, *Amp* is the change in absorbance and is calculated by subtracting the initial absorbance from the final absorbance, Abs_{inf} is the infinity reading, k is the observed rate constant and t the time. However, the linear function was also used to determine some of the k_{obs} values (Equation 23). Here, $[S]_o$ and $[S]_t$ represent the initial concentration of the substrate and that determined at time t respectively. A_o, A and A_{inf} represent the initial absorbance, the absorbance determined at time t of the reaction and the absorbance at infinity, respectively. The non-linear fitting was carried out using the software included in SigmaPlot, version 10.0.[40]

$$Abs_t = Amp.e^{-kt} + Abs_{inf} \quad (22)$$

$$\ln [S]_t = - kt + \ln [S]_o$$

$$\ln (A - A_{inf}) = - kt + \ln (A_o - A_{inf}) \quad (23)$$

Detection method

UV-vis spectrophotometry was used to follow the rate of reactions by recording the UV-vis spectra at certain time intervals. Since CDs are UV-inactive we were able to investigate the rate of degradation of UV-active guests in the presence of CDs. The UV spectra were recorded on a Shimadzu UV-2101 spectrophotometer.

REFERENCES

1. Soft Imaging System GmbH, *Digital Solutions for Imaging and Microscopy*, Version 3.1 for Windows (Copyright 1987-2000).
2. M. R. Caira, *Roum. Chim. Rev*., **2001**, 46, 371-386.
3. K. Yvon, W. Jeitschko and E. Parthé, *J. Appl. Crystallogr*., **1977**, 10, 73-74.
4. Paratone N oil (Exxon Chemical Co., Texas, USA).
5. APEX2, Version 1.0-27, Bruker AXS Inc., Madison, Wisconsin, USA.
6. Z. Otwinowski and W. Minor, Processing of X-ray Diffraction Data in Oscillation Mode, in *Methods in Enzymology*, eds. C.W. Carter and R.M. Sweet, Academic Press, New York, **1996**, vol. 276, 307-326.
7. Program SAINT, Version 7.60a, Bruker AXS Inc., Madison, WI, USA, **2006**.
8. G. M. Sheldrick, Program SADABS, Version 2.05, University of Göttingen, Germany, **2007**.
9. XPREP, *Data Preparation and Reciprocal Space Exploration*, Version 5.1, © Bruker Analytical X-ray Systems*,* **1997***.*
10. G. M. Sheldrick, SHELXH-97, *Acta Crystallogr.,* **2008**, A64, 112-122.
11. L. J. Barbour, *Supramol. Chem*., **2001**, 1, 189-191.
12. G. M. Sheldrick, *Direct Methods for Solving Macromolecular Structures*, ed. S. Fortier, Dordrecht: Kluwer Academic Publishers, **1998**, 401-411.
13. T. R. Schneider and G. M. Sheldrick, *Acta Crystallogr*., **2002**, D58, 1772-1779.
14. R. Miller, S. M. Gallo, H. G. Khalak and C. M. Weeks, *J. Appl. Crystallogr.*, **1994**, 27, 613-621.
15. I. Uson and G. M. Sheldrick, *Curr. Opin. Struct. Biol.*, **1999**, 9, 643-648.
16. G. M. Sheldrick, H. A. Hauptman, C. M. Weeks, R. Miller, and I. Uson, International Tables for Crystallography, eds. E. Arnold and M. Rossmann, Dordrecht: Kluwer Academic Publishers, **2001**, vol. F, 333-351.
17. R. Miller, G. T. DeTitta, R. Jones, D. A. Langs, C. M. Week and H. A. Hauptman, *Science*, **1993**, 259, 1430-1433.
18. J. Karle, *Acta Crystallogr*., **1968**, B24, 182-186.
19. J. Karle and H. Hauptman, *Acta Crystallogr*., **1956**, 9, 635-651.
20. IUCr Webmaster, *Data Validation Procedures*, Copyright © International Union of Crystallography, http://journals.iucr.org/services/cif/checking/validlist.html, 11/07/2011.

21. Cambridge Structural Database and Cambridge Structural Database system, Version 5.32, Cambridge Crystallographic Data Centre, University Chemical Laboratory, Cambridge England, February 2011.
22. A. L. Spek, PLATON, A multipurpose crystallographic tool, Version 10500 © **1980-2000**.
23. POV-Ray for Windows, Version 3.1e.watcom.win32, The Persistence of Vision Development Team, © **1991-1999**.
24. Mercury CSD 2.4, © CCDC **2001-2010**, Cambridge, UK.
25. L. J. Barbour, *J. Appl. Crystallogr.*, **1999**, 32, 351-352.
26. P. Job, *Ann. Chim. Phys.,* **1928**, 9, 113-203.
27. G. Scatchard, *Ann. N.Y. Acad. Sci.,* **1949**, 51, 660.
28. H. A. Benesi and J. H. Hildebrand, *J. Am. Chem. Soc.,* **1949**, 71, 2703-2707.
29. R. L. Scott, *Recl. Trav. Chim. Pays-Bas.,* **1956**, 75, 787-789.
30. D. Salvatiera, C. Díez, and C. Jaime, *J. Incl. Phenom.,* **1997**, 27, 215-231.
31. R. E. Jr. Barrans and D. A. Dougherty, *Supramol. Chem.,* **1994**, 4, 121-130.
32. P. C. Kearney, L. S. Mizoue, R. A. Kumpf, J. E. Forman, A. McCurdy and D. A. Dougherty, *J. Am. Chem. Soc.,* **1993**, 115, 9907-9919.
33. M. A. Petti, T. J. Shepodd, R. E. Barrans and D. A. Dougherty, *J. Am. Chem. Soc.,* **1988**, 110, 6825-6840.
34. C. Floare, F. Balibanu and M. Bogdan, *Studia UBB, Physica, Special Issue*, **2005**, L. 4a, 451-454.
35. L. Fielding, *Tetrahedron,* **2000**, 56, 6151-6170.
36. W. B. Turnbull and A. H. Daranas, *J. Am. Chem. Soc.*, **2003**, 125, 14859-14866.
37. T. Wiseman, S. Williston, J. F. Brandts and L. N. Lin, *Anal. Biochem.,* **1989**, *179*, 131-137.
38. L. Indyk and H. F. Fisher, *Methods Enzymol.,* **1998**, *295*, 350-364.
39. L. F. Fieser, Experiments in Organic Chemistry, ed. D. R. Heath, Boston, 2nd edn., **1941**, 360.
40. Sigma Plot, Version 10.0, Systat Software Inc., USA, © **2010**.

Chapter 3: Cycluron

This chapter is divided into two parts. First, the solid-state inclusion complexes of cycluron with four cyclodextrins are investigated using the method of single crystal X-ray diffraction and other solid-state characterisation techniques. This is followed by a study of the inclusion complexes formed in solution with three native CDs using two methods, namely Proton Nuclear Magnetic Resonance spectroscopy (^{1}H NMR) and Isothermal Titration Calorimetry (ITC).

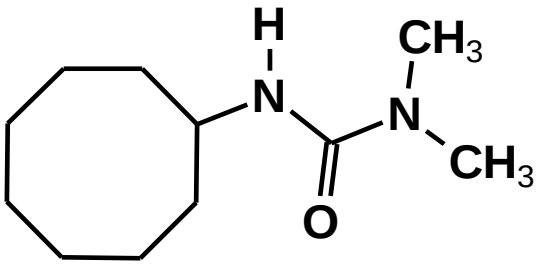

PART 1: COMPLEXATION IN THE SOLID STATE

THE GUEST: CYCLURON

The crystal structure of cycluron has never been elucidated before. It was important to determine it so that the CD complexes formed with this guest could be modelled correctly and a comparison between the complexed and uncomplexed form of the guest in the solid state be made.

Preparation of single crystals

The recrystallisation of cycluron was performed by dissolving 10 mg (0.05 mmol) of cycluron in 2 cm^3 of an 80:20 v/v water-ethanol solution at 60 °C. After stirring the solution for an hour it was filtered and left to crystallise under ambient conditions. Single crystals were obtained within two days.

Crystal structure analysis

Data-collection and space group determination

Crystal intensity data were collected on a Nonius KappaCCD single crystal X-ray diffractometer. The program LAYER was used to determine the crystal system and space group of cycluron.[1] The Laue symmetry was found to be *mmm* indicating the orthorhombic crystal system. Examination of the reciprocal lattice displayed the following reflection conditions: *hkl: none; 0kl: k = 2n; h0l: l = 2n; hk0: h = 2n*. These indicated the space group *Pbca*, as confirmed by the program X-PREP.[2]

Structure solution and refinement

Crystal and refinement data are shown in Table 1. The unit cell refinement and data reduction were performed with the program DENZO-SMN.[3] The structure was solved with SHELXS-97 which revealed all the non-hydrogen atoms.[4] The atoms were placed and refined isotropically on F^2 in SHELXH-97.[5] Two of the cyclooctyl carbon atoms were disordered over two positions. The site occupancy factor (s.o.f.) of each major component was refined as *x* while the minor component refined as *1-x*. The value of *x* settled at 0.82. All ordered atoms were subsequently refined anisotropically. All the hydrogen atoms except the amide hydrogen were placed in idealised positions based on a riding model. They were refined isotropically with temperature factors related to those of the parent atoms to which they were attached. The methylene and methine hydrogens were refined with U_{iso} values 1.2 times those of their parent atoms while the methyl hydrogens refined with U_{iso} values 1.5

times those of the carbon atoms to which they were attached. The amide hydrogen was located in the difference Fourier synthesis map and allowed to refine freely with an N-H constraint of 0.88(1) Å being applied. A planar geometry was found to occur around the N atom.

Table 1. *Data-collection and refinement parameters for the herbicide cycluron.*

Chemical formula	$C_{11}H_{22}N_2O$
Formula weight	198.31
Crystal system	Orthorhombic
Space group	*Pbca*
Unit cell constants	
a (Å)	10.6735(3)
b (Å)	10.1804(6)
c (Å)	21.5476(1)
$\alpha = \beta = \gamma$ (°)	90
Volume (Å^3)	2341.4(2)
Z	8
Density$_{calc}$ (g cm^{-3})	1.125
μ [MoKα] (mm^{-1})	0.072
F (000)	880
Temperature of data collection (K)	173(2)
Crystal size (mm)	0.12 x 0.09 x 0.03
Range scanned θ (°)	2.69 – 25.57
Index ranges	h: -12, 12; k: -12, 11; l: -26, 24
ϕ and ω scan angle (°)	1.0
Total no. of frames	174
Dx (mm)	30.00
Total no. of reflections collected	13405
No. of independent reflections	2161
No. of reflections with I > 2σ(I)	1465
No. of parameters	130
R_{int}	0.0850
S	1.031
R_1 [I > 2σ(I)]	0.0664
No. of reflections omitted	7
wR_2	0.1498
Weighting scheme parameters	a = 0.0636 and b = 2.1476
$(\Delta / \sigma)_{mean}$	< 0.001
$\Delta\rho$ excursions (e Å^{-3})	0.34 and -0.35

Molecular structure

A diagram of the molecule with the labelling scheme is shown in Figure 1. The C-C bond lengths in the cyclooctyl ring range between 1.458(6) Å and 1.539(5) Å and the bond angles between 113.9(3)° and 118.8(3)°. The urea moiety shows a relatively planar geometry while all other geometrical parameters are normal.

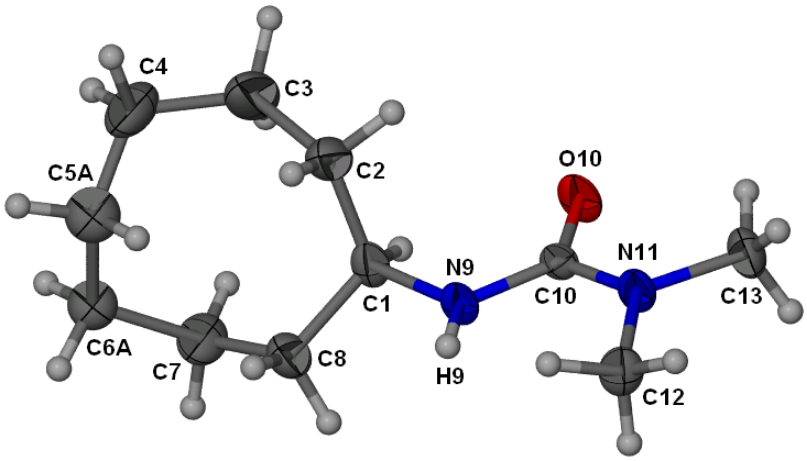

Figure 1. *Molecular structure of cycluron showing the thermal ellipsoids at the 50% probability level. Only the major components of the disordered ring (carbon atoms C5A and C6A) are shown for clarity.*

Conformation and disorder

An eight-membered ring such as that present in cycluron can adopt ten idealised symmetrical conformations.[6] The conformation of the major component here, as confirmed by the endocyclic torsion angles, is that of a boat-chair. When solving the X-ray crystal structure of cycluron there was evidence of high electron density peaks ~1.5 Å away from two of the cyclooctyl carbon atoms. These were modelled accordingly and resulted in a slightly strained boat-chair conformer. Figure 2 shows the deconvolution of the disordered components with their respective pseudo-mirror planes and endocyclic torsion angles.

Crystal packing and hydrogen bonding

The unit cell contains eight symmetry related molecules. The space group P*bca* contains three glide planes. Each molecule is reflected through these planes and translated a distance of ½ along all three axes. The most important feature of the crystal packing is the formation of the hydrogen bond N9–H9•••O10^{i} (2.909(2) Å, *i* = *3/2-x, -1/2+y, z*) which links the molecules in infinite chains parallel to the *b*-axis (Figure 3).

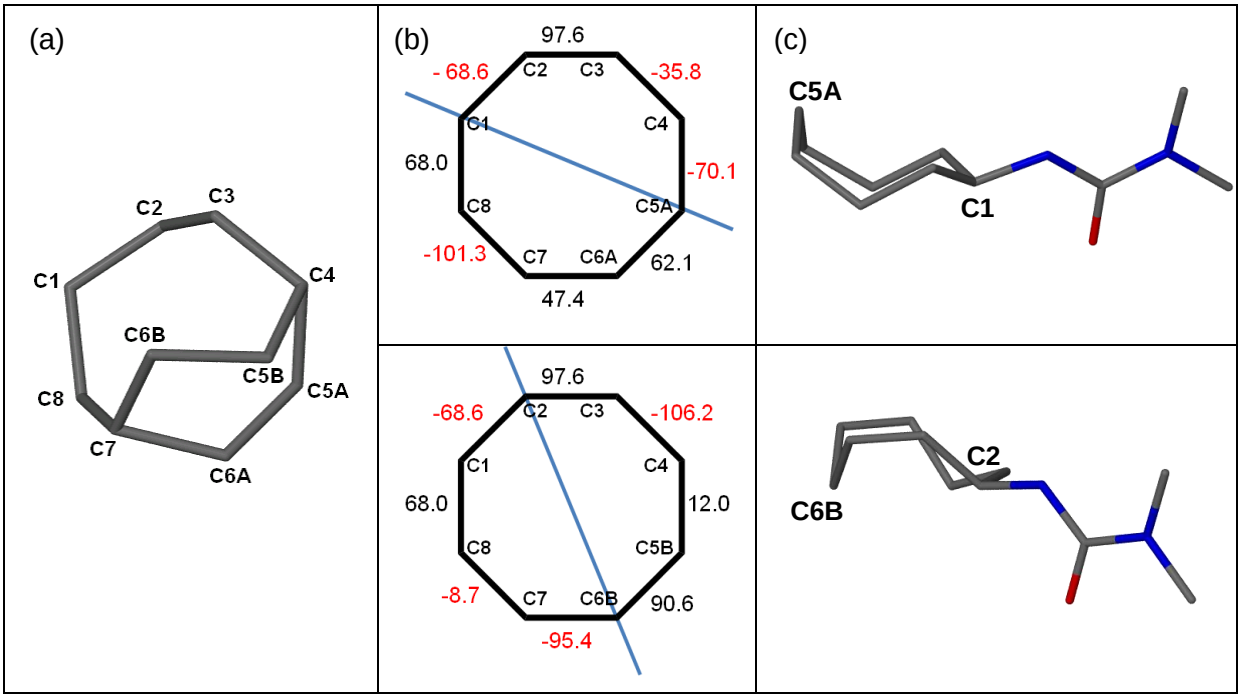

Figure 2. *(a) Disordered cyclooctyl ring of cycluron, (b) schematic representation of the rings with their associated endocyclic torsion angles and the pseudo-mirror plane shown in blue and (c) the cycluron molecules adopting the boat-chair conformation in both cases.*

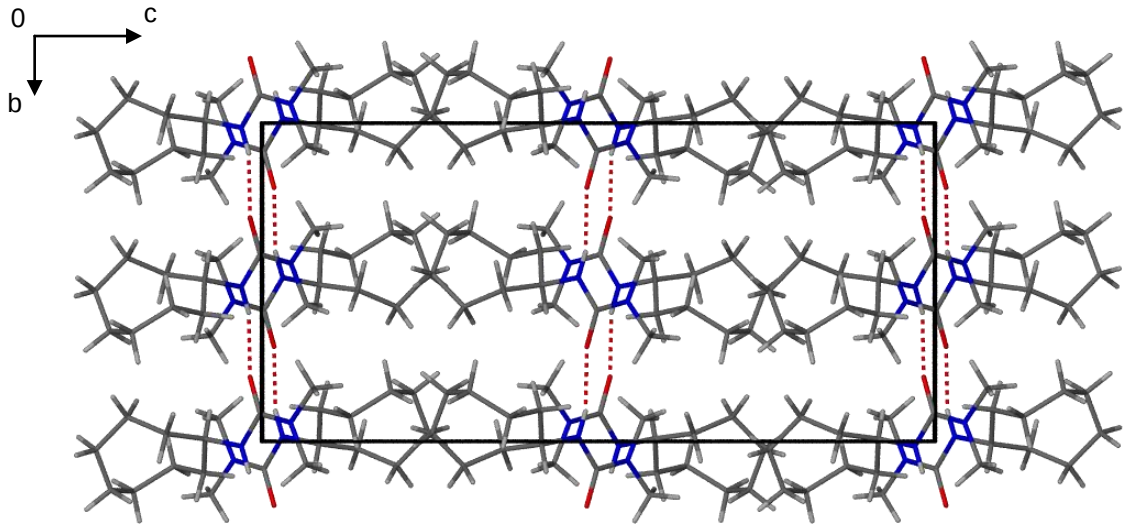

Figure 3. *Crystal packing projected along [100] showing the intermolecular hydrogen bonds which link the molecules to form infinite chains.*

β-CYCLODEXTRIN INCLUSION COMPLEX WITH CYCLURON

Complex preparation

Both the kneading and co-precipitation method resulted in complexation between cycluron and the native β-CD. Single crystals of the β-CD·cycluron complex were obtained using a 1:1 host-guest ratio. 65 mg of β-CD (0.05 mmol) was dissolved in 2 cm^3 of distilled water at 60 °C. Once the β-CD material had dissolved, 10 mg (0.05 mmol) of the guest was added over a 5 min period. The solution was stirred at 60 °C until there was no evidence of the solid guest material. The solution was immediately filtered into a clean vial and left to crystallise at room temperature. The vial was covered with parafilm and holes were made to assist with the process of slow evaporation. Single crystals appeared within two days. The solid-state β-CD·cycluron complex will be referred to as BCDCYC henceforth.

Confirmation of stoichiometry

Since cycluron and β-CD are UV-inactive compounds, a technique such as ^{1}H NMR spectroscopy was necessary to confirm the stoichiometry of the BCDCYC crystals. The complex crystals were dissolved in D_2O and the ^{1}H NMR spectrum was recorded. Integration of the proton signals for H**1**, H**2** and H**4** of the CD molecule and the methyl protons of cycluron revealed a 1:1 host-guest stoichiometry for the BCDCYC complex (Table 2, Appendix A).

Table 2. *Integrals of the host and guest protons for BCDCYC used to confirm the stoichiometry.*

Proton (CD/G) – [Total no. of protons]	δ (ppm)	Integration of peaks		Experimental peak integral/ Theoretical proton number
		Experimental	Integer	
7 × H**1** (CD) – [7]	5.081	7.000*	7	1
7 × H**2** (CD) – [7]	3.671	7.073	7	1
7 × H**4** (CD) – [7]	3.591	7.162	7	1
7 × C$\underline{H}_2$ (G) – [14]	1.701	13.710	14	1
2 × C$\underline{H}_3$ (G) – [6]	2.885	5.716	6	1

* Reference integral.

Thermal Analysis

The TG and DSC traces for BCDCYC are illustrated in Figure 4. The TG curve shows an immediate mass loss with two distinct gradients which can be reconciled with the broad asymmetric shape of the dehydration endotherm on the DSC trace between 30 and 100 °C. This is an indication that the water loss from the crystal is a multi-step process with the weakly bound water molecules being released first, followed by the more strongly bound

water molecules. The observed mass loss in the TG curve of 11.9 ± 0.4 % (n = 3) is equivalent to 20.0 ± 0.3 water molecules per CD dimer. The second broad endotherm starting at 290 °C is characteristic for the decomposition of β-CD complexes. This is in agreement with the very large mass loss observed in the TG trace from 270 °C to 350 °C. The HSM photographs (Figure 5) associate the thermal events with the physical appearance of the crystals. The crystallinity of the sample is lost as soon as the water is expelled and the darker appearance confirms this.

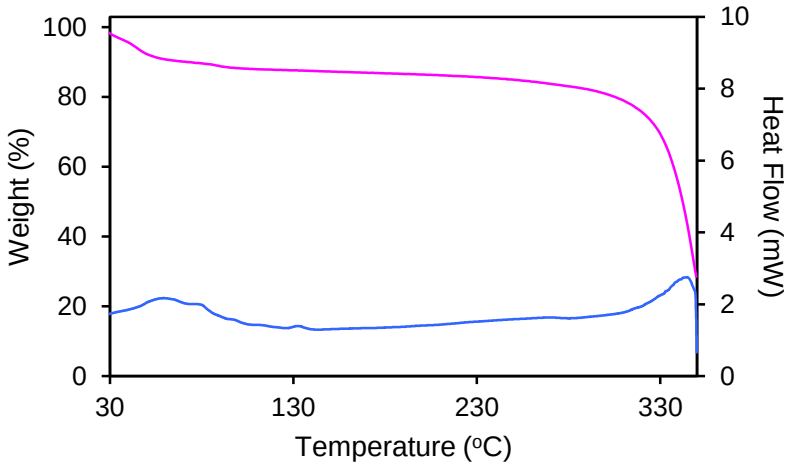

Figure 4. *Representative TG (pink) and DSC (blue) traces for BCDCYC.*

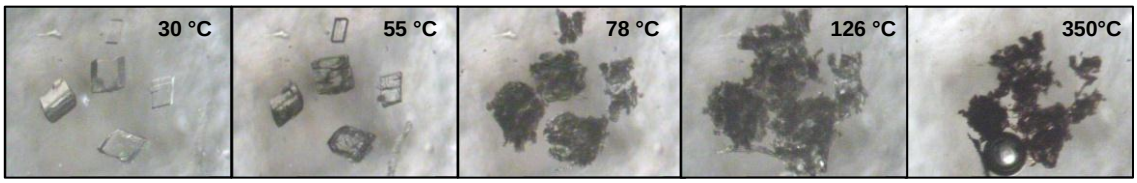

Figure 5. *HSM photographs of the BCDCYC crystals recorded at various temperatures.*

Crystal structure analysis

Data-collection and space group determination

Crystal intensity data were collected on a Nonius KappaCCD single crystal X-ray diffractometer. The program LAYER was used to determine the crystal system which was found to be triclinic and as cyclodextrins are chiral molecules the space group *P*1 was inferred.[1] X-PREP subsequently confirmed the crystal system and space group.[2]

Structure solution and refinement

The crystallographic data and data-collection parameters for BCDCYC are shown in Table 3.

Table 3. *Data-collection and refinement parameters for the BCDCYC complex.*

Chemical formula	$C_{42}H_{70}O_{35}\cdot C_{11}H_{22}N_2O\cdot 11.5H_2O$
Formula weight	1540.47
Crystal system	Triclinic
Space group	*P*1
Unit cell constants	
a (Å)	15.320(1)
b (Å)	15.464(2)
c (Å)	15.979(1)
α (°)	79.549(4)
β (°)	85.134(6)
γ (°)	74.971(7)
Volume (Å^3)	3592.5(5)
Z	2
Density$_{calc}$ (g cm^{-3})	1.424
μ [MoKα] (mm^{-1})	0.126
F (000)	1654
Temperature of data collection (K)	133(2)
Crystal size (mm)	0.25 x 0.20 x 0.10
Range scanned θ (°)	0.41 – 26.37
Index ranges	h: -18, 19; k: -18, 19; l: -19, 19
ϕ and ω scan angle (°)	1.0
Total no. of frames	601
Dx (mm)	33.00
Total no. of reflections collected	66486
No. of independent reflections	14453
No. of reflections with I > 2σ(I)	8948
No. of parameters	1721
R_{int}	0.1170
S	1.025
R_1 [I > 2σ(I)]	0.1005
No. of reflections omitted	61
wR_2	0.2462
Weighting scheme parameters	a = 0.1344 and b = 10.0885
$(\Delta / \sigma)_{mean}$	< 0.001
$\Delta\rho$ excursions (e Å^{-3})	0.85 and -0.65

The asymmetric unit contains two crystallographically independent CD molecules each containing a guest molecule disordered over two positions and 23 water molecules surrounding the host molecules. The *a*, *b* and *c* unit cell parameters match those of four other fully elucidated β-CD complexes.[7] However, the interaxial α and β parameters differ from these by up to 10°. This complex X-ray crystal structure is therefore not isostructural with any known β-CD complexes and was solved by *ab initio* direct methods using SHELXD.[8] SHELXD solved the structure partially by revealing most of the non-hydrogen host molecules and some atoms of the non-hydrogen guest molecules as well as some water molecules. The carbon and oxygen atoms of the host were then assigned correctly and the model was refined using SHELXH-97.[5] The difference Fourier map revealed the positions of further atoms which were assigned and refinement continued. This was repeated until all the host atoms had been accounted for. The glucopyranose units of the two independent host molecules were labelled A1-A7 and B1-B7. The primary hydroxyl groups on A1, A7 and B7 were disordered over two positions (s.o.f. = 0.51, 0.58 and 0.52 for the major components, respectively). All the host atoms were refined anisotropically except the disordered primary hydroxyl groups. Hydrogen atoms were geometrically placed on the host using the riding model. The isotropic temperature factors assigned to the hydrogen atoms were 1.2 times those of their parent atoms.

Twenty-nine positions were located for water molecules with 17 being fully occupied oxygen sites and the other 6 oxygen atoms were each disordered over two positions (Table 4).

Table 4. *Site-occupancy values of the water molecules present in the asymmetric unit.*

Water molecule/s	s.o.f.	Water molecule/s	s.o.f.
O1WA	0.68	O1WB	0.32
O2WA	0.32	O2WB	0.68
O3WA	0.52	O3WB	0.48
O7WA	0.55	O7WB	0.45
O8WA	0.39	O8WB	0.61
O9WA	0.32	O9WB	0.68
O4W-O6W	1.00	O10W-O23W	1.00

The TG analyses accounted for only 20.0 ± 0.3 water molecules per dimer which is slightly lower than the number (23) modelled in the BCDCYC X-ray crystal structure. This discrepancy can be explained by the different preparation methods employed before a TG measurement and X-ray data-collection. Prior to X-ray data-collection the crystals were taken directly from the mother liquor and placed into paratone oil to prevent loss of any

crystalline water molecules, whereas for TG analysis the crystals were first surface-dried on filter paper and then quickly transferred into an open crucible. The TG curve (Figure 4) shows an immediate mass loss indicating that water may have diffused out of the crystals prior to TG measurement and are therefore not accounted for, resulting in a lower mass loss.

Disordered water molecules O3WA and O3WB form hydrogen bonds with the disordered primary hydroxyl group on glucopyranose unit B7 (O6B7•••O3WB 2.62 Å and O7B7•••O3WA 2.76 Å). When modelling these atoms, both the host atom and the water molecule were assigned a common s.o.f. which settled at 0.52 for the major component.

Modelling of the cycluron guest

Integration of the ^{1}H NMR signals of the BCDCYC crystals in D_2O revealed that a single cycluron molecule was included per β-CD molecule. During the course of refinement it became apparent that the guest molecules in both CDs were disordered as there were many residual peaks of high electron density close to the guest atoms that had already been placed. From the high quality of the X-ray data it was possible to resolve the disordered guest molecules utilising the geometrical parameters of the uncomplexed cycluron crystal structure. Several distance constraints were used to ensure reasonable geometries and prevent the least-squares refinement from diverging. The two disordered guest molecules in host B were labelled A and B and were assigned a global isotropic temperature factor which settled at 0.099 Å^2. The disordered guest molecules in host A were labelled C and D and were also assigned a global isotropic temperature factor which settled at 0.083 Å^2. Disordered guests B and C were refined with *x* to determine their s.o.f. while guests A and D were refined with *1-x*. An initial value of 0.5 was set and refined to 0.62. All guest atoms were refined isotropically and the hydrogen atoms were placed in idealised positions in a riding model. No attempt was made to locate the amide hydrogen atoms as the electron density was very low owing to the many disordered atoms. The methylene hydrogens, methine hydrogen and amide hydrogen refined with a U_{iso} value 1.2 times those of their parent atoms while the methyl hydrogens refined with a U_{iso} value 1.5 times those of their parent atoms. The same numbering scheme was used as for the uncomplexed guest.

Geometrical analysis of the BCDCYC structure

Host conformation

The structure and numbering scheme of host molecule A is shown in Figure 6. An analgous labelling scheme was used for host molecule B. The geometrical data for each β-CD molecule of the BCDCYC complex are listed in Table 5. The parameters listed are defined explicitly in Chapter 1.

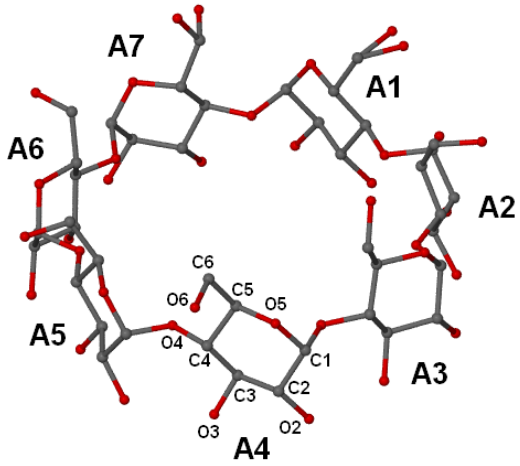

Figure 6. *Macrocyclic structure and numbering scheme of glucose residues. Hydrogen atoms have been omitted for clarity.*

Table 5. *Geometrical parameters for the host molecules of BCDCYC.*

Residue	*l* (Å)	*D* (Å)	ϕ (°)	*d* (°)	α^a (Å)	$D_3{}^b$ (Å)	$\tau_1{}^c$ (°)	$\tau_2{}^d$ (°)
A1	4.99	4.34	129.9	2.6	0.003	2.80	4.5	5.9
A2	5.05	4.38	128.2	-0.4	0.055	2.74	7.0	8.8
A3	5.07	4.34	127.7	2.3	-0.052	2.75	6.4	8.0
A4	5.00	4.43	129.6	0.3	-0.002	2.77	4.0	4.6
A5	5.04	4.34	128.2	-0.6	0.029	2.72	2.0	3.1
A6	5.06	4.37	128.5	-0.6	0.002	2.77	4.8	5.0
A7	5.05	4.40	127.8	0.1	-0.030	2.75	5.8	7.2
B1	5.14	4.34	125.9	4.5	0.057	2.81	10.6	11.5
B2	4.92	4.47	132.0	-2.6	-0.055	2.86	4.2	6.3
B3	5.06	4.32	127.4	-0.5	0.001	2.78	9.9	10.3
B4	5.11	4.38	127.7	1.4	0.033	2.77	5.7	6.6
B5	5.02	4.37	128.9	0.6	-0.011	2.81	6.8	7.1
B6	4.93	4.41	129.8	1.0	-0.015	2.74	3.3	4.2
B7	5.07	4.35	128.3	-3.1	-0.010	2.72	3.6	4.9

[a] mean e.s.d. = 0.005 Å; [b] mean e.s.d. = 0.01 Å; [c] mean e.s.d. = 0.3° ; [d] mean e.s.d = 0.2°.

The usual $^4C_1$ chair conformation is adopted by all glucose residues. The heptagonal parameters for the two host molecules of BCDCYC do not deviate significantly from those parameters reported for a heptagon formed by the O4 atoms of β-CD.[9,10] The distances between each O4 atom of the heptagon (*D*) as well as the distances between each O4 atom and a generated centroid (*l*) for the BCDCYC complex have small ranges, demonstrating the seven-fold symmetry of the β-CD molecules. The dihedral angles (τ_1 and τ_2) are all positive confirming the inward tilt of the primary rims of the glucopyranose units towards the centre of the CD cavity which results in the toroidal shape of the β-CD molecules. Table 5 also lists other important parameters such as the deviation of O4 atoms from the mean O4 plane (α), the distance between O2n and O3(n-1) (D_3) and the angle between the O4 atoms of the glucopyranose units (ϕ) which is 128.57° or 5π/7 radians for a regular heptagon.

The primary hydroxyl torsion angle ω (O5-C5-C6-O6) describes the rotation of the C6-O6 bond relative to the cyclodextrin cavity. For the BCDCYC complex most of the primary hydroxyl torsion angles (ω) have a *(-)-gauche* orientation and the C6-O6 bonds are directed away from the CD cavity. There are, however, a few glucopyranose units, namely A3, B5 and the minor component of A7, that have a *(+)-gauche* orientation, the C6-O6 bonds being directed towards the middle of the β-CD cavity. These *(+)-gauche* torsion angles allow for weak, long-range C-H•••O hydrogen bonds to occur between the host and guest molecules.

The O4 mean planes of host molecules A and B comprising the dimer are essentially parallel to one another with an angle of 1.27(4)° between them.

Guest inclusion and conformation

The asymmetric unit of BCDCYC contains two guest molecules. Each guest molecule is disordered over two positions with the major guest components being labelled B and C (Figure 7 - blue), each being located in one of the host molecules comprising the β-CD dimer. Minor guest components A and D (green) are also each located in one of the host molecules comprising the β-CD dimer. With regard to any symmetry between the disordered pairs, there is evidence of a pseudo-mirror plane within the CD cavity that relates the disordered components (A to B and C to D). Molecules A and B are further displaced from each other when compared to molecules C and D. When looking at the A-D and B-C pairs, one can relate the two partial guest molecules by performing a pseudo-twofold rotation around the *a*-axis. All four disordered guest components of the BCDCYC complex have the same boat-chair conformation and cyclooctyl geometry as that of the major component of

the uncomplexed guest, with the mirror plane passing through atoms C1 and C5 of the cyclooctyl group (Figure 2).

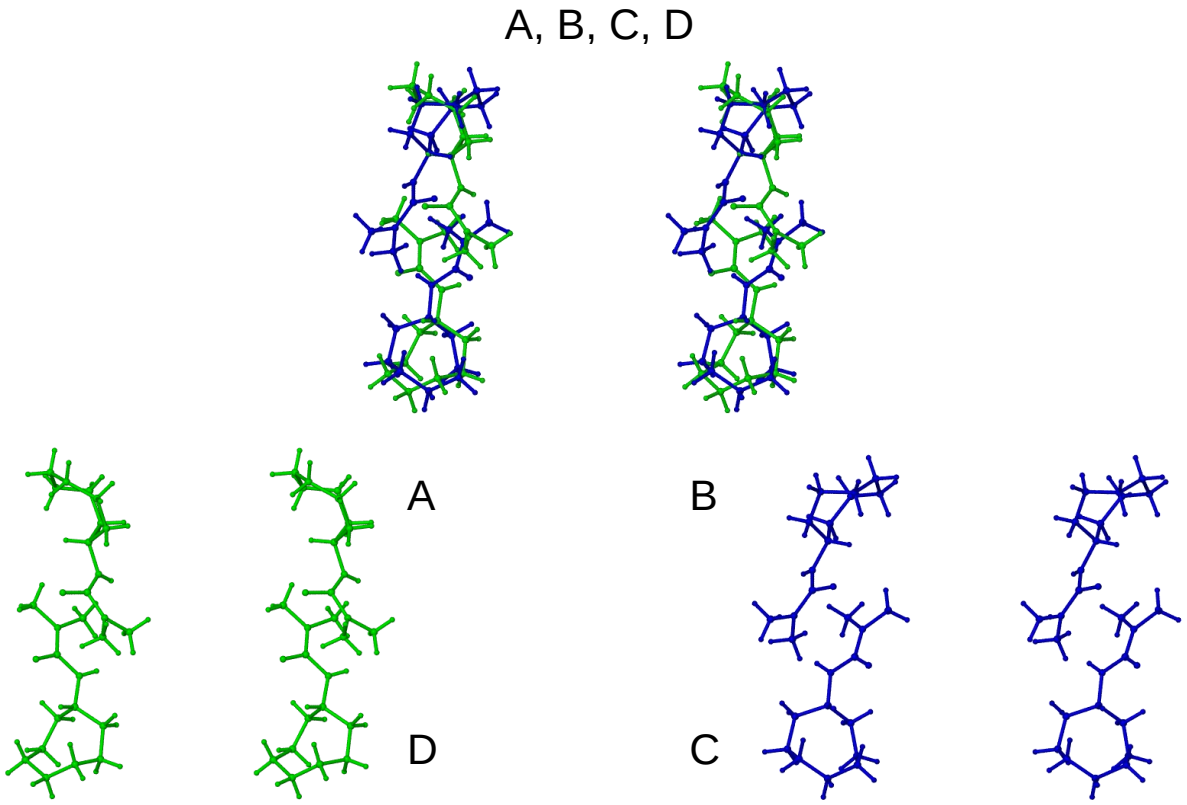

Figure 7. *Stereoviews of the disordered guests A, B, C and D of the BCDCYC complex and the deconvoluted disordered components A/D (green) and B/C (blue).*

The guest components are located with the cyclooctyl group positioned at the primary rims of the CD molecules and the urea moieties at the secondary rims (Figure 8). The two cycluron molecules are fully encapsulated by the β-CD molecules, with only a very small portion of the cyclooctyl ring extending beyond the primary rim of the CD into the adjacent dimer which is slightly offset. The guests are tilted with respect to the O4-heptagon of each CD molecule.

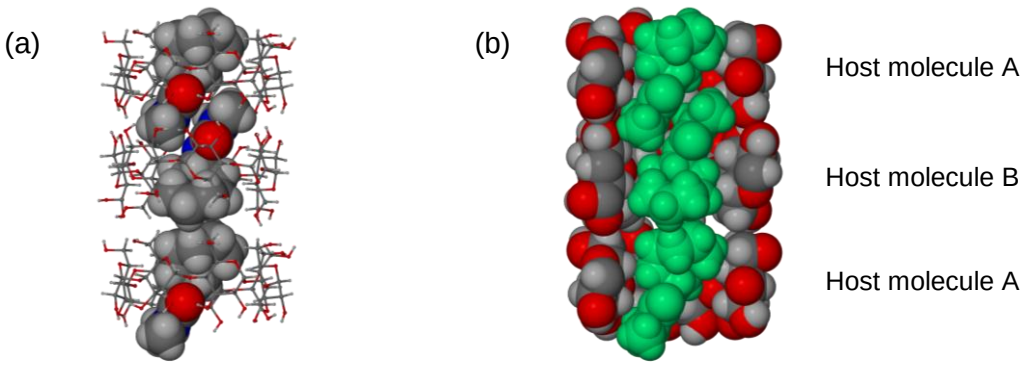

Figure 8. *(a) The tilted guest molecules in the dimer cavity (b) A cross-sectional view of the BCDCYC complex. Only the major guest components are shown and the water molecules have been omitted.*

Hydrogen bonding interactions

Host interactions

A β-CD molecule is normally stabilised by seven intramolecular O2n•••O3(n-1) hydrogen bonds that can form between adjacent glucopyranose units. The BCDCYC complex has 12 of 14 possible intramolecular hydrogen bonds. The other two O2 atoms form intra-layer hydrogen bonds with adjacent β-CD molecules. At the secondary rim interface of the β-CD dimer there are 14 intermolecular interactions, eleven of which are slightly weaker hydrogen bonds (O2–H•••O3) and two which have a more favourable distance and therefore stabilise the dimer to a greater extent (O3–H•••O3) (Table 6).

Table 6. *Summary of the intra- and intermolecular hydrogen bonds for the CD molecules.*

Interaction	Type	Number	Mean bond length, Å O•••O / C•••O	Mean bond angle,° O–H•••O / C–H•••O
Host intramolecular	O2–H•••O3	12	2.78(1)	145
Host-host intermolecular	O2–H•••O3	11	3.07(1)	148
	O3–H•••O3	2	2.81(1)	167
Intra-layer	O2–H•••O2	2	2.75(1)	107
	O6–H•••O6	3	2.80(1)	127
	C2–H•••O3	4	3.39(1)	158
	C1–H•••O2	4	3.38(1)	142
Inter-layer	O6–H•••O6	1	2.77(2)	160

The β-CD dimers stack on top of one another to form columns parallel to the *c*-axis. These columns pack to produce layers in the *xy*-plane. Interactions within and between these layers are known as intra- and inter-layer interactions respectively and they link the β-CD dimers to one another (Figure 9). There are six long range C–H•••O hydrogen bonds and four stronger O–H•••O hydrogen bonds that make up the intra-layer hydrogen bonding network while only one strong inter-layer hydrogen bond is evident for the BCDCYC complex.

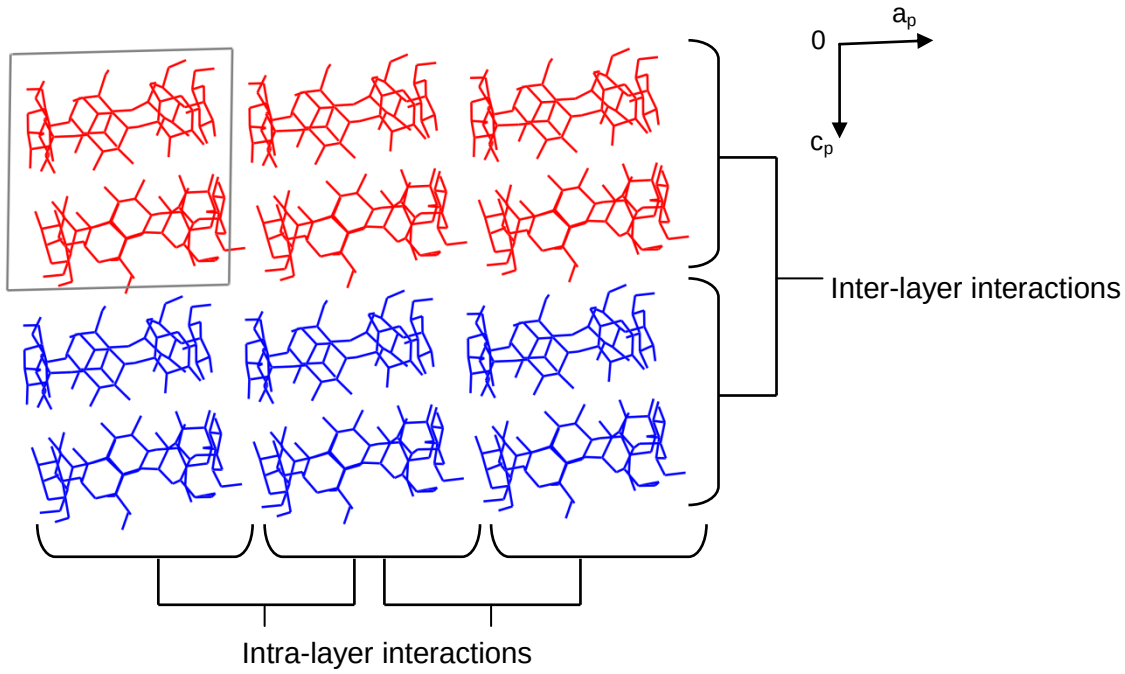

Figure 9. *The difference between intra- and intermolecular interactions for a crystal structure containing β-CD dimers.*

Guest interactions

There are two weak C–H•••O hydrogen bonds between the host and guest molecules at the secondary interface. One methyl group of both guest molecule A (C13A) and B (C13B) form hydrogen bonds with atoms O3B2 and O3A7 of the host molecules. The C•••O contact distances between the two guest and host molecules are 2.94(1) and 3.56(3) Å respectively. The former contact distance is unusually short for a C-H•••O type hydrogen bond but due to the extensive disorder of the guest molecules, and the slight deviation from planarity of the urea moiety of guest molecule A, this bond length can be justified.

Water interactions

The 29 water molecule sites are found between the columns of dimers, as shown in Figure 10. The six disordered water atoms are labelled A and B to distinguish the major and minor

components. Atoms O5W, O7WA, O7WB and O14W (green atoms and labels) are the only four atoms that do not form hydrogen bonds with the cyclodextrin directly but rather bond to other water molecules, forming an intricate hydrogen bonding system that stabilises the crystal packing to a greater extent.

Thirteen of the fourteen primary hydroxyl groups present within the asymmetric unit bond to at least one water molecule. Neither component of the disordered primary hydroxyl group on glucose residue A7 bonds to a water molecule. Atoms O6A3, O6A5 and O6B6 act as hydrogen bond acceptors to water molecules O12W, O15W and O22W with the following O•••O distances: 2.73, 2.63 and 2.71 Å. The remaining primary hydroxyl groups are hydrogen bond donors and the respective atoms involved, with their distances and angles, are listed in Table 7. The water molecules that interact with the secondary rim include O2WB, O6W, O8WA, O8WB, O13W, O20W, and O21W. All of these water molecules act as hydrogen atom donors, since the hydroxyl oxygen atoms donate their hydrogen atoms to an adjacent glucopyranose unit or to the accompanying dimer CD unit. There are 40 water-water close contacts which range from 2.48 to 3.04 Å with a mean distance of 2.73 Å. No water molecules are present between the guest and β-CD molecules.

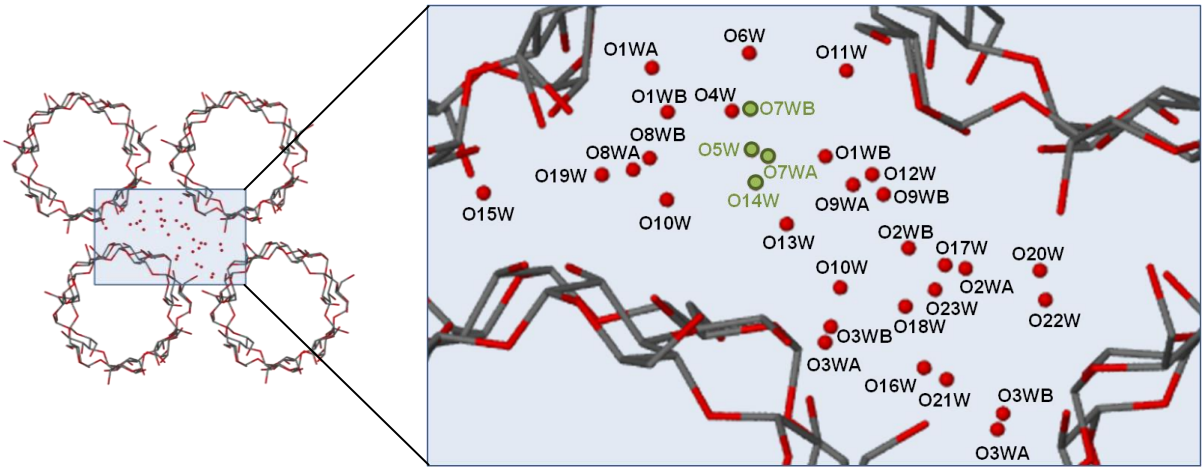

Figure 10. *The interstitial water molecules with their respective labels. Atoms shown in green are not directly bonded to the CD.*

Table 7. *Host(O6)-water interactions for the BCDCYC complex.*

Interaction	H•••A (Å)	D•••A (Å)	D-H•••A (°)
O7A1*–H7A3•••O15W[a]	1.74	2.54(2)	160
O6A2–H6A5•••O17W[a]	2.00	2.62(1)	130
O6A4–H6A9•••O16W	1.88	2.66(1)	153
O6A6–H6AA•••O3WA[b]	2.29	2.78(1)	117
O6B1–H6B3•••O11W	1.78	2.61(2)	170
O6B2–H6B5•••O19W	1.87	2.68(1)	163
O6B3–H6B7•••O4W	1.96	2.77(2)	161
O6B4–H6B9•••O3WA[c]	2.32	2.90(2)	126
O6B4–H6B9•••O23W[c]	2.27	2.76(2)	118
O6B5–H6BY•••O15W[d]	1.93	2.731)	158
O6B1–H6B3•••O22W	2.04	2.71(1)	137
O7B7*–H7B7•••O3WA	2.00	2.77(2)	153

Symmetry codes: [a] *-1+x, y, z;* [b] *x, -1+y, 1+z;* [c] *x, -1+y, z;* [d] *x, y,-1+z.*

* O7A1 and O7B7 are disordered O6 atoms.

Crystal packing

The head-to-head β-CD dimers of BCDCYC include two disordered guest molecules. Figure 11 (a) is a packing diagram of the BCDCYC structure projected down the *c*-axis illustrating the infinite channels produced by the cavities of the CD dimers. Throughout the crystal structure water molecules are positioned in the interstitial sites between these channels. Figure 11 (b) shows the packing of the BCDCYC structure as viewed down the *b*-axis. This figure illustrates the stacking of the dimers in columns parallel to the *c*-axis. Upon closer inspection the respective layers parallel to the *a*-axis are seen to be displaced along this direction by ~3.0 Å. This shift is necessary to reduce close contacts between the hydrophobic cyclooctyl groups of the guest molecules in adjacent dimers.

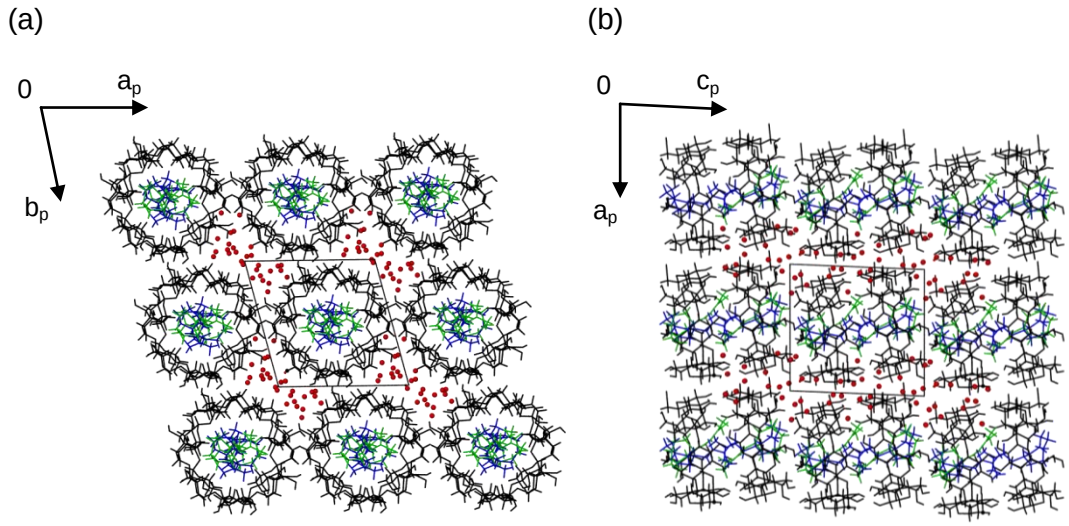

Figure 11. *Packing diagrams of the BCDCYC structure, viewed along (a) [001] and (b) [010]. Water molecules are presented in red, the host in black and the disordered guests in blue and green.*

Comparative PXRD

The calculated and experimental PXRD traces for the BCDCYC complex are shown in Figure 12. The shift of peaks to higher 2θ values for the calculated pattern is due to shrinkage of the crystal upon cooling during data-collection on the single crystal X-ray diffractometer. The level of agreement between the two traces is however still good, which confirms that the single crystal is representative of the bulk sample.

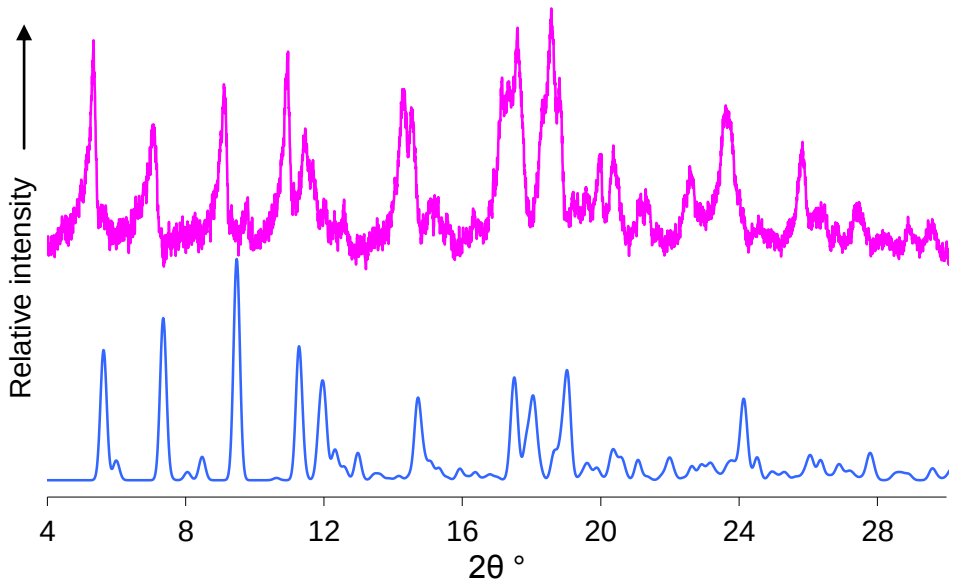

Figure 12. *Calculated (blue) and experimental (pink) PXRD traces of BCDCYC.*

The BCDCYC complex has unit cell dimensions very similar to those of two other triclinic (*P*1) isostructural series which were referred to as B4:*P*1 and B5:*P*1 by S. Lubhelwana.[7] The members of the isostructural series B4 have the following average unit cell parameters: *a* = 15.52(4) Å, *b* =15.52(5) Å, *c* = 15.78(6) Å, α = 102.0(1)°, β = 102.1(2)°, γ = 103.7(1)° and for B5 the parameters are as follows: *a* = 15.23(3) Å, *b* =15.67(6) Å, *c* = 16.0(4) Å, α = 89(2)°, β = 97.6(7)°, γ = 103.4(1)°. BCDCYC also crystallises in the triclinic crystal system (*P*1) and has similar *a*, *b*, *c* and γ unit cell parameters of 15.32 Å, 15.46 Å, 15.98 Å and 105.0°, respectively. However, the interaxial angles α and β differ significantly in all three cases. This influences the stacking of these three dimeric structures which can be seen by comparing their respective PXRD traces (Figure 13). Even though they all have a channel-type packing arrangement the locations of the water molecules, as well as host and guest molecules within the asymmetric unit are substantially different, thus causing slight shifts in peak positions and differences in peak intensities. The crystal structure of BCDCYC discussed here, demonstrates a new packing arrangement for dimeric β-CD inclusion complexes.

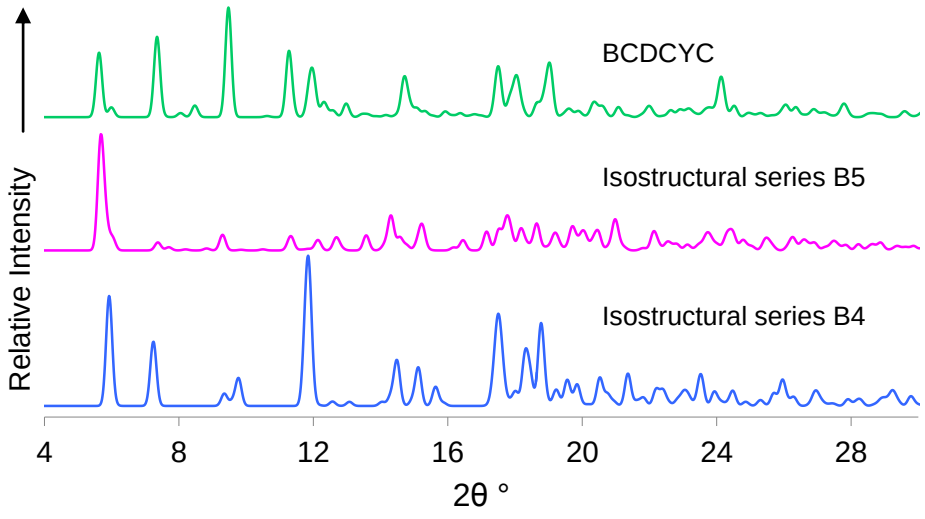

Figure 13. *Calculated PXRD traces of three structurally similar triclinic (P1) dimeric β-CD inclusion complexes.*

γ-CYCLODEXTRIN INCLUSION COMPLEX WITH CYCLURON

Complex preparation

A solid-state inclusion complex of γ-CD with cycluron was prepared using the kneading method. 65 mg of γ-CD was placed in a mortar with ~2 drops of distilled water. An equimolar quantity of cycluron (0.05 mmol) was added to the γ-CD paste with simultaneous kneading over a 5 min period. Kneading continued for 40 min and required additional drops of water to keep the material moist. Complexation between the host and guest molecule was then confirmed using PXRD.

Powder X-ray diffraction

The PXRD pattern obtained from the γ-CD·cycluron material prepared by kneading (Figure 14 – green) was compared to the PXRD patterns of the uncomplexed host molecule (pink) and guest molecule (blue) as well as to a reference pattern for the one known isostructural series of γ-CD inclusion complexes (orange).[7] There is excellent agreement between the γ-CD·cycluron complex PXRD pattern and the reference pattern for γ-CD complexes, verifying the formation of an inclusion complex between γ-CD and cycluron. The slight shift of peaks to higher 2θ° values for the reference pattern can be attributed to the different temperatures at which the data were collected.

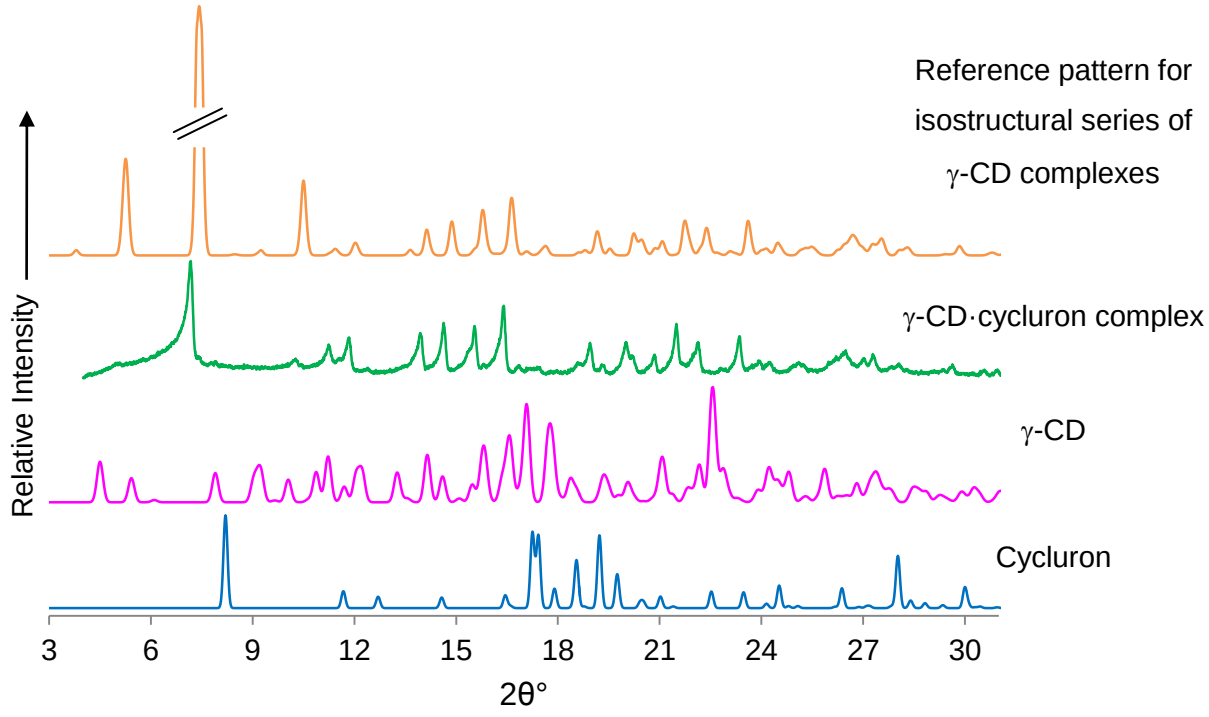

Figure 14. *PXRD traces illustrating complexation between γ-CD and cycluron.*

The preparation of single crystals for this particular complex was not pursued; this is due to the highly symmetrical tetragonal space group, $P4_12$, in which these complexes crystallise and the indiscernible guest molecules within the γ-CD cavities once the crystal structure has been solved. Only a few crystal structures have been published of γ-CD inclusion complexes and these have unit cell dimensions $a \sim b \sim 23.8$ and $c \sim 23.2$ Å.[11]

The packing arrangement of γ-CD complexes is shown schematically in Figures 15 (a) and (b) with the crystallographic symmetry elements of the space group $P4_12$ indicated. In the crystalline phase, γ-CD molecules stack on top of one another to form infinite channels parallel to the tetragonal *c*-axis. These channels are unique in that they have three CD molecules per asymmetric unit. Consequently, the number of symmetry-independent glucose residues is six, amounting to ¾ of a γ-CD molecule.[12] The CD molecules pack in a square pattern generating large channels between the columns. These interstitial sites are normally filled with solvent molecules such as water. The crystallographically independent γ-CD molecules form a trimer, two of which are parallel and one is antiparallel. The columns are then built by translation of these units. The intermolecular contacts involve head-to-head (A), tail-to-tail (B) and head-to-tail (C) interactions. A complicated hydrogen bonding system helps maintain the host framework. The fourfold rotation axis runs through the centre of the γ-CD cavity, requiring fourfold disorder of the guest, which usually renders the latter unable to be modelled satisfactorily.

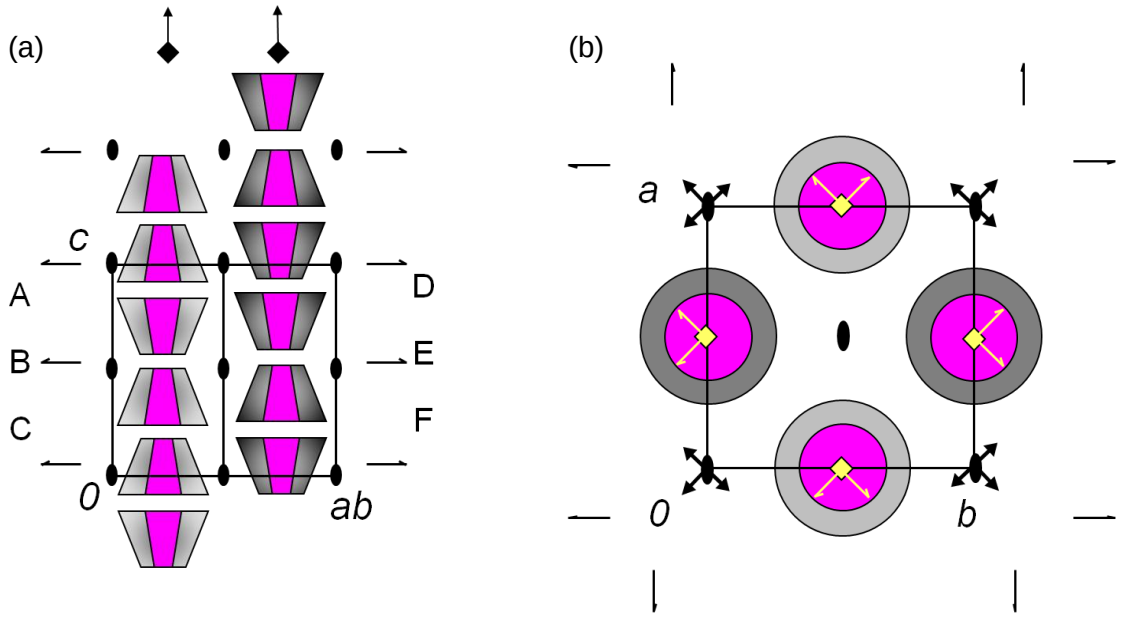

Figure 15. *(a) Schematic diagram showing the stacking motif of the γ-CD molecules along the c-direction and the two independent columns (light and dark) parallel to c. (b) A projection onto the xy-plane illustrating the crystallographic tetrads positioned at the centre of each column (b).*[12]

TRIMEA INCLUSION COMPLEX WITH CYCLURON

Complex preparation

Only the method of co-precipitation was used when forming inclusion complexes with derivatised CDs and cycluron. Single crystals were obtained by adding an equimolar amount of cycluron (10 mg, 0.05 mmol) to an aqueous solution of TRIMEA (72 mg, 0.05 mmol) which was stirred at room temperature for 24 h. A total of 4 cm^3 of water was required to ensure a clear solution. The latter was filtered into a clean vial and placed in an oven set at 65 °C. Single crystals were obtained within five days.

Complex stoichiometry and thermal analysis

Figure 16 illustrates the thermal events recorded for the TRIMEA·cycluron complex (TMEACYC). There is a broad endothermic event (A) associated with crystal dehydration in the temperature range 30-100 °C. This corresponds to an observed mass loss in the TG curve of 4.3 ± 0.1 % (n = 2), yielding 6.5 ± 0.1 water molecules per CD dimer. The second two-step mass loss of 7.6 ± 0.5 % in the temperature range 100-270 °C corresponds to release of a guest molecule from the CD dimer (calcd. for a 2:1 host-guest stoichiometry 7.2 %). There is no significant mass loss in the TG curve corresponding to the small endotherm B on the DSC trace. This endotherm, with an onset temperature of ~120 °C, is interpreted as being associated with initial rearrangement of the solid complex to yield a structurally modified complex phase. PXRD patterns were acquired at different temperatures in order to follow this rearrangement (Figure 17).

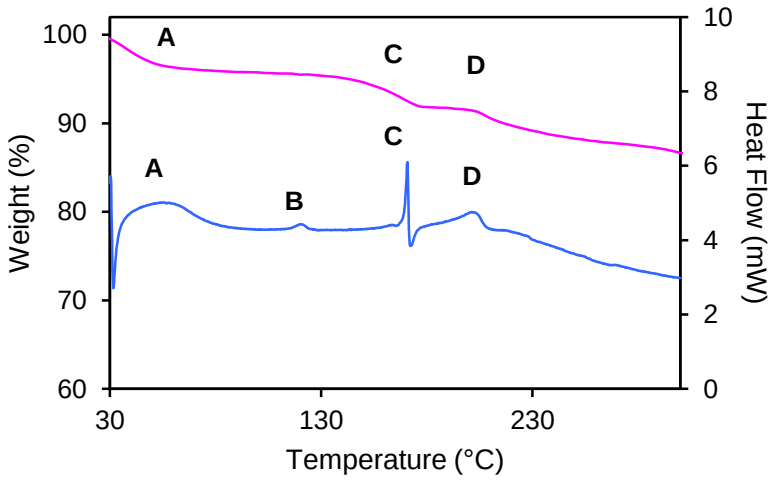

Figure 16. *Representative TG (pink) and DSC (blue) traces for TMEACYC.*

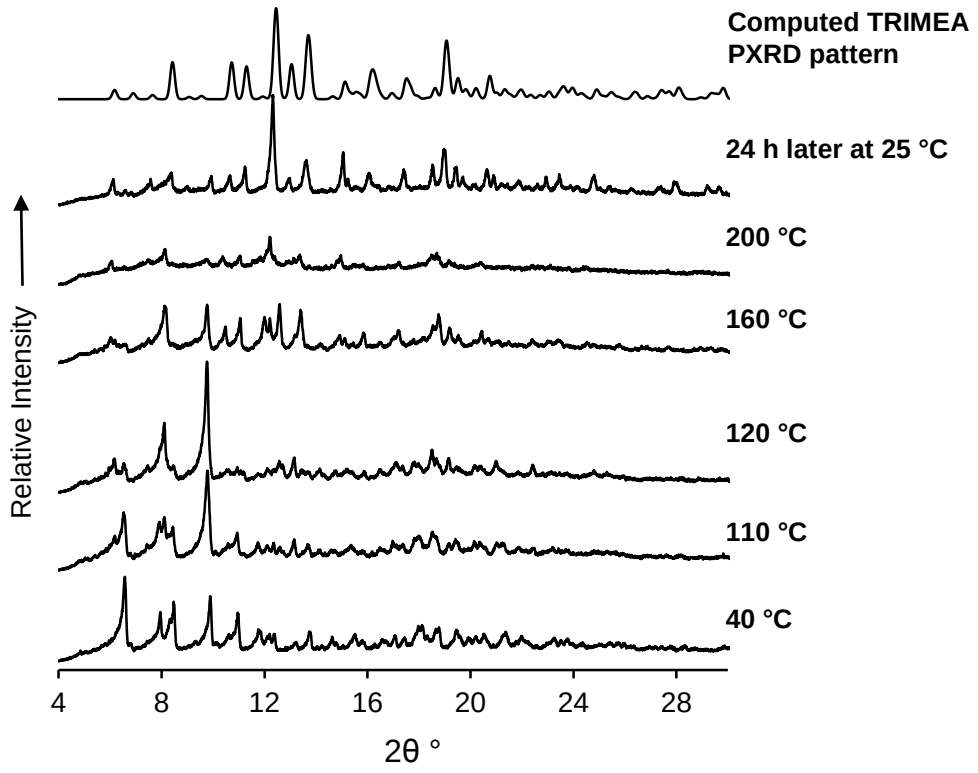

Figure 17. *Experimental PXRD patterns of TMEACYC at various temperatures. The experimental trace recorded 24 h later is shown to compare with the computed PXRD pattern of the host TRIMEA.*

In keeping with the above TG/DSC interpretation, it can be noted that the PXRD trace recorded at 110 °C shows some significant differences from that recorded at 40 °C (the effect of the dehydration process), while another significant change in the PXRD pattern, occurring between 120 and 160 °C, accounts for the interpretation of the DSC event B. The sharp endotherm C, immediately followed by an exotherm (Figure 16) is attributed to successive melting of the anhydrous complex and its rapid recrystallisation to a new phase that subsequently releases the guest, yielding a final solid phase that melts at ~200 °C (endotherm D). The variable-temperature PXRD data (Figure 17) again support the above interpretation of the DSC features in that the PXRD pattern at 160 °C does not match that of the single known crystalline form of the host TRIMEA,[13] whereas at 200 °C, the trace is in good agreement with that of pure TRIMEA.

The HSM images (Figure 18) show two complex crystals under silicone oil. Bubbles appear at 68 °C indicating dehydration. At 110 °C the crystals appear opaque and continue to bubble more vigorously. There is evidence of recrystallisation occurring at 213 °C followed by an immediate melt at 222 °C. This correlates with what is observed in the TG and DSC traces.

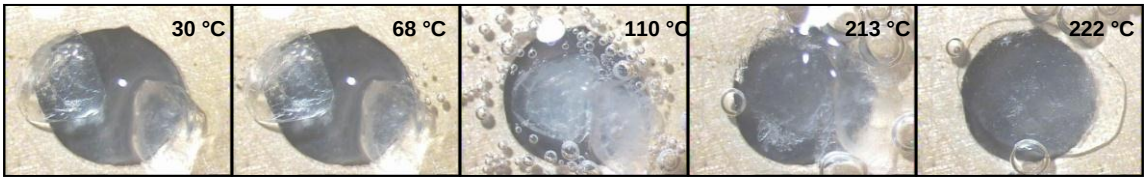

Figure 18. *HSM photographs of the TMEACYC crystals recorded at various temperatures.*

Crystal structure analysis

Data-collection and space group determination

Intensity data were collected on a Nonius KappaCCD single crystal X-ray diffractometer from a single crystal coated with paratone N oil.[14] The preliminary unit cell parameters and space group were determined using the program LAYER.[1] The Laue symmetry was found to be *mmm* indicating the orthorhombic crystal system. Further examination of the systematic absences (*hkl: none, h00: h =2n, 0k0: k = 2n, 00l: l = 2n*) confirmed the space group $P2_12_12_1$. TMEACYC crystallises with a 2:1 host-guest unit in the asymmetric unit.

Structure solution and refinement

The crystallographic data and data-collection parameters for TMEACYC are shown in Table 8. The TMEACYC complex was solved by direct methods using the program SHELXD as no isostructural complex existed.[8] The resultant solution had a correlation coefficient (CC) value of 82.2 and revealed most of the non-hydrogen atoms of the host and a few non-hydrogen guest atoms. The primary and secondary methoxyl groups of the host as well as possible water molecules were temporarily deleted to allow for correct placement of these atoms after an initial refinement of a stable starting model. Refinement was performed using the full-matrix least-squares method implemented in SHELXH-97.[5] All the non-hydrogen host and guest atoms were located in successive difference Fourier maps. The glucose units were labelled A1 - A6 and B1 - B6 for the two independent TRIMEA molecules (host molecules A and B). All non-hydrogen host atoms were refined anisotropically except three secondary methoxyl carbon atoms (C7B1, C8B1 and C7B3), which showed abnormally high thermal motion. The eight cyclooctyl carbon atoms of the guest were refined isotropically

and the C-C bonds were refined with a restrained bond length of 1.52(1) Å. The C-C-C angles of the cyclooctyl group were allowed free variation during refinement.

Table 8. *Data-collection and refinement parameters for the TMEACYC complex.*

Chemical formula	$(C_{54}H_{96}O_{30})_2 \cdot C_{11}H_{22}N_2O \cdot 7H_2O$
Formula weight	2774.92
Crystal system	Orthorhombic
Space group	$P2_12_12_1$
Unit cell constants	
a (Å)	17.1400(3)
b (Å)	28.2883(4)
c (Å)	30.0478(5)
$\alpha = \beta = \gamma$ (°)	90
Volume (Å^3)	14569.0(4)
Z	4
Density$_{calc}$ (g cm^{-3})	1.265
μ [MoKα] (mm^{-1})	0.103
F (000)	6000
Temperature of data collection (K)	173(2)
Crystal size (mm)	0.40 x 0.22 x 0.18
Range scanned θ (°)	1.0 – 25.0
Index ranges	h: -20, 20; k: -33, 33; l: -35, 35
ϕ and ω scan angle (°)	0.5
Total no. of frames	860
Dx (mm)	44.00
Total no. of reflections collected	25686
No. of independent reflections	13851
No. of reflections with I > 2σ(I)	8162
No. of parameters	1645
R_{int}	0.0631
S	1.017
R_1 [I > 2σ(I)]	0.0677
No. of reflections omitted	19
wR_2	0.1655
Weighting scheme parameters	a = 0.1165 and b = 4.2231
$(\Delta / \sigma)_{mean}$	< 0.001
$\Delta\rho$ excursions (e Å^{-3})	0.66 and -0.44

The hydrogen atoms of the host and the methine, methylene and methyl protons of the guest were geometrically constrained to their parent atoms and refined with linked temperature factors. The amide hydrogen (H9) of the guest molecule was not geometrically constrained to an idealised position as this hydrogen was apparent in the difference Fourier map and did not conform to the regular trigonal planar geometry but rather presented a slightly pyramidal arrangement at the N atom.

In total, nine oxygen atoms were placed as water molecules of which four had full site-occupancy (O1W, O2W, O3W and O4W). The s.o.f.s of the remaining five sites refined to 0.77, 0.74, 0.52, 0.48 and 0.49 for O5W, O6W, O7W, O8W and O9W, respectively. This led to a total of 7 water molecules per asymmetric unit which is in reasonable agreement with the TG estimate of 6.5 water molecules per CD dimer. The modelling of the water molecules was difficult due to the many partially occupied sites. The hydrogen atoms of the water molecules were not located.

Geometrical analysis of the TMEACYC structure

The asymmetric unit of the TMEACYC complex consists of two TRIMEA molecules encapsulating one ordered guest molecule and a partial water molecule (Figure 19 (a)). The remaining water molecules surround the host molecules. The labelling scheme of host molecule A is shown in Figure 19 (b) (the same scheme is used for host molecule B). The guest molecule has been consistently labelled in this chapter.

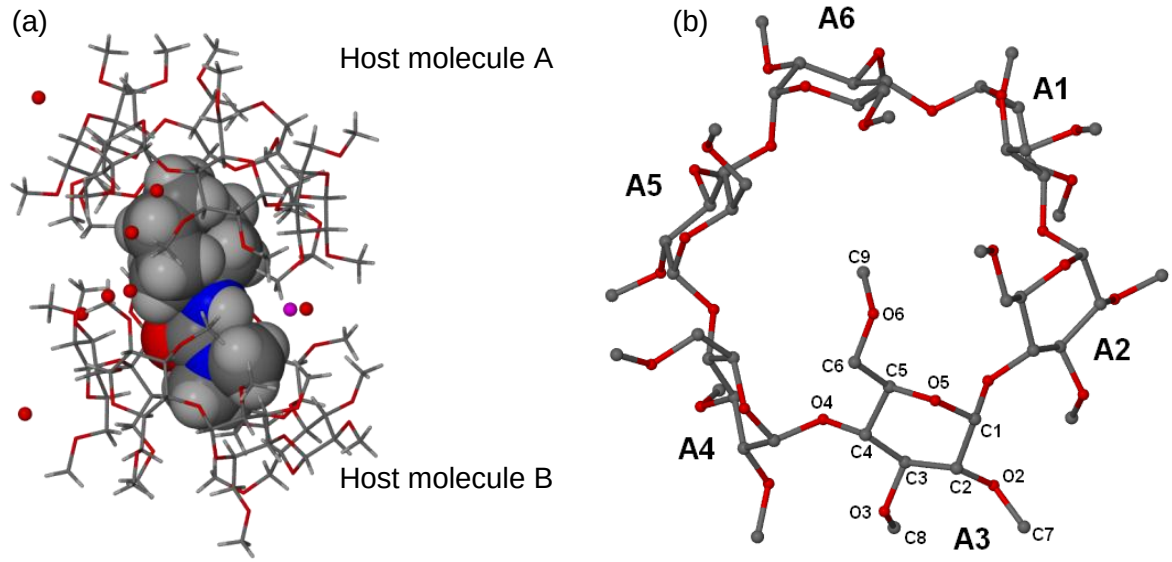

Figure 19. *(a) The asymmetric unit of the TMEACYC complex (the partially included water molecule is shown in pink) (b) Macrocyclic structure of host molecule A and numbering scheme of the TRIMEA glucose residues.*

Host conformation

The torsion angle ω (O5-C5-C6-O6) that describes the rotation around the C6-O6 bond of each glucose unit is noteworthy with regard to derivatised CDs. This parameter, together with the tilt angle τ_1 (the angle between the O4 mean plane and the mean plane through the six atoms of the glucose ring) demonstrates the extent to which a specific glucose unit contributes to folding over and blocking the primary side of the CD. Host molecules A and B of the TMEACYC complex contain glucopyranose units A2, A3, A6, B4 and B6 with positive ω torsion angles indicating a (+)-*gauche* conformation and an inward rotation towards the centre of the CD cavity. All other glucose units have a negative ω torsion angle with atoms C6, O6 and C9 pointing away from the CD cavity. On the secondary rim of both CD molecules the O2-C7 bonds point away from the cavity while the O3-C8 bonds point toward the cavity.

The geometrical parameters used to describe the structural features of the two α-CD host molecules are listed in Table 9. The parameters listed have been previously defined in Chapter 1. Host molecule B shows slight ellipticity as indicated numerically by parameters *l, D* and ϕ; this is due to accommodating the planar dimethyl urea moiety of the guest. In comparison, host molecule A is 'round' in overall shape. The maximum deviations of the O4 atoms from the mean plane are ~0.27 Å and ~0.33 Å for host molecules A and B respectively (Table 9). All the τ_1 and τ_2 tilt angles are positive indicating an inward tilt of the primary methoxyl side for all the glucose units. Glucose units A2, A3 and A6 have large tilt angles as well as primary methoxyl groups that are in the (+)-*gauche* conformation and as a result these residues act as a lid for host molecule A. Glucose units B1 and B6 of host molecule B have large positive tilt angles but the C6-O9 bonds are directed away from the CD cavity and therefore only glucose unit B4 of host molecule B performs the same function as glucose units A2, A3 and A6 of host molecule A.

Table 9. *Geometrical parameters for the host molecules of the TMEACYC complex.*

Residue	*l* (Å)	*D* (Å)	ϕ (°)	*d* (°)	α^a (Å)	$D_3{}^b$ (Å)	$\tau_1{}^c$ (°)	$\tau_2{}^d$ (°)
A1	4.35	4.35	119.6	11.9	-0.223	3.421	8.4	9.3
A2	4.32	4.40	119.5	-3.9	0.202	3.498	22.5	21.7
A3	4.33	4.26	121.5	-9.8	0.046	3.383	33.6	32.7
A4	4.44	4.51	116.1	16.5	-0.269	3.439	9.9	13.2
A5	4.27	4.27	121.5	-9.0	0.256	3.715	24.7	24.1
A6	4.37	4.34	119.3	-5.4	-0.013	3.252	28.5	31.9
B1	4.10	4.36	124.9	0.3	0.164	3.429	28.2	31.0
B2	4.18	4.27	121.3	14.5	0.165	3.465	1.1	1.8
B3	4.49	4.15	112.6	-15.0	-0.333	3.339	24.1	24.4
B4	4.09	4.38	124.6	0.5	0.165	3.383	28.1	32.0
B5	4.17	4.28	121.9	14.0	0.166	3.492	3.7	3.7
B6	4.53	4.22	111.4	-14.5	-0.328	3.501	26.3	27.5

[a] mean e.s.d. = 0.003 Å; [b] mean e.s.d. = 0.005 Å; [c] mean e.s.d. = 0.2 ° ; [d] mean e.s.d. = 0.4 °.

In accommodating very different residues, the host molecules have their secondary faces slightly offset from one another. As an angle of 7.23(9)° exists between the two O4 mean planes of the host molecules, parameters R_A and R_B (defined on pg. 8) were calculated as 2.3 Å and 3.1 Å respectively. These numerical values convey the extent of the lateral displacement of the host molecules comprising the dimeric assembly (Figure 20).

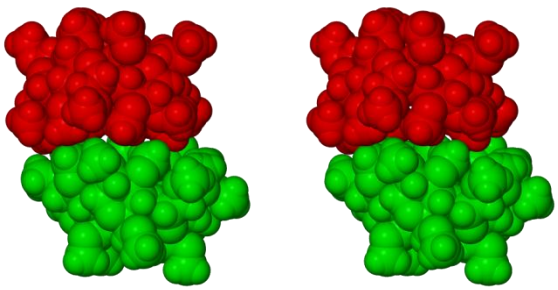

Figure 20. *Stereoview of the host dimer (host A in red, B in green) illustrating their lateral displacement.*

Guest inclusion and conformation

The guest molecule is encapsulated in a head-to-head host dimer in which host molecule A accommodates the cyclooctyl residue of the guest molecule and host B the amide moiety. Several primary methoxyl groups on both host molecules A and B close their narrower sides, effecting complete encapsulation of the cycluron molecule. Only one water molecule, with s.o.f. 0.76, is situated within the dimeric capsule: it serves as a bridge between the guest

amide nitrogen atom and a secondary oxygen atom (O2) of the nearest methylated glucose unit of the host. Figures 21 (a)-(d) are space-filling diagrams presenting different views of TMEACYC with the included water molecule.

The cyclooctyl ring of the guest molecule, cycluron, has the same boat-chair conformation as discribed for the uncomplexed guest. The disposition of the urea 'tail' is similar to that of the minor component of the uncomplexed guest with the pseudo-mirror plane of the boat-chair conformation passing through atoms C2 and C6 of the cyclooctyl ring. This specific geometry allowed for an optimum fit of the hydrophobic portion of the guest molecule within the small α-CD cavity. It must be noted that the guest molecule is not deeply embedded within the TRIMEA cavities. The C5 atom of the cyclooctyl ring is situated 1.24 Å below the O4 mean plane of host molecule A while the methyl urea atom C12 is situated on the O4 mean plane of host molecule B.

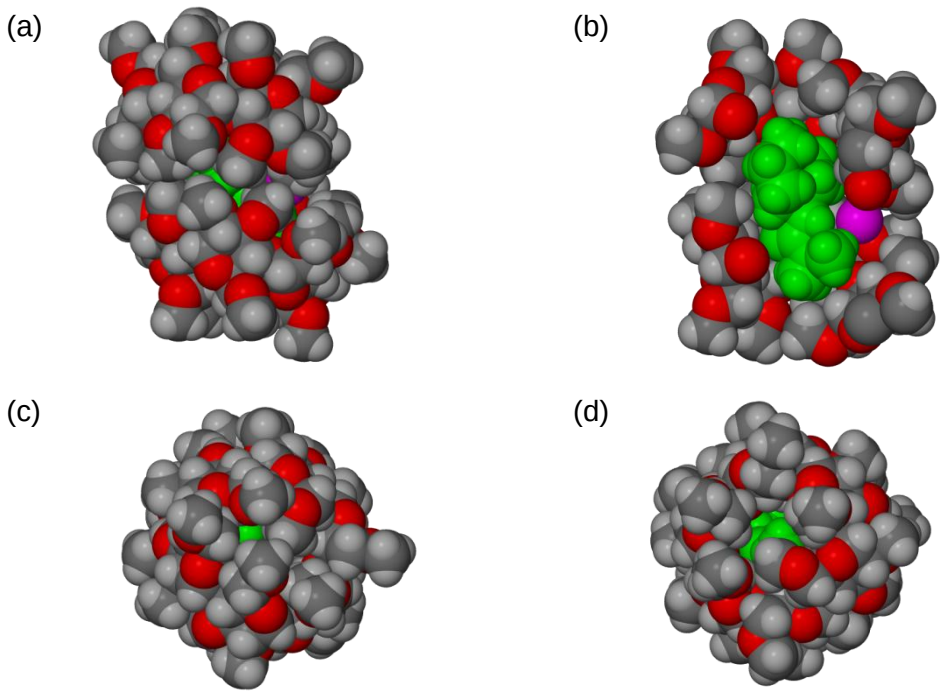

Figure 21. *The guest molecule encapsulated within the TRIMEA dimer. The partial water molecule is shown in pink. (a) A side view, (b) a cross-sectional view, (c) a view from the primary rim of host molecule A and (d) a view from the primary rim of host molecule B.*

Intra- and intermolecular interactions

Figure 22 displays the intramolecular, host-host, host-guest, guest-water and host-water interactions that occur within the TMEACYC complex while Table 10 lists these interactions and their respective distances and angles.

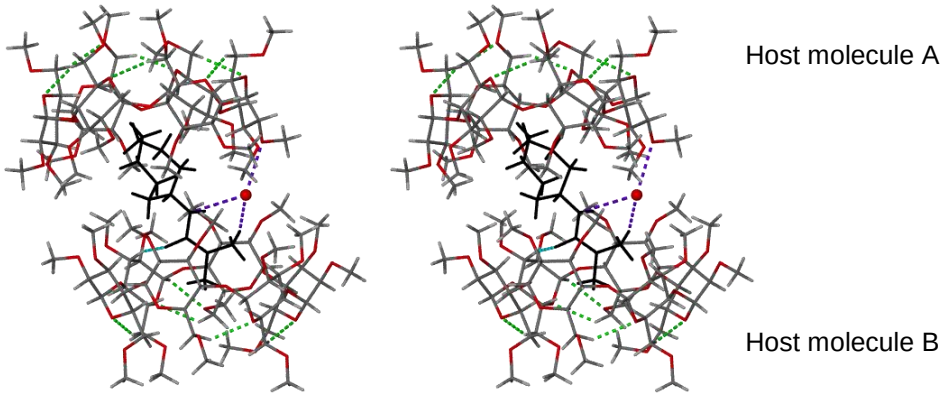

Figure 22. *The stereogram shows the intramolecular hydrogen bond interactions between and within the glucose molecules (green) as well as the direct host-guest interaction (light blue) and the hydrogen bonds from the bridging water molecule (purple).*

Table 10. *Hydrogen bonding interactions for TMEACYC.*

Interaction	H•••A (Å)	D•••A (Å)	D-H•••A (°)
Intramolecular			
C6A1–H6A2•••O6A2	2.38	3.29(1)	151
C6A2–H6A3•••O5A3	2.31	3.20(1)	149
C6A3–H6A5•••O5A4	2.57	3.41(1)	142
C6A4–H6A8•••O5A5	2.25	3.13(1)	147
C6A5–H6AX•••O5A6	2.50	3.23(1)	131
C6A6–H6AY•••O5A1	2.40	3.31(1)	153
C6B2–H6B4•••O5B3	2.43	3.21(1)	135
C6B3–H6B6•••O5B4	2.40	3.23(1)	141
C6B5–H6BX•••O5B6	2.45	3.15(1)	127
C6B6–H6BY•••O5B1	2.34	3.25(1)	152
C9B5–H9BC•••O5B5	2.51	3.11(1)	120
C1B6–H1B6•••O6B5	2.49	3.14(1)	122
Host-host			
C2A3–H2A3•••O5B2[a]	2.43	3.35(1)	153
C2A5–H2A5•••O5B6[b]	2.52	3.44(1)	153
C1B2–H1B2•••O3A3[c]	2.52	3.39(1)	145
Host-guest			
C3B6–H3B6•••O10	2.62	3.52(2)	149
Guest-Water			
C13–H13A•••O5W	2.20	3.15(1)	162
Host-water*			
C9A1–H9A2•••O4W[d]	2.55	3.14(1)	118
C8A4–H9AZ•••O5W	2.54	3.49(1)	161
C1A6–H1A6•••O2W[d]	2.49	3.31(1)	139
C4B3–H4B3•••O7W[e]	2.40	3.23(1)	161

Symmetry codes: [a] *3/2-x*, *1-y*, *1/2+z*; [b] *-1+x*, *y*, *z*; [c] *3/2-x*, *1-y*, *-1/2+z*; [d] *-1/2+x*, *3/2-y*, *1-z*; [e] *1/2+x*, *1/2-y*, *1-z*. * Since H atoms of water molecules were not located, only the host-water interactions with donor hydrogen atoms from the host have been listed.

Host interactions

There are several intramolecular host hydrogen bonds that stabilise the structure of the TRIMEA molecules in the TMEACYC complex (Figure 22). Weak hydrogen bonds form between atoms C6 of one methylglucose unit and O5 of the neighbouring unit. These contribute to the large tilt angles displayed by the methylglucose units. One C6–H•••O6′

hydrogen bond forms on glucose residue A1 and this limits the rotation around the C5-C6 bond. Due to the extreme rotation around the C6-O6 bond for methylglucose unit B5 (C5-C6-O6-C9 = -75.3°), an intraglucose hydrogen bond between atoms C9B5 and O5B5, as well as an intramolecular hydrogen bond between atoms O6B5 and C1B6, were formed. Only three weak C–H•••O host-host hydrogen bonds are evident.

Guest interactions

The guest forms a weak C–H•••O hydrogen bond with included water molecule O5W (Figure 22-purple bond). The closest (C•••O) contact distance between the cyclooctyl portion of the guest and host molecule A is ~3.8 Å. The carbonyl group forms a long range hydrogen bond with a C•••O contact distance of 3.52(1) Å (Figure 22-light blue bond). Interestingly, the potential hydrogen bonding donor ability of the N-H group in cycluron is not utilised in the crystal.

Water interactions

For the dimeric complex unit, there is a complement of seven water molecules distributed over nine sites. Water molecule O5W acts as linker between the guest and host molecule forming a hydrogen bond motif N•••H–O–H•••O2. The hydrogen bond to nitrogen is weak (N•••O 3.30(1) Å) while that to O2 is of average strength (O•••O 2.87(1) Å).

All the other water molecules are either within normal hydrogen bonding distance of a host oxygen atom or another water molecule. Table 11 lists the atoms involved in the hydrogen bonds and their hydrogen bonding distances. Additional weaker C•••O hydrogen bonds exist but have not been listed. This cumulative hydrogen bonding effect contributes to the overall stability of the TMEACYC complex.

Table 11. *OW•••OW close contacts and OW•••O(Host) close contacts.*

Interaction	Distance (Å)	Symmetry operator	Interaction	Distance (Å)	Symmetry operator
O1W•••O3A5	2.82(1)		O1W•••O2A6	3.22(1)	
O1W•••O2W*	2.73(1)	*-1/2+x*, *3/2-y*, *1-z*	O1W•••O6W	2.76(1)	
O2W•••O6A1	2.73(1)		O2W•••O3W*	2.73(1)	*-1/2+x*, *3/2-y*, *1-z*
O3W•••O3B6	2.73(1)		O3W•••O6A5	2.93(1)	*1+x*, *y*, *z*
O4W•••O5A4*	2.93(1)	*3/2-x*, *1-y*, *-1/2+z*	O4W•••O6W*	2.72(1)	*1+x*, *y*, *z*
O5W•••O2A4	2.87(1)		O5W•••O2B5	3.00(1)	
O6W•••O8W	2.90(1)		O7W•••O6B3*	2.76(1)	*-1/2+x*, *1/2-y*, *1-z*
O9W•••O3B5	2.99(2)				

*Atom to which the symmetry operator refers.

Crystal packing

The CD dimers of TMEACYC pack in a modified herringbone formation when viewed down the crystal *c*-axis. The primary (narrower) side of each CD dimer is blocked by side-on contact with another CD dimer, as shown in Figure 23. The encapsulated guest molecules are completely isolated from one another.

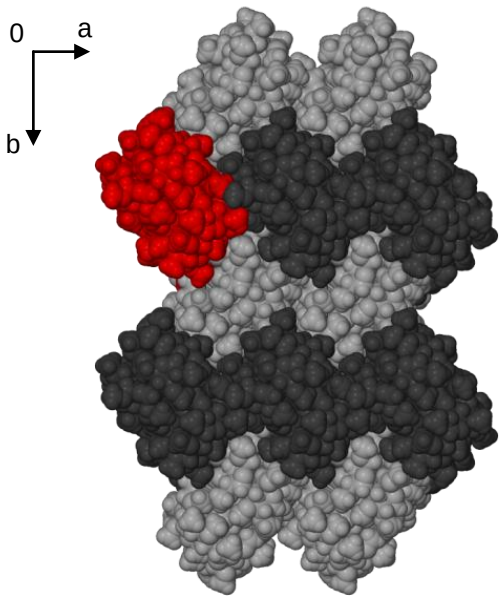

Figure 23. *Space-filling representation of the molecular packing in the TMEACYC complex viewed along [001]. Different shading is used to distinguish the symmetry-related dimeric capsules.*

Comparative PXRD

The computed and experimental PXRD traces for TMEACYC are shown in Figure 24. The two traces were obtained at different temperatures and as a result there is a slight shift of peaks for the computed pattern to higher 2θ values. Their profiles are, however, very similar, indicating that the single crystal is representative of the bulk material.

The first TRIMEA complex containing two crystallographically independent host molecules has been described by Caira *et al*.[15] In this complex a 2:1 host-guest ratio was found and an interesting bimodal guest inclusion was described, with two host molecules packing in a head-to-tail mode. The TMEACYC complex discussed here also contains two crystallographically independent host molecules but packs in a completely different arrangement with the two head-to-head host molecules forming a cage around the guest molecule. A similar arrangement will be seen in Chapter 5 of this thesis when the TRIMEA complex of the agrochemical fenitrothion is discussed. It is noteworthy, however, that these two crystal structures are not isostructural with each other or with any other previously

published TRIMEA complexes.[11] The dimeric TMEACYC capsule described here is thus a novel entity.

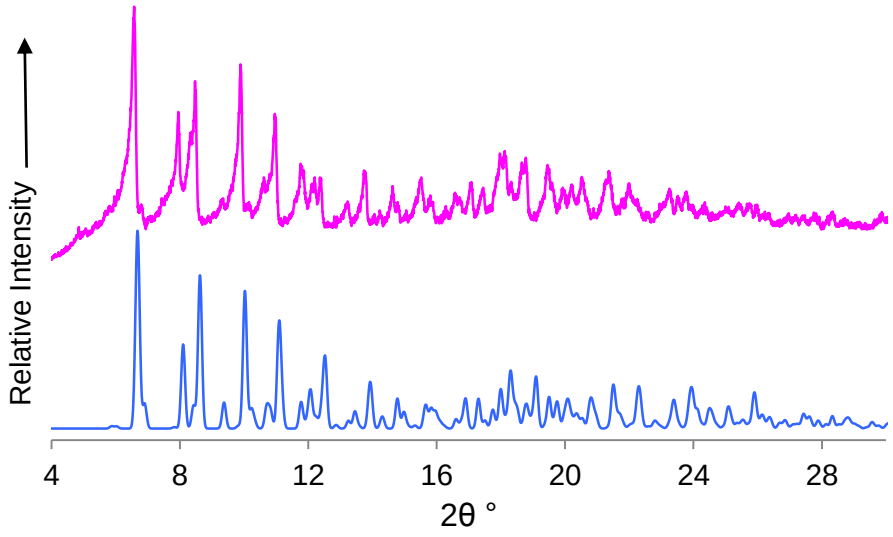

Figure 24. *Calculated (blue) and experimental (pink) PXRD traces of TMEACYC.*

TRIMEB INCLUSION COMPLEX WITH CYCLURON

Complex preparation

The crystalline inclusion complex TRIMEB·cycluron (TMBCYC) was prepared using the method of co-precipitation. 72 mg of TRIMEB (0.05 mmol) was weighed into a vial to which 2 cm^3 of distilled water was added. The solution went clear immediately. 10 mg (0.05 mmol) of the herbicide, cycluron, was added and this was stirred for 6 h at ~20 °C after which it was filtered through a 0.45 µm filter into a clean vial and placed in an oven at 65 °C. Single crystals were obtained within 12 h.

Complex stoichiometry and thermal analysis

Figures 25 and 26 illustrate the TG and DSC traces recorded for TMBCYC and the HSM photographs recorded at various temperatures. Crystals of TMBCYC showed an initial mass loss of 1.4 ± 0.1 % (n = 2) which can be seen from the TG trace. This mass loss is associated with crystal dehydration. The second mass loss of 10.5 ± 0.1 % (n = 11) measured from 130 to 280 °C is due to the guest molecule dissociating from the host. When calculated for an ideal 1:1 host to guest stoichiometry, the mass loss should be 12.1%. The slightly lower TG result for the host-guest stoichiometry is a consequence of the two events of melting and decomposition overlapping, i.e. occurring without a definite plateau between each process. This renders it difficult to estimate the final mass after guest loss. The small endotherm on the DSC curve occurring at 148 °C may be due to rearrangement of the complex structure to one that is more favourable for guest loss. Following melting of the complex at 160 °C (indicated by the large, sharp endotherm in the DSC trace), there is immediate loss of the guest molecule.

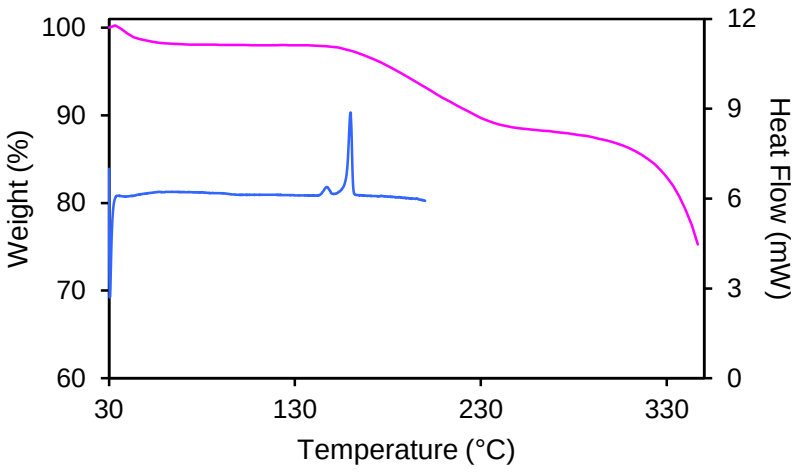

Figure 25. *Representative TG (pink) and DSC (blue) traces for TMBCYC.*

The HSM photographs show the rod-like shape of the crystals and their colourless appearance. The crystals are stable up to a temperature of 150 °C and then start to melt at 160 °C. The melting point lies in the range of reported melting points for other known TRIMEB inclusion complexes and differs from that of the known crystalline forms of TRIMEB itself (148 °C, 157 °C).[16]

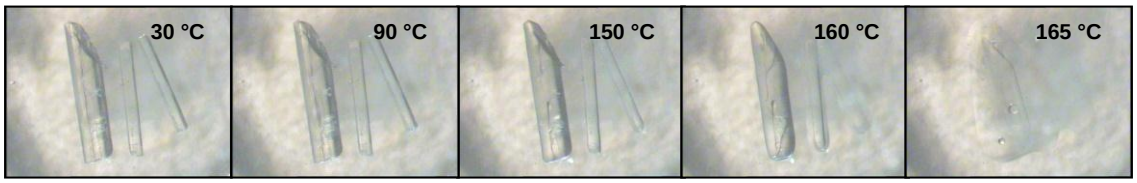

Figure 26. *HSM photographs of the TMBCYC crystals recorded at various temperatures.*

Crystal structure analysis

Data-collection and space group determination

Intensity data were collected on a Nonius KappaCCD single crystal X-ray diffractometer. The X-ray diffraction pattern revealed Laue symmetry *mmm*, corresponding to the orthorhombic crystal system. Further examination of the systematic absences (*hkl: none, h00: h =2n, 0k0: k = 2n, 00l: l = 2n*) confirmed the space group $P2_12_12_1$. The asymmetric unit contains one cycluron molecule included within a TRIMEB molecule.

Structure solution and refinement

The refinement parameters and crystal data are reported in Table 12. The TMBCYC complex structure was solved using the method of isomorphous replacement. This was done by using the rigid skeleton of the isostructural complex TRIMEB·*p*-iodophenol as a trial model.[17] The rigid skeleton included the α-1,4 glucopyranose rings without their flexible methoxyl groups. The glucopyranose units were labelled G1-G7 with disordered moieties labelled A and B. All the remaining non-H atoms of the host and guest were located in successive difference electron density maps. Several atoms of the host were disordered over two positions; these were modelled by assigning s.o.f.s of *x* and *1-x*, with *x* variable. Two primary methoxyl groups (methylglucose units G2 and G7) and one secondary methoxyl group (G3) were found to be disordered over two positions and were refined isotropically. Three methoxyl carbon atoms (C9G5, C9G3 and C7G6) of the host showed abnormally high thermal motion but were finally modelled isotropically since anisotropic treatment yielded unreasonable thermal ellipsoids. For the guest molecule, atoms C4, C5 and C6 of the cyclooctyl ring as well as atoms O10, N11, C12 and C13 were refined

isotropically. All other non-hydrogen atoms of the TMBCYC complex were refined anisotropically.

Table 12. *Data-collection and refinement parameters for the TMBCYC complex.*

Chemical formula	$C_{63}H_{112}O_{35}\cdot C_{11}H_{22}N_2O\cdot 0.9H_2O$
Formula weight	1644.27
Crystal system	Orthorhombic
Space group	$P2_12_12_1$
Unit cell constants	
a (Å)	14.8872(4)
b (Å)	21.2437(6)
c (Å)	27.9334(5)
$\alpha = \beta = \gamma$ (°)	90
Volume (Å^3)	8834.2(4)
Z	4
Density$_{calc}$ (g cm^{-3})	1.236
μ [MoKα] (mm^{-1})	0.098
F (000)	3556
Temperature of data collection (K)	173(2)
Crystal size (mm)	0.25 x 0.23 x 0.18
Range scanned θ (°)	2.4 - 25.0
Index ranges	h: -17, 17; k: -25, 25; l: -33, 33
ϕ and ω scan angle (°)	1.0
Total no. of frames	622
Dx (mm)	50.00
Total no. of reflections collected	15583
No. of independent reflections	8496
No. of reflections with I > 2σ(I)	6806
No. of parameters	988
R_{int}	0.0209
S	1.048
R_1 [I > 2σ(I)]	0.0801
No. of reflections omitted	22
wR_2	0.2137
Weighting scheme parameters	a = 0.1346 and b = 7.8964
$(\Delta / \sigma)_{mean}$	< 0.001
$\Delta\rho$ excursions (e Å^{-3})	0.65 and -0.54

With one exception, all the hydrogen atoms of the complex were placed in idealised positions using a riding model and were assigned isotropic temperature factors 1.2-1.5 times those of their parent atoms. The exception, the amide hydrogen (H9) of the guest molecule, was not placed in an idealised position as it could be located on the difference Fourier map. This atom was assigned and refined with a U_{iso} value of 0.09 $Å^2$.

Two sites were revealed for water molecules from the electron density maps. Initially full s.o.f.s were applied but the resulting refined temperature factors were unrealistically large. Through successive refinements varying s.o.f.s and fixing temperature factors, followed by fixing the s.o.f.s and varying the temperature factors, the two water oxygen atoms O1W and O2W refined with s.o.f.s of 0.44 and 0.47 and U_{iso} values of 0.084 and 0.088 $Å^2$ respectively. Ultimately, the crystal structure was modelled with 0.9 water molecules per host molecule. In this case, the somewhat higher experimental TG mass loss of 1.4%, which is equivalent to 1.3 water molecules per asymmetric unit, can be attributed to the crystalline material that grows in a rosette formation, rendering surface-drying of the crystals prior to thermal analysis a difficult operation. The hydrogen atoms of the water molecules were not located.

Geometrical analysis of the TMBCYC structure

The asymmetric unit of the TMBCYC complex comprises one TRIMEB molecule, its associated guest and a water molecule with s.o.f. 0.9. The asymmetric unit and numbering scheme of the glucose units are shown in Figures 27 (a) and (b) respectively.

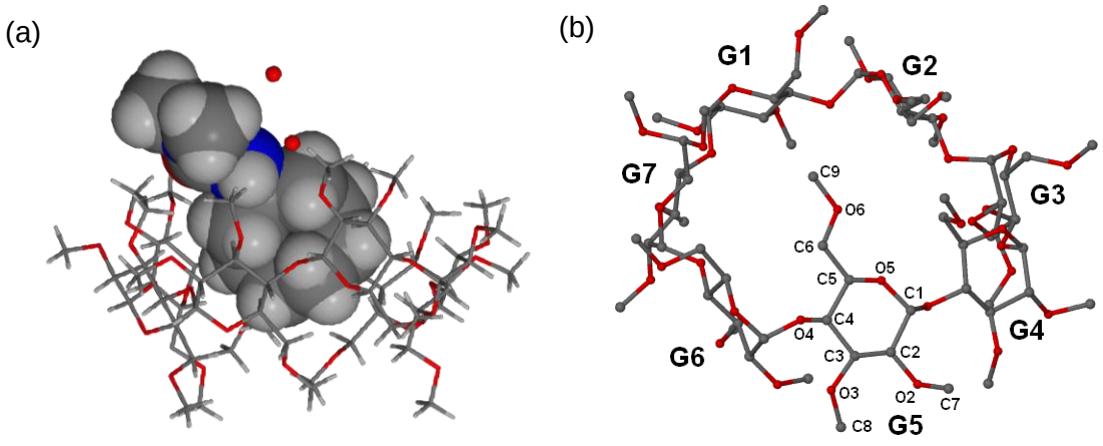

Figure 27. *(a) The asymmetric unit of the TMBCYC complex. (b) Macrocyclic structure and numbering scheme of the TRIMEB glucose residues (hydrogen atoms have been omitted for clarity).*

Host conformation

The major components of methyl glucose units G2 and G7, as well as the fully occupied methyl glucose G5, have a positive ω torsion angle (O5-C5-C6-O6) indicating a (+)-*gauche* conformation. The O6-C9 groups of these residues act as lids closing off the primary side of the TRIMEB cavity. The torsion angles (ω) of the minor components of G2 and G7, as well as those of all other methylglucose units (G1, G3, G4 and G6) indicate a (-)-*gauche* conformation, with the O6-C9 bonds directed away from the cavity.

The geometric parameters of the O4-heptagon, deviations of each O4 atom from the mean O4 plane, the O2n•••O3(n-1) distance and τ_1 and τ_2 tilt angles for the TMBCYC complex are listed in Table 13. It was possible to solve this structure using the co-ordinates of the TRIMEB host from the published TRIMEB·*p*-iodophenol structure.[17] The parameters shown in Table 13 are therefore in agreement with these for the TRIMEB host molecule of the TRIMEB·*p*-iodophenol complex. The TRIMEB molecule has a distorted elliptical conformation with a saddle-like curvature, as can be seen in Figure 28. This type of conformation is associated with relatively large deviations of the O4 atoms from the mean O4 plane as well as larger than normal τ_1 and τ_2 tilt angles.

Table 13. *Geometrical parameters for the host molecule of the TMBCYC complex.*

Residue	*l* (Å)	*D* (Å)	ϕ (°)	*d* (°)	α^a (Å)	$D_3{}^b$ (Å)	$\tau_1{}^c$ (°)	$\tau_2{}^d$ (°)
G1	4.91	4.37	128.1	-25.4	0.439	3.107	28.4	29.2
G2	4.67	4.37	135.6	3.6	-0.410	3.297	31.8	37.6
G3	5.25	4.40	121.1	24.5	-0.320	3.468/3.678	9.0	8.7
G4	5.20	4.27	120.7	-20.3	0.625	3.769	37.6	36.9
G5	4.60	4.55	138.3	-12.5	-0.035	3.354	40.3	44.5
G6	5.03	4.26	124.9	20.3	-0.558	3.546	10.1	12.1
G7	5.31	4.42	121.7	4.6	0.260	3.428	14.1	16.2

[a] mean e.s.d. = 0.003 Å; [b] mean e.s.d. = 0.006 Å; [c] mean e.s.d. = 0.2 ° ; [d] mean e.s.d = 0.2 °.

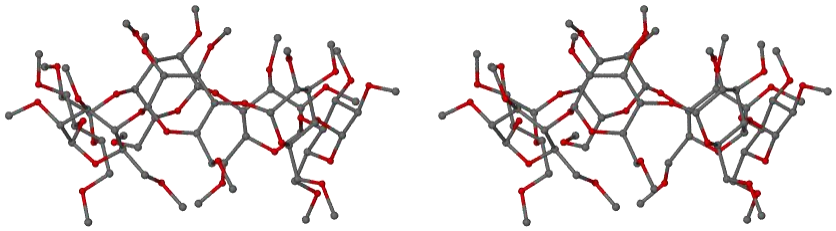

Figure 28. *Stereoview illustrating the saddle-like curvature of the TRIMEB host molecule. Hydrogen atoms and minor disordered components of the host have been omitted for clarity.*

Guest inclusion

The cycluron molecule is positioned within the TRIMEB cavity with the hydrophobic cyclooctyl ring extending towards the primary side and the polar dimethyl urea 'tail' protruding from the secondary rim into the interstitial spaces, where the 'tail' interacts with one of the two water molecules. Figures 29 (a)-(d) are space-filling diagrams presenting different views of the TMBCYC complex with the two partial water molecules. It can be seen that the TRIMEB molecule forms a cup shape around the guest molecule with the primary rim almost totally sealed off by the methoxyl groups and the secondary rim of the cavity showing a large portion of the guest molecule.

The cyclooctyl residue of the guest molecule retains the boat-chair conformation on complexation with TRIMEB. The attachment position of the urea 'tail' is comparable to that observed in the major component of the uncomplexed guest, with the pseudo-mirror plane passing through atoms C1 and C5 of the cyclooctyl ring. Atom C4 of the guest molecule is positioned ~0.4 Å above the O4 mean plane, which is somewhat deeper into the CD cavity than what was observed in the TMEACYC crystal structure.

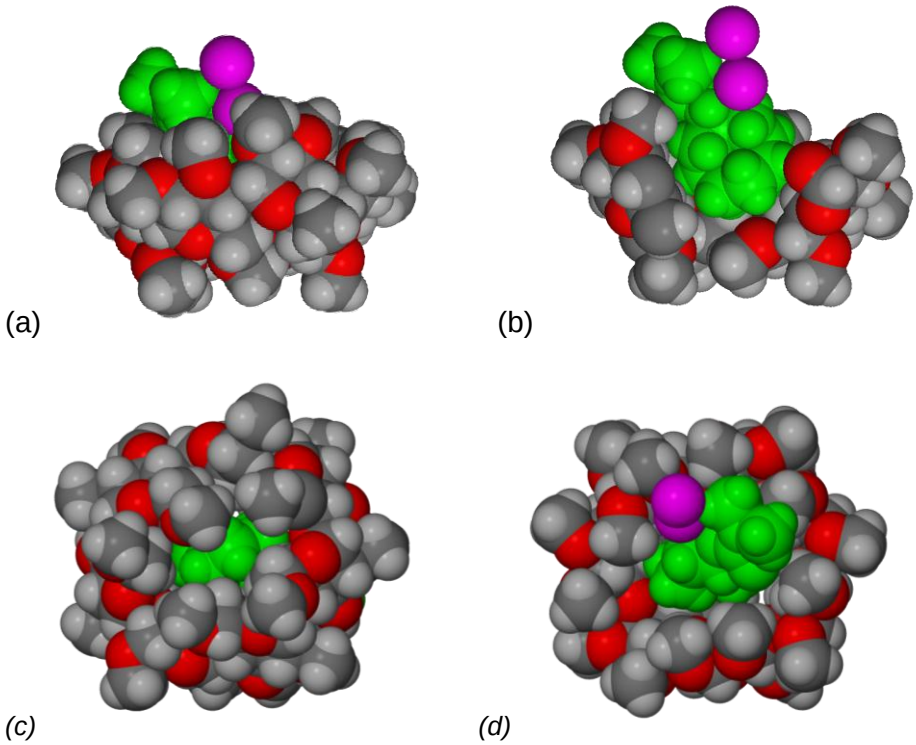

Figure 29. *(a) A side view, (b) a cross-sectional view, (c) a view from the primary rim and (d) a view from the secondary rim of the TMBCYC complex (oxygen atoms of partial water molecules are shown in pink).*

Hydrogen bonding interactions

Intramolecular, host-host and host-guest interactions

Table 14 lists the intramolecular, host-host and host-guest C–H•••O interactions that occur within the TMBCYC complex with their respective distances and angles. The distorted conformation of the TRIMEB molecule is partly a consequence of weak C–H•••O intramolecular hydrogen bonds that form between and within the methyl glucose residues. There are five C6–H•••O5′ hydrogen bonds which are thought to contribute towards the large tilt angles reported for TRIMEB molecules.[18] In addition there are three C1 atoms that act as hydrogen bond donors to the oxygen atoms of adjacent methoxyl groups. Atoms C6 and C8 of glucose residues G4 and G6 form hydrogen bonds with oxygen atoms of adjacent methoxyl groups as well.

Table 14. *Hydrogen bonding interactions for the TMBCYC complex.*

Interaction	H•••A (Å)	D•••A (Å)	D-H•••A (°)
Intramolecular			
C6G7–H6G2•••O5G1	2.51	3.39(1)	148
C1G6–H19•••O3G5	2.41	3.08(1)	124
C6G6–H25B•••O5G7	2.38	3.15(1)	134
C6G1–H26B•••O5G2	2.49	3.15(1)	124
C1G4–H37•••O6G3	2.43	3.17(1)	131
C6G4–H42B•••O5G5	2.44	3.14(1)	127
C6G4–H42B•••O6G5	2.59	3.53(1)	159
C1G3–H46•••O3G2	2.57	3.17(1)	118
C8G6–H52A•••O2G7	2.51	3.22(1)	129
C6G3–H60B•••O5G4	2.31	3.07(1)	133
Host-host			
C2G1–H2•••O5G4[a]	2.56	3.45(1)	147
C4G6–H22•••O3G2[b]	2.58	3.51(1)	154
C1G1–H23•••O6G3[a]	2.55	3.54(1)	167
C2G4–H38•••O6G1[c]	2.39	3.34(1)	156
C9G4–H45B•••O3G1[c]	2.52	3.20(1)	126
C2G2–H56•••O6G6[d]	2.55	3.50(1)	158
C9G3–H67A•••O3G5[d]	2.52	3.11(1)	119
Host-guest			
C8G7–H66A•••O10	3.02	3.52(2)	113

Symmetry codes: [a] *3/2-x, 1-y, 1/2+z*; [b] *1+x, y, z*; [c] *3/2-x, 1-y, -1/2+z*; [d] *-1+x, y, z*.

Seven host-host hydrogen bonds contribute to the stabilisation of the crystal structure in the absence of interstitial water molecules. Three of these bonds occur between contiguous TRIMEB molecules arrayed along the *a*-axis and the other four are between two TRIMEB molecules that are related by a twofold screw axis parallel to *c*. Only one host–guest hydrogen bond is present and it forms between a secondary methoxyl group of the host and the carbonyl oxygen atom of the guest.

Water interactions

There are two water molecule sites, O1W and O2W, with s.o.f.s of 0.44 and 0.47, respectively. The disordered water molecules are hydrogen bonded to one another with an O•••O contact distance of 2.88(2) Å. O1W is a hydrogen bond donor to both atom N9 of the guest molecule (2.82(2) Å) and the disordered methoxyl oxygen atom O2A3 (O•••O 2.96(2) Å). The O2W atom forms a hydrogen bond to oxygen atom O5G6 of a neighbouring host molecule ((O2W•••O5^{i} 3.06(1) Å, *i = 2-x, -1/2+y, 1/2-z*) and a second hydrogen bond forms between O2W and O6B2 which is situated on a third host molecule (O2W•••O6^{ii} 2.83(2) Å, *ii = 1-x, -1/2+y, 1/2-z*) (Figure 30). As in the TMEACYC complex, the hydrogen atom of the N-H functionality does not appear to engage in hydrogen bonding.

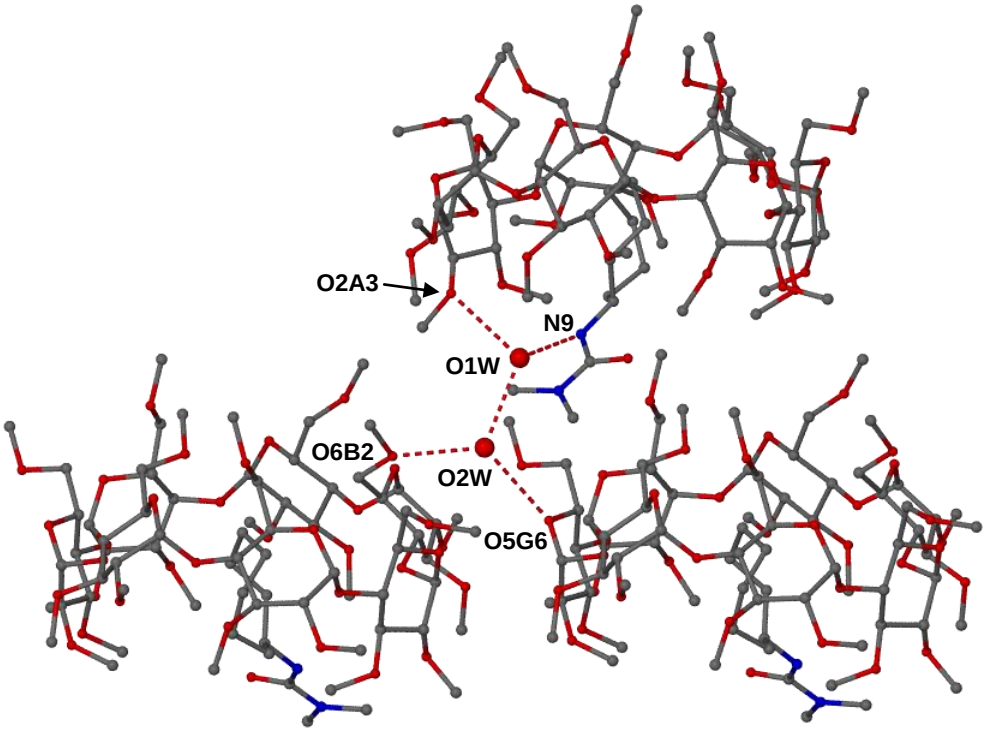

Figure 30. *The host-water, host-guest and water-water intermolecular interactions.*

Crystal packing

Molecules of the TMBCYC complex pack in a screw-channel mode in a head-to-tail fashion. An undulating, discontinuous host 'channel' is generated parallel to the crystal *b*-axis but guest molecules are isolated from one another due to the host molecules being slightly offset from one another in the *x*-direction. A stereoview of the complex packing arrangement down [100] is shown in Figure 31.

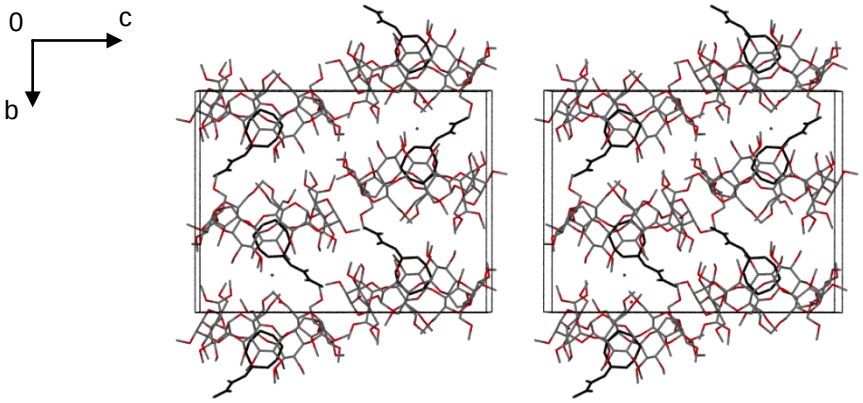

Figure 31. *Stereoview of the crystal packing for the TMBCYC complex viewed along [100]. Guest molecules are shown in black.*

Comparative PXRD

The experimental and calculated PXRD traces are in good agreement confirming that the sample of the TMBCYC crystals prepared was homogeneous (Figure 32) and that the two phases correspond. Differences in the relative intensities of the peaks are attributed to some degree of preferred orientation in the sample, while the generally higher angular positions of the peaks in the calculated trace arise from differences in the respective sample temperatures (294 K for the experimental PXRD trace, 173 K for the single crystal X-ray diffraction data).

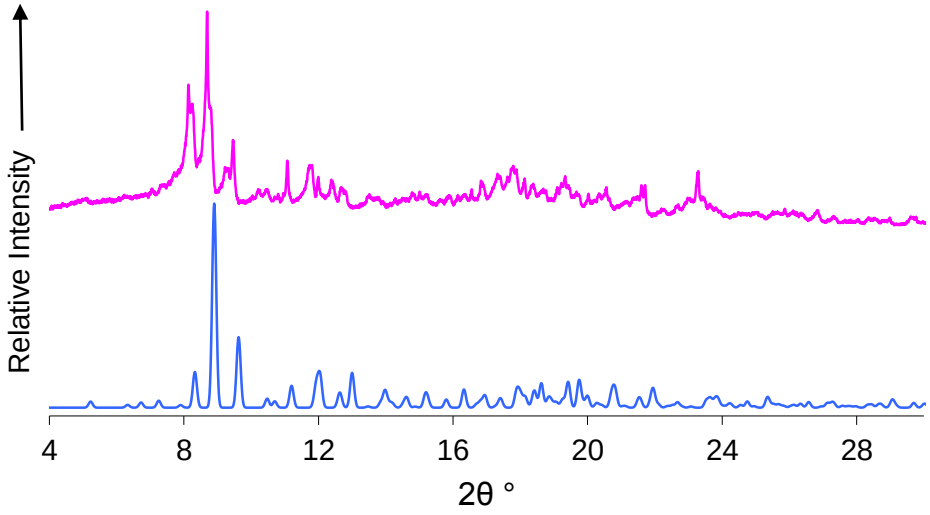

Figure 32. *Calculated (blue) and experimental (pink) PXRD traces of TMBCYC.*

DIMEB INCLUSION COMPLEX WITH CYCLURON

Complex preparation

The DIMEB·cycluron (DMBCYC) complex was prepared by dissolving 0.050 mmol (67 mg) of DIMEB in distilled water (2 cm^3) at 20 °C. Once the CD had dissolved an equimolar amount of cycluron (10 mg) was added. The solution was stirred for 6 h and then filtered into a clean vial and placed in an oven set at 65 °C. Within five days single crystals appeared.

Complex stoichiometry and thermal analysis

Figure 33 shows the TG and DSC curves for the DMBCYC complex. The TG curve indicates an initial mass loss of 3.6 ± 0.5 % (n = 2), which is equivalent to 3.2 ± 0.3 water molecules per complex unit if a 1:1 host-guest stoichiometry is assumed. Corresponding to this process, the DSC curve depicts an initial broad endotherm in the range ~30-100 °C. The second mass loss shown on the TG trace of 11.72 ± 0.04 % (n = 2) commencing at ~180 °C is interpreted as the dissociation of the guest from the host (calcd. for 1:1 host-guest stoichiometry 12.5%) and is reflected in the DSC trace as the second broad endotherm spanning the range 200-280 °C. The latter evidently comprises two distinct events, first a broad peak in the range ~200-260 °C and secondly a sharp endotherm peaking at 275 °C. These two events can be related to the change in the slope of the TG trace at ~245 °C as well. Host decomposition occurs beyond 350 °C. The DSC trace for DMBCYC is similar to those recorded for other DIMEB complexes containing organic guest molecules.[19] The HSM images (Figure 34) display the colourless, rectangular-shaped single crystals of the DMBCYC complex. The crystals become opaque and lose their crystallinity upon dehydration. At 340 °C the crystals start to decompose as can be seen by the change in colour.

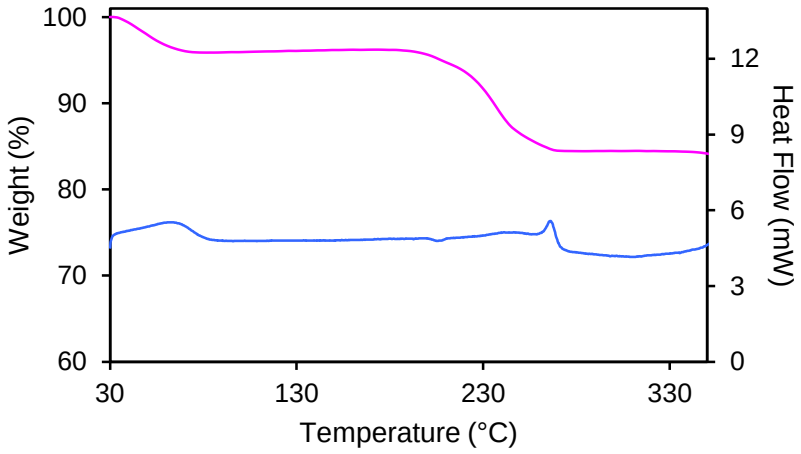

Figure 33. *Representative TG (pink) and DSC (blue) traces for DMBCYC.*

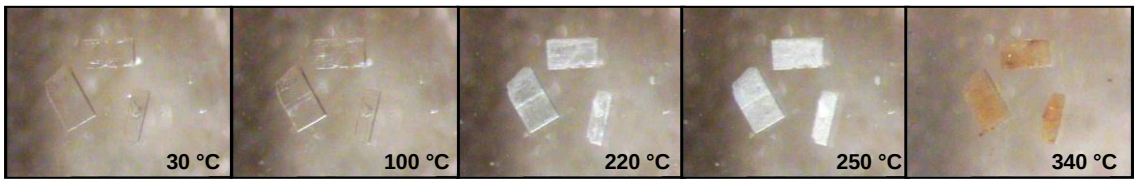

Figure 34. *HSM photographs of the DMBCYC crystals recorded at various temperatures.*

Crystal structure analysis

Data-collection and space group determination

Intensity data were collected on a Nonius KappaCCD single crystal X-ray diffractometer. The Laue symmetry was found to be *mmm*, indicating the orthorhombic crystal system. The reflection conditions (*hkl: none, h00: h =2n, 0k0: k = 2n, 00l: l = 2n*) confirmed the space group $P2_12_12_1$. The crystal was maintained at a lower temperature (143 K) during data-collection than the other cycluron complexes. The diffraction quality deteriorated rather quickly at 173 K due to the longer exposure times that were required. The choice of a lower temperature led to successful data-collection and subsequent analysis.

Structure solution and refinement

The data-collection and refinement parameters for the DMBCYC complex are reported in Table 15. This structure was solved by direct methods using the program SHELXD[8] as an isostructural complex did not exist.[11] The solution with the highest correlation coefficient of 71.69 revealed the majority of the non-hydrogen host atoms and a few guest atoms. There was, however, already evidence of guest disorder as well as disordered methoxyl groups. The glucopyranose units were labelled G1-G7 with disordered guest components and disordered host moieties labelled A and B. The host molecule of the DMBCYC complex has three primary methoxyl groups on glucose residues G4, G5 and G6, each disordered over two positions with the major components having s.o.f. values of 0.59, 0.82 and 0.74 respectively. In addition a secondary methoxyl group of methyl glucose unit G2 has the terminal carbon of the methoxyl group disordered over two positions with s.o.f.s of 0.56 and 0.44. All of the methoxyl carbon atoms on the secondary and primary rim of the CD have unusually high thermal parameters which resulted in their refinement using an isotropic model. Hydrogen atoms were placed in idealised positions using a riding model for both the guest and host. The guest is disordered over two positions with only one atom (C1) being shared by each disordered component. The C-C bonds in the cyclooctyl rings were refined with a restrained bond length of 1.52 Å (σ = 0.01 Å) but the C-C-C angles were allowed free variation during refinement. The 2.9 water molecules per complex unit are disordered,

occupying five extra-cavity sites. O1W, O2W, O3W, O4W and O5W have s.o.f. values of 0.92, 0.30, 0.72, 0.60 and 0.40 respectively (sum = 2.9). This is consistent with the number of water molecules determined from the TG results, namely 3.2 ± 0.3 water molecules per asymmetric unit.

Table 15. *Data-collection and refinement parameters for the DMBCYC complex.*

Chemical formula	$C_{56}H_{98}O_{35}\cdot C_{11}H_{22}N_2O\cdot 2.9H_2O$
Formula weight	1582.57
Crystal system	Orthorhombic
Space group	$P2_12_12_1$
Unit cell constants	
a (Å)	10.387(2)
b (Å)	15.092(3)
c (Å)	51.86(1)
$\alpha = \beta = \gamma$ (°)	90
Volume (Å^3)	8130(3)
Z	4
Density$_{calc}$ (g cm^{-3})	1.293
μ [MoKα] (mm^{-1})	0.106
F (000)	3413
Temperature of data collection (K)	143(2)
Crystal size (mm)	0.38 x 0.30 x 0.18
Range scanned θ (°)	2.7 - 24.9
Index ranges	h: -12, 8; k: -17, 17; l: -61, 56
ϕ and ω scan angle (°)	0.5
Total no. of frames	1558
Dx (mm)	84.30
Total no. of reflections collected	45501
No. of independent reflections	7718
No. of reflections with I > 2σ(I)	4714
No. of parameters	858
R_{int}	0.0781
S	1.298
R_1 [I > 2σ(I)]	0.1118
No. of reflections omitted	22
wR_2	0.3049
Weighting scheme parameter	a = 0.2
$(\Delta / \sigma)_{mean}$	< 0.001
$\Delta\rho$ excursions (e Å^{-3})	0.66 and -0.53

Modelling of the cycluron guest

The host-guest ratio of the DMBCYC complex was confirmed to be 1:1 from the thermal analysis results. After numerous refinements of the DMBCYC complex many additional high electron density peaks were noticeable around the initially modelled single guest molecule. Furthermore, the temperature factors of the initially placed guest molecule atoms were abnormally high. Taking this into consideration, the guest atoms were deleted and the difference Fourier map was reanalysed taking into account the possibility of two different guest positions within the DIMEB cavity. Two guests were eventually modelled with s.o.f.s 0.59 and 0.41 for guest molecules A and B respectively. Separate global temperature factors were applied to each guest and these refined to the same value of 0.12 $Å^2$. C1 is the only atom shared by each component of disorder. Several distance restraints were used to ensure reasonable geometries and to prevent the least-squares refinement from diverging. All the hydrogen atoms were placed in idealised positions in a riding model and no attempt was made to locate the amide hydrogen as the electron density was low owing to the many disordered atoms. The methine proton on C1 was not placed either due to limitations of the SHELX-97 program. (Two methine protons would need to be placed on atom C1 with slightly different geometries in order to satisfy both disordered models). Figure 35 illustrates the disordered guest molecules in the absence of the DIMEB host molecule.

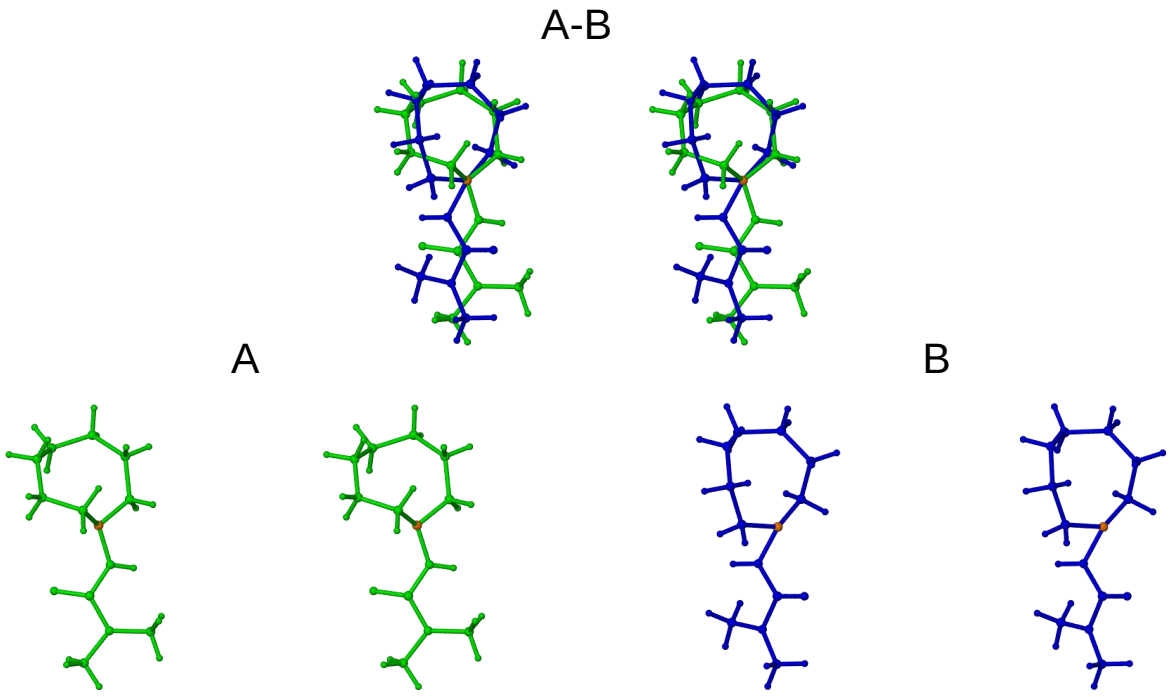

Figure 35. *Stereoviews of the disordered guests A-B of the DMBCYC complex and the deconvoluted disordered components A (green) and B (blue). The common atom C1 is shown in orange.*

Geometrical analysis of the DMBCYC structure

The crystallographic asymmetric unit of the DMBCYC complex comprises a hydrated monomeric complex. The asymmetric unit and numbering scheme employed for the glucose units are shown in Figure 36 (a) and (b) respectively.

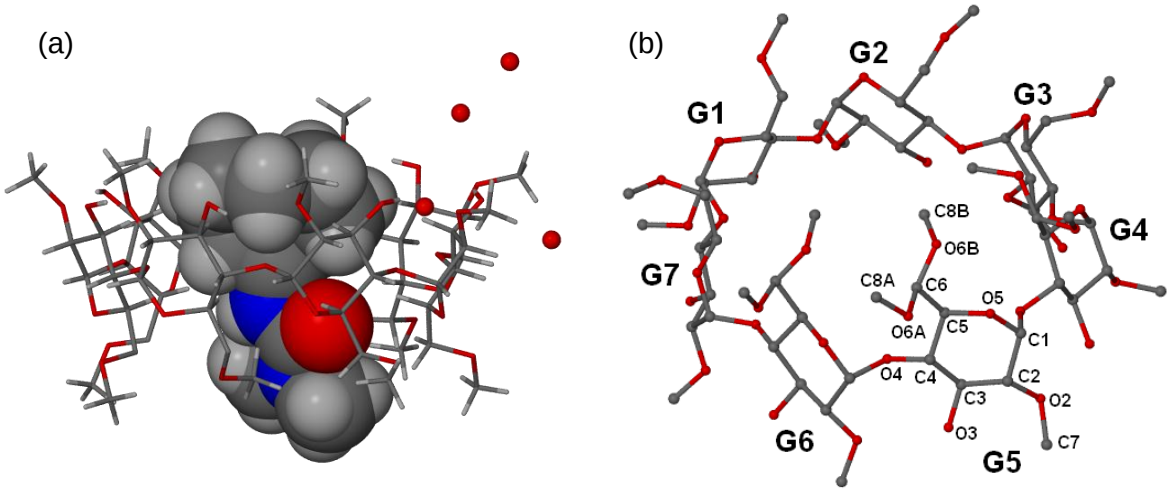

Figure 36. *(a) The asymmetric unit of the DMBCYC complex. (b) Macrocyclic structure and numbering scheme of the DIMEB glucose residues (hydrogen atoms and all minor components have been omitted for clarity).*

Host conformation

The primary hydroxyl torsion angles (ω) for the DIMEB molecule have been tabulated in order to illustrate the (-)-*gauche* and (+)-*gauche* conformations of the major and minor components for glucose residues G4, G5 and G6 (Table 16). All of the major primary methoxyl groups, except the major component of G6, are directed away from the DIMEB cavity. Close contacts are evident between the primary methoxyl group of G6 and guest component B; however, these two sets of atoms have s.o.f.s that preclude their simultaneous presence. The same can be said for minor components of glucose residues G4 and G5 and guest component A. All the O2-C7 bonds of the secondary methoxyl group are directed away from the CD cavity.

The geometrical parameters of the O4-heptagon, deviations of each O4 atom from the mean O4 plane, the O2n•••O3(n-1) distance and τ_1 and τ_2 tilt angles for the DMBCYC complex are listed in Table 17. The DIMEB molecule adopts its usual round and symmetrical structure as can be seen by the narrow range in the values of parameters *l, D and* ϕ. This round and rigid conformation can be attributed to the well-known intramolecular O2n•••H–O3(n-1) hydrogen bonds that link neighbouring methylglucose residues. The deviation of O4 atoms

from the O4 mean plane are small but the positive tilt angles τ_1 and τ_2 are slightly larger than those observed in the native β-CD molecule.

Table 16. *Torsion angles (ω) for DMBCYC.*

Glucose residue	Major ω (°)/ (+)- or (-) - *gauche* conformation	Minor ω (°)/ (+)- or (-) - *gauche* conformation
G1	-67.4(1) / (-)	
G2	-68.8(1) / (-)	
G3	-68.4(1) / (-)	
G4	-68.4(1) / (-)	67.4(1) / (+)
G5	-76.2(1) / (-)	64.8(1) / (+)
G6	72.6(1) / (+)	-41.9(1) / (-)
G7	-79.0(1) / (-)	

Table 17. *Geometrical parameters for the host molecule of the DMBCYC complex.*

Residue	*l* (Å)	*D* (Å)	ϕ (°)	*d* (°)	α[a] *(Å)*	D_3[b] (Å)	τ_1[c] (°)	τ_2[d] (°)
G1	5.11	4.39	126.5	-12.9	-0.170	2.83	19.7	21.3
G2	4.83	4.44	132.3	7.4	0.248	2.84	10.4	14.0
G3	5.03	4.30	128.8	6.0	0.039	2.81	1.1	3.4
G4	5.25	4.32	122.8	-6.1	-0.232	2.89	17.9	17.5
G5	4.88	4.48	133.1	-6.9	0.032	2.83	15.0	18.2
G6	4.95	4.38	128.8	11.6	0.246	2.80	9.8	10.9
G7	5.18	4.32	125.8	0.3	-0.163	2.93	9.1	10.5

[a] *mean e.s.d. = 0.005 Å;* [b] *mean e.s.d. = 0.01 Å;* [c] *mean e.s.d. = 0.2°;* [d] *mean e.s.d = 0.4°.*

Guest inclusion

The guest molecule, which is disordered over two positions, has both disordered components A and B located in the CD cavity in the opposite orientation to that found in the TMBCYC and BCDCYC complexes. Lichtenthaler *et al* have used computational methods to illustrate the molecular lipophilicity patterns of CDs.[20,21] They have found the primary rim of a DIMEB molecule to be relatively hydrophilic while the opposite is true for the secondary rim. The guest molecule, cycluron, conforms to this arrangement with the hydrophobic cyclooctyl group positioned at the secondary rim and the polar dimethyl urea group at the primary rim. Figures 37 (a)-(d) are space-filling diagrams presenting different views of the DMBCYC complex.

The cyclooctyl ring of the guest molecule retains the boat-chair conformation on complexation with DIMEB. The point of attachment for the dimethyl urea group is very unlike the minor and major component of the uncomplexed cycluron molecule for guest A. The plane of symmetry for the cyclooctyl ring passes through atoms C3A and C7A rather than atoms C1A and C5A or C2A and C6A which has been observed thus far for all other CD inclusion complexes with cycluron. In the case of guest B the mirror plane contains atoms C1 and C5B, similar to that seen in the TMBCYC complex. Due to the more 'round' and symmetrical shape of the host molecule, cycluron is deeply embedded within the CD cavity. The guest molecule is also positioned in a more vertical orientation relative to the O4 mean plane to reduce the steric interference between the primary rim of the CD and dimethyl groups of the guest molecule (Figure 37 (b)).

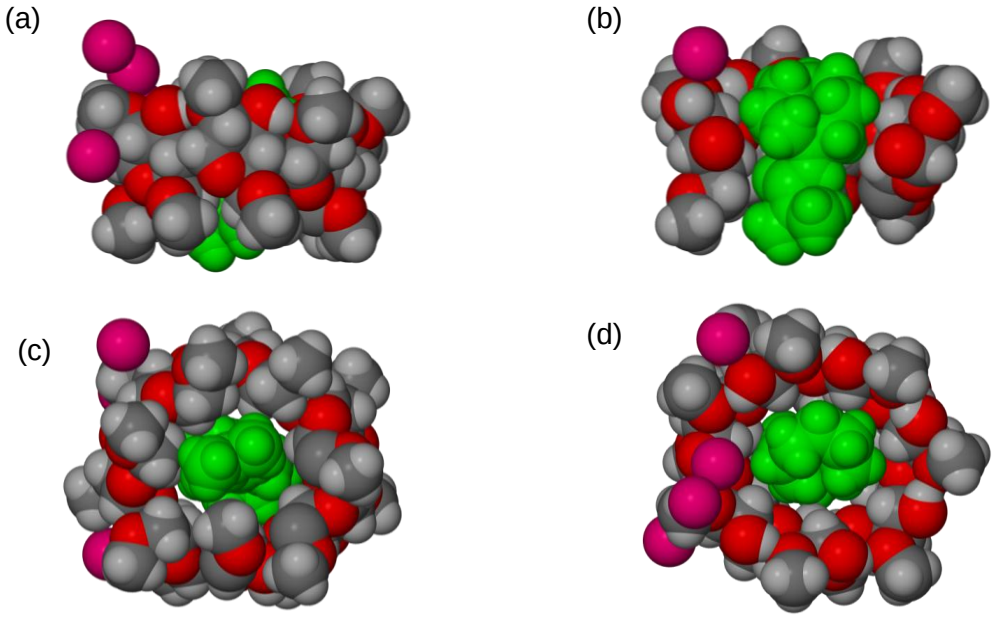

Figure 37. *(a) A side view, (b) a cross-sectional view, (c) a view from the primary rim and (d) a view from the secondary rim of the DMBCYC complex. All minor disordered components have been omitted and the water molecules are shown in pink.*

Hydrogen bonding interactions

Intramolecular and host-host interactions

There are seven, well-known intramolecular hydrogen bonds (O2n•••H–O3(n-1)) that link adjacent methylglucose units of a DIMEB molecule. Table 17 lists the D•••A distances (D_3) for each of these hydrogen bonds and the D–H•••A angles range from 129–161°. The host-host interactions are only of the type C–H•••O and are shown in Table 18. These

interactions occur between the secondary and primary methoxyl groups, as well as between C2–H functions of the glucose residues which act as hydrogen bond donors to neighbouring methoxyl oxygen atoms. There are no hydrogen bonding interactions between the host and guest molecules; the mode of inclusion of the cycluron molecule is based entirely on weak van der Waals forces and hydrophobic interactions.

Table 18. *Host-host hydrogen bonding interactions for the DMBCYC complex.*

Interaction	H•••A (Å)	D•••A (Å)	D-H•••A (°)
C8A4–H8A3•••O3G5[a]	2.19	2.98(3)	137
C7G1–H7G2•••O6G7[b]	2.47	3.25(2)	136
C2G3–H2G3•••O3G6[c]	2.52	3.29(1)	134
C2G4–H2G4•••O6A5[a]	2.37	3.31(1)	157
C2G5–H2G5•••O5G4[d]	2.54	3.51(2)	164
C8A5–H8GY•••O3G4[d]	2.53	3.33(2)	139
C7G7–H7GG•••O3G2[e]	2.51	3.39(1)	149

Symmetry codes: [a] *1-x, 1/2+y, 1/2-z;* [b] *-1/2+x, 1/2-y, 1-z;* [c] *x, 1+y, z;* [d] *1-x, -1/2+y, 1/2-z;* [e] *x, -1+y, z.*

Water interactions

Intermolecular hydrogen bonds form between the five partial water molecules and between the water molecules and the host oxygen atoms. Table 19 lists these significant hydrogen bonds. Water molecules O4W and O5W have a total s.o.f. value of 1.0 and are separated by only 0.72 Å. Both oxygen atoms can bond to equivalent atoms; however, the hydrogen bonds differ in strength depending on which disordered oxygen atom is bonding to the particular host atom or neighbouring water atom. All five water sites are found within the interstitial spaces between the DIMEB molecules.

Table 19. *Contact distances for the water-water and water-host interactions.*

Interaction	Distance (Å)	Symmetry operator	Interaction	Distance (Å)	Symmetry operator
O1W•••O3G7	2.92(1)		O1W•••O6G1*	2.79(1)	*-1/2+x, 1/2-y, 1-z*
O1W•••O2W*	2.72(1)	*1/2+x, 1/2-y, 1-z*	O1W•••O3W*	2.85(1)	*x, y, 1-z*
O2W•••O3G1	2.87(3)		O2W•••O5W	2.77(4)	
O2W•••O4W	2.67(1)		O2W•••C8G7*	3.20(4)	*-1/2+x, 1/2-y, 1-z*
O3W•••C2G2*	3.36(2)		O3W•••O2G2*	2.98(2)	*1/2+x, 3/2-y, 1-z*
O4W•••O6G2*	2.82(3)	*-1/2+x, 3/2-y, 1-z*	O4W•••O5G2*	3.38(2)	*-1/2+x, 3/2-y, 1-z*
O5W•••O6G2*	2.88(3)	*-1/2+x, 3/2-y, 1-z*	O5W•••O5G2*	3.22(2)	*-1/2+x, 3/2-y, 1-z*

*Atom to which the symmetry operator refers.

Crystal packing

The DIMEB complex packs in a head-to-tail manner forming infinite columns along the crystal *a*-axis. A zigzag layer pattern is evident in the [010] projection (Figure 38). These herringbone-type chains form sheets parallel to the *xy*-plane. The twofold screw axis parallel to *a* does not pass through the CD cavity and as a result complex units related by the 2_1-axis in this direction are members of adjacent columns. As there is a strong inclination of the macrocyclic O4-plane to the *a*-axis direction, a given guest molecule is blocked within its CD cavity by atoms of neighbouring host molecules at the primary and secondary sides.

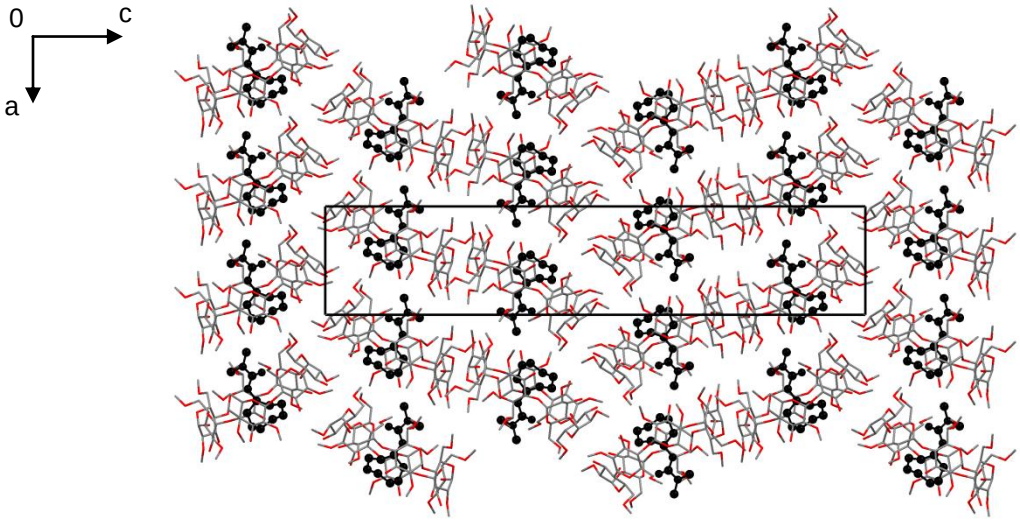

Figure 38. *Packing arrangement of DMBCYC viewed along [010]. Guest molecules are represented using the ball and stick model. (Hydrogen atoms and water molecules have been excluded for clarity).*

Comparative PXRD

The experimental and calculated PXRD traces are in good agreement confirming that the single crystal selected for X-ray analysis is representative of the bulk material (Figure 39). The general shift of the calculated peaks to higher 2θ values is due to shrinkage of the crystal on cooling. The shift is greater for this complex when compared to the other three complexes discussed in this chapter as the data-collection was performed at a significantly lower temperature of 143 K.

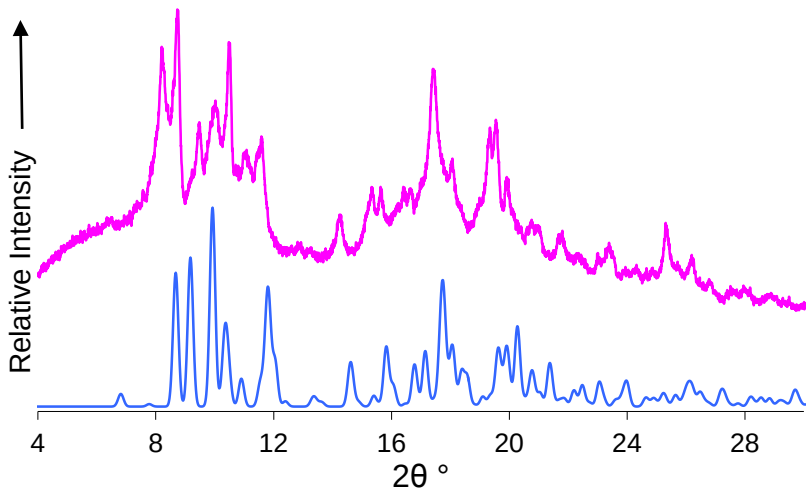

Figure 39. *Calculated (blue) and experimental (pink) PXRD traces of DMBCYC.*

A CSD search was initially undertaken in order to determine whether an isostructural complex existed from which the host atom co-ordinates were available and could be used to solve the DMBCYC structure.[11] Two DIMEB inclusion complexes, with methyl- and ethyl-paraben as guests with similar unit cell dimensions to that of DMBCYC had been deposited in the CSD. However, the difference of 4 Å in the *c*-axes results in these crystal structures overlapping only partially with DMBCYC (Figure 40). The methyl- and ethyl-paraben host molecules pack in a very similar arrangement and this similarity is reflected in their corresponding PXRD patterns (Figure 41). The longer *c*-axis of the DMBCYC complex results in a significantly different PXRD trace which can be attributed to the different arrangement of its primary methoxyl groups and the water molecule positions when compared to the paraben DIMEB complexes.

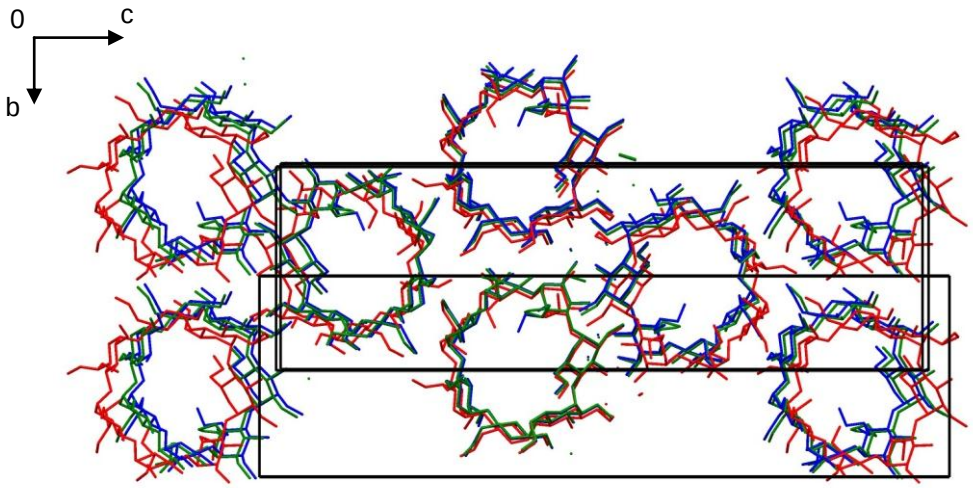

Figure 40. *Overlay of the host molecules for three DIMEB inclusion complexes. [DIMEB·methyl-paraben (blue), DIMEB·ethyl-paraben (green) and DMBCYC (red)]*

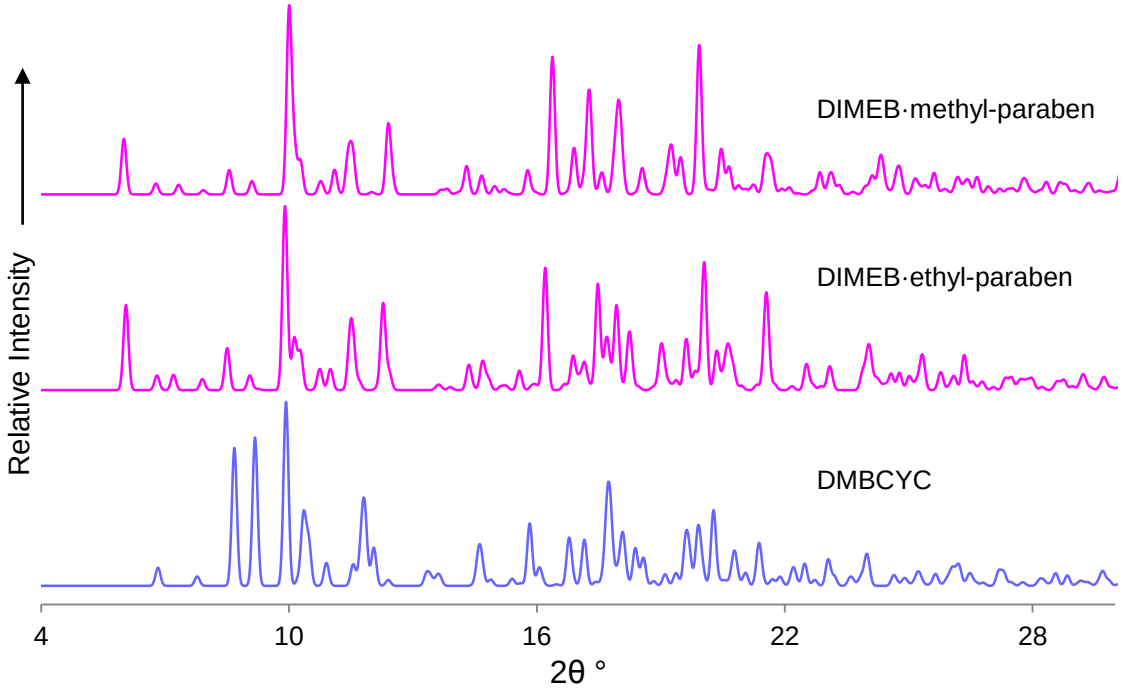

Figure 41. *Calculated PXRD traces of the structurally related DIMEB complexes.*

SOLUBILITY STUDY

A semi-quantitative solubility test was performed with cycluron to determine whether its aqueous solubility would increase in the presence of β-CD. The aqueous solubility of cycluron at 25 °C is 1.2 g dm^{-3}.[22]

A 10 mM aqueous β-CD solution was prepared to which an accurately weighed quantity of the cycluron sample was added. After continuous stirring for 72 h at 25 °C the excess cycluron material was separated from the solution and weighed. Based on the masses of cycluron before and after the experiment a twofold increase for the solubility of cycluron was found, relative to the solubility of cycluron in pure water. This is an approximate value and other analytical techniques such as gas chromatography or high performance liquid chromatography would provide a more accurate determination. Due to the large amount of error associated with this method of determining the concentration of cycluron in solution, only β-CD was investigated; however, it would be beneficial to carry out these tests with the other native and derivatised CD molecules.

DISCUSSION

Complex stoichiometry and thermal analysis

Three of the CD complexes discussed contain seven glucose/methyl glucose units and each of these complexes displays a 1:1 host-guest ratio. The TMEACYC complex is the only host with six methylglucose units and it displays an unusual 2:1 host-guest ratio. Two methods were used to deduce these ratios. For the methylated CDs there was a definite step in the TG traces indicating guest loss, from which the guest content could be assessed. The TG traces for β-CD complexes have a tendency to show only water loss and then decomposition which means that an alternative method such as ^{1}H NMR spectroscopy was required to confirm the stoichiometry.

The TG trace for each complex shows an initial mass loss which is due to the included water molecules being released. The BCDCYC and DMBCYC complexes decompose whereas the TMEACYC and TMBCYC complexes melt. β-CD shows the highest level of guest thermal stabilisation as the complex decomposes only above 290 °C and there is no evidence of guest loss prior to decomposition. DIMEB on the other hand stabilises the guest up to a temperature of 190 °C which is considerably higher than the corresponding temperatures for the hosts TRIMEA and TRIMEB, namely 120 °C and 140 °C respectively. The TMEACYC complex shows a complicated behaviour upon heating and is the only documented TRIMEA complex that recrystallises into the known crystalline form of TRIMEA once the guest has been released. Variable-temperature PXRD proved to be a useful tool in interpreting the thermal events for this particular complex.

Conformations of the host and guest molecules

The four host molecules discussed in this chapter have significant differences in their chemical constitutions, resulting in very different cavity geometries. Firstly, the geometrical parameters for the heptagonal rings of β-CD (*l*, *D* and ϕ), formed by the O4 atoms of each glucose unit, have small ranges illustrating the regular, 'round' shape that β-CD normally displays. The deviations (*d*) of the O4 atoms from their least-squares plane are also small, as are the tilt angles τ_1 and τ_2. All these parameters suggest the usual symmetrical, truncated, cone-like appearance of a β-CD molecule. The conformation of the DIMEB host molecule does not differ significantly from that of β-CD. It also adopts a rather round and symmetrical structure which is maintained by the same seven intramolecular O2n•••H–O3(n-1) hydrogen bonds occurring in β-CD. The geometries of the host molecules TRIMEA and TRIMEB are rather different from those of β-CD and DIMEB, which is mainly

due to the loss of the O2n•••H–O3(n-1) hydrogen bonds upon methylation of the O3 hydroxyl groups.[17] This reduces the symmetry of the TRIMEA and TRIMEB molecules and creates greater flexibility around the glycosidic linkage. This is evident from the deviation of the O4 atoms from their mean plane which range from 0.03 to 0.63 Å in the TRIMEB structure and only from 0.001 to 0.056 Å in the β-CD structure. Another significant difference is found in the tilt angles (τ_1) of the TRIMEA and TRIMEB glucose residues which are in the range 1.1 to 33.6° for TRIMEA and 9.0 to 40.3° for TRIMEB while β-CD has a much narrower range, namely 1.9 to 10.6°. All the host molecules of the cycluron complexes have only positive τ_1 and τ_2 values, indicating the inward inclination of the primary hydroxyl/methoxyl groups.

The different nature of the host molecules affects the orientation, position and geometry of the cycluron molecule within the respective cavities. The TRIMEA complex demonstrates how both the urea moiety of the guest and the hydrophobic cyclooctyl portion have a certain binding affinity for the interior of the host. The cyclooctyl moiety of the guest is situated at the primary rim of the β-CD molecule and the TRIMEB molecule but the orientation is reversed for the DIMEB complex. These guest arrangements are in accordance with what was documented by Lichtenthaler and the molecular lipophilicity patterns he found for the various CDs, using computational visualisation methods.[20,21,23] The symmetrical, wider β-CD and DIMEB molecules include the entire guest, while the urea 'tail' portion protrudes from the secondary rim of the TRIMEB complex molecule. Finally, two TRIMEA molecules are required to encapsulate cycluron entirely; hence, the extent of inclusion for each complex is significantly different.

An overlay of the dimethyl urea residue of the guest molecules occurring in the four complexes shows the various orientations adopted by the cyclooctyl ring (Figure 42). The major and minor components of the uncomplexed guest are also included for comparison. The guest molecule in the BCDCYC complex differs only slightly from the major component of the uncomplexed guest with a ~120° angle of rotation between atoms C2-C3-C4 and C6-C7-C8 to obtain a more linear geometry in order for the guest to have an optimum fit within the CD cavity (Figure 43). The cyclooctyl ring of the guest in the TMEACYC complex has completely different torsion angles for the eight-membered ring from that of the uncomplexed guest but still retains the low energy boat-chair conformation. The latter conformation as well as the point of attachment for the amide moiety of the guest molecule within the TMBCYC complex is comparable to the major component of the uncomplexed guest. As the orientation of the guest in the CD cavity of the DMBCYC complex is reversed, there is

greater orientational freedom for the cyclooctyl residue. This is probably why the guest was disordered and hence challenging to model. The point of attachment for the amide moiety differs significantly from that of the uncomplexed guest but the boat-chair conformation of the cyclooctyl ring is maintained.

The guest molecules are all tilted with respect to the O4-polygon planes and in the case of the BCDCYC complex the guests are rotated with respect to each other in the CD dimer. This maximises the use of available space inside the cavity and minimises close contacts and steric interference between the host and guest molecules.

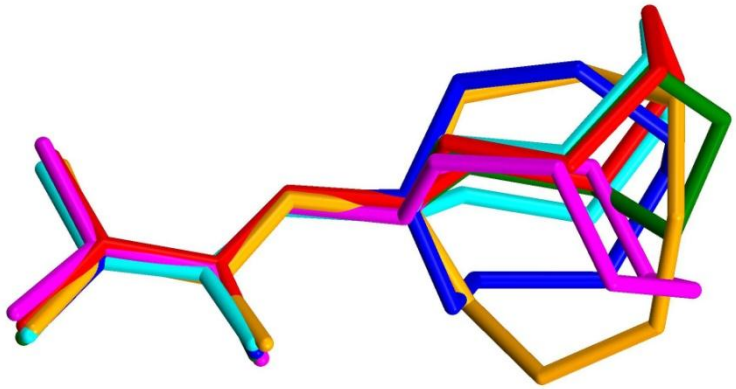

Figure 42. *Overlay of the cycluron conformers occurring in the cycluron complexes. The colours are as follows: uncomplexed guest (major component-red, minor component-green), complexed guest in BCDCYC (pink), TMEACYC (dark blue), TMBCYC (light blue) and DMBCYC (orange). In the case of the DMBCYC complex, only the major component of guest disorder is shown for simplicity.*

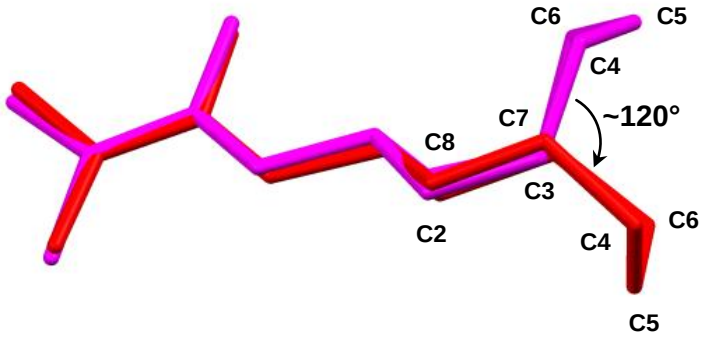

Figure 43. *An overlay of the uncomplexed guest molecule (red) and the guest molecule from the BCDCYC complex (pink). A rotation of approximately 120° is responsible for the different cyclooctyl geometries.*

Intra- and intermolecular interactions

The BCDCYC complex contains many intra- and intermolecular interactions due to the profusion of hydroxyl groups. The formation of the β-CD dimer is facilitated by O3•••O3 and O2•••O3 intermolecular hydrogen bonds of which the former are stronger. The inter- and

intra-layer interactions (including those mediated by water) stabilise the two-dimensional layers as well as the overall three-dimensional structure of the BCDCYC structure.[24]

The TMEACYC complex is dominated by weak C-H•••O interactions that form within the host molecules and between the host molecules. There are also four weak C-H•••O host-water and 15 stronger O•••O contacts between water molecules or between a water molecule and oxygen atom of the methoxyl groups which add to the overall stability. The TMBCYC complex has several C6-H•••O5 intramolecular hydrogen bonds which have the effect of narrowing the O6 rim of the TRIMEB molecule and producing a more cup-shaped and sealed conformation. Numerous other weak C-H•••O hydrogen bonds stabilise this complex in the absence of additional water molecules. Finally, the DMBCYC structure is held together through the common intramolecular O2n•••H–O3(n-1) interactions and many other C•••O intermolecular contacts involving the O3 and O6 groups of the host. Host-host and host-water hydrogen bonds are also present.

Water molecules

Native CD complexes such as those containing β-CD normally contain many included water molecules. Most water molecules are located near the primary or secondary rim of the native CD molecules as they can form strong hydrogen bonds with the numerous hydroxyl groups present. The BCDCYC complex has 40 water (O•••O) close contacts and many more host-water interactions too. There are, however, no water molecules present between the host cavity and guest molecules.

The derivatised CD complexes contain few or no water molecules normally and this is due to their decreased hydrogen bonding capacity and the presence of methoxyl groups which have a greater degree of rotational freedom and can therefore maximise the efficiency of crystal packing. The TMEACYC complex contains a water molecule which acts as a bridge between the host and guest. The water molecule donates a hydrogen atom to the amide nitrogen of the guest and to a methoxyl oxygen atom of the host. The TMBCYC complex also contains a water molecule that donates a hydrogen atom to the amide nitrogen of the guest. This water molecule then links to a further water molecule rather than the host. The DMBCYC complex contains no guest-water interactions. The host-guest interactions are primarily hydrophobic in nature for all four complexes with not one significant hydrogen bond occurring between the amide group and the CD cavity walls.

Crystal packing

The guests are completely isolated from one another in three of the four complexes discussed. The BCDCYC complex contains dimeric β-CD units that form infinite channels in which the cycluron molecules are positioned. At the primary interface of two β-CD dimers the cyclooctyl rings are in close proximity to one another and are surrounded by the primary hydroxyl groups which isolate the guest molecules from the aqueous environment between the channels. The TMEACYC complex shows a novel packing arrangement in which the primary rims of the cage-like structure are further blocked by a side-on contact with another CD dimer. The hydrophilic dimethyl urea moiety of the cycluron molecule in the TMBCYC complex extends beyond the CD cavity into the interstitial vacant sites and interacts with a water molecule. This increases the packing efficiency of the crystal structure. The monomeric units of the DMBCYC complex pack in what seem to be infinite columns; however, the secondary and primary rims of the DIMEB molecules are abutted by the neighbouring DIMEB molecule in the channel due to the strong inclination of the DIMEB molecules to the *yz*-plane forming a herringbone packing arrangement.

PART 2: COMPLEXATION IN SOLUTION

^{1}H NMR SPECTROSCOPY OF CYCLURON WITH THE NATIVE CYCLODEXTRINS IN SOLUTION

The only guest that was studied in solution using ^{1}H NMR spectroscopy was the urea herbicide, cycluron. This was due to the higher solubility of cycluron in water (1.2 g dm^{-3} at 25 °C) when compared to the other guest molecules investigated here. The cycluron molecule is shown in Figure 44 with the methyl (H_a), methine (H_b) and methylene (H_c) protons labelled. It is noteworthy that the methylene protons are not all chemically equivalent but have been assigned with a common label (H_c) to simplify the analysis and interpretation of the ^{1}H NMR spectra.

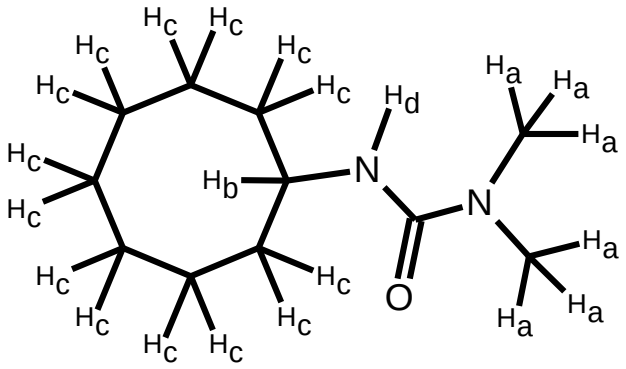

Figure 44. *Chemical structure of cycluron with the respective protons labelled.*

The ^{1}H NMR signals for all three sets of protons mentioned above undergo complexation-induced shifts (CISs) when interacting with α-, β- and γ-CD molecules in solution. However, the magnitudes of these CISs depend on the depth of the protons included within the CD cavity. The amino (H_d) and hydroxyl protons of the host are exchanged with the solvent D_2O and are as a result not present in the ^{1}H NMR spectra. The large peak at 4.70 ppm in the spectra is due to residual HDO molecules in the D_2O solvent and was used as an internal standard for the measurement of the chemical shifts.

Figure 45 illustrates the upfield and downfield CISs of the proton signals for β-CD and cycluron. In the absence of cycluron the CD proton signal H_5 overlaps with the CD proton signal H_6 (Figure 45 (a)); conversely, when the concentration of the guest molecule increases the proton signal, H_5, shifts upfield and can be seen as a doublet of triplets (Figure 45 (b) and (c)). The proton signal for H_3 of the host also moves upfield towards H_6 while the

signals for host protons H_2 and H_4 do not shift significantly. The CIS values for the methine proton of the guest molecule (H_b) could not be determined for this particular case with β-CD as a result of severe overlap between the host and guest signals. It is however clear that the signal for the guest molecule proton, H_c, moves downfield with increasing CD concentrations (Figure 45 (c)).

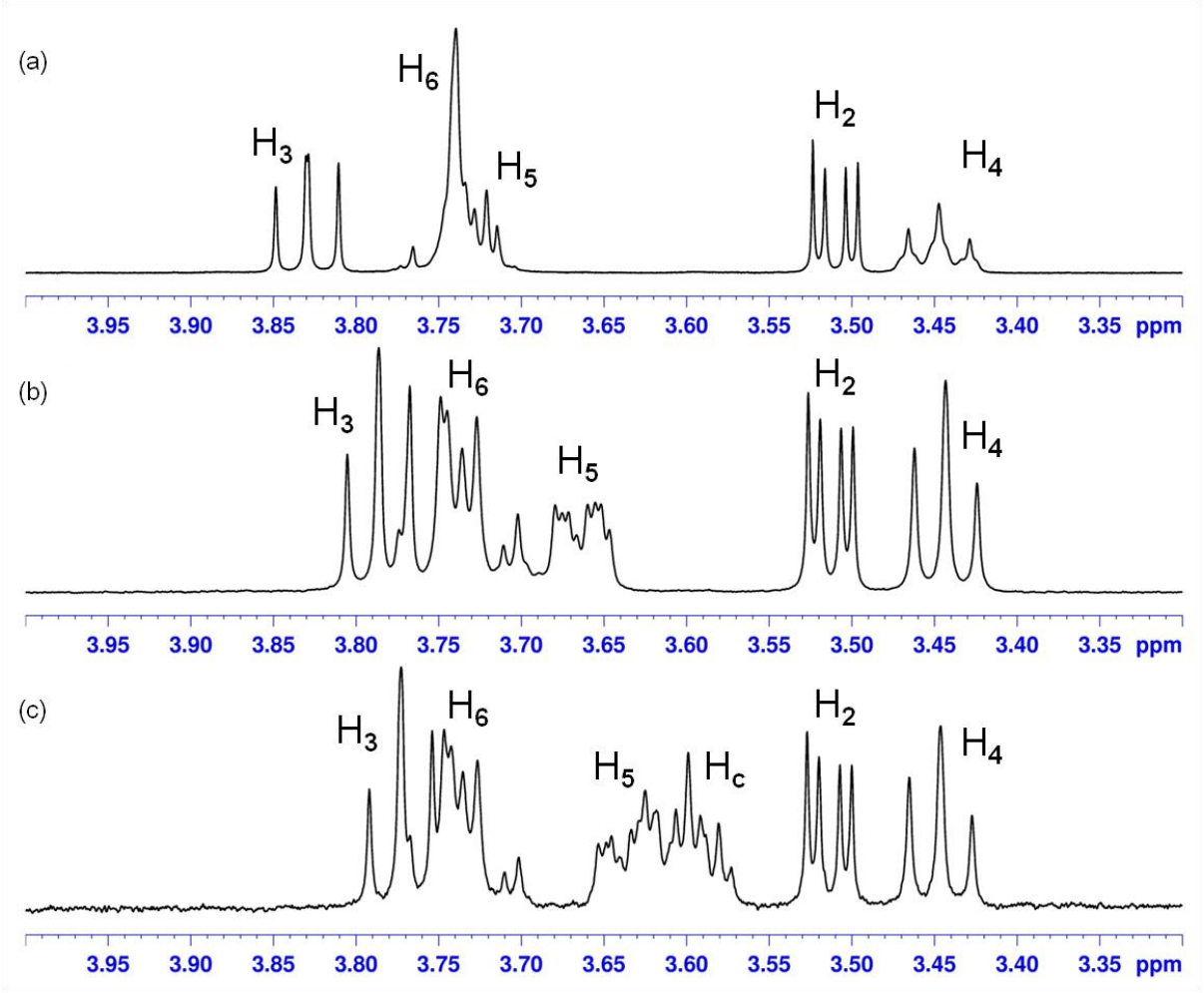

Figure 45. *Partial ^{1}H NMR spectra (500 MHz) of β-CD with cycluron (r = [H] / ($[H]_t$+ $[G]_t$)) (a) r = 1 (b) r = 0.5 and (c) r = 0.1.*

In separate experiments using the other native host molecules (α-CD and γ-CD), similar trends were observed. The CIS values were considerably smaller than those observed for the β-CD·cycluron interaction.

Stoichiometry and mode of inclusion

The stoichiometries of the cycluron inclusion complexes with α-, β- and γ-CD were determined using the continuous variation method. The stock solution concentrations were 2.5 mM in each case. The protons showing the largest changes in their chemically induced

shift values were monitored and Job plots for complexation with each cyclodextrin were obtained (Figure 46).[25] All the Job plots have a maximum at r = 0.5 indicating a 1:1 host-guest ratio.

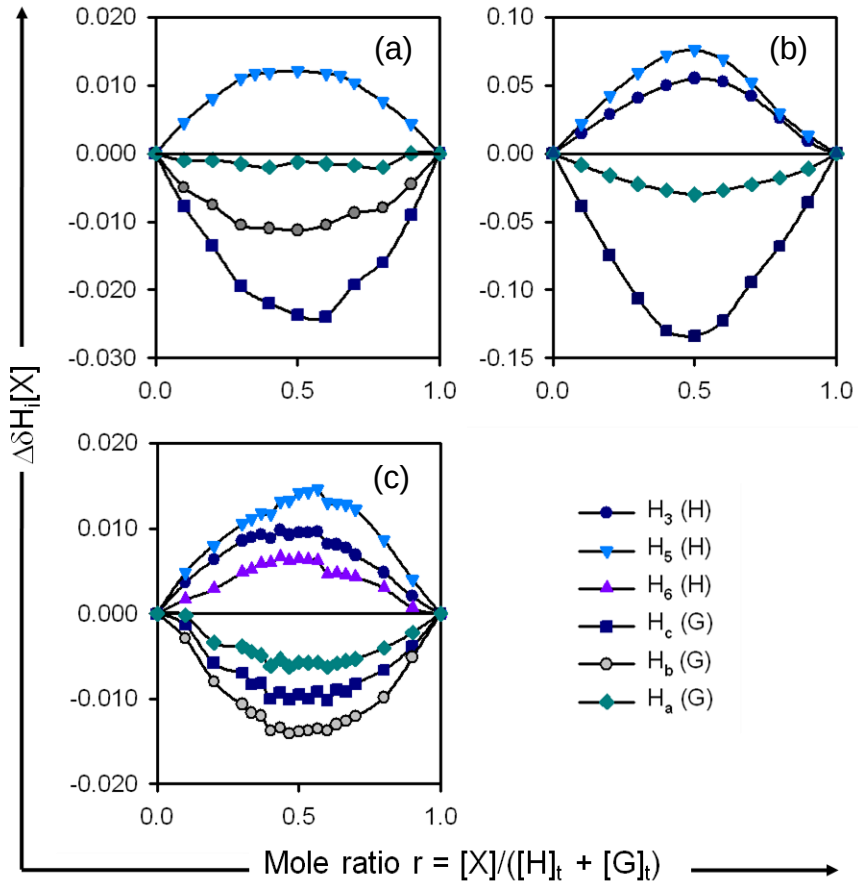

Figure 46. *Job plots for cycluron with (a) α-CD, (b) β-CD and (c) γ-CD.*

The order of the magnitudes of the CIS values determined from the Job plots in Figure 46 for each CD with cycluron is slightly different. For α-CD the magnitudes of the CIS values are in the order $H_c > H_5 > H_b > H_a$. For β-CD, the order is $H_c > H_5 > H_3 > H_a$ and for γ-CD $H_b > H_5 > H_c > H_3 > H_a > H_{6a,b}$. The protons associated with the the cylooctyl ring (H_b and H_c) of the guest showed the greatest CIS values followed by the methyl protons (H_a). The host protons most affected are H_3 and H_5, with the latter having a greater CIS value, suggesting that the closest interaction between the host and guest takes place at the primary rim of the CD cavity with the cyclooctyl residue of the guest molecule. As the methyl protons (H_a) of the guest display only small CISs it can be deduced that they are not in close contact with the CD walls and are situated closer to the wider secondary rim of the CD. The change in chemical shift multiplied by the concentration of the host/guest proton ($\Delta\delta H_i[X]$) is an order of magnitude greater for β-CD than that for α-CD and γ-CD (Figure 46) indicating a stronger interaction between β-CD and cycluron. All CIS values are shown in Table 20.

Table 20. *Maximum observed chemically induced shifts for cycluron with α-CD, β-CD and γ-CD at 298 K.*

	$\Delta\delta_{obs}^{max}$ H_3 (ppm)	$\Delta\delta_{obs}^{max}$ H_5 (ppm)	$\Delta\delta_{obs}^{max}$ H_6 (ppm)	$\Delta\delta_{obs}^{max}$ H_a (ppm)	$\Delta\delta_{obs}^{max}$ H_b* (ppm)	$\Delta\delta_{obs}^{max}$ H_c (ppm)
α-CD	0.005	0.021	0.006	-0.004	-0.020	-0.031
β-CD	0.059	0.088	0.005	-0.034	-	-0.154
γ-CD	0.014	0.018	0.006	-0.010	-0.022	-0.017

* Due to overlapping of the H_5 proton of the host and H_b proton of the guest it was not possible to determine $\Delta\delta_{obs}^{max}$ H_b for β-CD

Association constants

The association constants for the inclusion complexes α-CD·cycluron and β-CD·cycluron were evaluated using the same data used to construct the Job plots. In determining the association constant between γ-CD and cycluron a new set of NMR measurements was performed owing to their very weak association. For these experiments the cycluron concentration was kept constant at 2.5 mM and the γ-CD concentration was varied from zero to 40 mM (well in excess).

The association constants for each of the 1:1 host-guest complexes was determined using a non-linear least-squares regression analysis of the observed chemical shift changes of cycluron with α-, β- and γ-CD NMR lines as a function of the CD concentration. Equation 1 was used for the evaluation of K, where [X] is the concentration of the host or guest of a sample and $[M] = [G]_t + [H]_t$.

$$\Delta\delta_{obs}^{(X)} = \frac{\Delta\delta_c^{(X)}}{2\,[X]_t} \times \left\{ [M] + \frac{1}{K} \pm \left[\left([M] + \frac{1}{K} \right)^2 - 4\,[H]_t\,[G]_t \right]^{\frac{1}{2}} \right\} \qquad (1)$$

Table 21 lists the association constant (K) obtained for each complex as well as the correlation coefficient (R) and the error loss function (E). The program CONSTEQ was used to obtain the parameters in the case of α- and β-CD while a modified program ConstEQV was used for γ-CD. Satisfactory convergence of these values was obtained in the case of α-CD and β-CD with the correlation coefficients reaching a value very close to unity. Again, due to the very small ^{1}H NMR shifts the correlation coefficient was slightly further from unity for the γ-CD case.

Table 21. *K, E and R values for the α-CD, β-CD and γ-CD complexes at 293 K.*

	α-CD	β-CD	γ-CD
K *	228	3254	155
R	0.999	0.999	0.953
E	1.2×10^{-5}	1.2×10^{-4}	6.7×10^{-3}

* The association constants are dimensionless as the concentrations are expressed in mol dm^{-3} relative to the standard concentration of 1 mol dm^{-3}.

For any solution containing a host and guest mixture it is possible to calculate the concentration of the complex in solution [C] from the association constant using Equations 2 and 3. When the maximum of a Job plot occurs at 0.5 it is known that $[H]_t = [G]_t$ (1.25 mM). [C] can then be calculated and the percentage of the guest that forms a complex in solution with each CD can be determined. It is obvious that a stronger association constant will result in a greater concentration of the complex in solution (Table 22).

$$d = [H]_t + [G]_t + \frac{1}{K} \tag{2}$$

$$[C] = \frac{d - \sqrt{d^2 - 4\,[H]_t\,[G]_t}}{2} \tag{3}$$

Table 22. *Percentage of guest included in the CD cavity and the concentration of the complexes formed in solution.*

	α-CD	β-CD	γ-CD
K	228	3254	155
[C] (mM)	0.23	0.77	0.18
% of guest included	19 %	61 %	14 %

ISOTHERMAL TITRATION CALORIMETRY INVESTIGATION OF THE INTERACTION BETWEEN CYCLURON AND THE NATIVE CDs

The ITC technique was employed to investigate the thermodynamics of inclusion of cycluron with the native CDs. Table 23 lists the concentrations of the cycluron and CD solutions as well as the injection volume and number of injections for each ITC experiment conducted. The association constants from the ^{1}H NMR studies conducted between cycluron and the hosts α-CD and γ-CD were found to be 228 and 155 respectively, indicating weak binding forces between these host molecules and cycluron. In order to produce a measurable heat change, in both cases it was necessary to use much higher concentrations of the CD solutions as well as greater injection volumes. Due to the poor aqueous solubility of β-CD we were limited to lower concentrations of β-CD. However, the strong association constant between cycluron and β-CD allowed an accurate binding isotherm to be obtained.

Table 23. *Experimental parameters for the ITC experiments performed with cycluron and the native CDs*

	[CD] (mM)	[Cycluron] (mM)	Injection volume (10^{-6} dm^3)	Number of injections
α-CD	60	0.75	10	25
β-CD	15	0.75	5	40
γ-CD	60	0.75	10	20

In Figure 47 plots of the power exchange versus time are shown for a solution of cycluron titrated with solutions of α-, β-, and γ-CD. A binding isotherm is created by plotting the integrated power signals against the ratio of total CD concentration and the total guest concentration ($[CD_i]_{tot}$ / $[G]_{tot}$). An exothermic reaction is observed for both the α-CD and β-CD experiments as the power supplied to the sample cell decreases indicating that heat is being released. For the γ-CD binding reaction, heat is absorbed, resulting in an increase in power to the sample vessel, indicative of an endothermic process. The changes in heat for the α-CD and γ-CD complexation processes are an order of magnitude smaller than that for β-CD complexation.

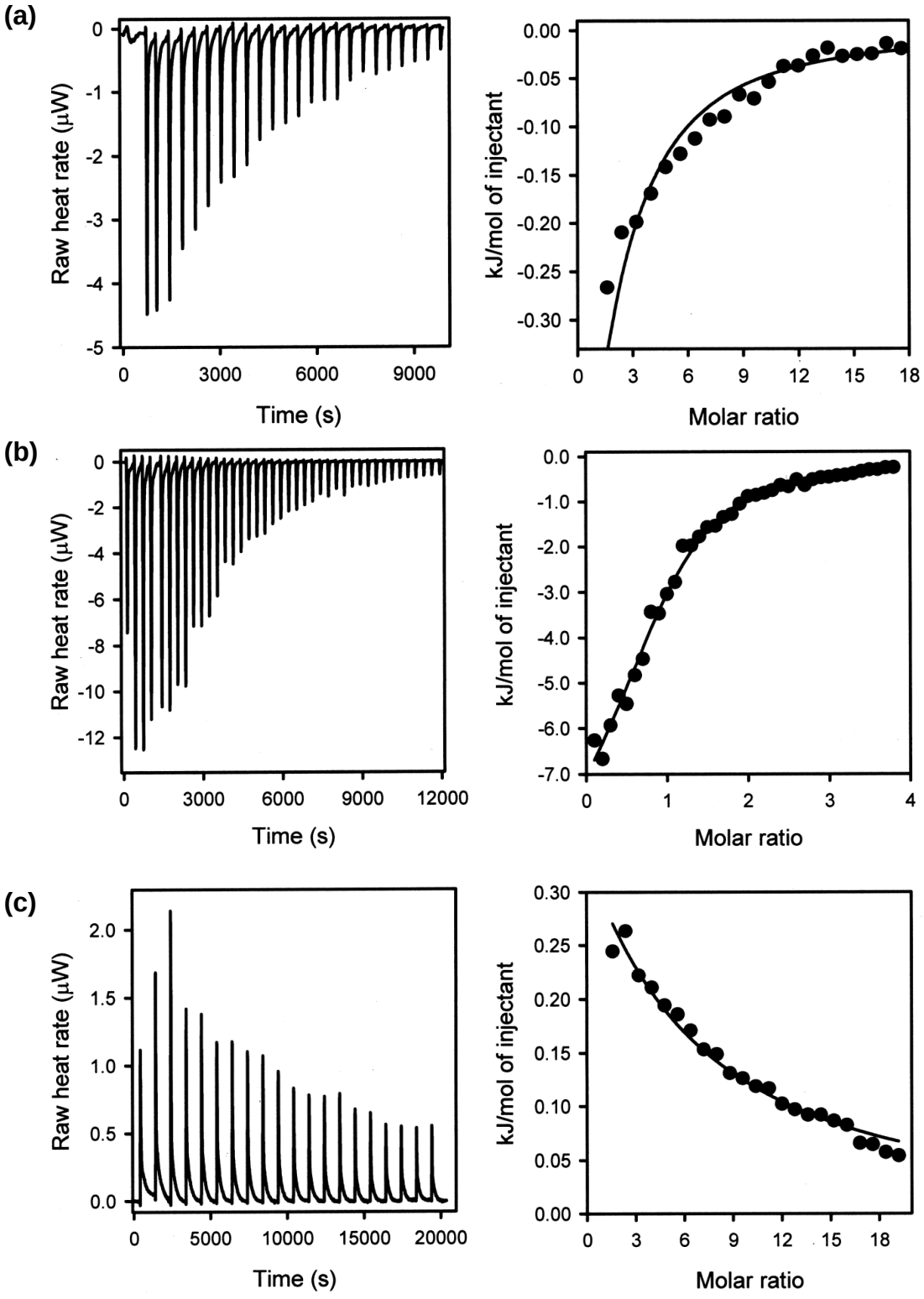

Figure 47. *Calorimetric titration of cycluron with the native cyclodextrins: (a) α-CD, (b) β-CD and (c) γ-CD. Left: Raw data for the sequential injections of the CD solution into the cycluron solution. Right: Reaction heat isotherms obtained from the integration of the calorimetric curves. The fitted curve is based on the thermodynamic parameters obtained in Table 23.*

Association constant, change in enthalpy and complex stoichiometry

The association constant (K), change in enthalpy ($\Delta H°$) and complex stoichiometry were determined using the least-squares non-linear adjustment based on the Wiserman isotherm discussed in Chapter 2 (Equation 4, reproduced below). The data are summarised in Table 24. In all three cases the stoichiometric ratio between the host and guest molecules in solution was found to be 1:1 and negative $\Delta G°$ values were obtained, demonstrating that all three binding processes are spontaneous at 298 K. The standard formation enthalpies ($\Delta H°$) are negative for α- and β-CD and positive for γ-CD correlating with what was previously mentioned regarding the feedback mechanism of the ITC instrument. For all three cases the change in entropy values multiplied by the temperature are positive and larger than the standard enthalpy changes indicating that the interactions between the agrochemicals and CDs in solution are entropically-driven.

$$\frac{dq}{d[CD]_T} = \Delta H^o \, V_0 \left[\frac{1}{2} + \frac{1 - X_R - r}{2\sqrt{(1 + X_R + r)^2 - 4X_R}} \right] \quad (4)$$

Table 24. *Formation constants K and thermodynamic parameters $\Delta H°$, $T\Delta S°$, $\Delta G°$ for complexation between cycluron and the native cyclodextrins at 298 K.*

	K*	$\Delta G°$ (kJ mol^{-1})	$\Delta H°$ (kJ mol^{-1})	$T\Delta S°$ (kJ mol^{-1})
α-CD	459 ± 7	-15 ± 5	-2.0 ± 0.1	13.2
β-CD	4753 ± 31	-21 ± 9	-8.9 ± 0.1	12.1
γ-CD	74 ± 1	-11 ± 1	5.68 ± 0.01	16.3

* The association constants are dimensionless as the concentrations are expressed in mol dm^{-3} relative to the standard concentration of 1 mol dm^{-3}.

Discussion of ^{1}H NMR and ITC results

The association constants (K) obtained from both the ^{1}H NMR and ITC experiments for cycluron complexing with β-CD are an order of magnitude greater than those for its complexation with α- and γ-CD. The actual values do differ quite considerably for each method (e.g. β-CD: 3254 for ^{1}H NMR and 4753 for ITC) but this is expected due to the differences between the techniques. ^{1}H NMR spectroscopy is an indirect technique that takes advantage of changes in physical observables, whereas ITC involves the direct measurement of the concentrations of free and bound guest molecules.

The association constant and thermodynamic parameters reported here are consistent with what has previously been discussed in the literature for guest molecules also containing a cyclooctyl ring moeity. Table 25 compares the values that were obtained for these parameters using the method of ITC for α- and β-CD forming complexes with cycluron (this study) and cyclooctanol respectively.[26,27] Matsui *et al* have also determined the association constants for the interaction between cyclooctanol and the hosts α- and β-CD using a spectrophotometric method and have obtained slightly lower values of 178 and 2000, respectively.[28] The lower values could be due to the fact that a buffer solution containing citrate (known to bind to β-CD) was used.

Table 25. *Comparison of association constants and thermodynamic parameters for complexation of cycluron and cyclooctanol with α- and β-CD.*

Host	Guest	K	ΔG° (kJ mol^{-1})	ΔH° (kJ mol^{-1})	TΔS° (kJ mol^{-1})
α-CD	Cycluron	459	-15.2	-2.0	13.2
α-CD[27]	Cyclooctanol	235	-13.5	-3.9	9.6
β-CD	Cycluron	4753	-21.0	-8.9	12.1
β-CD[27]	Cyclooctanol	4405	-20.8	-16.4	4.4

The binding strength between the CDs and cycluron can be ranked as follows: β-CD > α-CD > γ-CD. The size of the CD ring affects the depth of inclusion and the position of the guest with respect to the cavity walls of the CD once included. The top and bottom diameters of α-CD, β-CD and γ-CD are 4.7 to 5.3 Å, 6.0 to 6.5 Å and 7.5 to 8.3 Å, respectively.[29] When cycluron associates with γ-CD the exchange rate between the complexed and uncomplexed form is rapid due to the weak long-range forces that occur between the two molecules. The γ-CD cavity is too large to accommodate a single cycluron molecule with a good fit. The α-CD cavity on the other hand is too small which limits the depth of inclusion of the cycluron molecule as well as the number of interactions that can occur between the two molecules. The β-CD cavity is larger than that of α-CD and presents a perfect site for the cycluron molecule to position itself. Owing to the large upfield shifts of the H_3 and H_5 protons of β-CD upon increasing cycluron concentrations, one can confidently infer that the guest is deeply embedded within the CD cavity.

Attractive van der Waals interactions and hydrogen bonds are characterised by negative ΔH° values.[27] Since both of these interactions are critically dependent on the distance between the host and guest molecule, one expects the ΔH° value for γ-CD to be much larger than those for α- and β-CD, which is the case here. With regard to the positive ΔS° values, it

has been shown that increasing the molecular flexibility or the number of degrees of freedom in a guest molecule results in a more favourable complexation entropy since there are more possible conformers that can fit properly into the CD cavity.[26] The cyclooctyl ring of cycluron can adopt ten idealised symmetrical conformations which illustrates the flexibility of the molecule.[6] One can also see from the crystal structures how the geometry and position of the methyl urea 'tail' of the guest molecule can differ depending on the size of the CD cavity. Generally, the entropy of the system also increases because of the water molecules being displaced from the interior of the cavity upon inclusion of the guest molecule.[30]

The results of this investigation offer information regarding the stoichiometry, binding energies and binding strength. The method provides little or no information about the orientation of cycluron in the CD cavities, the mode of inclusion and whether the guest molecules enter the CD cavity from the primary side or secondary side. Other spectroscopic techniques such as 2D NMR spectroscopy would be valuable for exploring the conformations of these cyclodextrin complexes.

Complex formation has been confirmed in both the solid state and in solution, using X-ray crystallography, NMR spectroscopy and ITC. The structural features deduced for the β-CD cycluron complex are comparable for these techniques employed here even though a comparison is being made between two different phases of matter. Figure 48 shows the cross-sectional view of the 1:1 β-CD·cycluron complex determined using single crystal X-ray diffraction. Solution-state studies using ^{1}H NMR spectroscopy show large $\Delta\delta_{obs}$ values for the methylene protons of the guest molecules (H_c) and the H_5 and H_3 protons of the host molecules, suggesting similar modes of guest inclusion both in solution and in the solid state.

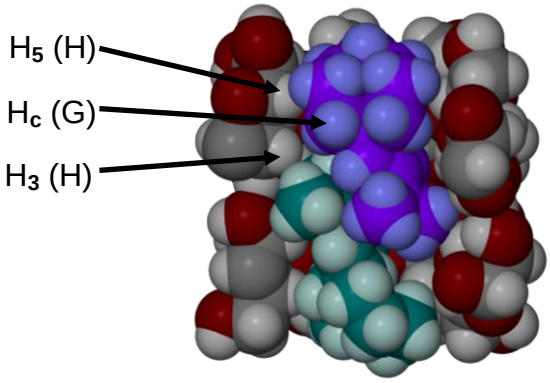

Figure 48. *A cross-sectional view of the 1:1 β-CD·cycluron crystal structure highlighting the host-guest H-atom contacts.*

REFERENCES

1. L. J. Barbour, *J. Appl. Crystallogr*., **1999**, 32, 351-352.
2. XPREP, *Data Preparation and Reciprocal Space Exploration*, Version 5.1, © Bruker Analytical X-ray Systems*,* **1997***.*
3. Z. Otwinowski and W. Minor, Processing of X-ray Diffraction Data in Oscillation Mode, in *Methods in Enzymology*, eds. C.W. Carter and R.M. Sweet, Academic Press, New York, **1996**, vol. 276, 307-326.
4. G. M. Sheldrick, *SHELXS-97*, *Program for Crystal Structure Solution*, Institüt für Anorganische Chemie der Universität, Tammanstrasse 4, D-3400 Göttingen, Germany, **1997**.
5. G. M. Sheldrick, *SHELXH-97, Acta Cryststallogr*., **2008**, A64, 112-122.
6. D. G. Evans, and J. C. A. Boeyens, *Acta Crystallogr*., **1988**, B44, 663-671.
7. S. Lubhelwana, MSc Dissertation, *Crystal Isostructurality and X-ray Diffraction studies of Cyclodextrin Inclusion Compounds*, University of Cape Town, South Africa, **2005**.
8. G. M. Sheldrick, *Direct Methods for Solving Macromolecular Structures*, ed. S. Fortier, Dordrecht: Kluwer Academic Publishers, **1998**, 401-411.
9. K. Harata, *Inclusion complexes*, eds. J. L. Atwood, J. E. D. Davies and D. D. MacNicol, Oxford University Press, London, **1984**, vol. 5, ch. 9.
10. K. B. Lipkowitz, K. Green and J. Yang, *Chirality*, **1992**, 4, 205-215.
11. Cambridge Structural Database and Cambridge Structural Database system, Version 5.32, Cambridge Crystallographic Data Centre, University Chemical Laboratory, Cambridge England, February **2011**.
12. T. Steiner and W. Saenger, *Acta Crystallogr*., **1998**, B54, 450-455.
13. T. Steiner and W. Saenger, *Carbohydr. Res*., **1996**, 282, 53-63.
14. Paratone N oil (Exxon Chemical Co., TX, USA).
15. M. R. Caira, W. T. Mhlongo and J. Li, *J. Optoelectron. Adv. M.*, **2008**, 10, 2255-2260.
16. M. R. Caira, S. A. Bourne, W. T. Mhlongo and P. M. Dean, *Chem. Commun*., **2004**, 2216-2217.
17. K. Harata, K. Uekama, M. Otagiri and F. Hirayama, *J. Inclusion Phenom. Mol. Recog. Chem*., **1984**, 1, 279-293.
18. M. R. Caira, V. J. Griffith, L. R. Nassimbeni and B. van Oudtshoorn, *Supramol. Chem*., **1996**, 7, 119-124.
19. E. J. C. de Vries and M. R. Caira, *Carbohydr. Res*., **2008**, 343, 2433-2438.
20. F. W. Lichtenthaler and S. Immel, *Starch*, **1996**, 48, 4, 145-154.

21. F. W. Lichtenthaler and S. Immel, *Starch*, **1996**, 48, 6, 225-232.
22. *The Pesticide Manual*, eds. C. R. Worthing and R. J. Hance, British Crop Protection Council: Lavenham, Suffolk, England, 8th edn., **1987**.
23. F. W. Lichtenthaler and S. Immel, *The Lipophilicity Patterns of Cyclodextrins and of Non-glucose Cyclooligosaccharides*, Proceedings of the Eighth International Symposium on Cyclodextrins, eds. J. Szetjli and L. Szente, Kluwer Academic Publishers, The Netherlands, **1996**, 3-16.
24. G. Le Bas and G. Tsoucaris, *Supramol. Chem.*, **1994**, 4, 13-16.
25. P. Job*, Ann. Chim. Phys*., **1928**, 9, 113-203.
26. M. V. Rekharsky and Y. Inoue, *Chem. Rev.*, **1998**, 98, 1875-1918.
27. M. V. Rekharsky, M. P. Mayhew and R. N. Goldberg, *J. Phys. Chem. B*, **1997**, 101, 87-101.
28. Y. Matsui and K. Mochida, *Bull. Chem. Soc. Jpn*., **1979**, 52, 2808-2814.
29. S. Li and W. C. Purdy, *Chem. Rev*., **1992**, 92, 1457-1490.
30. M. L. Doyle, *Curr. Opin. Biotechnol*., **1997**, 8, 31-35.

Chapter 4: Endosulfan

Solid-state inclusion complexes of endosulfan with four cyclodextrins (β-CD, γ-CD, DIMEB and randomly methylated β-CD) have been investigated primarily using powder and single crystal X-ray diffraction methods.

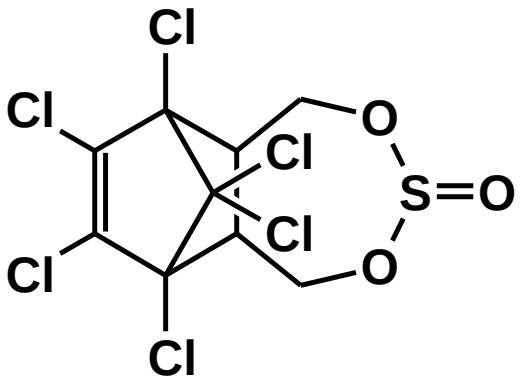

THE GUEST: ENDOSULFAN

The commercial product of endosulfan is a white powder comprising two conformational isomers, α- and β-endosulfan in the ratio 7:3. The difference between these two conformational isomers is defined by the geometry of the seven-membered cyclic sulfite residue as can be seen in Figure 1. β-endosulfan is a symmetrical molecule with both sets of methylene protons in equivalent positions. In order to convert β-endosulfan into α-endosulfan a 'twisting' of one of the equatorial hydrogen atoms, on the CH_2 group, to an axial position is required. This breaks the internal symmetry of the molecule. The conversion of β-endosulfan to α-endosulfan has been studied extensively using thermodynamic, spectroscopic and computational methods.[1,2,3]

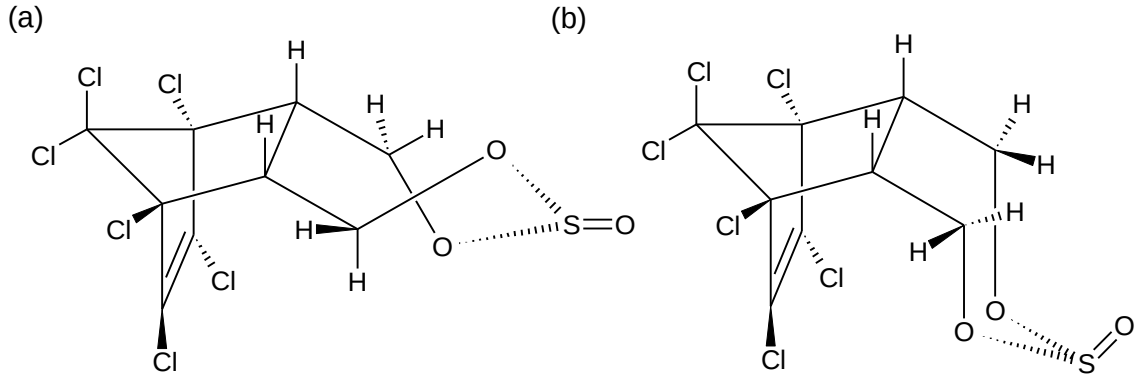

Figure 1. *Structures of (a) α- and (b) β-endosulfan.*

The crystal structure of the symmetrical β-conformer was published in 1977 by two separate groups and this form was shown to crystallise in two different space groups, namely $P2_1/c$ and $P6_3/m$.[4,5] An additional paper was published by Schmidt *et al* [2] in 1997, who quoted X-ray data for both the α- and β-endosulfan molecules; however, no atom coordinates were published. From the ORTEP diagrams shown in the journal article by Schmidt (Figure 2), both the α- and β-endosulfan molecules appear to be symmetrical, even though it is stated in the text that the α-endosulfan molecule is asymmetrical and similar diagrams to that of Figure 1 above were provided.[2] The difference between the two ORTEP pictures depicted relates to the positions of the methylene protons on the seven-membered ring. For the 'α-endosulfan' molecule the axial hydrogen atoms of the methylene groups are situated *trans* to the methine protons while for the β-endosulfan molecule the hydrogen atoms are situated on the same face. There is also a change in configuration at the sulfite atom, but this does not affect the symmetrical nature of either molecule illustrated. From this information we believe that the article is contradictory and the true α-endosulfan structure has not been elucidated to date.

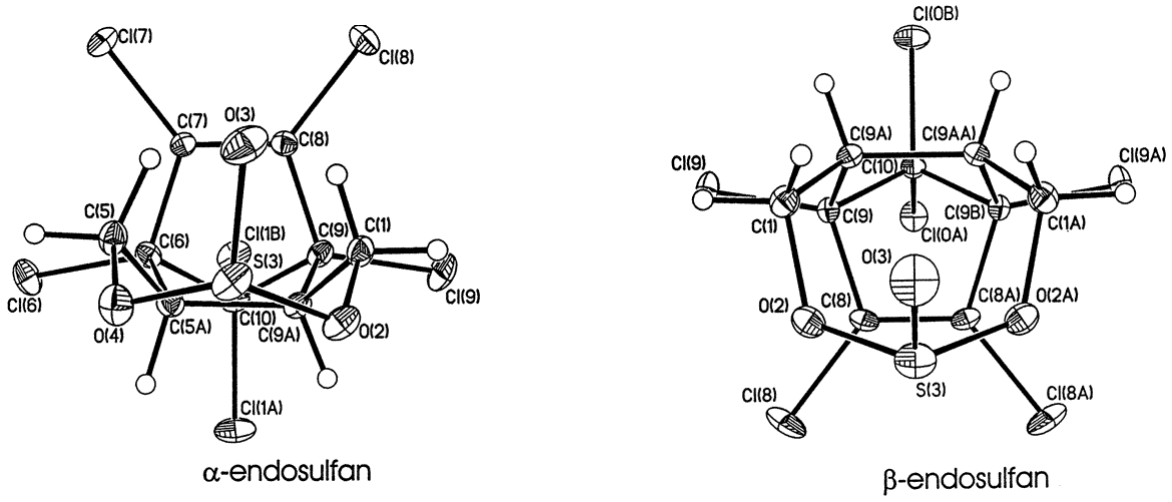

Figure 2. *ORTEP drawings of α- and β-endosulfan from the Schmidt et al journal article.* [2]

β-CYCLODEXTRIN INCLUSION COMPLEXES WITH ENDOSULFAN

β-CD inclusion complexes with both the individual isomers of endosulfan as well as the commercial sample of endosulfan were investigated in the present study.

Complex preparation

Both the kneading method and the co-precipitation method resulted in the formation of a β-CD inclusion complex containing a mixture of conformational isomers of endosulfan (BCD**C**END). The kneading method required 65 mg of β-CD (0.05 mmol) and 20 mg of the commercial endosulfan sample. These two samples were co-ground in the presence of water for 40 min. Once complexation had been confirmed with PXRD, the sample was dissolved in 6 cm^3 of distilled water and stirred at 80 °C for 8 h in an attempt to obtain single crystals of the complexed material.

The co-precipitation method used the same masses of both the guest and host samples, as those for the kneading method. The β-CD material was dissolved in 8 cm^3 of distilled water. The solid guest material was added over a 5 min period to the aqueous β-CD solution. This was then stirred continuously for 8 h at 80 °C. For both the recrystallisation of the kneaded material and co-precipitation method each solution was filtered through a 0.45 μm filter, capped and placed in a Dewar flask at 80 °C for 5 days. Single crystals formed within that time period.

The co-precipitation method explained above was also used to form β-CD inclusion complexes with both individual isomers of endosulfan. During preparation of the β-CD·α-

endosulfan (BCD**A**END) and β-CD·β-endosulfan (BCD**B**END) complex materials, the aqueous solutions of β-CD containing each isomer did not appear clear prior to filtration. The yields of BCD**A**END and BCD**B**END were much lower than that obtained when using the commercial sample of endosulfan.

Confirmation of stoichiometry

The host-guest stoichiometry for the BCD**C**END complex was determined using elemental analysis. For a 2:1 host-guest ratio, the formula $(C_{42}H_{70}O_{35})_2 \cdot C_9H_6Cl_6O_3S \cdot 19.3H_2O$ requires % C, 36.6, % H, 7.0 and % S, 1.0. The experimentally determined values of % C, 37.2(1), % H, 5.7(2) and % S, 0.7(1) (n = 2) are within reasonable agreement with the theoretical values for a 2:1 host-guest complex thereby confirming the complex stoichiometry. The slight discrepancy between the theoretical and experimental values can be attributed to a higher or lower water content present within the sample prior to elemental analysis of the material (a value of 19.3 water molecules was used based on the TG results).

Thermal analysis

The TG and DSC traces for the BCD**C**END complex are shown in Figure 3. The TG curve shows an immediate mass loss due to expulsion of water from the crystalline sample. This mass loss is a two-step process as the gradient changes significantly between 30 and 160 °C and can be explained by the more weakly bound water molecules being expelled first followed by the more strongly bound ones. A mass loss of 11.5 ± 0.1 % (n = 2) between 30 and 160 °C is equivalent to 19.3 ± 0.1 H_2O molecules (calcd. for a 2:1 host-guest stoichiometry). The DSC trace displays the multi-step dehydration process with an irregular-shaped endotherm occurring from 30 to 90 °C. The second DSC endotherm is due to host-guest decomposition and this can be reconciled with the sharp mass loss seen in the TG trace.

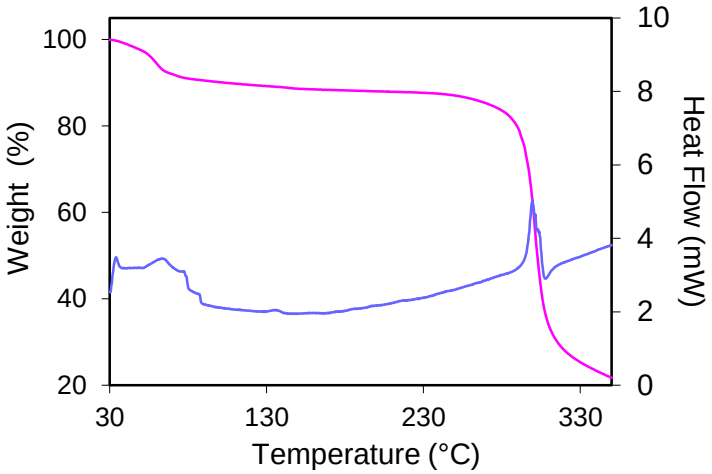

Figure 3. *Representative TG (pink) and DSC (blue) traces for the inclusion complex BCD**C**END.*

The HSM photographs (Figure 4) of the BCD**C**END complex illustrate a single regular, tabular crystal that loses its crystallinity rapidly, due to expulsion of water, once removed from the mother liquor. At 80 °C extensive cracking occurs and the crystal starts to fragment. Bubbles were first seen at 86 °C and became more vigorous as the crystal started to decompose at 245 °C. Decomposition can be seen by the discolouration of the crystal.

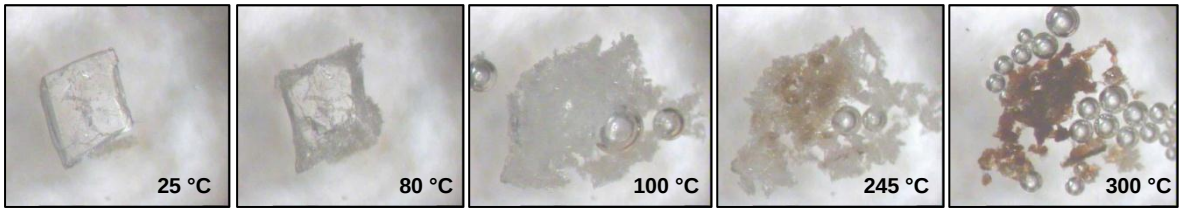

Figure 4. *HSM photographs of a BCD**C**END complex crystal immersed in silicone oil.*

Crystal structure analysis

The stoichiometric and thermal analyses which have been discussed above were performed only on the BCD**C**END complex. The latter crystallised in the triclinic crystal system in space group *P*1. This X-ray crystal structure was only partially solved due to the entire dimeric β-CD unit being disordered over two positions, one laterally displaced from the other by ~1.0 Å. There were insufficient data available to obtain a reliable structure solution.

The yields of BCD**A**END and BCD**B**END crystals were very low in comparison to the yield obtained when a complex was formed with the commercial endosulfan material. Consequently, no accurate host-guest ratios could be determined using methods such as ^{1}H NMR spectroscopy and elemental analysis for either the BCD**A**END or the BCD**B**END complexes. Similarly, TG and DSC measurements could not be performed as it was impossible to remove a sufficient quantity of complex material from the vials in which the complexes were prepared.

The crystal systems, space groups and unit cell dimensions for the three β-CD-endosulfan inclusion complexes are listed in Table 1. It has previously been shown by Mentzafos *et al* [6] that there is a metric relationship between the monoclinic and triclinic crystal systems for β-CD inclusion complexes that contain similar unit cell dimensions to those listed below. If one were to apply a metric transformation of $a' = a + b$, $b' = b - a$ and $c' = c$ to the *P*1 unit cell it is possible to obtain a unit cell with dimensions similar to those of the *C*2 structure (a = ~19, b = ~24 and c = ~16 Å) (Figure 5). This indicates a direct relationship between the β-CD·endosulfan complexes and therefore the physical properties (host-guest ratio and

thermal profiles) recorded for the BCD**C**END (space group *P*1) are assumed to be similar for the β-CD complexes containing the individual isomers.

Table 1. *Crystal systems, space groups and unit cell dimensions for the three endosulfan-β-CD complexes formed.*

Complex	Crystal system	Space group	Unit cell dimensions					
			a **(Å)**	***b*** **(Å)**	***c*** **(Å)**	***α*** **(°)**	***β*** **(°)**	***γ*** **(°)**
BCD**C**END	Triclinic	*P*1	15.354(1)	15.473(2)	15.480(2)	104.919(5)	103.638(5)	100.823 (6)
BCD**A**END	Monoclinic	*C*2	19.239(2)	24.450(3)	15.888(2)	90	109.544(2)	90
BCD**B**END	Monoclinic	*C*2	19.280(1)	24.431(2)	15.900(1)	90	109.586(1)	90

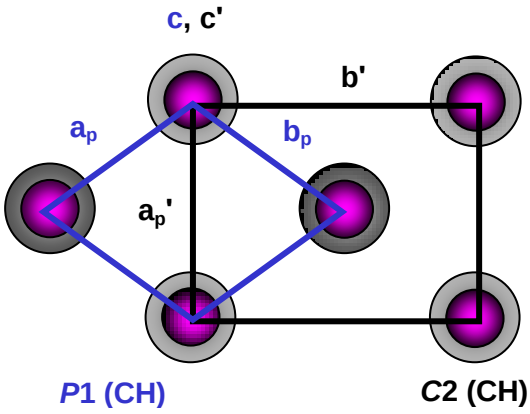

Figure 5. *Schematic diagram of the metrically related unit cells P1 (solid blue line) and C2 (solid black line)*

Single crystal X-ray diffraction data-collections were performed for both the BCD**A**END and BCD**B**END complexes; however, the size and shape of the crystals (thin plates) did not lead to satisfactory data-sets, especially in the case of the BCD**A**END complex. Therefore, only the single crystal X-ray structure of BCD**B**END will be reported and a brief comparison with what was discernible from the partial structure solution of the BCD**A**END complex will be made.

β-CD-β-ENDOSULFAN INCLUSION COMPLEX

Data-collection and space group determination

The single crystal X-ray diffraction data were measured on a Bruker KAPPA APEX II DUO diffractometer. Upon inspection of the reciprocal lattice layers with the program LAYER the Laue symmetry was found to be 2/*m* indicating the monoclinic crystal system.[7] The reflection conditions were *hkl: h + k = 2n, h0l: h = 2n.* Based on these reflection conditions, there were three possible space groups: *C*2, *Cm* and *C*2/*m*. The non-centric space group *C*2 was selected as the host cyclodextrin is chiral.

Structure solution and refinement

Structure solution and guest modelling were particularly challenging for this inclusion complex. The asymmetric unit of the BCD**B**END complex comprises one cyclodextrin molecule, half a guest molecule and 9.8 water molecules. Crystal data and refinement parameters are reported in Table 2. Unit cell refinement and data reduction were performed with the program SAINT.[8] BCD**B**END was found to be isostructural with the complex β-CD·(0.5)((*Z*)-9-dodecen-1-ol)·0.5(C_2H_6O)·9.6H_2O (refcode: ZUZXOH).[9,10] The structure of BCD**B**END was solved by isomorphous replacement using only the host coordinates of ZUZXOH. Data were corrected for absorption by a numerical procedure (face-indexing using SADABS[11]). The primary hydroxyl groups of the host were deleted prior to the first refinement in order to model any possible disorder of the O6 atoms in BCD**B**END. The structure was refined with SHELXH-97 with successive difference Fourier maps revealing the O6 atoms.[12] The glucose units of the host were systematically labelled G1-G7 as shown in Figure 6.

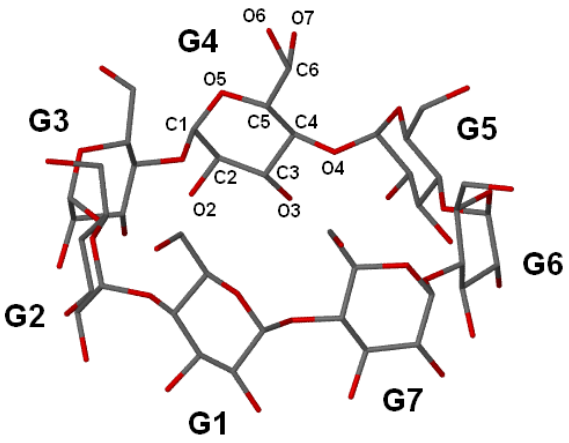

Figure 6. *Macrocyclic structure and numbering scheme of the β-CD glucose units. The disordered primary hydroxyl group is shown with labels O6 and O7 (hydrogen atoms have been omitted for clarity).*

Table 2. *Data-collection and refinement parameters for the BCD**B**END complex.*

Chemical formula	$C_{42}H_{70}O_{35}\cdot(C_9H_6Cl_6O_3S)_{0.5}\cdot 9.8H_2O$
Formula weight	1514.82
Crystal system	Monoclinic
Space group	*C*2
Unit cell constants	
a (Å)	19.239(2)
b (Å)	24.450(3)
c (Å)	15.888(2)
α (°)	90
β (°)	109.544(2)
γ (°)	90
Volume ($Å^3$)	7043.1(1)
Z	4
$Density_{calc}$ ($g\ cm^{-3}$)	1.429
μ [MoKα] (mm^{-1})	0.250
F (000)	3204
Temperature of data collection (K)	100(2)
Crystal size (mm)	0.30 x 0.23 x 0.14
Range scanned θ (°)	1.7 – 24.8
Index ranges	h: -22, 22; k: -28, 28; l: -18, 18
ϕ and ω scan angle (°)	0.5
Total no. of frames	1302
Dx (mm)	60.00
Total no. of reflections collected	20232
No. of independent reflections	6107
No. of reflections with $I > 2\sigma(I)$	4590
No. of parameters	750
R_{int}	0.0381
S	1.867
R_1 [$I > 2\sigma(I)$]	0.1570
No. of reflections omitted	10
wR_2	0.4044
Weighting scheme parameters	a = 0.2, b = 0
$(\Delta / \sigma)_{mean}$	<0.001
$\Delta\rho$ excursions ($e\ Å^{-3}$)	1.90 and -1. 37

One primary hydroxyl oxygen host atom was disordered over two positions and labelled O6G4 and O7G4 (Figure 6). These atoms were modelled by assigning s.o.f.s of *x* and *1-x*, with *x* variable. The value of *x* refined to 0.68. Host atoms O5G7, C5G7, C6G7, O6G7, C6G2, O6G2 and disordered components O6G4 and O7G4 were refined isotropically due to unrealistic thermal ellipsoids resulting when they were treated anisotropically. In order to satisfy the n/p ratio (no. of reflections/total number of parameters defined) which was just below eight, a decision was made to select five well-behaved host atoms (C4G1, C1G2, C1G3, C1G4 and C1G5) and refine them isotropically, thereby reducing the number of parameters and increasing the n/p ratio. These atoms were selected as they form part of the rigid skeleton structure of the CD host molecule and thus have very small and practically isotropic thermal motion.

All host hydrogen atoms were placed in idealised positions using a riding model, except for hydroxyl hydrogen atoms which were refined using a hydrogen bonding searching model (AFIX 83). The hydrogen atoms were refined isotropically with U_{iso} values 1.2 times those of their parent atoms. Fifteen sites for water molecules were located in the difference Fourier map, five of these being refined with full occupancy (O2W, O8W, O9W, O11W and O13W). Water molecules O1W, O4W and O12W are situated on a twofold rotation axis and have an s.o.f. of 0.5. The remaining oxygen sites were assigned a fixed isotropic thermal factor of 0.10 $Å^2$ while the site-occupancies were allowed to vary. Once the site-occupancies had converged after many refinement cycles the s.o.f. values were fixed and the U_{iso} values were allowed to vary. The final site-occupancies and temperature factors for these oxygen atoms are reported in Table 3. A total of 9.8 H_2O molecules per asymmetric unit were accounted for, which is in agreement with that obtained from the TG results, namely 9.7 per CD molecule.

Table 3. *Site-occupancies and U_{iso} values of disordered water molecules for BCD**B**END.*

Atom	Site-occupancy	U_{iso} ($Å^2$)
O3W	0.33	0.11
O5W	0.49	0.12
O6W	0.27	0.10
O7W	0.43	0.13
O10W	0.69	0.12
O14W	0.69	0.10
O15W	0.39	0.08

Modelling of the endosulfan guest

The host-guest ratio is 2:1 for this particular complex and as a result half a guest molecule is present in the asymmetric unit (Figure 7). Atoms C2A, Cl2A, C5A and Cl5A have full site-occupancy while all other atoms in the asymmetric unit have a fixed s.o.f. value of 0.5.

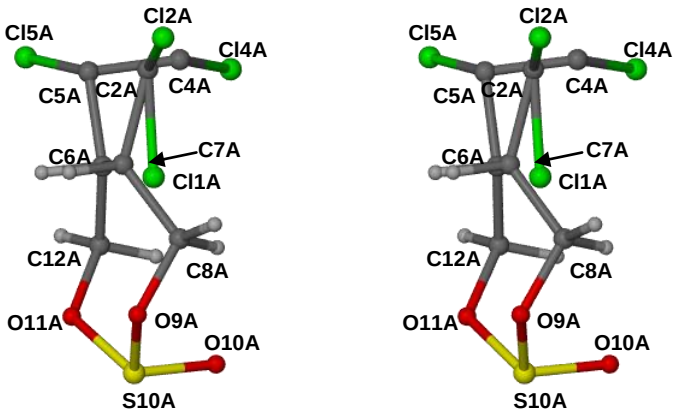

***Figure 7**. Stereoview displaying the guest atoms present in the asymmetric unit.*

The carbon, oxygen and sulphur atoms were assigned a global U_{iso} variable which refined to 0.09 $Å^2$. The individual chlorine atoms were refined isotropically as unrealistic thermal ellipsoids resulted when they were refined anisotropically. Three large difference electron density peaks were found within an equal distance from the centre of the CD cavity. A 180° rotation of the guest molecule around the seven-fold symmetry axis of the β-CD molecule resulted in chlorine atoms Cl2A, Cl4A and Cl5A of the guest overlapping with the residual electron density peaks. Attempts at modelling a second guest component in the asymmetric unit were made; however, the difference Fourier synthesis map did not show any evidence of the carbon atoms of the norbornenyl ring to which the chlorine atoms would attach themselves. Distance restraints were applied to each bond of the guest molecule modelled, since without these restraints, the high difference Fourier electron density peaks belonging to the additional unmodelled chlorine atoms caused the atoms to move away from their original positions. Hydrogen atoms were placed on the partial guest molecule in idealised positions based on a riding model with U_{iso} values 1.2 times those of their parent atoms.

The resultant high R-factor (R_1), weighted R-factor (wR_2) and goodness-of-fit (S) (Table 2) are due to the large number of atoms being refined isotropically, many restraints being used and large residual electron density peaks that were not assigned. There is also some deviation of the modelled guest molecule from its ideal geometry in order to satisfy the twofold-related guest component i.e. the formal double bond in the norbornenyl moiety of one guest molecule is simultaneously required to be represented by a single C-C bond in its

twofold-disordered counterpart and *vice versa*. Further explanation regarding the symmetry-generated guest components will be described under the heading 'Guest inclusion and conformation'.

Geometrical analysis of the BCDBEND structure

Host conformation

The asymmetric unit of the BCD**B**END structure contains a single β-CD molecule (refer to Figure 6 for the labelling scheme used). The seven glucose residues of the β-CD molecule adopt the usual $^4C_1$ chair conformation. The C6-O6 bonds of each glucose unit, except the minor component of G4, are directed away from the CD cavity and are in the (-)-*gauche* conformation relative to the C4-C5 and O5-C5 bonds. The geometrical parameters of the O4-heptagon for the BCD**B**END structure are listed in Table 4. The narrow ranges of the O4-centroid distances (*l*), O4n•••O4(n+1) distances (*D*) and O4(n-1)•••O4n•••O4(n+1) angles (ϕ) illustrate the seven-fold symmetry of the β-CD molecule. The dihedral angles (τ_1 and τ_2) describe the orientation of each glucose unit relative to the O4 mean plane. These values are all positive indicating that the primary rim of each glucose unit tilts towards the centre of the CD cavity.

Table 4. *Geometrical parameters for the host molecules of BCD**B**END.*

Residue	*l* (Å)	*D* (Å)	ϕ (°)	*d* (°)	α[a] (Å)	D_3[b] (Å)	τ_1[c] (°)	τ_2[d] (°)
G1	5.10	4.42	126.8	-0.2	0.011	2.82	9.5	11.1
G2	5.06	4.31	128.2	0.6	0.012	2.83	9.4	11.9
G3	4.97	4.43	129.9	0.5	-0.017	2.76	4.6	4.7
G4	5.02	4.39	128.7	-2.6	-0.016	2.76	8.3	9.0
G5	5.12	4.27	126.9	3.1	0.046	2.86	12.1	12.6
G6	5.01	4.49	128.9	-1.7	-0.032	2.83	6.0	7.6
G7	4.95	4.27	130.6	0.1	-0.004	2.79	15.2	13.4

[a] *mean e.s.d. = 0.008 Å;* [b] *mean e.s.d. = 0.03 Å;* [c] *mean e.s.d. = 0.4°;* [d] *mean e.s.d = 0.4°.*

Guest inclusion and conformation

Through the twofold symmetry operation inherent in the space group *C*2, the guest molecule is completed and a second guest component is generated. Ultimately, there is one guest molecule per β-CD dimer, disordered over two positions (Figure 8). Atoms C4A and Cl4A are positioned on the crystallographic diad and therefore only have site-occupancy values of 0.5 and are shared between the two guest components. A norbornenyl group does not

possess a twofold rotation axis under normal circumstances; thus, the geometry of the norbornenyl moeity is slightly distorted. Nevertheless, there is strong evidence of a single guest molecule being included within the β-CD dimer.

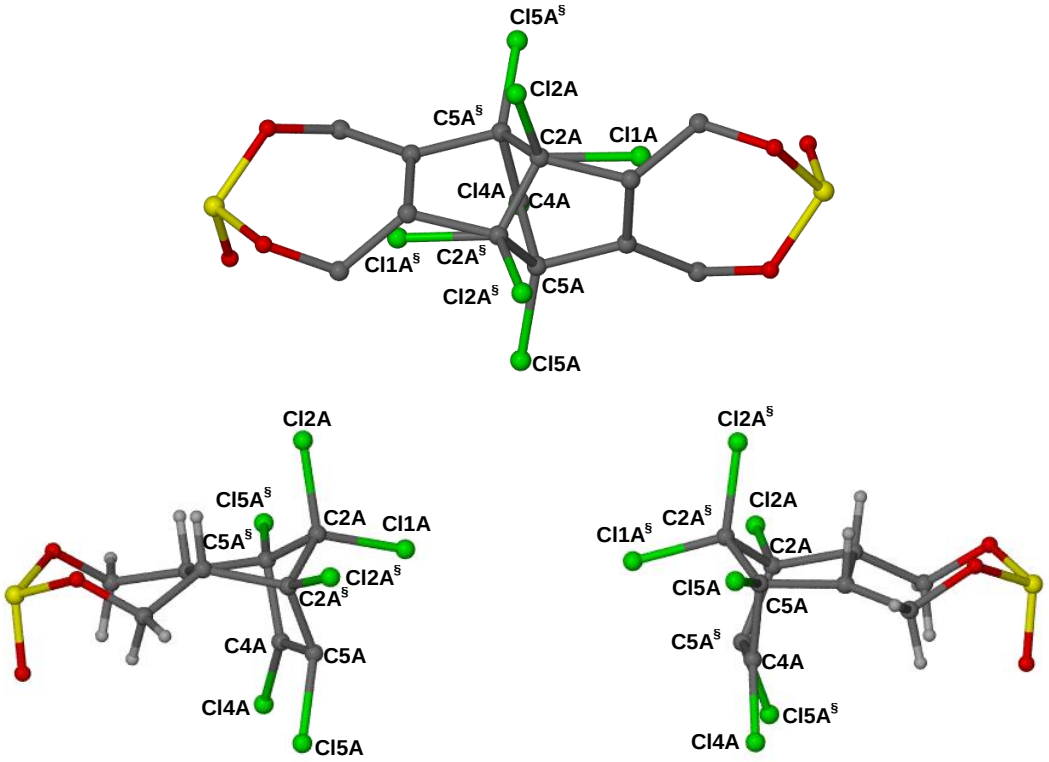

Figure 8. *Deconvolution of the twofold symmetry-related guest molecules present within the β-CD dimer (§Twofold related counterpart).*

Each guest component is situated with five of the six chlorine atoms at the secondary interface of the β-CD dimer and the seven-membered sulfite ring is directed towards the primary rim of the β-CD molecule (Figure 9). A large void is apparently created when only one endosulfan molecule is positioned within the β-CD dimer; however, a single crystal X-ray structure is an averaged representation of what occurs in the crystal. The guest molecule can be positioned so that the dioxathiepine oxide group is either in one half of the β-CD dimer or the other half.

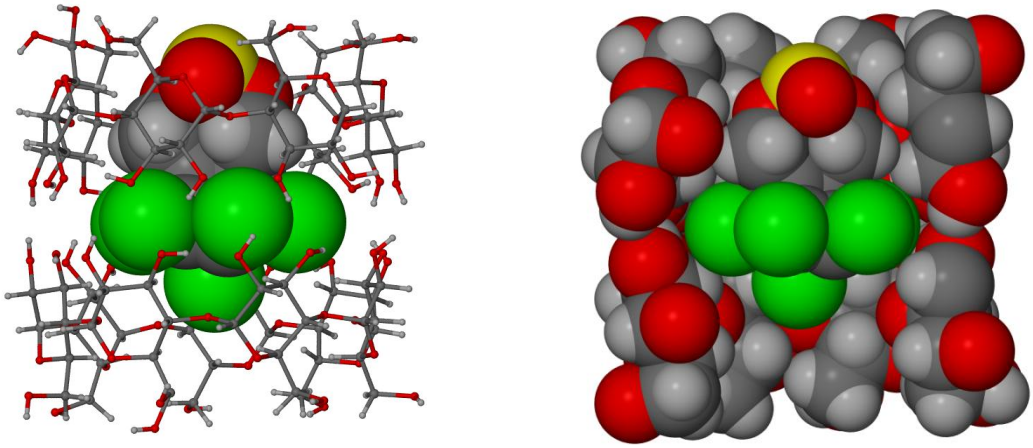

Figure 9. *(a) The relative position of one complete guest component within the β-CD dimer and (b) a cross-sectional space-filling view of a single guest component within the β-CD dimer.*

An important feature of the included β-endosulfan molecule is the conformation of the cyclic sulfite moiety, which is significantly different from that of uncomplexed β-endosulfan, with which the complex was prepared. Uncomplexed β-endosulfan has both the methine and methylene H atoms situated on the same face (*cis* to one another, Figure 10(a)), while the β-endosulfan molecule within the BCD**B**END complex has these two sets of H atoms situated *trans* to one another (Figure 10(b)). In order for the original uncomplexed β-endosulfan molecular conformation to convert to that observed in the BCD**B**END X-ray crystal structure, epimerisation at the sulphur atom is necessary as well as a change in conformation of the seven-membered dioxathiepine oxide ring. The high temperatures used during complex preparation of the BCD**B**END complex may have been sufficient to overcome the energy barrier associated with epimerisation at a sulfite atom. The other possibility is that the β-endosulfan sample contains a mixture of epimers and only one of the epimers can undergo the necessary conformational change, and is then included in the CD. The conformational change may be induced by the CD molecule. According to Schmidt *et al*,[1] who performed MNDO computational studies of the heats of formation for the conformations of endosulfan, the change in conformation we are observing has an energy barrier of ~419 kJ mol^{-1}. These MNDO calculations are, however, based on molecules in the vapour phase at room temperature.

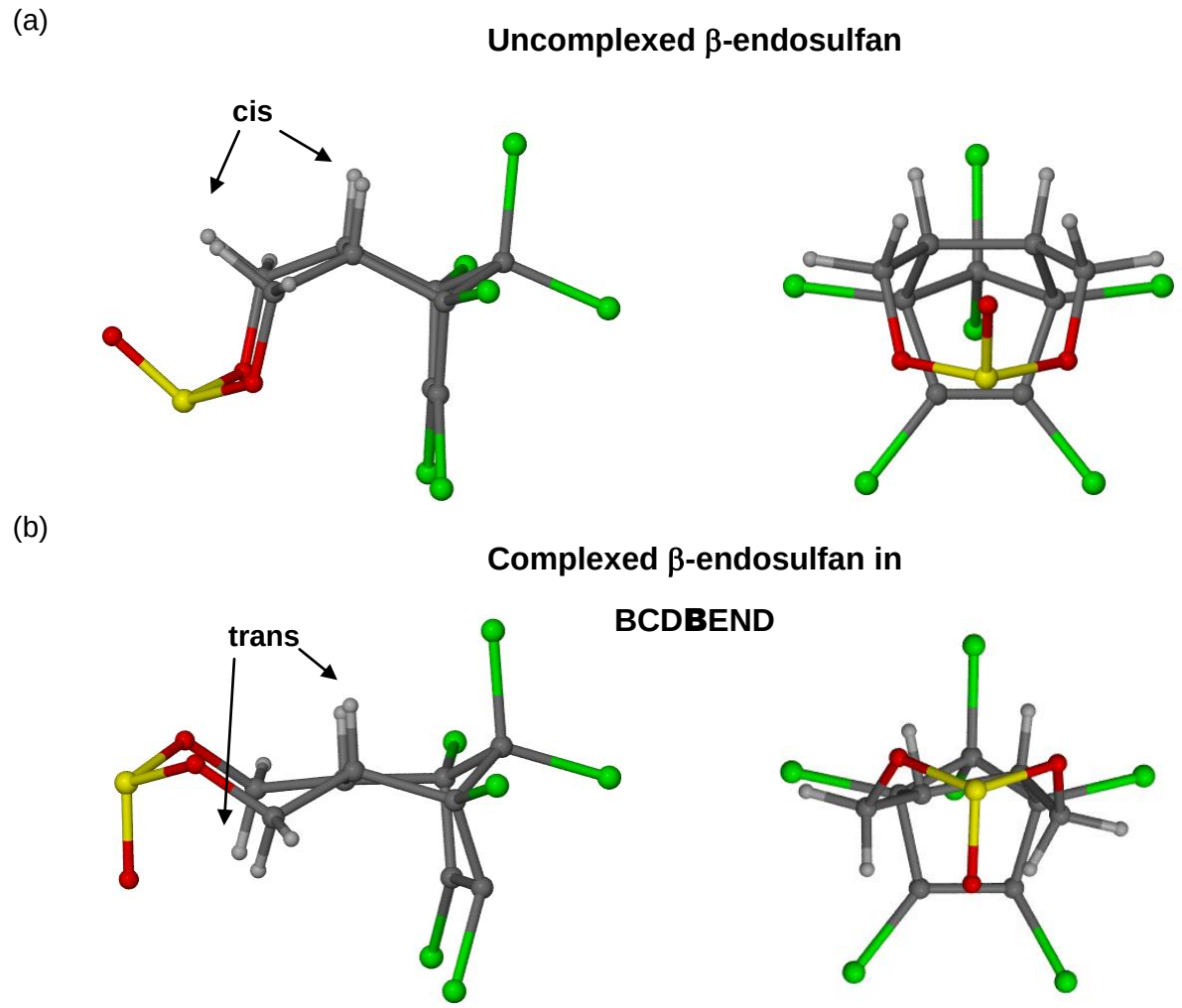

Figure 10. *A side-on and end-on view of the uncomplexed β-endosulfan molecule (a) versus the conformation of β-endosulfan within the BCD**B**END complex (b).*

Intra- and intermolecular interactions

Host interactions

The BCD**B**END structure comprises two host molecules forming a head-to-head dimer with C_2 symmetry. These host molecules are stabilised by a network of intra- and intermolecular interactions at the secondary face of the β-CD dimer. The intra- and intermolecular hydrogen bonds involving the β-CD molecules comprising the dimer as well as the intra- and interlayer hydrogen bonds between adjacent β-CD dimers have been summarised in Table 5. At the primary rim of the CD molecule there are two weak intramolecular (C6–H•••O5(n+1)) hydrogen bonds with an average C•••O distance of 3.39(3) Å and C–H•••O angle of 146°.

Table 5. *Summary of the intra- and intermolecular hydrogen bonds for the CD molecules.*

Interaction	Type	Number	Mean bond length, Å	Mean bond angle, °
Host intramolecular	O3–H•••O2	5	2.81(3)	149
Host-host intermolecular	O2–H•••O3[§]	6	3.11(2)	146
	O3–H•••O3[§]	2	2.81(2)	162
Intra-layer	C2–H•••O3[a]	1	3.37(4)	167
	C1–H•••O2[a]	1	3.37(3)	136
Inter-layer	C6–H•••O6[b]	1	3.51(4)	161

[§]Twofold related counterpart (*1-x, y, 1-z*), [a] *1/2+x, 1/2+y, z*; [b] *1-x, y, -z.*

Guest interactions

Two hydrogen bonds of the type C–H•••Cl are present between the host and guest molecule with a mean C•••Cl distance of 3.58(2) Å and C–H•••Cl angle of 136°. In addition to the halogen-type interactions there is one hydrogen bond that occurs between a carbon atom of the seven-membered ring of the guest and an ethereal oxygen atom of the host (C12A–H•••O4G4; C•••O, 3.39(3) Å and C–H•••O angle of 140°). These interactions are both very weak.

Water interactions

The water molecules are situated between the columns of β-CD dimers (Figure 11). Three of these water molecules (O1W, O6W and O12W) are positioned on a crystallographic twofold rotation axis (Figure 11-green) and have a partial occupancy of 0.5. All the ordered and disordered water molecules form hydrogen bonds with at least one other water molecule or host molecule and are therefore essential in the overall framework of this complex.

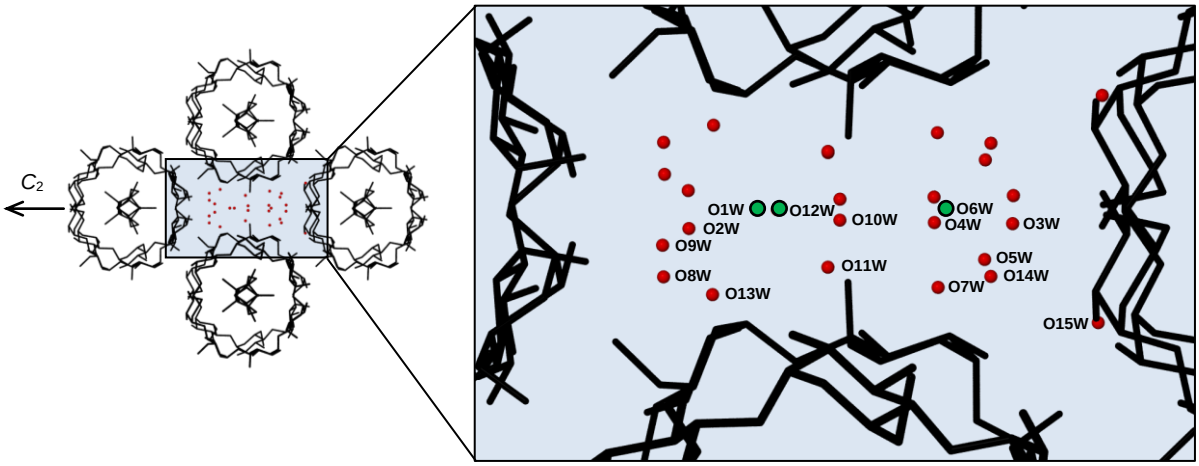

Figure 11. *The interstitial water molecules with their respective labels.*

At the secondary rim of the β-CD molecule, atoms O2G2, O2G4 and O2G6 are hydrogen bond donors to water molecules O12W, O8W and O2W, respectively. At the primary rim, atoms O6G2, O6G3, O6G5 and O6G6 also donate their hydroxyl hydrogen atoms to water molecules O11W, O9W, O4W and O9W, respectively. The mean O•••OW distance for these hydrogen bonds is 2.82(2) Å. O15W is the only oxygen atom of a water molecule that does not bond to any other water molecules. Instead it acts as a link between two adjacent glucose units. Close contact distances apparently exist between water molecules O5W, O6W and O14W; however, when the low s.o.f. values of these disordered atoms are taken into account (Table 3), such contacts are seen to be artefacts. Table 6 lists the OW•••OW hydrogen bond contact distances for the BCD**B**END complex.

Table 6. *OW•••OW contact distances for the BCD**B**END structure.*

Interaction	Distance (Å)	Symmetry operator*
O1W•••O9W	2.80(4)	*-1/2+x, -1/2+y, z*
O2W•••O13W	2.81(3)	*-1+x, y, z*
O2W•••O8W	2.79(3)	*1/2-x, -1/2+y, 1-z*
O3W•••O4W	2.79(7)	*x, y, z*
O3W•••O7W	2.69(8)	*-x, y, -z*
O6W•••O7W	2.68(8)	*x, y, z*
O8W•••O8W	3.11(2)	*1-x, y, 1-z*
O9W•••O13W	2.75(2)	*-1/2+x, 1/2+y, z*
O10W•••O11W	2.83(4)	*2-x, y, 1-z*
O11W•••O13W	2.75(5)	*x, y, z*
O11W•••O7W	2.59(8)	*1+x, y, z*
O12W•••O8W	3.03(5)	*1/2+x, -1/2+y, z*
O12W•••O10W	2.68(4)	*x, y, z*
O14W•••O14W	3.05(5)	*1-x, y, 1-z*
O14W•••O6W	2.59(8)	*1/2+x, -1/2+y, z*
O14W•••O6W	2.97(8)	*1/2-x, -1/2+y, 1-z*

*The symmetry operators refer to the second O atoms.

Crystal packing

Figures 12 (a) and (b) are packing diagrams of the BCD**B**END structure viewed down the *c*- and *a*-axes respectively. These figures illustrate the endless channels formed by the dimeric β-CD units parallel to the *c*-axis. The twofold axes run parallel to the *b*-axis and are present at positions 0, ½ and 1 along both the *a*- and *c*-axes. These twofold axes relate the two β-CD molecules of a dimer to one another as well as relating adjacent dimers. This packing arrangement is characteristic of the channel-type packing motif for β-CD molecules and has been found to occur for many dimeric β-CD inclusion complexes.[6,13] The dimers are arranged in *C*-centred layers and are stacked above one another parallel to the *c*-axis. The relative average shift of consecutive dimers for the BCD**B**END complex is 2.62 Å (R_A value), which is in agreement with the reported average value of 2.7(2) Å for the channel-type structures crystallising in the space group *C*2.[6] Excessive guest disorder is often observed for complexes of the channel-type packing mode.[10,14] Consequently, it is rather remarkable that the guest molecule in the BCD**B**END structure could be successfully modelled even though the overall crystal structure refinement is not of the same standard as those of other β-CD inclusion complexes.

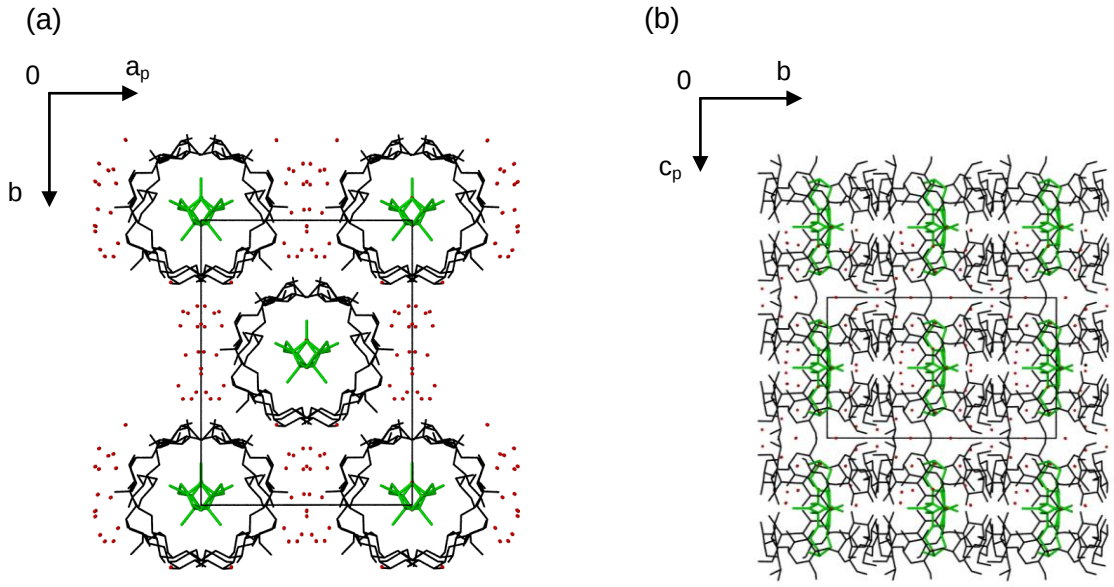

Figure 12. *Packing diagrams of the BCD**B**END structure viewed along [001] (a) and [100] (b).*

Comparative PXRD

Figure 13 displays the calculated PXRD patterns for the BCD**A**END, BCD**B**END and BCD**C**END complexes that were generated from the best structural solutions obtainable from the X-ray data sets of each complex. There is a high degree of similarity among these three patterns. Earlier in this chapter, we reported the unit cell dimensions for these

complexes which showed BCD**A**END and BCD**B**END crystallising in a different space group (*C*2) from that of BCD**C**END (*P*1). As seen from the PXRD patterns, there is a close relationship between the *P*1 and *C*2 dimeric β-CD inclusion complexes. One cannot unequivocally distinguish between the *P*1 and *C*2 β-CD complexes using PXRD methods only. The space group choices for these three complexes were justified based on the Laue symmetries identified from the single crystal X-ray data obtained. The space group *C*2 is specifically characterised by a crystallographic diad at the interface of each dimer, while the *P*1 structure normally possesses a pseudo-twofold rotation axis at the dimer interface.

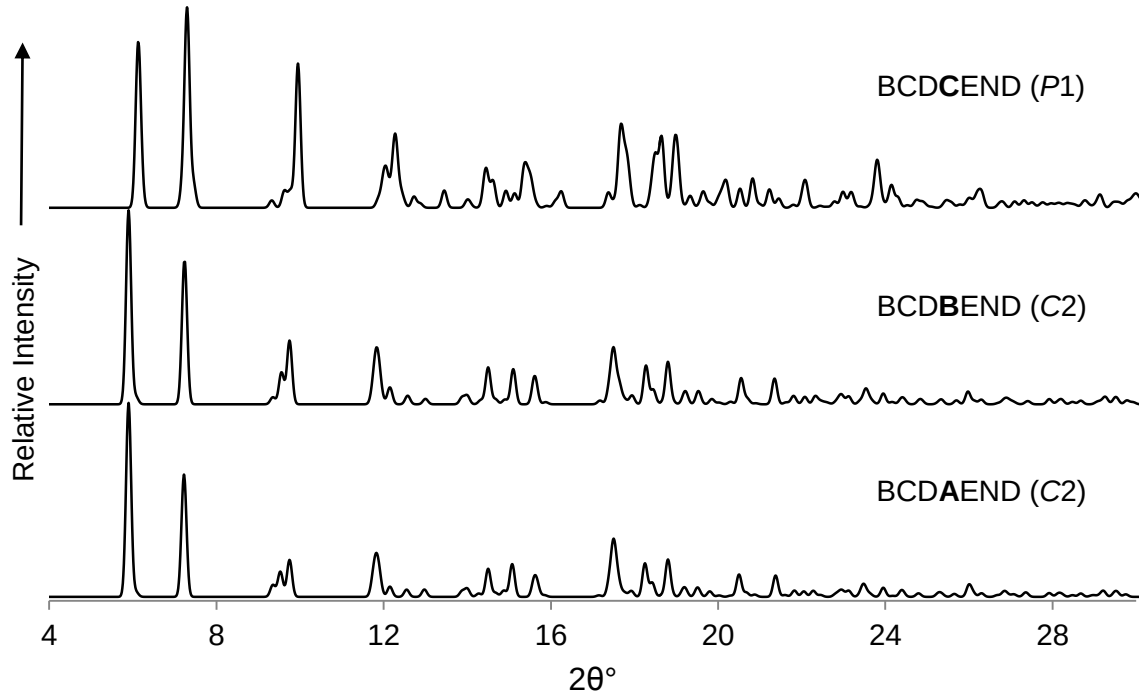

Figure 13. *Calculated PXRD patterns for the BCD**A**END, BCD**B**END and BCD**C**END complexes.*

The BCD**A**END structure was very similar to that of the BCD**B**END complex especially with regard to the host and guest conformations. The initial difference Fourier map after refining the BCD**A**END complex using the host atom coordinates of an isostructural complex, clearly showed the same symmetrical endosulfan molecule as that discussed for the BCD**B**END complex. There were, however, many more electron density peaks surrounding the cyclic sulfite residue, suggesting more than one conformation for the ring.

γ-CYCLODEXTRIN INCLUSION COMPLEX WITH ENDOSULFAN

Complex preparation

A complex of γ-CD with the isomeric mixture of endosulfan was formed using the kneading method. Equimolar quantities (0.025 mmol) of both the CD (35 mg) and endosulfan sample (10 mg) were placed in a mortar with a few drops of distilled water. Together, the two materials were kneaded for 45 min with additional drops of water being added so as to maintain a paste-like consistency throughout the entire process. A PXRD pattern was recorded to confirm whether or not a complex had formed.

Powder X-ray diffraction

The PXRD pattern recorded for the material obtained by kneading was compared to the reference pattern for the one known isostructural series of γ-CD complexes (Figure 14). There is generally a good correlation between the peak positions of each PXRD trace, from which one infers that the inclusion complex is isostructural with the known series. However, the relative peak intensities differ, especially in the 2θ-range from 9 to 18°. The significant differences in the intensities of the corresponding peaks are easily explained. The reference pattern (blue trace) is an averaged pattern for a series of isostructural γ-CD inclusion complexes of small organic guest molecules containing light atoms (C, H, N, O). Instead, the experimental pattern is that of a γ-CD inclusion complex of a highly chlorinated guest molecule; the Cl atoms have large scattering factors for X-rays and hence the magnitudes of the structure factors will be strongly influenced by their presence. The intensities (I_{hkl}) are in turn proportional to the squares of the structure factors (F^2_{hkl}), resulting in a unique intensity distribution in the experimental pattern (pink trace).

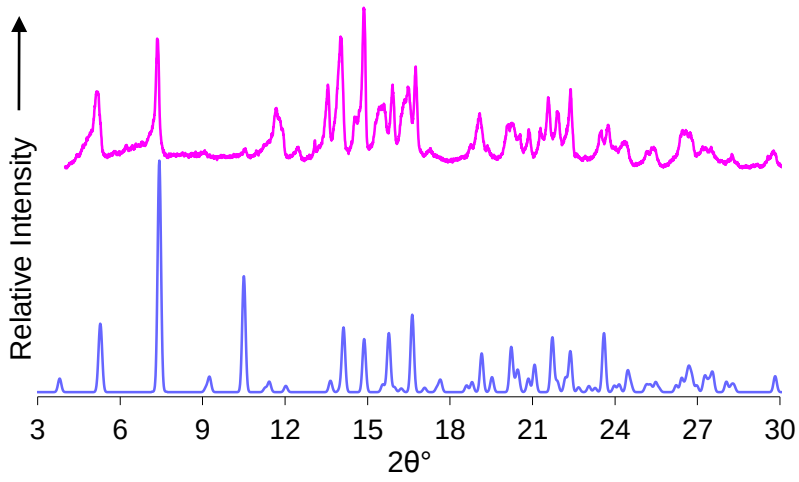

Figure 14. *Calculated reference pattern for γ-CD inclusion complexes (blue) and experimental γ-CD·endosulfan pattern (pink).*

What the comparison in Figure 14 shows is that the unit cell dimensions of the γ-CD·endosulfan inclusion complex are very similar to those of the isostructural series in question (*viz.* a = b ≈ 23.8 Å, c ≈ 23.2 Å), the common space group being $P42_12$ (tetragonal crystal system). This was discussed earlier (see pg. 69 for further details on the packing arrangement of γ-CD inclusion complexes). Given the fact that the host molecules are stacked in perfect alignment with sequence ABC along the crystal *c*-axis, and that the crystallographic tetrad coincides with this arrangement, the guest molecules are invariably disordered within the γ-CD channels. Accurate modelling of the guest molecules under these circumstances is therefore generally very difficult or impossible and in the case of the γ-CD inclusion complex containing endosulfan, such modelling was not pursued, especially since the difference Fourier electron density peaks within the channel had heights typically less than 1 e $Å^{-3}$.

DIMEB INCLUSION COMPLEX WITH β-ENDOSULFAN

Many attempts were made to form inclusion complexes between DIMEB and the three endosulfan samples (α-endosulfan, β-endosulfan and the 7:3 isomeric mixture); however, we were only successful in forming an inclusion complex with the symmetrical β-endosulfan isomer.

Complex preparation

A crystalline complex of DIMEB·β-endosulfan (DMB**B**END) was prepared using the co-precipitation method. 33 mg of DIMEB (0.024 mmol) was dissolved in 2 cm^3 of water to which an equimolar amount of β-endosulfan (10 mg) was added. This solution was stirred continuously at room temperature for ~2 h. An additional 6 cm^3 of water was added and stirring continued. Before filtration took place the sample was heated to 50 °C and then cooled to room temperature. This process was repeated until a clear solution resulted. After filtration of the latter through a 0.45 µm filter the vial was sealed and placed in an oven at 60 °C for a period of one month, at which point single needle-like crystals appeared at the bottom of the vial. Smaller volumes of water resulted in uncomplexed DIMEB crystals forming.

Confirmation of stoichiometry

A 1:1 host-guest stoichiometry was established using ^{1}H NMR spectroscopy through integration of the respective host and guest signals for a sample of the complex crystals dissolved in $CDCl_3$ (Table 7, see Appendix A for full spectrum). TG analysis showed a two-step mass loss indicating the loss of guest prior to decomposition and confirmed the 1:1 host-guest stoichiometry, as explained below.

Table 7. *Integrals of the host and guest protons for DMB**B**END used to confirm the stoichiometry.*

Proton (CD/G) – [Total no. of protons]	δ (ppm)	Integration of peaks		Experimental peak integral/ Theoretical proton no.
		Experimental	Integer	
7 × H**3** (CD) – [7]	3.957	6.938	7	1
7 × H**2** (CD) – [7]	3.297	7.176	7	1
2 × H**3** (G) – [2]	4.143	2.000*	2	1
2 × H**1** (G) – [2]	3.172	1.964	2	1

* Reference integral.

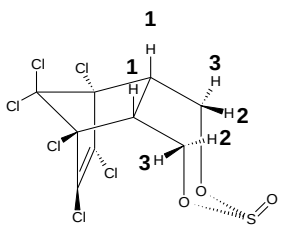

Thermal analysis

The TG and DSC traces for DMB**B**END are shown in Figure 15. There is no indication of water molecules being expelled from the complex at temperatures lower than 200 °C. A mass loss of 26.4 ± 0.2 % (n = 2) in the range 200 to 330 °C corresponds to one guest molecule being released per DIMEB molecule (calcd. for a 1:1 host guest stoichiometry 26.0 %). Guest loss is immediately followed by host decomposition. The DSC trace exhibits two endothermic peaks that correspond to the events described for the TG trace.

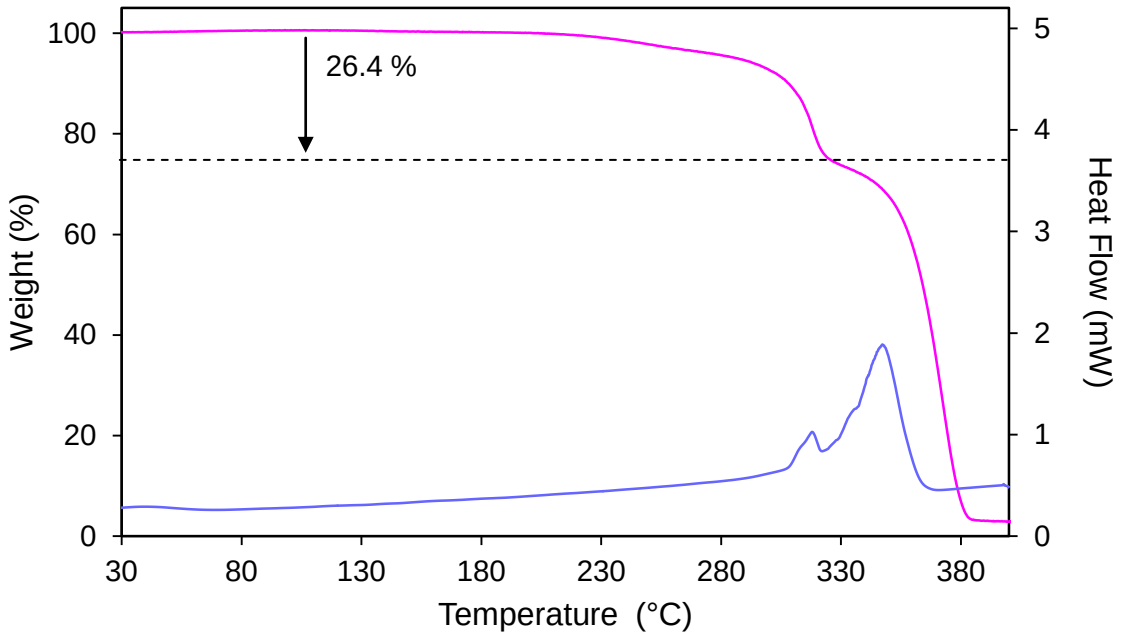

Figure 15. *Representative TGA (pink) and DSC (blue) traces of DMB**B**END.*

The HSM images (Figure 16) show the needle-like complex crystals of DMB**B**END that start to lose their crystalline form at 200 °C. At 300 °C the sample begins to change colour signifying the onset of decomposition. The orange-brown colour at 335 °C is suggestive of host decomposition. These images provide a visual representation of what is recorded in the TG and DSC traces.

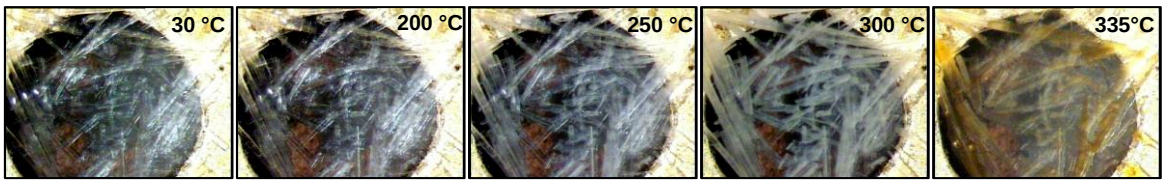

Figure 16. *HSM photographs of the DMB**B**END crystals recorded at various temperatures.*

Crystal structure analysis

Data-collection and space group determination

Intensity data-collection for DMB**B**END was performed on a Bruker KAPPA APEX II DUO diffractometer. The Laue system was found to be *mmm*, indicating the orthorhombic crystal system. Further examination of the systematic absences (*hkl: none, h00: h = 2n, 0k0: k = 2n*), using the program LAYER, confirmed the space group $P2_12_12$.[7] DMB**B**END crystallises with a 1:1 host-guest stoichiometry with two complex units in the asymmetric unit.

Structure solution and refinement

The data-collection and refinement parameters for the DMB**B**END complex are reported in Table 8. The DMB**B**END structure was solved by direct methods using the program SHELXD[15] as no isostructural complex could be identified.[9] The resultant structure solution revealed most of the atoms of the two host molecules and partial guest molecules. The carbon and oxygen atoms of the host were correctly assigned and the guest candidate atoms within the middle of the host cavity were initially deleted to prevent model bias. Refinement of the model was performed using the full-matrix least-squares method implemented in SHELXH-97.[12] The remaining host atoms were located in successive difference Fourier maps. Two guest molecules were easily modelled within the DIMEB host cavities; further discussion regarding the guest molecules will follow below. The host molecules were labelled A1-A7 and B1-B7 with guest molecules A and B positioned in hosts A and B respectively. Two of the non-hydrogen methoxyl atoms (O6 and C8) belonging to methyl glucose unit B5 were disordered over two positions and refined with s.o.f.s of *x* and *1-x*, with *x* variable. An initial value of 0.5 was set and it refined to 0.50. Methyl glucose unit B6 contained a similar type of disorder; however, three atoms (C6, O6 and C8) of the methyl glucose unit were each disordered over two positions and the variable *x* refined to 0.52. Most of the non-hydrogen atoms were refined anisotropically; exceptions included the disordered atoms and a few of the primary and secondary carbon atoms of the methoxyl groups, which showed abnormally large thermal motion. This is expected due to the flexible character of these methoxyl groups. All host hydrogen atoms were placed in idealised positions in a riding model with temperature factors 1.2-1.5 times those of the atoms to which they are attached. More specifically, the hydrogen atoms of the hydroxyl group on position 3 of the methyl glucose units were placed using a hydrogen bond searching model (AFIX 83). Nine of the fourteen residues had their hydrogen atoms placed in idealised positions after refinement, to form the intramolecular hydrogen bonding network typical of

DIMEB molecules. The other five hydrogen atoms required distance restraints as they were placed in a position where no hydrogen bond acceptor atoms were present.

Table 8. *Data-collection and refinement parameters for the DMB**B**END complex.*

Chemical formula	$C_{56}H_{98}O_{35}\cdot C_9H_{12}Cl_6O_3S\cdot 1.04H_2O$
Formula weight	1755.29
Crystal system	Orthorhombic
Space group	$P2_12_12$
Unit cell constants	
a (Å)	26.907(4)
b (Å)	29.784(4)
c (Å)	20.352(3)
$\alpha = \beta = \gamma$ (°)	90
Volume (Å^3)	16310(4)
Z	8
Density$_{calc}$ (g cm^{-3})	1.431
μ [MoKα] (mm^{-1})	0.328
F (000)	7411
Temperature of data collection (K)	133(2)
Crystal size (mm)	0.39 x 0.23 x 0.06
Range scanned θ (°)	1.66 – 25.82
Index ranges	h: -18, 32; k: -36, 33; l: -24, 18
ϕ and ω scan angle (°)	0.5
Total no. of frames	649
Dx (mm)	60.00
Total no. of reflections collected	62617
No. of independent reflections	16670
No. of reflections with I > 2σ(I)	9793
No. of parameters	1790
R_{int}	0.0721
S	1.045
R_1 [I > 2σ(I)]	0.1023
No. of reflections omitted	12
wR_2	0.2617
Weighting scheme parameters	a = 0.155 and b = 39.903
$(\Delta / \sigma)_{mean}$	< 0.001
$\Delta\rho$ excursions (e Å^{-3})	1.02 and -0.69

Three sites were identified as possible positions for water oxygen atoms in the asymmetric unit. Two of these three sites are located within the DIMEB host molecules and one is positioned outside the cavity. The respective water oxygen atoms have been labelled O1W, O2W and O3W and have final s.o.f.s of 1.0, 0.62 and 0.47, respectively. The TG trace did not show any evidence of water being expelled from the crystals prior to guest loss and decomposition. The mass loss expected would be ~1.1 % which is very small and as two of the three water sites are positioned within the DIMEB cavities it is quite possible that the two water molecules occupying them are expelled only upon guest loss and not before.

Modelling of the endosulfan guest molecule

Figure 17 illustrates the labelling scheme used for the endosulfan molecule in the DMB**B**END complex.

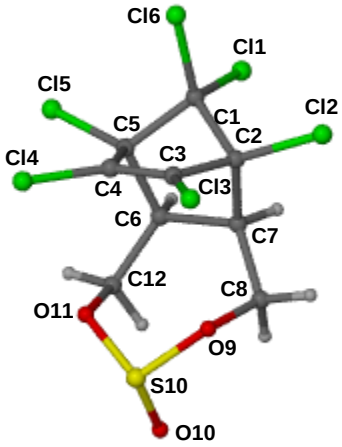

Figure 17. *Labelling scheme used for the endosulfan molecule of the DMB**B**END complex.*

Despite the data having been corrected for absorption using the multi-scan procedure (program SADABS),[11] the two initially placed guest molecules had large residual electron density peaks situated more than 1 Å away from chlorine atoms Cl1, Cl2, Cl3, Cl4 and Cl5. Upon inspection it became evident that by rotating the guest molecule around the seven-fold axis of the DIMEB molecule it was possible to model a second guest component in both host molecules A and B. The two guest components were labelled C and D (Figure 18). Guest molecules A and C are related by a ~54° rotation around the seven-fold host axis as well as a slight lateral displacement, whereas guest molecules B and D are related by a larger rotation angle of ~105° as well as a slight vertical and lateral shift.

Distance restraints were applied to all bonds of each molecule once the second components had been modelled to maintain reasonable guest geometries during refinement. Major guest

components (A and B) refined with a final s.o.f. of 0.72 and the minor guest components (C and D) had a final s.o.f. of 0.28. All guest atoms were refined isotropically with minor components C and D being assigned separate global U_{iso} values, which refined to 0.074 and 0.115 $Å^2$ respectively. Hydrogen atoms were placed on the four guest components in idealised positions based on a riding model. Their temperature factors and s.o.f.s were related to the parent atoms to which they were attached.

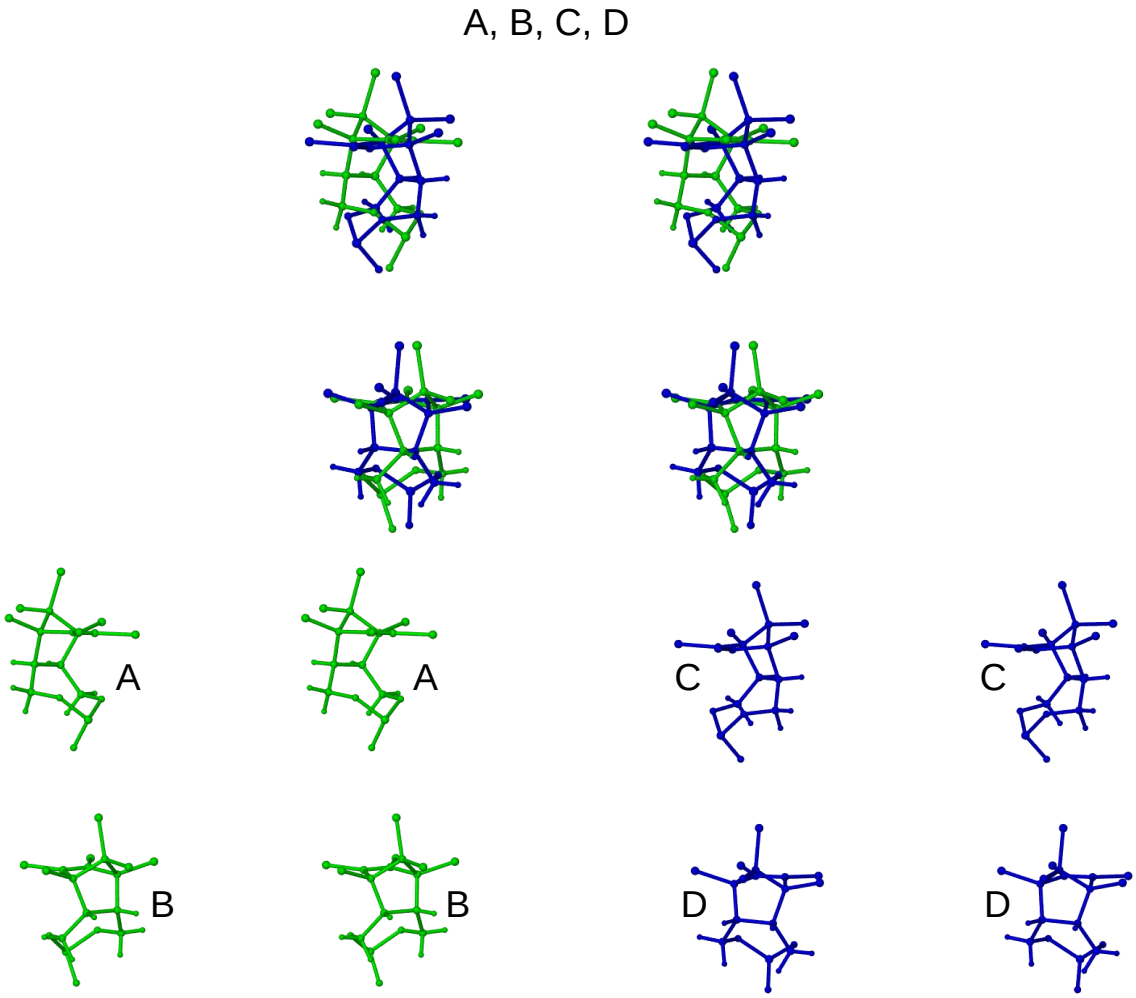

Figure 18. *Stereoviews of the disordered guests A, B, C and D of the DMB**B**END complex and the deconvoluted disordered components A/B (green) and C/D (blue).*

Geometrical analysis of the DMBBEND structure

The crystallographic asymmetric unit of the DMB**B**END complex comprises two DIMEB molecules each encapsulating a guest molecule (Figure 19(a)). Figure 19 (b) illustrates the numbering of atoms for a single methyl glucose unit and the labels used for the individual glucose units of the two host molecules. A geometrical analysis of the host will be made followed by a description of the guest locations and conformations.

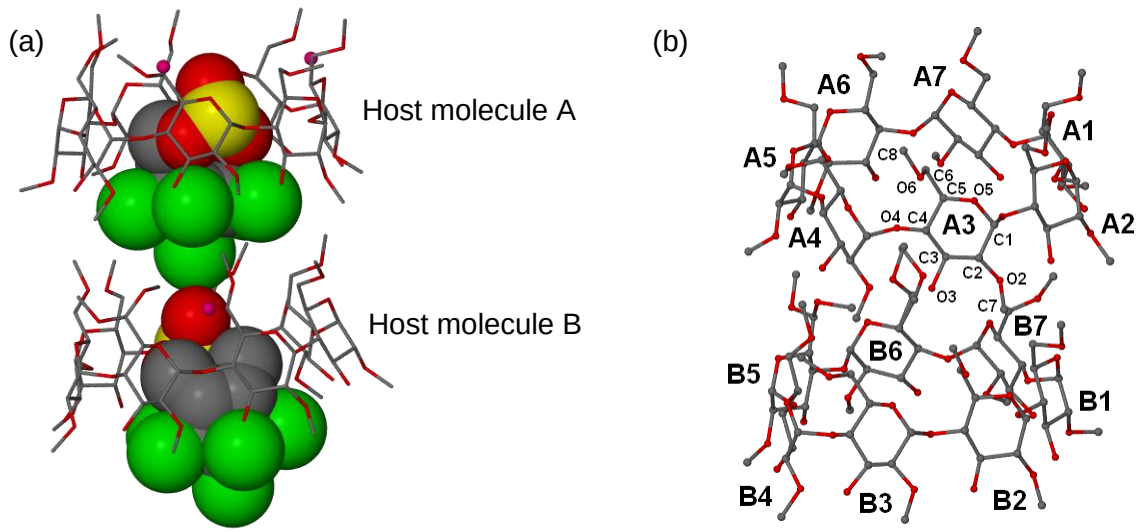

Figure 19. *(a) The asymmetric unit of the DMB**B**END complex with the two major guest components shown (water molecules are shown in pink). (b) Macrocyclic structure and numbering scheme of the DIMEB glucose residues (hydrogen atoms and all minor guest components have been omitted for clarity).*

Host conformation

The primary hydroxyl torsion angle ω (O5-C5-C6-O6) describes the rotation of the C6-O6 bond relative to the cyclodextrin cavity. For host molecule A of DMB**B**END, five of the seven primary methoxyl groups are directed away from the CD cavity with a (-)-*gauche* conformation. The C6-O6 bonds of glucose residues A6 and A7 are directed towards the centre of the CD cavity ((+)-*gauche* conformation). Both disordered methoxyl groups of host molecule B contain one component with a negative ω torsion angle and one with a positive ω torsion angle. The C6-O6 bonds of glucose residues B1, B2, B3 and B7 have a *(-)-gauche* orientation and are directed away from the CD cavity. The primary methoxyl group of glucose residue B4 adopts the (+)-*gauche* conformation.

Table 9 lists the geometrical parameters for the O4-heptagons of the two host molecules. In addition to these parameters, the deviation of O4 atoms from the mean O4 plane (α), the O2•••O3 intramolecular contact distances and the dihedral angles (τ_1 and τ_2) are listed. The range of values obtained for the distances between each O4 atom and the centroid of the CD (*l*) as well as the distances (*D*) and angles (ϕ) between successive O4 atoms of the heptagons are comparable for the two host molecules. The O4 atoms of the heptagon do not deviate significantly from the O4 mean plane, the largest distances being 0.113 and 0.149 Å for atoms O4A4 and O4B2. The τ_1 and τ_2 tilt angles are all positive indicating the general inward trend of all glucose residues towards the centre of the CD cavity.

Table 9. *Geometrical parameters for the host molecules of the DMB**B**END complex.*

Residue	*l* (Å)	*D* (Å)	ϕ (°)	*d* (°)	α^a *(Å)*	$D_3{}^b$ (Å)	$\tau_1{}^c$ (°)	$\tau_2{}^d$ (°)
A1	5.07	4.25	126.2	-1.7	-0.075	2.83	16.2	14.6
A2	5.04	4.39	129.1	-4.4	0.005	2.79	12.5	13.3
A3	5.00	4.31	128.0	8.8	0.105	2.71	9.8	10.2
A4	4.93	4.42	130.4	-6.8	-0.113	2.82	1.4	3.9
A5	5.08	4.31	127.7	2.7	0.024	2.85	13.6	15.8
A6	5.12	4.41	125.4	-2.4	0.018	2.84	6.2	5.8
A7	4.87	4.40	132.8	4.0	0.036	2.91	12.0	14.2
B1	4.94	4.47	130.5	8.6	0.070	2.78	8.0	9.3
B2	4.99	4.20	129.6	-7.4	-0.149	2.87	12.2	11.4
B3	5.12	4.46	126.1	0.0	0.051	2.84	18.7	21.6
B4	4.99	4.37	129.8	4.4	0.087	2.78	6.7	8.2
B5	5.02	4.37	128.7	-1.5	-0.070	2.79	11.1	12.9
B6	5.07	4.43	128.2	-1.3	-0.045	2.88	17.1	16.2
B7	5.10	4.28	126.7	-2.4	0.056	2.75	12.5	13.7

[a] mean e.s.d. = 0.006 Å; [b] mean e.s.d. = 0.01 Å; [c] mean e.s.d. = 0.3 °; [d] mean e.s.d = 0.3 °.

The overall geometries of these two independent host molecules are not significantly different. However, when relating the positions of the two independent macrocycles in the asymmetric unit to one another, we observe a lateral shift between them. As the two O4 mean planes are not parallel (interplanar angle 4.23(4)°), this lateral shift has minimum and maximum values of 1.3 Å (R_A) and 1.9 Å (R_B) respectively.

Guest inclusion and conformation

Space-filling diagrams Figures 20 (a) and (b) illustrate the position of the endosulfan molecule within the DIMEB molecules. In both host molecules A and B the hexachloronorbornene group is situated at the secondary rim of the DIMEB host molecules and the dioxathiepine oxide ring is positioned closer to the primary rim. Chlorine atoms Cl1, Cl2, Cl3, Cl4 and Cl5 of the guest molecules are roughly coplanar, with Cl6 extending into the narrower primary rim of a DIMEB molecule positioned above. Figure 20 (c) displays a projected view down the two DIMEB cavities and illustrates once again the wider secondary rim that accommodates the radial chlorine groups. The narrower primary rim contains the sulfite group which interacts with a water molecule that is deeply embedded within the DIMEB cavity (Figure 20 (d)).

A common conformation is adopted for all four guest component molecules. The bond lengths and angles are consistent with those reported for the uncomplexed β-endosulfan

molecule by Byrn *et al*.[4] There is no doubt that the DMB**B**END complex includes the β-endosulfan isomer in its original conformation. This is also evident from Figure 18.

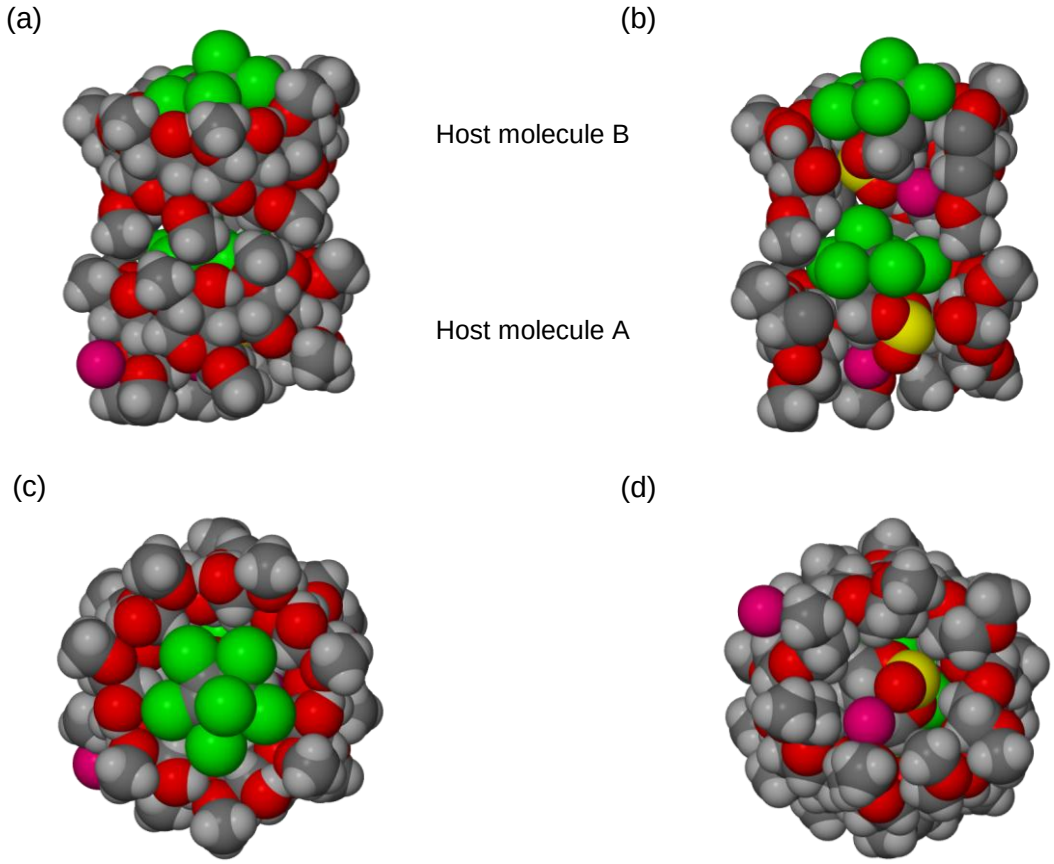

Figure 20. *Space-filling diagrams of the major guest components within the DIMEB cavities. The partial water molecules are shown in pink. (a) A side view, (b) a cross-sectional view, (c) a view from the secondary rim of host molecule B and (d) a view from the primary rim of host molecule A.*

Intra- and intermolecular interactions

Intramolecular, host-host and host-guest interactions

Fourteen intramolecular hydrogen bonds are shown in Figure 21 and their O2•••O3 contact distances (D_3) have been previously listed in Table 9. These hydrogen bonds have an average O–H•••O angle of 143° and are important in maintaining the 'round' shape of the DIMEB host molecules. Other intramolecular hydrogen bonds of the type C6–H•••O5(n+1) assist in stabilising the flexible primary methoxyl groups. There are several weak intraglucose interactions of the type C7–H•••O3 and C8–H•••O3/O5/O6. These hydrogen bonds have a mean C•••O contact distance of 3.14(2) Å and C–H•••O angles that range between 114 and 144°.

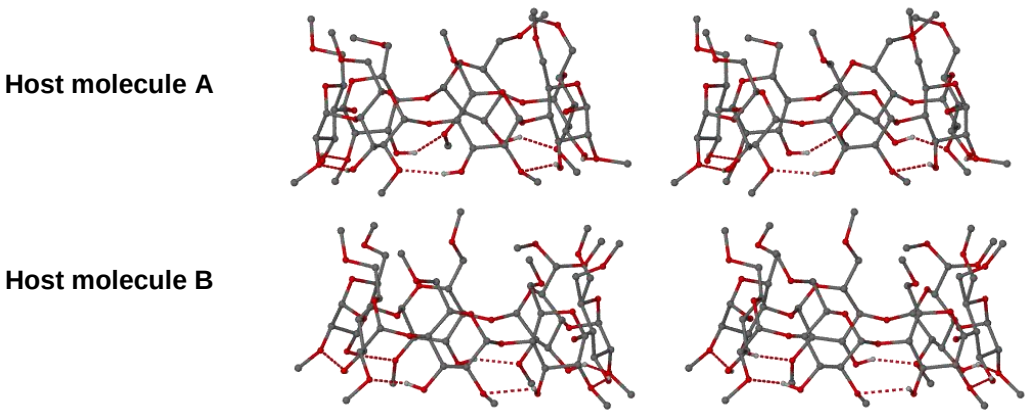

Figure 21. *Stereoview of the host intramolecular hydrogen bonding network for the DMB**B**END complex.*

The intermolecular host-host and host-guest hydrogen bonds are weak C–H•••O interactions (Table 10). The host-host interactions occur only between host molecules of adjacent columns with no significant hydrogen bonds being formed between the DIMEB molecules that stack on top of one another. Both guest molecules (A and B) form a C–H•••O hydrogen bond with host molecules A and B respectively. Guest components C and D do not form any significant host-guest interactions.

Table 10. *Host-host and host-guest hydrogen bonding interactions for the DMB**B**END complex.*

Interaction	H•••A (Å)	D•••A (Å)	D-H•••A (°)
Host-host			
C7A2–H7A5•••O3A5[a]	2.34	3.23(2)	151
C8A2–H8A6•••O3B6[b]	2.49	3.47(3)	176
C2A3–H2A3•••O5B7[b]	2.51	3.23(1)	129
C2A3–H2G3•••O6B7[b]	2.49	3.46(1)	163
C8A4–H8AY•••O6A3[c]	2.59	3.37(2)	137
C2A5–H2A5•••O6B1[d]	2.35	3.34(1)	167
C6A7–H6AB•••O3B2[e]	2.51	3.49(2)	170
C7B1–H7B1•••O6A4[a]	2.46	3.35(2)	150
C2B2–H2B2•••O5A7[b]	2.45	3.43(2)	168
C8B2–H8B5•••O3A7[b]	2.49	3.31(2)	140
C7B3–H7B7•••O5A1[b]	2.49	3.25(2)	134
Host-guest			
C12A–H12A•••O4A2	2.54	3.46(2)	155
C12B–H12D•••O4B2	2.48	3.41(1)	157

Symmetry codes: [a] *3/2-x, 1/2+y, 1-z;* [b] *-1/2+x, 3/2-y, 1-z;* [c] *1-x, 1-y, z;* [d] *3/2-x, -1/2+y, 1-z;* [e] *1/2+x, 3/2-y, 1-z.*

Water and guest-guest interactions

Water molecules O1W (full occupancy) and O3W (s.o.f. = 0.47) are situated within host molecules A and B respectively. These water molecules form hydrogen bonds with the terminal oxygen atom of the sulphite group of guest molecules A, B and C. Figure 22 displays two of these interactions, as the minor components (guest molecules C and D) have been omitted for clarity. Water molecule O1W is capable of forming a hydrogen bond with both major and minor guest components within host molecule A (O1W•••O10A, 2.87(2) Å and O1W•••O10C, 2.64(4) Å). The O•••O contact distance between partial water molecule O3W and atom O10B of guest molecule B is 2.71(3) Å. Water molecules O1W and O3W perform a bridging function as they bond to atoms O6A7 and O6B4 of the respective host molecules in which they are included (O1W•••O6A7, 2.87(2) Å and O3W•••O6B4, 2.83(3) Å). O2W (not shown) is located outside the host molecule and also acts as a bridging water molecule, this time, however, linking two host molecules rather than a guest and host molecule as seen for atoms O1W and O3W. O2W is a hydrogen bond donor to atoms O6A2 and O6C5^{i} of host molecule B with O•••O contact distances of 2.87(2) and 2.80(3) Å respectively (*i = 3/2-x, 1/2+y, 1-z*).

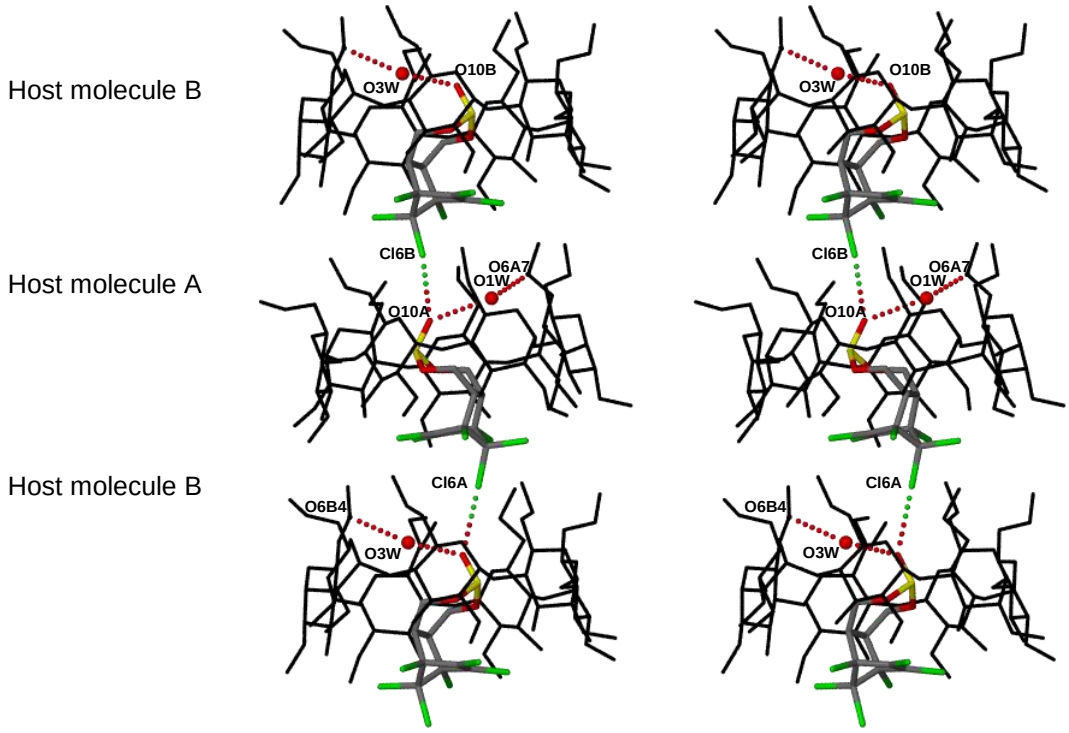

Figure 22. *The water-guest, water-host and the halogen bond interactions for the major guest components of the DMB**B**END complex.*

With regard to the interactions between the guest molecules, there is an intermolecular interaction between the chlorine atom (Cl6) of one guest and the oxygen atom (O10) of the guest situated below. This halogen-oxygen interaction links the guest molecules in infinite chains within the host molecules. The halogen-oxygen contact distances (Cl•••O) and C-Cl•••O bond angles are listed in Table 19. These values are in agreement with the mean Cl•••O contact distance (3.1(1) Å) and range of C-Cl•••O angles (136-174°) found from crystal structures deposited in the CSD.[9] The Cl•••O contact distances are less than the sum of their van der Waals radii indicating the attractive nature and hence their stabilising effect on the crystal structure.

Table 19. *Guest-guest contacts for the DMB**B**END complex.*

Interaction	Cl6•••O10 (Å)	C1-Cl6•••O10 (°)
C1A-Cl6A•••O10B	3.14(1)	169
C1C-Cl6C•••O10D	3.16(5)	157
C1B-Cl6B•••O10A[a]	3.12(1)	143
C1D-Cl6D•••O10C[a]	3.40(4)	173

Symmetry codes: [a] *x, y, 1+z*

Crystal packing

The DIMEB molecules pack head-to-tail in infinite columns parallel to the *c*-axis (Figure 23). These columns adopt a zig-zag arrangement in the *x*-direction of the [001] projection (Figure 24). The complex units assemble in close-packed layers parallel to the *xy*-plane with the chlorine atoms of each guest molecule occupying the space between these layers. The host and guest molecules of each column align in an anti-parallel arrangement as a result of the twofold screw axes in the *x*- and *y*-directions.

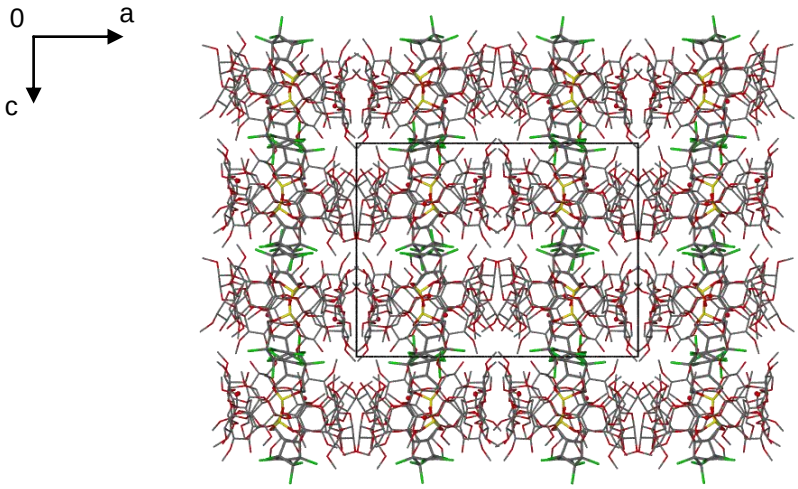

Figure 23. *Packing arrangement of DMB**B**END viewed along [010].*

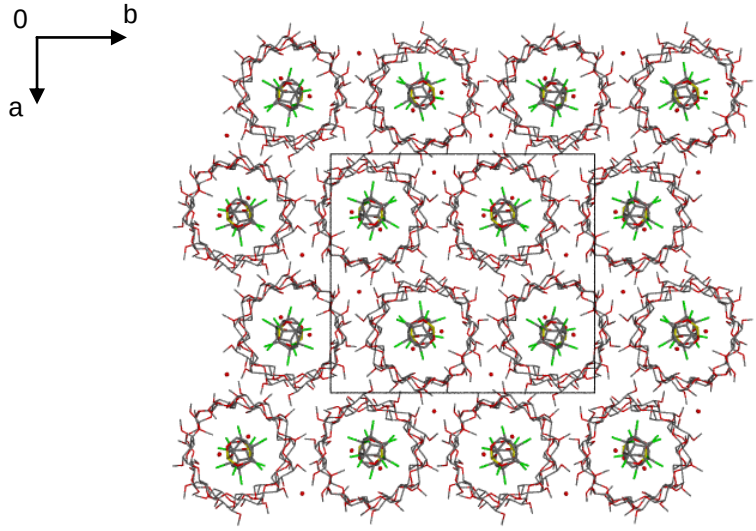

Figure 24. *Packing arrangement of DMB**B**END viewed along [001].*

Comparative PXRD

The calculated PXRD pattern generated from the final single crystal X-ray structure solution was compared with the experimental PXRD trace (Figure 25). There is good correlation of the peak positions and peak intensities between these two PXRD patterns indicating that the single crystal structure is representative of the bulk material. A slight shift of the experimental pattern to lower 2θ values when compared to the calculated pattern can be attributed to the different temperatures of data-collection for these two samples.

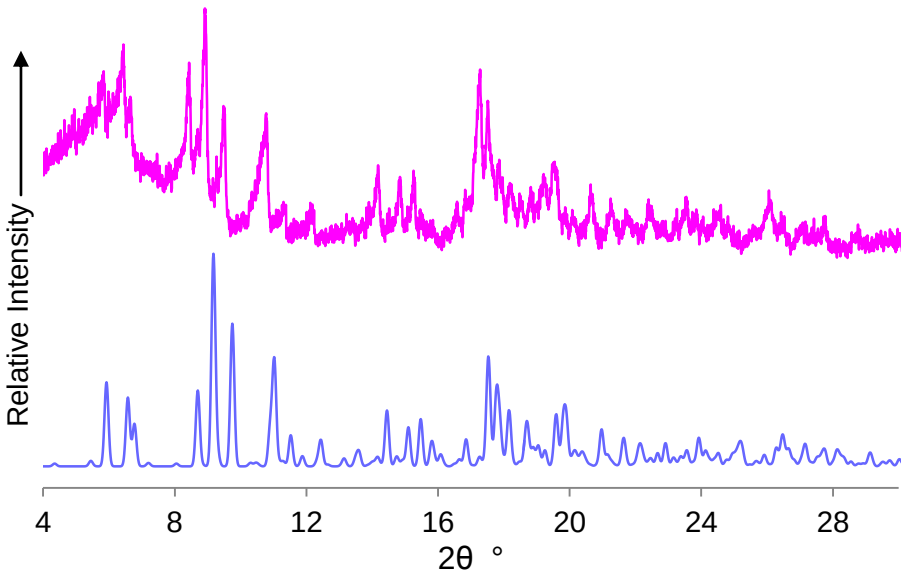

Figure 25. *Calculated (blue) and experimental (pink) PXRD traces of DMB**B**END based on data collected at 133 K and 294 K respectively.*

RAMEB COMPLEX WITH ENDOSULFAN

The derivatised CD, randomly methylated β-CD (RAMEB), was investigated for its possibility of forming an inclusion complex with the commercial sample of endosulfan. As RAMEB is a non-crystalline CD this question was investigated using powder X-ray diffraction only.

Complex preparation

Standard grade randomly methylated β-CD (RM-β-CD) with a degree of substitution (D.S.) of 1.6-1.9 methyl groups per glucose unit was used. A molecular weight of 1309 g mol^{-1} for RAMEB was employed to calculate the mass of sample required to prepare the kneaded and physical mixtures of RAMEB and endosulfan. 64 mg of RAMEB (0.05 mmol) and 20 mg (0.05 mmol) of endosulfan were placed in a mortar to which a single drop of distilled water was added. The mixture was kneaded for 45 min and analysed with PXRD. For the physical mixture, equimolar quantities of RAMEB and endosulfan were placed in a vial and gently mixed with a spatula to ensure homogeneity.

Powder X-ray diffraction

The PXRD patterns of the material obtained by kneading, the physical mixture as well as the individual components are shown in Figure 26.

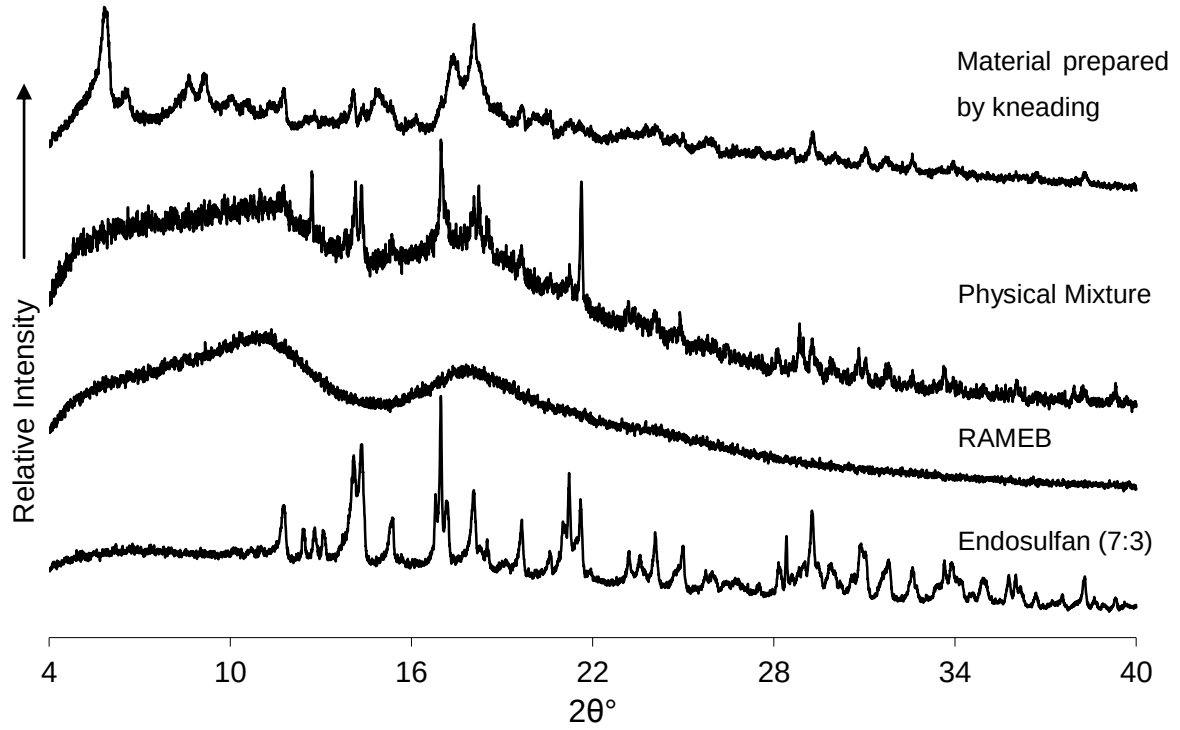

Figure 26. *PXRD patterns of the commercial sample of endosulfan, uncomplexed RAMEB, the physical mixture of RAMEB and endosulfan, and the sample obtained by kneading RAMEB and endosulfan.*

The pattern for the endosulfan sample presents a characteristic PXRD profile for a crystalline material. The RAMEB trace on the other hand shows a diffuse pattern typical of an amorphous product. The pattern shown for the physical mixture can be obtained by the superimposition of the pure component patterns. The pattern from the material obtained by kneading RAMEB and endosulfan is completely different, displaying sharp peaks, which is unusual for RAMEB complexes. Normally, one would expect the peaks of the crystalline guest component to disappear if an inclusion complex were formed as a result of the guest molecules being included within the non-crystalline RAMEB matrix. The sample obtained by kneading displays new peaks at low 2θ values that do not coincide with peaks from the uncomplexed endosulfan sample. This particular phenomenon has been reported previously when attempts at forming an inclusion complex with RAMEB and β-Lapachone were made by Cunha-Filho *et al*.[16] They suggested that the kneading process promotes partial crystallisation of RAMEB.

The PXRD pattern of the RAMEB and endosulfan sample that were kneaded together was compared with the calculated DIMEB·β-endosulfan complex pattern (Figure 27) and showed some similarities. This confirms that some order of the complex units is induced upon kneading the two materials together. Recrystallisation of the product from distilled water was attempted. However, only after all the water had evaporated was there a solid glassy precipitate at the bottom of the vial. The material was viewed under a polarising microscope but the material showed no birefringence, implying that it was optically isotropic and hence amorphous.

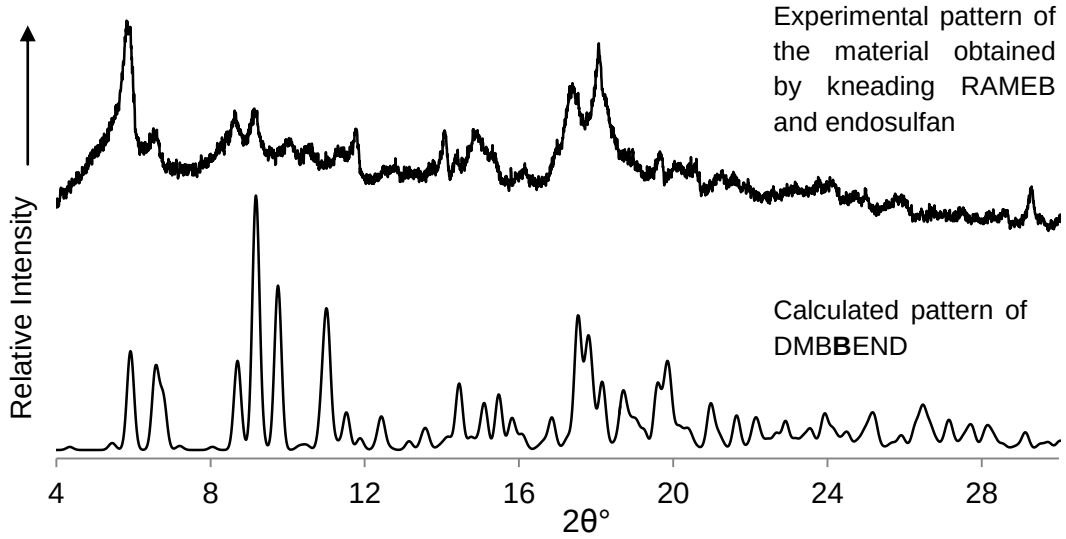

Figure 27. *PXRD pattern of the material obtained by kneading RAMEB and endosulfan (top) and the pattern calculated from the single crystal structure of the complex DMB**B**END (bottom).*

SEMI-QUANTITATIVE SOLUBILITY STUDIES

The reported aqueous solubility of endosulfan at 25 °C is 0.33 mg dm^{-3}.[17] Due to this very low solubility, semi-quantitative solubility studies were conducted in a 50:50 v/v water-ethanol solution. This particular solvent system allowed an accurate calibration curve to be obtained from which the concentration of endosulfan could be determined using UV spectrophotometry.

The solubility of endosulfan was investigated in the presence of five CDs, namely α-CD, β-CD, γ-CD, RAMEB and HP-β-CD. 10 mM solutions of each CD were prepared to which an excess quantity of the isomeric 7:3 endosulfan sample was added. These solutions were stirred continuously at 25 °C for ~72 h, after which the solutions were filtered through a 0.45 µm filter, and the UV-vis spectra recorded. The concentration of dissolved endosulfan was determined from the absorbance at a wavelength maximum of 213 nm. Table 20 lists the solubility enhancement factors (SEF) for endosulfan in the presence of each CD. The SEF was calculated by dividing the concentration of endosulfan in the presence of a CD molecule by the concentration of endosulfan determined in a 50:50 v/v water-ethanol solvent system. No conclusive results were obtained with β- and γ-CD as these were the only two samples that become turbid upon addition of endosulfan. The UV-vis spectra for these solutions did not show the typical spectra for endosulfan, suggesting that the CD molecules formed insoluble complexes with endosulfan which were filtered off before the UV-vis spectra were recorded. There were, however, 3.6- and 5.9-fold increases in the solubility of endosulfan in the presence of RAMEB and HP-β-CD respectively. It is well-documented that the solubility of many compounds is not sufficiently increased using unmodified CDs. Derivatised CDs can, however, increase the solubility of non-polar organic molecules to higher concentrations than can be achieved with unmodified CDs.[18] It is therefore not surprising that the highest SEF value for endosulfan occurs in the presence of HP-β-CD.

Table 20. *Solubility enhancement factor for endosulfan in 10 mM CD solutions.*

Cyclodextrin	Concentration of endosulfan (M)	Solubility Enhancement Factor
Absence of CDs	2.8×10^{-4}	1.0
α-CD	2.5×10^{-4}	0.9
β-CD	-	-
γ-CD	-	-
RAMEB	10.2×10^{-4}	3.6
HP-β-CD	16.6×10^{-4}	5.9

DISCUSSION

Complex preparation

Both the kneading and co-precipitation methods resulted in complexation of the commercial sample of endosulfan (a mixture of isomers) and β-CD. The individual isomers of endosulfan both formed a complex with β-CD using the co-precipitation method; however, only the BCD**B**END complex produced crystals that diffracted sufficiently well to enable collection of a full X-ray dataset from which the single crystal structure could be determined. The yields of crystals obtained for the complexes of the individual isomers with β-CD were exceptionally low, precluding their detailed characterisation. Complex formation between γ-CD and endosulfan (7:3), and between RAMEB and endosulfan, were achieved using the kneading method, while preparation of the DMB**B**END complex was accomplished using the co-precipitation method.

The latter method is ideal for forming single crystals of the complexes which can be fully characterised by the techniques described in this chapter; however, this method is not practical when applied to large-scale complex preparation due to the size of reaction vessels required and the problems associated with disposal of the wastewater. The β-CD, γ-CD and RAMEB endosulfan complexes could all be prepared using the kneading method, which is the preferred route to achieving complexation when large quantities of these complexes are required in an industrial setting.

Complex stoichiometry and thermal analysis

The host-guest stoichiometry of the β-CD·endosulfan complexes was deduced using elemental analysis. The DMB**B**END complex stoichiometry was determined using ^{1}H NMR spectroscopy which unequivocally demonstrated a 1:1 host-guest ratio. The thermal profiles of both the β-CD·endosulfan complex and DMB**B**END complex were evaluated using TGA and DSC. The DSC trace of the DMB**B**END complex displays two endotherms, which are associated with guest loss and decomposition. The first endothermic peak in the DSC trace of DMB**B**END occurs at only 317 °C. β-endosulfan itself, has been shown to undergo a solid-solid phase transition at 151 °C which is due to the conversion of β-endosulfan into α-endosulfan.[1] As DIMEB encapsulates the β-endosulfan isomer, it prevents the isomeric β-endosulfan to α-endosulfan conversion. The BCD**C**END complex is not as stable as the DMB**B**END complex as the crystals start to disintegrate as soon as the water molecules are

expelled at 80 °C. This highlights the importance of water molecules in maintaining the crystalline structure of a β-CD complex.

Conformation of the host and guest molecules

Single crystal X-ray diffraction allowed a complete analysis of the host and guest molecules for the BCD**B**END and DMB**B**END complexes. Both β-CD and DIMEB contain at least one hydroxyl group per glucose unit at the secondary rim of the macrocylic cavities. These hydroxyl groups are essential in maintaining the round conformation of the β-CD and DIMEB host molecules. The deviations of atoms from the O4 mean planes are smaller for the BCD**B**END complex (range 0.004 to 0.046 Å) than for the DMB**B**END complex (range 0.005 to 0.149 Å). The tilt angles (τ_1 and τ_2) for both BCD**B**END and DMB**B**END are positive and the range is once again smaller for the BCD**B**END complex. The methoxyl groups of a DIMEB host molecule induce a slightly greater tilt of the glucopyranose units towards the centre of the CD cavity; however, the tilting of the glucose units for the DIMEB molecule are not as large as that seen for the fully methylated CD series.

It is interesting to note that the TRIMEA and TRIMEB host molecules did not form solid-state inclusion complexes with either of the individual isomers of endosulfan nor with the commercially available 7:3 α/β mixture. This could be due to the narrow width of the CD cavity in the case of the TRIMEA host molecule and the highly distorted conformation the TRIMEB molecule typically adopts due to the lack of O-H•••O intramolecular hydrogen bonds.

The guest conformations in the BCD**B**END and DMB**B**END complexes are significantly different. The DMB**B**END complex contains β-endosulfan in a conformation that corresponds to that of the uncomplexed β-endosulfan isomer. The BCD**B**END complex, however, contains the endosulfan molecule in an alternative conformation which is rather similar to the purported 'α-endosulfan' crystal structure (Figure 28) that was shown in the 1997 paper of Schmidt *et al*.[2]

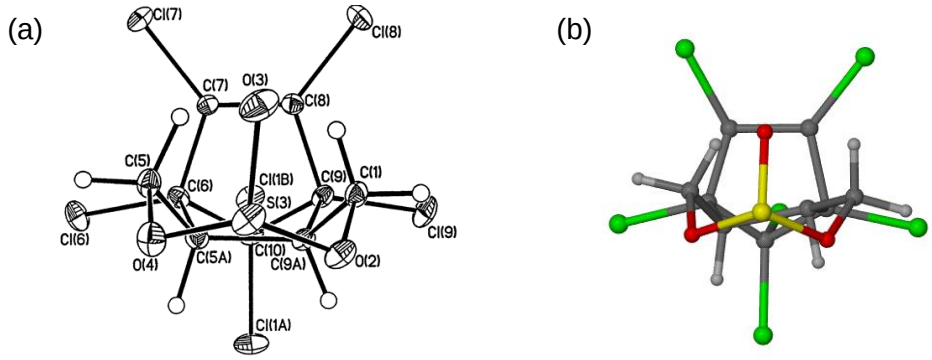

Figure 28. *(a) The 'α-endosulfan' ORTEP diagram obtained from the journal article by Schmidt et al [2] and (b) an end-on view of the endosulfan molecule found within the BCD**B**END complex.*

Knowing that this conformation has been observed previously [2] gives us confidence that its occurrence in the complex BCD**B**END is not extraordinary. The cyclodextrin molecule either induces this particular conformation of the β-endosulfan molecule (starting material) or the prolonged high temperatures maintained during the preparation of the complex may be responsible for the different guest conformation. An estimate of the energy required for epimerisation to occur at a cyclic sulfite group could not be found in the literature. The energy required to break bonds and reform them is in general nevertheless very high, leading us to suggest that the β-endosulfan sample is a mixture of epimers. This requires further investigation using ^{1}H NMR spectroscopy.

In both the BCD**B**END and DMB**B**END complexes the radial chlorine atoms of the hexachloronorbonenyl group are situated at the wider secondary rims of the CD molecules. The more polar seven-membered cyclic sulfite residue is directed towards the narrow, primary rim of the host molecules. In the case of the DMB**B**END complex, water molecules are positioned within the DIMEB cavities (closer to the primary rim) and play an important H-bonding bridging role in stabilising the guest molecules within the host molecules.

Intra- and intermolecular interactions

The strong intramolecular hydrogen bonds are present at the secondary interface of the DIMEB and β-CD molecules for the two complexes. The BCD**B**END complex is a dimeric complex containing hydrogen bonds of the flip-flop type which stabilise these dimeric units extensively. There are only two very weak host-guest interactions present within the BCD**B**END complex. The host molecules of the BCD**B**END complex are stabilised through a vast network of water-water and water-host interactions that occur between adjacent host molecules. Only one water molecule is present exterior to the host cavity in the DMB**B**END complex. This water molecule acts as a bridge linking four DIMEB units. The two water

molecules present within the two DIMEB cavities also form a bridge, but in this case between the guest and host molecules. The other important intermolecular interaction found in the DMB**B**END complex is a halogen bond C-Cl•••O which links the guest molecules in an infinite chain within the stacked DIMEB molecules. We are not aware of this feature appearing in previously reported X-ray structures of CD complexes.

Crystal packing

The β-CD-endosulfan complexes were found to be isostructural with other β-CD inclusion complexes. The *C*2 and *P*1 channel-type structures for dimeric β-CD inclusion complexes are well documented.[6] The BCD**B**END complex packs in such a way that there are no intermolecular interactions between the guest molecules in adjacent β-CD dimers. The guests are therefore isolated from one another and do not interact with the water molecules.

On the other hand, the DMB**B**END complex displays a novel packing arrangement for DIMEB inclusion complexes. DMB**B**END is one of the first DIMEB complexes to contain two independent DIMEB molecules in the asymmetric unit that are not related by a simple translation or rotation along a unit cell axis (as will be seen in Chapter 5 for the DIMEB·fenitrothion complex). The guest molecules are in contact with one another through a halogen bond. Most DIMEB inclusion complexes contain guests that are isolated from one another as the primary and secondary rims of neighbouring host molecules block these guest molecules. This occurs mainly as a result of a zig-zag arrangement of the DIMEB molecules. In the DMB**B**END complex the host molecules are not tilted relative to each other but instead form parallel layers along the *xy*-plane. The chlorine atoms are located at the secondary interfaces of the head-to-tail DIMEB columns forming their own layer in the *xy*-plane.

Complexation in solution

^{1}H NMR spectroscopy solution-state studies were attempted using the continuous variation method. Due to the very low aqueous solubility of endosulfan these experiments were performed using d_6-DMSO as a solvent. No chemical shifts were observed for the protons associated with either the CD molecules or the guest molecules investigated. The solvent DMSO has a relatively low association constant with β-CD (1.3 ± 0.2)[19] but endosulfan is highly soluble in organic solvents such as DMSO, therefore counteracting the inclusion capabilities of the CD molecules. Evidence of the significant contribution of hydrophobic interactions to the formation of the endosulfan inclusion complexes was provided by the fact that complexation does not occur in solvents other than H_2O. Application of other techniques

(ITC and ICD) for studying the complexation of endosulfan in CDs in solution was not possible either, due to the very poor aqueous solubility of endosulfan.

Final remarks

It must be emphasised that there were major challenges involved in the preparation, characterisation and structure refinements of the CD·endosulfan complexes presented in this chapter. Owing to the poor aqueous solubility of endosulfan as well as the small quantities of the individual isomers available (due to high cost), only limited studies were possible. The poor shape and size of the complex crystals prepared, especially in the case of the β-CD complexes, led to poor-quality X-ray diffraction data sets. In addition, excessive guest disorder within the CD cavities meant that many refinements and different modelling attempts were required before a final structure solution could be accepted and presented. Despite all these challenges significant new results have emerged from this study.

REFERENCES

1. W. F. Schmidt, S. Bilboulian, C. P. Rice, J. C. Fettinger, L. l. McConnell and C. J. Hapeman, *J. Agric. Food Chem.*, **2001**, 49, 5372-5376.
2. W. F. Schmidt, C. J. Hapeman, J. C. Fettinger, C. P. Rice and S. Bilboulian, *J. Agric. Food Chem*., **1997**, 45, 1023-1026.
3. S. E. Forman, A. J. Durbetaki, M. V. Cohen and R. A. Olofson, *J. Org. Chem*., **1965**, 30, 169-175.
4. S. R. Byrn and P. Y. Siew, *J. Chem. Soc. Perkin Trans*. 2, **1977**, 144-149.
5. G. Smith, C. H. L. Kennard and K. G. Shields, *Aust. J. Chem*., **1977**, 30, 911-916.
6 . D. Mentzafos, I. M. Mavridis, G. le Bas and G. Tsoucaris, *Acta Crystallogr*., **1991**, B47, 746-757.
7. L. J. Barbour, *J. Appl. Crystallogr*., **1999**, 32, 351-352.
8. Program SAINT, Version 7.60a, Bruker AXS Inc., Madison, WI, USA, **2006**.
9. Cambridge Structural Database and Cambridge Structural Database system, Version 5.32, Cambridge Crystallographic Data Centre, University Chemical Laboratory, Cambridge England, February **2011**.
10. D. Mentzafos, I. M. Mavridis and M. B. Hursthouse, *Acta Crystallogr. Sect. C, Cryst. Struct. Commun*., **1996**, 52, 1220-1223.
11. G. M. Sheldrick, Program SADABS, Version 2.05, University of Göttingen, Germany, **2007**.
12. G. M. Sheldrick, SHELXH-97, *Acta Crystallogr*., **2008**, A64, 112-122.
13 . M. R. Caira, *Rev. Roum. Chim.,* **2001**, 46, 371-386.
14. B. Klingert and G. Rihs, *J. Chem. Soc., Dalton Trans*., **1991**, 2749-2760.
15. G. M. Sheldrick, *Direct Methods for Solving Macromolecular Structures*, ed. S .Fortier, Dordrecht: Kluwer Academic Publishers, **1998**, 401-411.
16. M. S. S. Cunha-Filho, B. Dacunha-Marinho, J. J. Torres-Labandeira, R. Martínez-Pacheco and M. Landín, *AAPS PharmSciTech*, **2007**, 8, E68-E77.
17. *The Pesticide Manual*, eds. C. R. Worthing and R. J. Hance, British Crop Protection Council: Lavenham, Suffolk, England, 8th edn., **1987**.
18. A. R. Hedges, *Chem. Rev*., **1998**, 98, 2034-2044.
19. J. Taraszewska, *J. Inclusion Phenom. Mol. Recog. Chem.*, **1991**, 10, 69-78.

Chapter 5: Fenitrothion

The results based on the organophosphorus insecticide, fenitrothion, are separated into two parts. The work performed at the University of Cape Town on the formation of solid-state inclusion complexes between fenitrothion and various CDs will be presented in Part 1. Kinetic stability studies and circular dichroism results obtained during two three-month visits to the National University of Córdoba, Argentina will be shown in Part 2 of this Chapter.

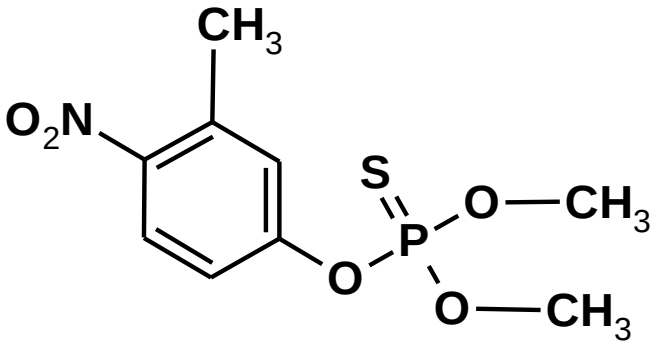

PART 1: COMPLEXATION IN THE SOLID STATE

THE GUEST: FENITROTHION

Fenitrothion is an oil at room temperature and practically insoluble in an aqueous medium.[1] The molecular structure of fenitrothion is shown in Figure 1 with the labelling scheme that will be used throughout this chapter. If more than one component is present in the asymmetric unit, a suffix A, B, C, etc. is used. As no X-ray crystal structure of fenitrothion has been reported to date, it was necessary to identify analogues of organophosphorus compounds from the Cambridge Structural Database (CSD) in order to facilitate the modelling of the fenitrothion molecules within the various CD complexes formed. The bond distances and angles of the following analogues were used: methylparathion, iodofenphos, famphur, ronnel and (*S*)-(-)-fenthion sulphoxide.[2]

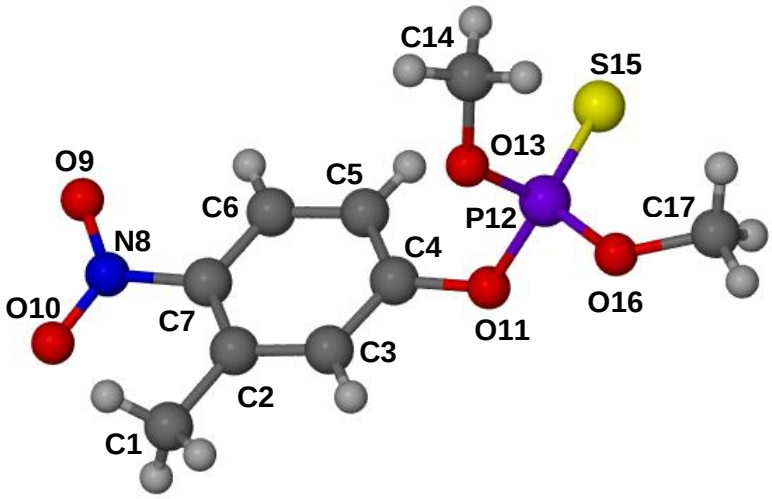

***Figure 1**. Molecular structure of fenitrothion and the labelling scheme that will be used throughout this chapter for all crystallographic analyses of the agrochemical.*

β-CYCLODEXTRIN INCLUSION COMPLEX WITH FENITROTHION

Complex preparation

Due to the very poor aqueous solubility of fenitrothion, various methods were employed to attempt formation of an inclusion complex between fenitrothion and β-CD. Initially, the method of co-precipitation with small volumes of water and high temperatures (~80 °C) resulted in a high yield of single crystals. However, a ^{31}P NMR spectrum recorded by dissolving these crystals in deuterated DMSO showed more than one phosphorus signal rather than a single signal for fenitrothion, indicating guest decomposition. As a result, lower temperatures and larger volumes of water were used but this resulted in low yields of poorly diffracting crystals. Other methods such as kneading and mechanical co-grinding were attempted to try to increase the yield but powder X-ray diffraction (PXRD) did not show evidence of complexation.

A detailed account of the preparation of the β-CD·fenitrothion complex (BCDFEN) is as follows: first, a drop of fenitrothion was weighed in a vial (~20 mg, 0.072 mmol) to which 2 cm^3 of distilled water was added. This was stirred vigorously for 5 min. In a separate vial an equimolar β-CD solution was prepared in 2 cm^3 of distilled water. The fenitrothion solution was quantitatively transferred to the β-CD solution using an additional 4 cm^3 of distilled water. The resulting solution was stirred for 24 h at 45 °C and then filtered through a 0.45 µm filter, even though the solution remained turbid. The vial was sealed and placed in a Dewar flask at 45 °C and left to cool to room temperature over two days. Very few single crystals appeared at the bottom of the vial, limiting the extent of possible characterisation. Consequently, only three methods of analysis were used to characterise the BCDFEN complex, namely ^{1}H and ^{31}P NMR spectroscopy, hot stage microscopy and single crystal X-ray diffraction.

Confirmation of stoichiometry and integrity of fenitrothion

A small quantity (~3 mg) of the BCDFEN sample was dissolved in deuterated DMSO and the ^{1}H and ^{31}P NMR spectra were recorded. Integration of the ^{1}H NMR signals revealed a 1:0.6 host to guest stoichiometry. Table 1 displays the relative integrals for some of the host and guest signals. (The complete ^{1}H NMR spectrum can be found in the Appendices).

Table 1. *Integrals of the host and guest protons for BCDFEN used to confirm the stoichiometry.*

Proton (CD/G) – [Total no. of protons]	δ (ppm)	Integration of peaks	Experimental peak integral/ Theoretical proton no.
7 × H**1** (CD) – [7]	4.792	7.000 *	1
7 × OH-**6** (CD) – [7]	4.363	7.148	1
7 × OH-**2** and 7 × OH-**3** (CD) – [14]	5.641, 5.603	14.309	1
H**1** and H**2** (G) – [2]	7.274, 7.226	1.238	0.6
H**3** (G) – [1]	8.043	0.609	0.6
Ar-C$\underline{H}_3$ (G) – [3]	2.505	1.941	0.6

* Reference integral.

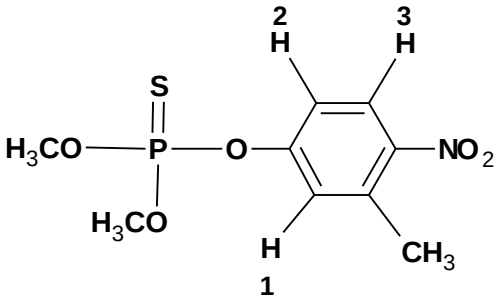

Previous work indicated that fenitrothion is readily distinguished from its thermal decomposition product, mainly the S-methyl isomer, O,S-dimethyl[O-(4-nitro-*m*-tolyl] phosphorothioate. This particular isomer has a ^{31}P NMR chemical shift occuring at 27.0 ppm in benzene-d_6 while fenitrothion has a ^{31}P NMR chemical shift that occurs at 66.1 ppm in the same solvent.[3,4,5] It was therefore necessary before each single crystal X-ray diffraction data-collection to confirm the integrity of fenitrothion using ^{31}P NMR spectroscopy. The same sample submitted for ^{1}H NMR spectroscopy was used to obtain a ^{31}P NMR spectrum. For the BCDFEN sample a single signal was observed at 65.351 ppm confirming the presence of fenitrothion and not a decomposition product.[6]

Hot stage microscopy

The HSM photographs (Figure 2) illustrate the two major events that occur upon heating the BCDFEN crystals under a drop of silicone oil. First, they lose their crystallinity due to expulsion of water; this commences at ~60 °C and continues above 100 °C. At 194 °C the crystals start to decompose as can be seen by the change in colour and presence of gas bubbles. This occurs up to a temperature of 360 °C. The events noted here are typical for β-CD complexes.[7,8]

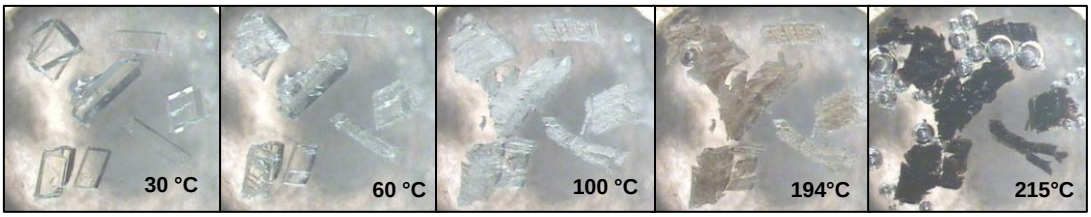

Figure 2. *HSM photographs of the BCDFEN crystals recorded at various temperatures.*

Crystal structure analysis

Solving the single crystal X-ray structure of the BCDFEN complex was not straightforward. Two sets of data were collected for two different single crystals prepared on separate days. Both sets of data showed the complex to crystallise in the same space group with almost identical unit cell dimensions; however, both data-sets resulted in poor structure solutions. Structure solution based on the second data-set did not reveal a coherent set of electron density peaks that could be sensibly modelled as the guest molecules. Furthermore, attempted anisotropic refinement of host CD atoms led to least-squares matrix singularities ('non-positive definite' indications). This data set was therefore abandoned and the results from the first data-set were pursued. The outcome is presented below.

Data-collection and space group determination

The single crystal X-ray diffraction data were measured on a Bruker KAPPA APEX II DUO diffractometer. The crystal was covered in paratone oil and placed under a constant stream of nitrogen gas in order to maintain a temperature of 173 K throughout the data-collection. The program LAYER was used to determine the crystal symmetry.[9] The Laue symmetry was found to be $\bar{1}$, indicating the triclinic crystal system. CDs are chiral molecules; as a result the space group *P*1 was inferred.

Structure solution and refinement

Table 2 contains the crystal data and refinement parameters for the BCDFEN complex. The asymmetric unit consists of a hydrated dimeric β-CD complex with two disordered guest molecules in each β-CD cavity. Data were corrected for absorption using the multi-scan procedure (program SADABS).[10] The structure was solved using the rigid non-hydrogen host atoms of an existing isostructural complex [2(β-CD)·2(1-Adamantane-carboxylic acid)·30H_2O].[11] The glucopyranose units for the two host molecules in the asymmetric unit were labelled A1-A7 and B1-B7. The structure was refined with SHELXH-97[12] and the successive difference Fourier maps revealed the remaining non-hydrogen host atoms, water

molecules and electron density peaks associated with the guest molecules within the CD cavity. All of the host atoms were refined anisotropically.

Table 2. *Data-collection and refinement parameters for the BCDFEN complex.*

Chemical formula	$C_{42}H_{70}O_{35}\cdot(C_9H_{12}O_5NPS)_{0.6}\cdot 12.5H_2O$
Formula weight	1525.91
Crystal system	Triclinic
Space group	*P*1
Unit cell constants	
a (Å)	17.889(2)
b (Å)	15.424(1)
c (Å)	15.482(1)
α (°)	103.016(2)
β (°)	113.256(2)
γ (°)	99.378(2)
Volume (Å^3)	3669.1(6)
Z	2
Density$_{calc}$ (g cm^{-3})	1.381
μ [MoKα] (mm^{-1})	0.154
F (000)	1625
Temperature of data collection (K)	173(2)
Crystal size (mm)	0.09 x 0.10 x 0.11
Range scanned θ (°)	1.6 – 28.0
Index ranges	h: -23, 23; k: -20, 20; l: -20, 20
ϕ and ω scan angle (°)	0.5
Dx (mm)	50.00
Total no. of reflections collected	71290
No. of independent reflections	17483
No. of reflections with I > 2σ(I)	15314
No. of parameters	1518
R_{int}	0.0381
S	1.394
R_1 [I > 2σ(I)]	0.1007
No. of reflections omitted	15
wR_2	0.3095
Weighting scheme parameters	a = 0.2, b = 0
$(\Delta / \sigma)_{mean}$	<0.001
$\Delta\rho$ excursions (e Å^{-3})	2.38 and -1.50

Many of the host hydrogen atoms were present in the difference Fourier maps; however, they were placed in geometrically calculated positions in a riding model using the AFIX instructions. An AFIX 83 instruction (hydrogen bond searching model) was used to place the hydrogen atoms of the hydroxyl groups; however, after refining the structure with this instruction the hydrogen atoms appeared in unrealistic positions so that many abnormally short contact distances resulted. Rotation of the hydrogen atoms around the C2–O2 bond or C3–O3 bond allowed these atoms to be placed in more physically reasonable positions so that the intramolecular hydrogen bonding network (O2•••H–O3(n-1)) within a β-CD molecule could be maintained. It should be noted that we could equally well have placed these hydrogen atoms in positions so that the host intermolecular hydrogen bond network (O3–H•••O3′) that exists within a β-CD dimer could be represented. Due to the 'flip-flop' nature of the H atoms in question, one of these alternatives had to be chosen in the static modelling. Isotropic temperature factors 1.2 times those of their parent atoms were assigned to each hydrogen atom of the host molecules.

A total of 25 water molecules per host dimer were located in the asymmetric unit over 26 sites. Only two of the 26 oxygen atom sites (O7WA and O7WB) showed partial occupancy and both of these atoms were situated near the centres of the primary rims of host molecules B and A respectively. These two water molecules had a combined site occupancy factor (s.o.f.) close to unity. Nineteen of the 25 water molecules were refined anisotropically while the others showed unrealistic thermal ellipsoids when refined anisotropically and were therefore refined isotropically. As TG analysis of this complex was not possible due to paucity of the material, an evaluation of the water content for 18 isostructural complexes found in the CSD was made. An average of 12 ± 3 H_2O molecules per CD molecule was determined. The BCDFEN structure was modelled with 12.5 water molecules per CD, which is in agreement with the other isostructural complexes.

Modelling of the fenitrothion guest

Initially two guest molecules were modelled relatively easily in each CD molecule but it was not possible for each of these guests to exist simultaneously as they were in positions that required overlap of their nitro groups. Furthermore, additional electron density peaks were present in the difference Fourier maps mimicking two more guest molecules, one in each CD cavity. The two additional guest molecules were modelled with difficulty and required many restraints and constraints in order to maintain their geometry. Modelling of these guests resulted in the atoms of the originally placed guest molecules deviating substantially from their initial positions and as a result further constraints and restraints were applied to them as well. At this stage there were two guest molecules present per CD molecule. The two

guests in each CD cavity were initially assigned and refined with s.o.f.s of *x* and *1-x*. The final values of *x* were close to 0.5 in both cases. With this result and taking into account the ^{1}H NMR analysis which showed a 1:0.6 host-guest ratio, each guest molecule (total of 4 disordered components per CD dimer) was assigned a fixed s.o.f. value of 0.3 which yielded a total of 1.2 guest molecules per β-CD dimer in accordance with the ^{1}H NMR result. Labelling of the four guest molecule components was as follows: host molecule A contained guest molecule components A and C while host molecule B contained guest molecule components B and D. Each guest component was assigned a global temperature factor which refined to 0.044, 0.099, 0.104 and 0.087 Å^2 for guest molecules A, B, C and D, respectively. The final refinement took place after placing hydrogen atoms on the four disordered guest molecules in idealised positions based on a riding model with U_{iso} values 1.2-1.5 times those of their parent atoms.

It must be emphasised that after many cycles of refinement and the application of several restraints and constraints, the geometry of the guest molecules was still not of the expected accuracy. The major deficiencies of the model included the nitro-groups' not maintaining a planar conformation and having unreasonable N–O bond lengths. The phosphorothioate groups also had unrealistic methoxyl and P=S bond lengths. In addition to these deficiencies there were still large difference electron density peaks surrounding the heavy atoms despite absorption corrections having been applied to the data. In order to present a reasonable model, sixteen non-hydrogen guest atoms were placed in geometrically correct positions by fixing their coordinates. Due to the low site-occupancy of the guests, this did not affect the refinement parameters significantly.

Geometrical analysis of the BCDFEN structure

Host conformation

The structure of the two host molecules in the asymmetric unit is comparable to that found in the BCDCYC complex (pg. 59) and a common numbering scheme has been employed. The primary hydroxyl torsion angles (ω) for all glucose units on both CD molecules indicate a (-)-*gauche* conformation with a range of values from -58 to -67°. The (-)-*gauche* conformation means that the C6–O6 bonds are directed away from the CD cavity. All glucose units adopt the usual $^{4}C_{1}$ conformation.

Table 3 lists the macrocyclic geometrical data for each β-CD molecule. The narrow ranges of the *l*, *D* and ϕ parameters (defined on pg. 6) illustrate the near ideal seven-fold symmetry

of the O4-heptagons. The torsion angles involving the O4 atoms of the heptagon (*d*) and the parameter α which describes the deviation of each O4 atom from the mean plane are very small for both host molecules, which further demonstrates the seven-fold symmetry of the O4-heptagons. The τ_1 and τ_2 tilt angles are all positive indicating that the primary rims of all the glucose units are inclined towards the centre of the cavity. Finally, the O4 mean planes of the two host molecules (A and B) are essentially parallel to one another with an interplanar angle of 1.16(5)°.

Table 3. *Geometrical parameters for the host molecules of BCDFEN.*

Residue	*l* (Å)	*D* (Å)	ϕ (°)	*d* (°)	α^a *(Å)*	D_3 [b] (Å)	τ_1 [c] (°)	τ_2 [d] (°)
A1	4.94	4.44	130.5	-0.4	-0.011	2.80	5.6	7.5
A2	5.02	4.40	129.2	-0.5	0.001	2.70	4.8	6.4
A3	5.20	4.24	124.3	1.2	0.013	2.79	8.5	8.6
A4	4.92	4.51	132.0	-1.3	-0.015	2.82	5.3	7.3
A5	4.96	4.27	129.7	1.0	0.009	2.80	12.3	13.2
A6	5.14	4.43	126.3	-1.0	-0.007	2.80	8.3	10.2
A7	5.07	4.33	128.0	1.0	0.011	2.83	9.5	10.0
B1	5.03	4.39	128.7	1.5	-0.031	2.75	5.0	5.8
B2	5.06	4.31	128.5	-0.4	0.016	2.87	10.8	11.2
B3	5.05	4.43	127.9	-0.3	0.016	2.75	4.1	6.0
B4	4.99	4.34	130.0	-0.9	-0.011	2.86	11.3	12.2
B5	5.07	4.37	127.6	2.1	-0.025	2.78	7.3	7.8
B6	5.05	4.38	128.7	-1.3	0.036	2.82	7.3	8.1
B7	5.03	4.38	128.6	-0.8	-0.001	2.70	4.0	5.1

[a] *mean e.s.d. = 0.003 Å;* [b] *mean e.s.d. = 0.03 Å;* [c] *mean e.s.d. = 0.2° ;* [d] *mean e.s.d = 0.2°.*

Guest inclusion and conformation

As stated earlier, there are two disordered guest molecules per β-CD molecule, each with equal s.o.f. values of 0.3. Figure 3 illustrates these disordered guest molecules and how guest molecules A and C or B and D can be present simultaneously. We are hesitant to make any comments regarding possible pseudo symmetry elements relating the four guest molecules as certain atoms were placed in fixed geometrical positions. The most well-behaved guest molecule (A) did, however, show the usual tetrahedral geometry around the phosphorus atom as well as a slight rotation of the nitro group out of the plane of the phenyl ring.

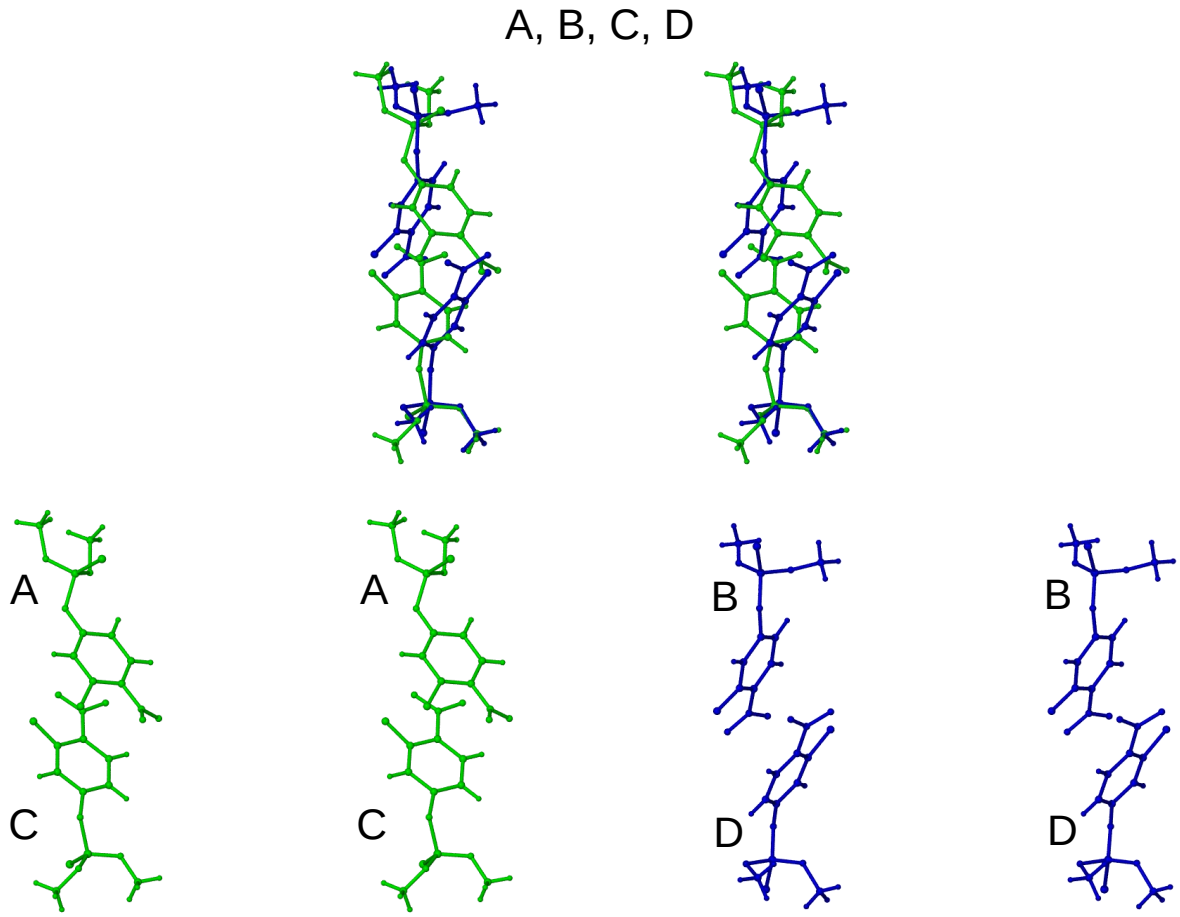

Figure 3. *Stereoviews of the disordered guests A, B, C and D of the BCDFEN complex and the deconvoluted disordered components A/C (green) and B/D (blue).*

All four guest components are positioned with the *O,O*-dimethyl phosphorothioate moiety at the primary rim of the CD molecule and the methyl nitro-phenyl ring planes at the secondary rim interface of the CD dimer (Figure 4 (a)). Space-filling diagrams (Figures 4 (b)-(d)) illustrate the extent to which the methoxyl groups of the phosphorothioate unit of the guest molecule protrude from the primary rim. The phenyl rings of guest molecules A and C are in effect parallel to one another (Figure 4 (c)); likewise for guest molecules B and D. The guest molecules are all tilted with respect to the O4 mean plane of each β-CD molecule in order to occupy most of the available space in the CD cavity, as well as to prevent close contacts between the nitro-groups at the secondary interface of the β-CD dimer.

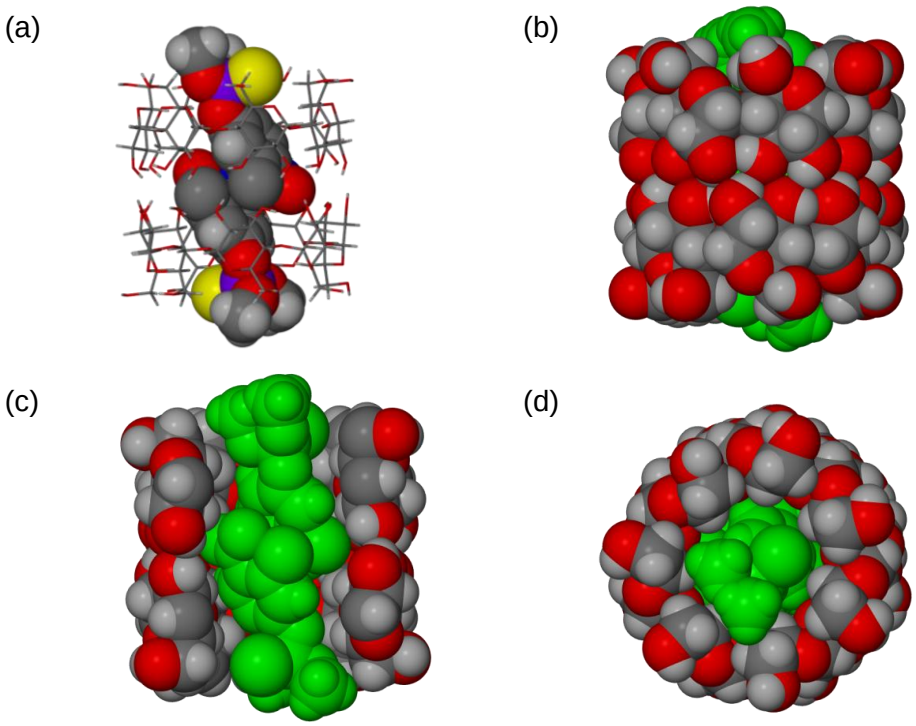

Figure 4. *(a) The relative positions of guest molecules A and C within the β-CD dimer of BCDFEN. Space-filling diagrams of BCDFEN; (b) a side view, (c) a cross-sectional view and (d) a view from the primary rim of host molecule A (for clarity only guests A and C are shown as representative).*

Hydrogen bonding interactions

Host-host interactions

A summary of the host-host interactions is shown in Table 4. The characteristic β-CD intramolecular hydrogen bonds (O2•••H–O3(n-1)) are present and have previously been listed in Table 3 (D_3, O2•••O3(n-1) distances). Fourteen hydrogen bonds exist between the two β-CD molecules of the dimer and these are of the type O2–H•••O3′, due to the way in which the hydrogen atoms for the secondary hydroxyl groups were modelled. Neutron diffraction studies have shown that both O2–H•••O3′ and O3–H•••O3′ intermolecular hydrogen bonds are capable of forming between the β-CD molecules at the secondary interface of a β-CD dimer due to the dynamic nature of the hydrogen atoms even in the solid state.[13] The O3•••O3′ interdimer contact distances within the BCDFEN structure range between 2.70 and 2.83 Å.

There are 12 intermolecular hydrogen bonds that occur between the β-CD dimers and six of these are weaker C–H•••O interactions. Eleven of the 12 interactions occur between adjacent β-CD molecules (intra-layer) and only one occurs between two β-CD molecules positioned one above the other (inter-layer).

Table 4. *Summary of the intra- and intermolecular hydrogen bonds for the CD molecules.*

Interaction	Type	Number	Mean bond length, Å	Mean bond angle, °
Host intramolecular	O2-H•••O3	14	2.79(3)	147
Host-host intermolecular	O2-H•••O3	14	3.09(3)	154
Intra-layer	O6-H•••O6	5	2.84(3)	133
	C2-H•••O3	4	3.33(3)	163
	C1-H•••O2	2	3.37(3)	140
Inter-layer	O6-H•••O6	1	2.87(3)	154

Guest interactions

There are no host-guest interactions present within the BCDFEN complex. The final structure presented here shows only one reasonable O•••OW contact distance between atoms O13B and O7WB (2.88(3) Å). Both of these atoms have a s.o.f. of 0.3. Water molecule O7WA is either too close to, or too far away from, all four carbon and oxygen atoms of the phosphorothioate moiety of guest molecules D and C. As a result, this water molecule which has a s.o.f. of 0.7 is only present in the absence of a guest molecule. The lack of hydrogen bonds between the host and guest molecules means that the host-guest interactions are primarily attributable to weak van der Waals forces and hydrophobic interactions.

Water interactions

A total of 25 water molecules per β-CD dimer were accounted for in the crystallographic analysis. Only two water molecules showed partial occupancy (O7WA and O7WB). All water molecules are situated at the periphery of the CD molecules, filling the intermolecular spaces between the CD units (Figure 5). Every primary hydroxyl group is within hydrogen bonding distance of at least one water molecule; furthermore, all water molecules are within hydrogen bonding distance of at least one host atom. The O3 atoms of the hydroxyl groups of host molecules A and B act as hydrogen bond acceptor atoms to the water molecules as their hydrogen atoms are already involved in the H-bonding scheme within the β-CD molecules. Table 5 lists the host atoms which act as hydrogen bond donors to water

molecules surrounding the host. Finally, there are 28 water-water close contacts whose O•••O distances range from 2.58 to 3.12 Å with a mean distance of 2.81 Å.

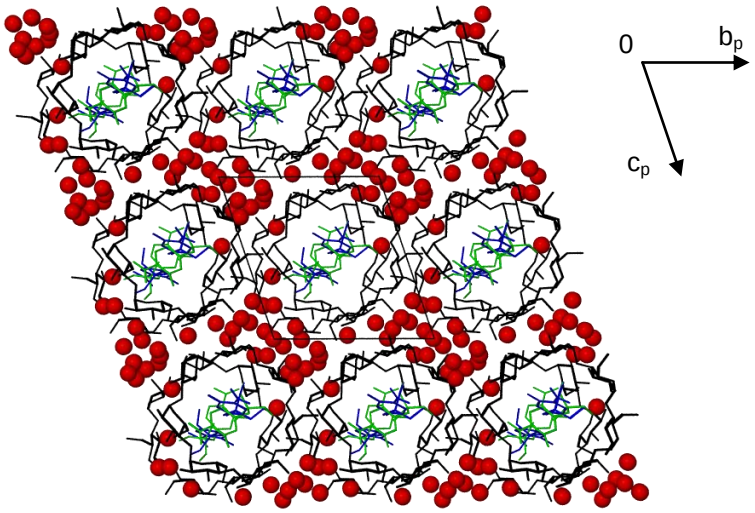

Figure 5. *The interstitial water molecules of the BCDFEN complex.*

Table 5. *Host-water interactions for the BCDFEN complex.*

Interaction	H ••• A (Å)	D ••• A (Å)	D-H ••• A (°)
O2A2–H2A2•••O24W[a]	2.32	2.73(3)	110
O2A5–H2A5•••O5W	2.17	2.68(3)	119
O6A5–H6A9•••O23W[b]	1.97	2.71(3)	147
O6A7–H6AA•••O18W	2.18	3.01(3)	175
O6B2–H6B3•••O23W	1.98	2.74(3)	149
O6B3–H6B5•••O1W	1.92	2.743)	162
O2B4–H2B4•••O12W[c]	2.10	2.71(3)	130
O3B4–H3B4•••O3W	2.46	2.93(3)	117
O6B4–H6B7•••O20W[d]	1.97	2.69(3)	144
O6B6–H6BY•••O9W	2.12	2.94(3)	165
C2A5–H8•••O4W	2.49	3.43(3)	156
C1A2–H1A2•••O10W[e]	2.55	3.41(3)	144
C2B2–H16•••O3W[e]	2.58	3.14(3)	116
C1A5–H1A5•••O7WA[b]	2.60	3.20(3)	119
C1B1–H1B1•••O25W[a]	2.55	3.43(3)	147

Symmetry codes: [a] *x, -1+y, z;* [b] *-1+x, y, -1+z;* [c] *x, 1+y, z;* [d] *x, y, -1+z;* [e] *x, y, 1+z.*

Crystal packing

The crystalline complex, BCDFEN, consists of head-to-head β-CD dimers, each containing a partially disordered guest molecule. Figure 6 is a stereoview projection down the *a*-axis illustrating the infinite channels formed by the host molecules. Figure 6 (a) and (b) are projections down the *b*- and *c*-axes, respectively. These packing diagrams illustrate the stacking of the dimers parallel to the *a* axis.

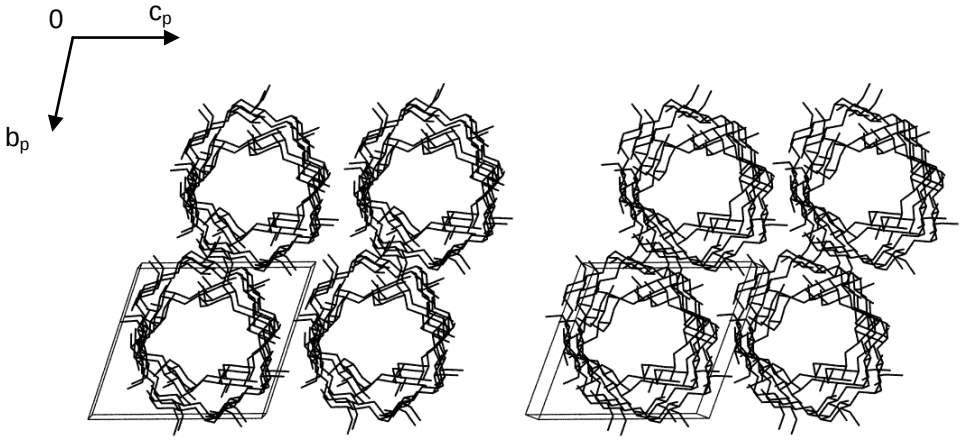

Figure 6. *Stereo packing diagram of the host molecules of BCDFEN viewed along [100].*

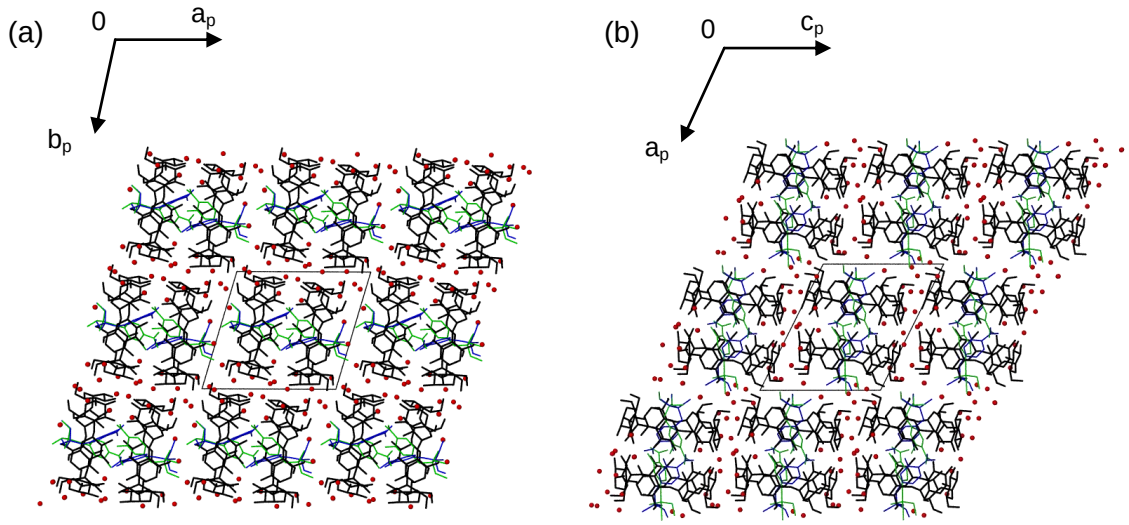

Figure 7. *Packing diagrams of the BCDFEN structure, viewed along (a) [001] and (b) [010]. Water molecules are presented in red, the host in black and the disordered guests in blue and green.*

The packing arrangement shown here is termed an 'intermediate-type packing arrangement' and is characteristic for β-CD complexes that crystallise in the space group *P*1 with unit cell dimensions similar to those reported here.[14] Figure 7 (b) clearly shows how the β-CD dimers

in adjacent parallel layers are shifted somewhat ($R_A = R'_B$ = 6.0 Å, defined on pg. 8) with the primary rim of one β-CD molecule positioned close to the seven-fold symmetry axis of another β-CD molecule one layer below. The channel-type structures such as the BCDCYC complex discussed in Chapter 3 display only a slight shift of ~3 Å between two adjacent layers. The channels of the BCDFEN structure are therefore said to be deformed at the interdimeric interface.[14] This large shift results in the guest molecules being isolated from one another and justifies the term 'cage-type' used by Saenger.[15]

Comparative PXRD

The calculated PXRD pattern from the single crystal X-ray structure of BCDFEN was compared to the reference pattern for an isostructural series of β-CD inclusion complexes. The reference pattern shown is an average of 18 PXRD traces computed from single crystal X-ray data. There is excellent agreement between the BCDFEN computed PXRD trace and the reference pattern for the known isostructural series (Figure 8). The peak intensities of the two patterns do differ slightly but this is due to the heavy atoms present in the BCDFEN complex and the fact the other trace is an average of the traces for 18 different structures all containing significantly different guest molecules. The important feature, however, is the peak positions which are indistinguishable.

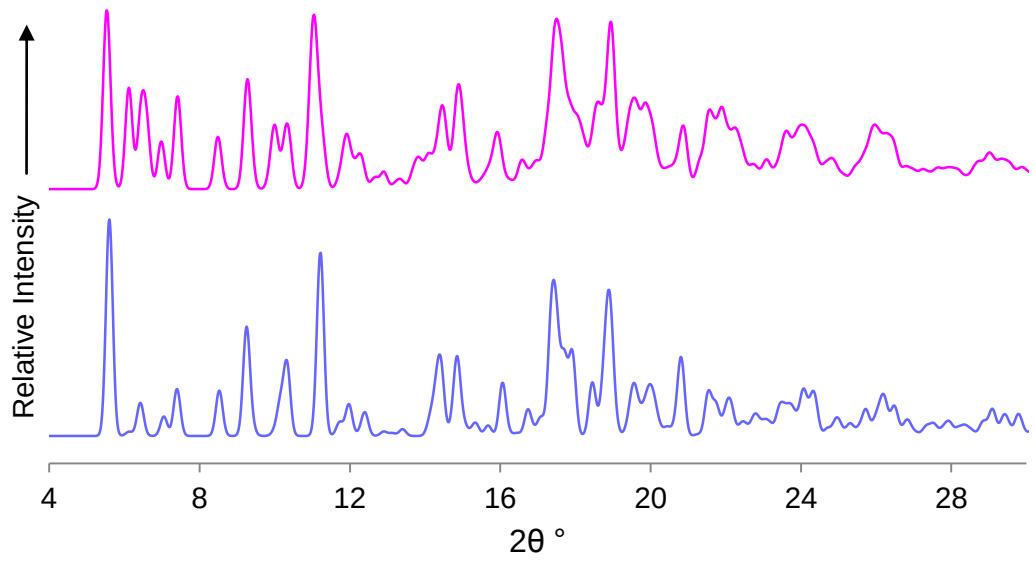

Figure 8. *Calculated PXRD trace of BCDFEN (blue) and the reference PXRD pattern for the isostructural series (pink).*

γ-CYCLODEXTRIN INCLUSION COMPLEX WITH FENITROTHION

Complex preparation

A similar procedure to that of the BCDFEN complex preparation was employed in order to obtain complex crystals of γ-CD with fenitrothion. Equimolar amounts of the host and guest molecules were used. γ-CD (103 mg, 0.072 mmol) was first dissolved in 2 cm^3 of distilled water at 45 °C. Once the γ-CD sample had dissolved, 20 mg of fenitrothion (0.072 mmol) and an additional 6 cm^3 of water were added. The latter was stirred continuously for 24 h and the total volume of water was maintained at 8 cm^3. The solution was then filtered into a clean vial, capped and placed in a Dewar flask at 45 °C. Complex crystals of γ-CD·fenitrothion (GCDFEN) formed within two days. Throughout the preparation, the CD solution containing fenitrothion did not appear translucent, but remained turbid until filtration took place. The low yield of single crystals obtained was comparable to that for the BCDFEN complex.

Confirmation of complexation

Owing to the very low yield of complex material, the only form of characterisation adopted was that of single crystal X-ray diffraction. A single crystal was mounted on a cryoloop and subjected to X-ray radiation using the Bruker KAPPA APEX II DUO diffractometer. The unit cell constants determined were similar to those of other γ-CD inclusion complexes that crystallise in the highly symmetrical tetragonal space group $P42_12$ (Table 6).

***Table 6**. A comparison of the mean unit cell dimensions for eight isostructural γ-CD inclusion complexes with that obtained for GCDFEN.*

	Space group	*a* (Å)	*b* (Å)	*c* (Å)	*α* (°)	*β* (°)	*γ* (°)	Vol. (Å^3)
Isostructural series*	$P42_12$	23.8	23.8	23.2	90	90	90	13103
GCDFEN	$P42_12$	23.7	23.7	22.9	90	90	90	12830

*Averaged values from eight γ-CD inclusion complexes found in the CSD.[2]

Full single-crystal X-ray data-collection of this particular complex was not pursued as the high symmetry of the space group requires the guest molecule to possess fourfold symmetry or the guest molecule will be disordered, invariably preventing its crystallographic modelling. Additional analyses to further support the crystal structure were also not possible due to the small quantity of sample available. Details regarding the essential packing features of the γ-CD host molecules for a γ-CD inclusion complex have been discussed previously in Chapter 3.

TRIMEA INCLUSION COMPLEX WITH FENITROTHION

Complex preparation

The TRIMEA·fenitrothion complex (TMEAFEN) was prepared by adding 20 mg (0.072 mmol) of fenitrothion to a 4 cm^3 aqueous solution of TRIMEA (88 mg, 0.072 mmol) at 20 °C. Stirring for several hours at room temperature followed by subsequent heating to 60 °C led to a turbid solution. This solution was then removed from the hot plate and stirred at room temperature. This process was repeated two to three times which resulted in a clear solution that was filtered (0.45 μm filter) and placed in an oven at 60 °C. Colourless single crystals appeared over a 12 h period.

Confirmation of stoichiometry and integrity of fenitrothion

The crystals of TMEAFEN were dissolved in $CDCl_3$ and the ^1H NMR spectrum was recorded. Integration of the host and guest protons revealed a 2:1 host-guest ratio. (Table 7; see Appendix A for full spectrum).

Table 7. *Integrals of the host and guest protons for TMEAFEN used to confirm the stoichiometry.*

Proton (CD/G) – [Total no. of protons]	δ (ppm)	Integration of peaks	Experimental peak integral/ Theoretical proton no.
6 × H**1** (CD) – [6]	5.044	12.3	2.0
6 × H**2** (CD) – [6]	3.164	13.6	2.3
Ar-C<u>H</u>$_3$ (G) – [3]	2.622	3.0*	1

* Reference integral.

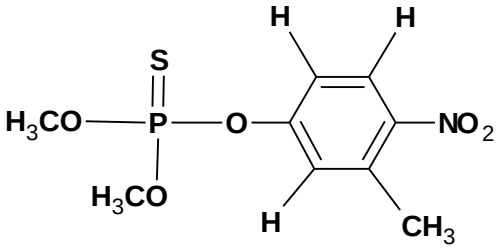

^{31}P NMR spectroscopy was used once again as a tool for confirming the presence of the intact fenitrothion molecule within the TRIMEA cavity. The ^{31}P NMR spectra for a freshly prepared sample of uncomplexed fenitrothion and the TMEAFEN complex in $CDCl_3$ were recorded and these yielded a single peak at δ = 65.456 and 65.459 ppm respectively.

Thermal analysis

The TG trace for the TMEAFEN complex has two distinct slopes with no clear plateaus in between them (Figure 9). Between 130 and 270 °C a total mass loss of 7.2 ± 0.3 % (n = 2) has been calculated but this is not due to complete guest dissociation as we would expect a mass loss of 11.3 % for a 2:1 host to-guest ratio. Instead, this initial mass loss can be interpreted as partial guest loss from the TRIMEA cavity that continues to occur during decomposition which commences at ~290 °C. The initial mass loss seen in the TG trace is accompanied by a broad endothermic peak at 131 °C in the DSC trace. The second endotherm, peaking at 204 °C corresponds to the fusion of the host TRIMEA.

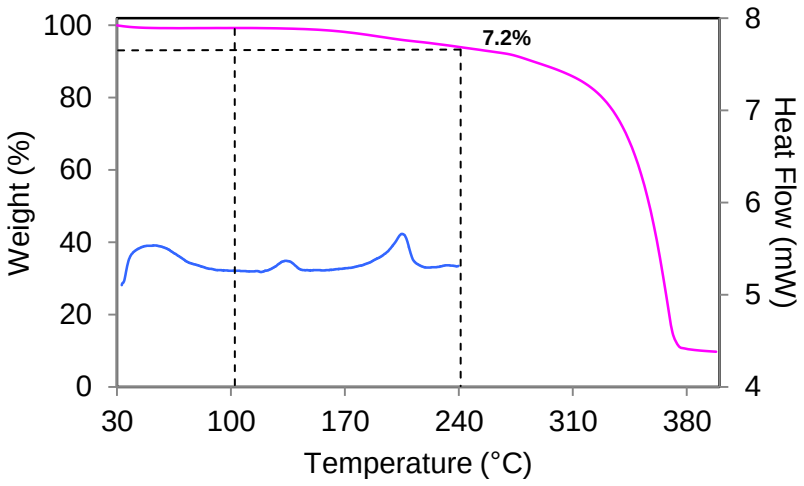

Figure 9. *Representative TG (pink) and DSC (blue) traces for TMEAFEN.*

The HSM images support the above interpretation of the TG and DSC events (Figure 10) as the clear crystalline features of the rod-shaped crystals at 30 °C become diffuse around the crystal edges at 130 °C followed by melting of the crystals at ~210 °C.

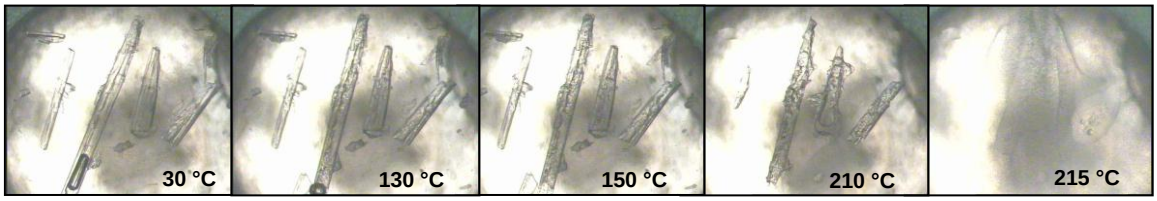

Figure 10. *HSM images of the TMEAFEN crystals recorded at various temperatures.*

Crystal structure analysis

Data-collection and space group determination

Intensity data-collection for TMEAFEN was performed on a Bruker KAPPA APEX II DUO diffractometer. The Laue system was found to be *mmm*, indicating the orthorhombic crystal system and the common space group $P2_12_12_1$ was identified from systematic absences. TMEAFEN crystallises with two host molecules and one guest molecule present in the asymmetric unit.

Structure solution and refinement

The crystallographic data and data-collection parameters for TMEAFEN are shown in Table 8. The unit cell refinement and data reduction were performed using the program SAINT[16] and structure solution for TMEAFEN was achieved by *ab initio* methods using the program SHELXD.[17] Data were corrected for Lorentz-polarisation effects and for absorption using the program SADABS.[10] When a reasonable structure solution was obtained through *ab initio* methods, host atoms were assigned correctly and refinement using SHELXH-97 took place.[12] Once all the host atoms had been placed the glucopyranose units of the two independent host molecules were systematically labelled A1-A6 and B1-B6.

Twofold-disordered methoxyl groups of the host were modelled by allowing the two components to refine isotropically with s.o.f.s *x* and *1-x*. These included one secondary methoxyl group on glucose residue B5 and the primary methoxyl groups on residues B2 and B5 which refined with final *x* values of 0.55, 0.59 and 0.55, respectively. The rest of the host atoms were treated anisotropically. Only the *O,O*-dimethyl phosphorothioate unit of the guest molecule was disordered over two positions. All guest atoms except those attached to the phosphorus atom were refined anisotropically and even though some of the host and guest hydrogen atoms were apparent in the electron density maps, all hydrogen atoms were placed in idealised positions in a riding model with temperature factors 1.2-1.5 times those of their parent atoms.

Table 8. *Data-collection and refinement parameters for the TMEAFEN complex.*

Chemical formula	$(C_{54}H_{96}O_{30})_2 \cdot C_9H_{12}O_5NPS$
Formula weight	2727.84
Crystal system	Orthorhombic
Space group	$P2_12_12_1$
Unit cell constants	
a (Å)	15.097(2)
b (Å)	24.278(3)
c (Å)	38.385(4)
$\alpha = \beta = \gamma$ (°)	90
Volume ($Å^3$)	14069(3)
Z	4
$Density_{calc}$ ($g\ cm^{-3}$)	1.288
μ [MoKα] (mm^{-1})	0.129
F (000)	5856
Temperature of data collection (K)	173(2)
Crystal size (mm)	0.11 x 0.04 x 0.03
Range scanned θ (°)	1.91 – 25.09
Index ranges	h: -18, 6; k: -27,28; l: -45,34
ϕ and ω scan angle (°)	0.5
Total no. of frames	568
Dx (mm)	60.00
Total no. of reflections collected	47709
No. of independent reflections	24600
No. of reflections with $I > 2\sigma(I)$	14645
No. of parameters	1661
R_{int}	0.0462
S	1.010
R_1 [$I > 2\sigma(I)$]	0.0638
No. of reflections omitted	3
wR_2	0.1401
Weighting scheme parameters	a = 0.0807 and b = 2.5525
$(\Delta / \sigma)_{mean}$	< 0.001
$\Delta\rho$ excursions ($e\ Å^{-3}$)	0.61 and -0.39

Modelling of the fenitrothion guest

Initially, all atoms expected for the fenitrothion molecule, except those of the *O*,*O*-dimethyl phosphorothioate unit, were clearly discernible and refined satisfactorily. The appearance of more than the expected number of difference Fourier peaks around the phosphorus atom suggested either molecular disorder or possible decomposition of the fenitrothion molecule (fenitrooxon, the *S*-methyl isomer of fenitrothion, and 3-methyl-4-nitrophenol being known decomposition products).[3] At this point, the ^{31}P NMR spectra of the crystal batch gave unequivocal proof that the included fenitrothion molecule was intact (*cf*. pg. 166 where details were provided). Subsequent refinement and careful examination of the difference Fourier maps revealed twofold disorder of both the sulphur atom and one of the methoxyl groups. Appropriate distance restraints (four O-C and two P-O bonds) were applied to the disordered moieties. The s.o.f.s. of the major and minor components of guest disorder refined to 0.57 and 0.43 respectively.

Geometrical analysis of the TMEAFEN structure

The asymmetric unit of the TMEAFEN complex consists of two TRIMEA molecules encapsulating one guest molecule (Figure 11). The host atoms are labelled in a similar manner to the TMEACYC complex (pg. 74).

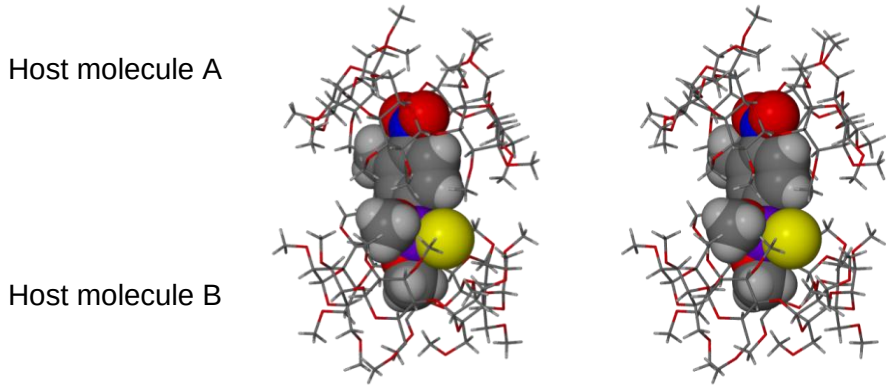

Figure 11. *Stereoview of the 2:1 host-guest asymmetric unit of TMEAFEN with only the major disordered guest component being shown.*

Host conformation

If one were to consider only the major components of the disordered methoxyl groups on methyl glucose residues B2 and B5, host molecules A and B each contain three primary methoxyl groups in a (+)-*gauche* conformation and three in a (-)-*gauche* conformation. Atoms C6, O6 and C9 of each methylglucose unit are therefore either directed inwards ((+)-

gauche conformation), acting as 'lids' closing off the primary rim, or are directed outwards ((-)-*gauche* conformation) forming intermolecular C–H•••O bonds with adjacent TRIMEA molecules.

From the geometric parameters for the crystallographically non-equivalent host molecules A, B listed in Table 9, it is evident that host molecule A is considerably more distorted than host molecule B. The former adopts an elliptical shape to accommodate the planar methyl-nitrophenyl moiety, while the latter, containing the more isotropically shaped *O*,*O*-dimethyl phosphorothioate unit, adopts a more 'round' shape. Figure 12 shows perspective views of host molecules A and B, containing respectively the aromatic and dimethyl phosphorothioate groups, viewed from within the cavity, i.e. from the secondary rims of the respective TRIMEA molecules.

Table 9. *Geometrical parameters for the host molecules of the TMEAFEN complex.*

Residue	*l* (Å)	*D* (Å)	ϕ (°)	*d* (°)	α[a] *(Å)*	D_3[b] (Å)	τ_1[c] (°)	τ_2[d] (°)
A1	4.52	4.05	113.1	-13.5	0.231	3.321	27.75	28.7
A2	4.50	4.39	113.9	9.5	-0.259	3.347	20.39	24.1
A3	3.82	4.44	130.8	5.6	0.035	3.590	5.5	6.8
A4	4.45	3.95	116.4	-12.0	0.219	3.369	31.7	32.2
A5	4.58	4.55	111.0	7.4	-0.239	3.301	16.6	20.2
A6	3.79	4.38	132.5	7.1	0.013	3.699	14.1	14.3
B1	4.41	4.12	114.4	-3.4	-0.084	3.306	1.2	3.4
B2	4.10	4.47	126.5	-0.8	0.005	3.800	36.9	38.7
B3	4.40	4.15	114.8	2.3	0.058	3.561	7.1	7.2
B4	4.26	4.42	122.6	0.6	-0.043	3.683	31.1	30.7
B5	4.31	4.19	117.3	-5.4	-0.041	3.237	10.0	9.8
B6	4.18	4.33	124.2	6.6	0.105	3.450	27.1	27.8

[a] *mean e.s.d. = 0.002 Å;* [b] *mean e.s.d. = 0.006 Å;* [c] *mean e.s.d. = 0.1° ;* [d] *mean e.s.d. = 0.2°.*

The ellipticity of the O4-hexagon in host molecule A is evident from the wide range of radii values (*l*), namely 3.79-4.58 Å. The transannular distance O4A3•••O4A6, normal to the plane of the included aromatic ring, is only 7.61 Å, whereas distance O4A1•••O4A4, which is roughly parallel to the included ring plane, is 8.95 Å. Instead, for host molecule B, the values of parameter *l* span the narrow range 4.10-4.41 Å. The more severe distortion of host molecule A is also reflected in wider ranges of the parameters *D* and ϕ when compared with data for host molecule B, larger magnitudes in torsion angles (*d*) and more significant deviations from the O4-plane (α). In accommodating the phosphate ester residue, host

molecule B maintains a 'round' shape (based on the uniform radii *l*), though the individual glucose rings tilt (as reflected in the parameters τ_1 and τ_2) with a range of angles wider than that for host molecule A. The host molecules are somewhat offset from one another (R_A = 3.1 Å and R_B = 2.3 Å, defined on pg. 8) with an angle of 3.25(6)° between the two O4 mean planes. These two features allow for optimal guest encapsulation.

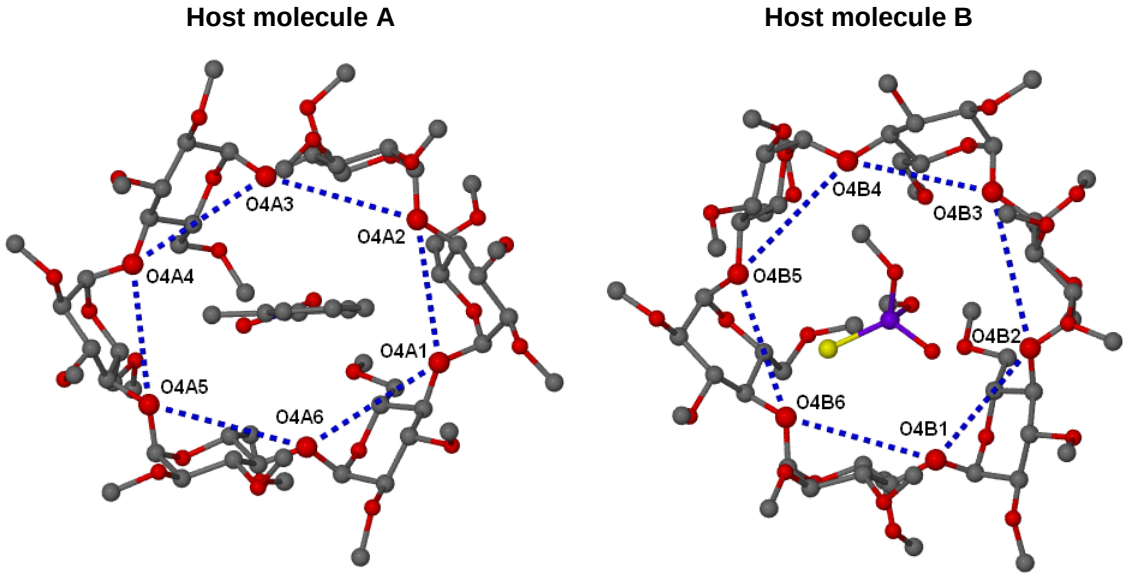

Figure 12. *Host molecules A and B viewed from their secondary sides and including their respective guest moieties. The blue dashed lines link the O4 atoms of each glucose unit showing a schematic representation of the two macrocycles.*

Guest inclusion and conformational disorder

As can be seen from Figure 12 above, host molecule A accommodates the aromatic portion of the fenitrothion molecule while the disordered *O*, *O*-dimethyl phosphorothioate unit is contained within the cavity of host molecule B. The primary methoxyl groups act as lids sealing off the primary rims. A cross-sectional space-filling representation of TMEAFEN emphasises the extent to which the host molecules are offset as well as the mode of encapsulation (Figure 13). The guest molecule is not deeply situated within the two TRIMEA cavities, as atom O9 of the nitro group is only 0.17 Å above the O4 mean plane of host molecule A while atom C17A of the phosphorothioate unit is 0.09 Å below the O4 mean plane of host molecule B (see Figure 13).

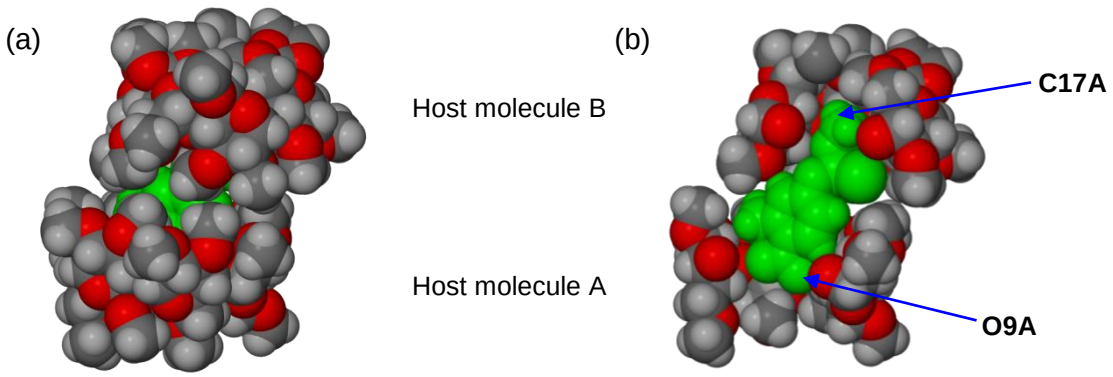

Figure 13. *A space-filling (a) side-on and (b) cross-sectional view of TMEAFEN.*

The nature of the guest disorder in TMEAFEN is shown in Figure 14, where for clarity the entire molecules (a) and (b) are drawn for what are essentially two rotamers, the *O,O*-dimethyl phosphorothioate groups being rotated by 107° with respect to one another around the O11-P12 bond. The two components thus share all atoms except the sulphur atom and one of the methoxy groups. Conformational differences are reflected in a range of torsion angles (Table 10). There is a slight twist of the nitro-group out of the plane of the aromatic ring and a *gauche* conformation around the bond C6-O11 linking the aromatic group to the phosphorothioate unit. The angles around the phosphorus atom indicate a tetrahedral geometry for both components.

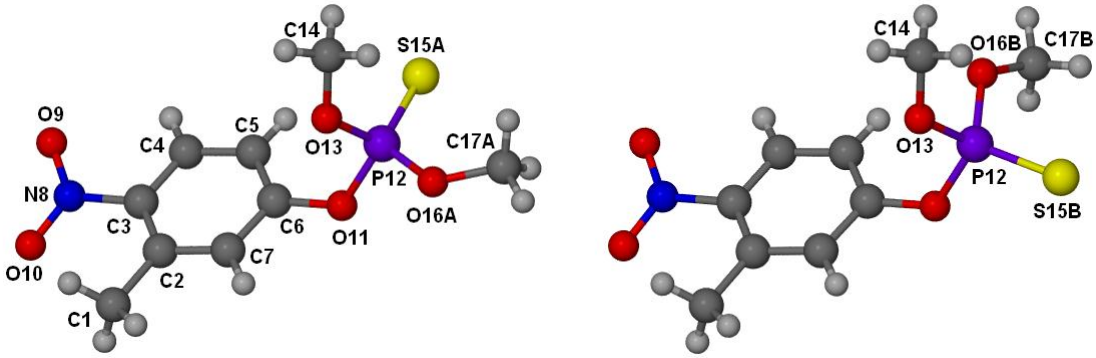

Figure 14. *Rotamers of fenitrothion giving rise to twofold disorder in TMEAFEN.*

Table 10*. Selected torsion angles of the fenitrothion molecule in TMEAFEN.*

Atoms	Torsion angle (°)	Atoms	Torsion angle (°)
C4-C3-N8-O9	-16.4(7)	C5-C6-O11-P12	57.9(7)
S15A-P12-O16A-C17A	8.3(2)	S15B-P12-O16B-C17B	50.2(7)
S15A-P12-O13-C14	-40.1(6)	S15B-P12-O13-C14	73.8(7)

Intra- and intermolecular interactions

Host interactions

As there are no hydroxyl groups or water molecules present in the TMEAFEN structure the principal hydrogen bonds are weak C–H•••O interactions. There are twelve intramolecular C6–H•••O5(n+1) interactions with an average C•••O distance of 3.27 Å and an average C–H•••O angle of 139°. These particular hydrogen bonds are responsible for the large tilt angles experienced by the methyl glucose units. Numerous intraglucose hydrogen bonds (C8–H•••O2, C9–H•••O5) exist as a result of the flexible primary and secondary methoxyl groups. A total of nine C–H•••O intermolecular host-host interactions occur with host molecule A acting as a hydrogen bond donor in three cases to oxygen atoms from an adjacent host molecule B, and *vice versa* for the other six interactions. These hydrogen bonds are listed in Table 11.

Table 11. *Host-host intermolecular interactions for TMEAFEN.*

Interaction	D ••• A (Å)	D-H ••• A (°)	Symmetry operator*
C2A4–H2A4•••O3B3	3.40(1)	163	*1/2+x, 1/2-y, 1-z*
C1A6–H1A6•••O6B6	3.41(1)	165	*1/2-x, 1-y, 1/2+z*
C7A6–H7AF•••O6B5	3.46(1)	169	*1/2-x, 1-y, 1/2+z*
C7B2–H7B5•••O3A1	3.14(1)	115	*-1/2+x, 3/2-y, 1-z*
C7B2–H7B6•••O3A2	3.43(1)	144	*-1+x, y, z*
C2B3–H2B3•••O3A4	3.43(1)	159	*-1/2+x, 1/2-y, 1-z*
C9B3–H9B8•••O5A5	3.11(1)	133	*-1/2+x, 1/2-y, 1-z*
C8B4–H8BZ•••O3A5	3.28(1)	136	*1/2+x, 1/2-y, 1-z*
C9B4–H9BY•••O6A6	3.36(1)	145	*1/2-x, 1-y, -1/2+z*

*The symmetry operators refer to the O atoms.

Guest interactions

Only two significant hydrogen bonds were found between the host and guest molecules namely C7–H7•••O2B3 (H•••O 2.53 Å, C•••O 3.309(6) Å and angle C–H•••O 167°), linking a phenyl hydrogen atom to a host methoxy oxygen atom, and C5A6–H5A6•••O10 (H•••O 2.53 Å, C•••O 3.482(6) Å and angle C–H•••O 159°), linking a host methine H atom to an oxygen atom of the guest nitro-group.

Crystal packing

Packing of the 2:1 host-guest complex units is of the 'cage' variety (Figure 15), the primary ends of each dimeric unit being abutted by side-on contact with host molecules of complex units related by the twofold screw axis parallel to *c*. Fenitrothion molecules are isolated from one another by complete encapsulation within the dimers.

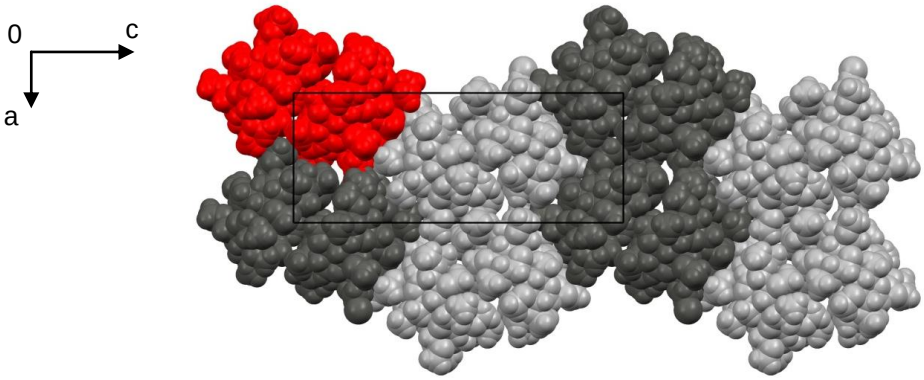

Figure 15. *Space-filling representation of the cage-type packing of TMEAFEN. The asymmetric unit is shown in red and the other screw-related dimeric complex units are distinguished by their shading.*

Comparative PXRD

Figure 16 shows the experimental and calculated PXRD patterns of the TMEAFEN complex. These display similar peak positions and peak intensities. There is a small shift of peaks for the calculated PXRD pattern to higher 2θ values. This is a result of the X-ray diffraction data being collected at a much lower temperature (173 K) for the single crystal than the experimental pattern (294 K) of the bulk sample. Nevertheless, the correspondence below confirms that the single crystal used for determination of the X-ray crystal structure is representative of the bulk sample.

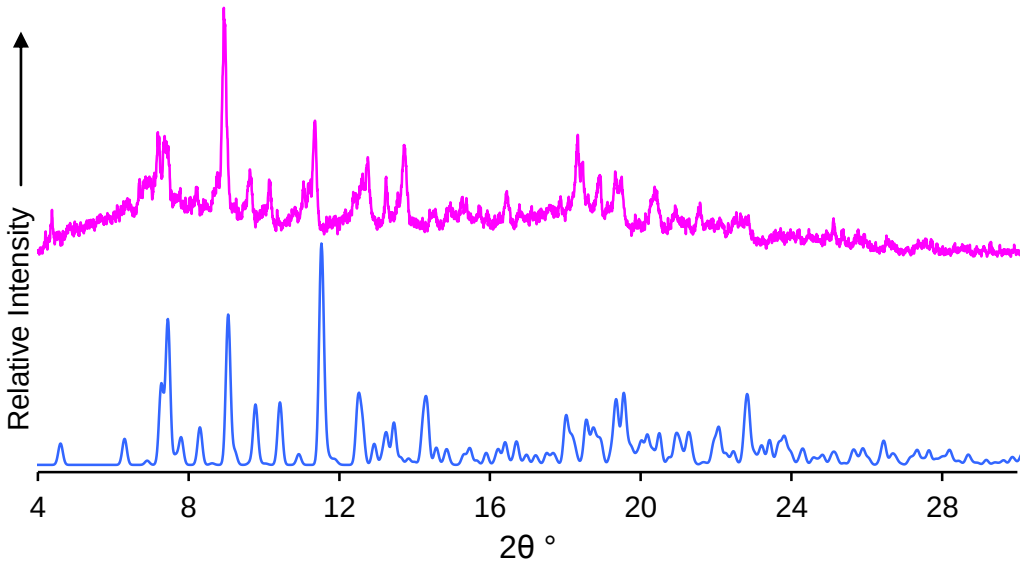

Figure 16. *Calculated (blue) and experimental (pink) PXRD traces of TMEAFEN.*

TRIMEB INCLUSION COMPLEX WITH FENITROTHION

Complex preparation

The preparation of the TRIMEB·fenitrothion inclusion complex (TMBFEN) commenced with a solution of TRIMEB (0.072 mmol) in 2 cm^3 of distilled water at 40 °C, to which an equimolar quantity of fenitrothion was added. Continuous stirring and cycling through heating and cooling stages as well as addition of a further 2 cm^3 of distilled water yielded a clear solution that was placed in a Dewar flask containing water at 50 °C. After 5 days a powder precipitated. Upon standing at room temperature for one month, colourless single crystals appeared. It is noteworthy that the method described here is significantly different from the conventional procedure for preparing single crystals with derivatised CDs.

Confirmation of stoichiometry

The host-guest stoichiometry for TMBFEN was established from elemental analysis. For a 1:1 host-guest stoichiometry, the formula $C_{63}H_{112}O_{35}·C_9H_{12}O_5NPS$ requires % C, 50.67, % H, 7.32 and % N, 0.82. The experimentally determined elemental analysis results of % C, 50.60, % H, 7.43 and % N, 0.61 agree with the theoretical 1:1 percentages, therefore confirming the 1:1 host-guest ratio. Further confirmation was obtained from the TG trace.

Thermal analysis

Figure 17 displays the TG and DSC traces obtained for TMBFEN.

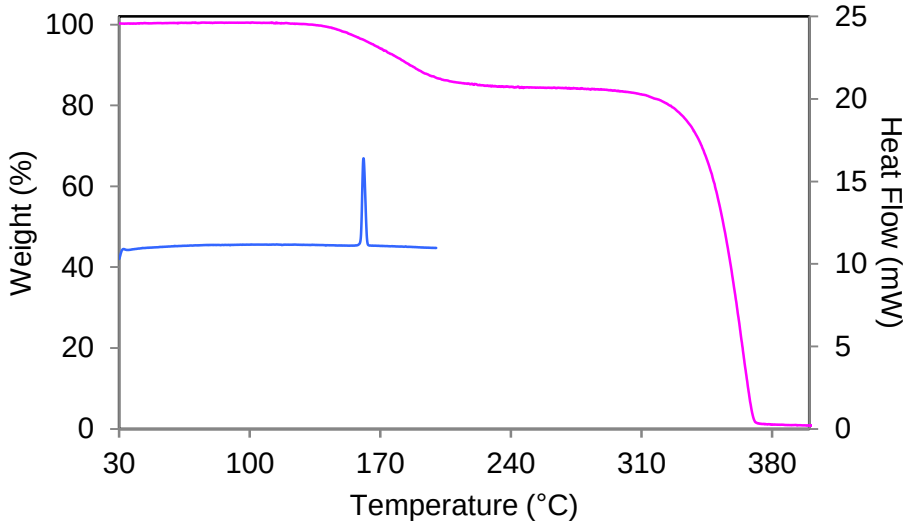

Figure 17. *Representative TG (pink) and DSC (blue) traces for TMBFEN.*

The initial plateau on the TG trace from 30 °C to beyond 100 °C indicates the absence of any water molecules. The mass loss of 16.5 ± 0.1 % (n = 2) measured from 100 to 250 °C is

due to the guest molecule dissociating from the host (calcd. for 1:1 host-guest stoichiometry 16.2%). The onset of guest loss precedes fusion (161 °C) of the complex (blue trace). Melting of this complex occurs at a temperature significantly different from those of the three known crystalline forms of TRIMEB itself. These are 157 °C for Form 1 and 148 °C for Forms 2 and 3,[18] which were also measured using DSC. Host decomposition is reflected in the second mass loss on the TG curve. The HSM images display the irregularly shaped single crystals that are stable up to a temperature of 154 °C (Figure 18). The two different preparative methods and instrumental capabilities are responsible for the slight discrepancies in the melting points obtained for the TMBFEN complex from DSC and HSM.

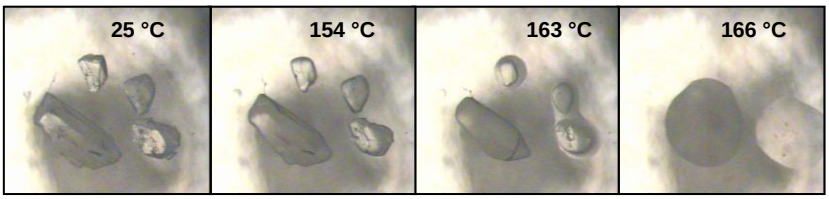

Figure 18. *HSM photographs of the TMBFEN crystals recorded at various temperatures.*

Crystal structure analysis

Data-collection and space group determination

Intensity data-collection for the complex TMBFEN was performed on a Nonius KappaCCD diffractometer. The Laue system was found to be *mmm*, indicating the orthorhombic crystal system and the space group $P2_12_12_1$ was clearly identified from systematic absences. The asymmetric unit contains one fenitrothion molecule included within a TRIMEB molecule.

Structure solution and refinement

The crystal data and refinement parameters are reported in Table 12. Structure solution of TMBFEN was achieved by using the host atomic coordinates of the isostructural complex TRIMEB·(*S*)-naproxen as a trial model.[19] All non-hydrogen atoms except O6, C7, C8 and C9 of each methyl glucose unit were included in the fragment serving as the trial model. The glucopyranose units were labelled G1-G7. Only one carbon atom of a primary methoxyl group belonging to the host was disordered over two positions and modelled by assigning s.o.f.s of *x* and *1-x*, with *x* variable. All host atoms except those of the disordered component were treated anisotropically in full-matrix least-squares refinement (program SHELXH-97).[12] Hydrogen atoms for the host were placed in idealised positions using a riding model and were assigned isotropic temperature factors 1.2-1.5 times those of their parent atoms.

Table 12. *Data-collection and refinement parameters for the TMBFEN complex.*

Chemical formula	$C_{63}H_{112}O_{35}\cdot C_9H_{12}O_5NPS$
Formula weight	1706.75
Crystal system	Orthorhombic
Space group	$P2_12_12_1$
Unit cell constants	
a (Å)	15.1588(4)
b (Å)	21.1279(4)
c (Å)	27.5575(7)
$\alpha = \beta = \gamma$ (°)	90
Volume (Å^3)	8825.9(4)
Z	4
Density$_{calc}$ (g cm^{-3})	1.284
μ [MoKα] (mm^{-1})	0.144
F (000)	3656
Temperature of data collection (K)	173(2)
Crystal size (mm)	0.24 x 0.13 x 0.11
Range scanned θ (°)	2.69 – 25.70
Index ranges	h: -18, 18; k: -25, 25; l: -33, 33
ϕ and ω scan angle (°)	1.0
Total no. of frames	642
Dx (mm)	39.00
Total no. of reflections collected	121751
No. of independent reflections	16732
No. of reflections with I > 2σ(I)	11175
No. of parameters	959
R_{int}	0.0568
S	1.021
R_1 [I > 2σ(I)]	0.0626
No. of reflections omitted	33
wR_2	0.1428
Weighting scheme parameters	a = 0.0782 and b = 6.3303
$(\Delta / \sigma)_{mean}$	< 0.001
$\Delta\rho$ excursions (e Å^{-3})	0.71 and -0.74

Modelling of the fenitrothion guest

During initial refinement of the host atoms it was relatively easy to model a single guest molecule within the TRIMEB cavity. However, large electron density peaks were still present in the vicinity of the guest molecule and certain atoms had unsatisfactorily large thermal parameters, suggesting guest disorder, i.e. evidence of a second guest component. From the high quality of the X-ray data set, a second component could be modelled. Two AFIX 66 instructions, which constrained the phenyl rings as rigid hexagons, as well as several distance restraints were applied to both guest molecule components in order to maintain reasonable geometries. The two guest components, labelled A and B, were refined with global s.o.f.s of *x* and *1-x*. The value of *x* refined to 0.66 for the major component, A. Each guest atom was refined with individual isotropic thermal parameters. The aromatic hydrogens were refined with thermal parameters 1.2 times the U_{iso} values of their parent atoms, while the methyl hydrogens refined with U_{iso} values 1.5 times those of their parent atoms.

Geometrical analysis of the TMBFEN structure

The asymmetric unit of TMBFEN comprises one TRIMEB molecule and the included fenitrothion molecule (Figure 19 (a)). The numbering scheme of the glucose units are shown in the accompanying figure (Figure 19 (b)).

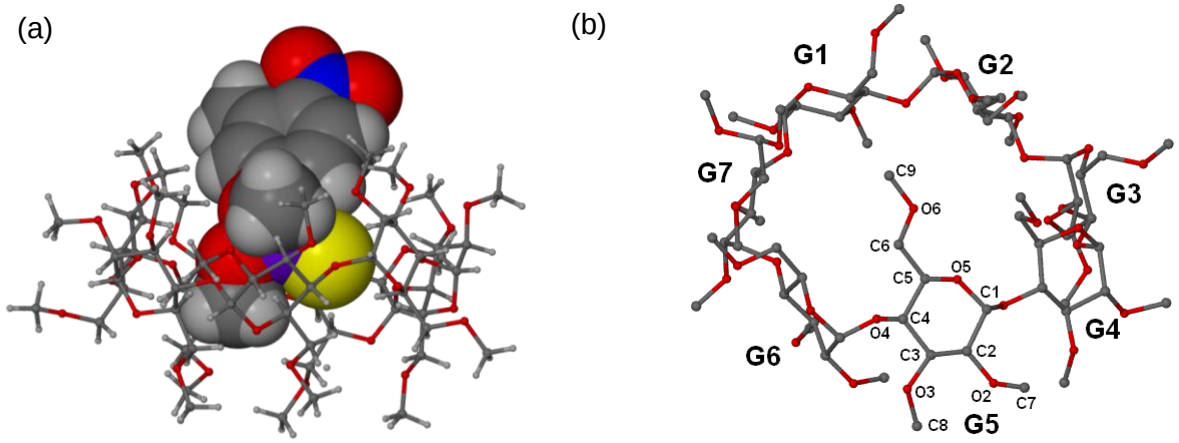

Figure 19. *(a) The asymmetric unit of TMBFEN with only the major disordered guest component shown. (b) The macrocyclic structure and numbering scheme of the TRIMEB glucose residues (hydrogen atoms have been omitted for clarity).*

Host conformation

Methyl glucose units G1, G3, and G6 all have positive ω torsion angles (O5-C5-C6-O6) indicating a (+)-*gauche* conformation. The other four methyl glucose units contain primary

methoxyl groups with a negative ω torsion angle and their C6-O6 bonds are directed away from the TRIMEB cavity. The host geometrical parameters (Table 13) compare favourably with those for the isostructural complex TRIMEB·(*S*)-naproxen[19] as well as the TMBCYC complex reported earlier in this thesis. The distorted, saddle-like conformation of the TRIMEB molecule can be seen from the large range of τ_1 and τ_2 tilt angles as well as the large range of positive and negative deviations (α) of the O4 atoms from the O4 mean plane. The torsion angles (*d*) involving the O4 atoms of the TRIMEB molecule are also relatively large. This illustrates the lack of planarity between the O4 atoms, which is due to excessive tilting of the methyl glucose units.

Table 13. *Geometrical parameters for the host molecule of the TMBFEN complex.*

Residue	*l* (Å)	*D* (Å)	ϕ (°)	*d* (°)	α[a] *(Å)*	D_3[b] (Å)	τ_1[c] (°)	τ_2[d] (°)
G1	5.18	4.49	124.5	5.7	0.239	3.404	15.5	16.4
G2	4.89	4.26	129.2	-23.5	0.441	3.088	27.2	28.0
G3	4.83	4.41	131.3	0.8	-0.384	3.242	29.2	35.2
G4	5.14	4.40	124.4	25.5	-0.340	3.569	14.5	15.3
G5	5.15	4.29	120.7	-19.0	0.603	3.831	37.8	36.5
G6	4.65	4.47	138.2	-12.1	-0.017	3.341	39.4	44.2
G7	5.11	4.28	122.6	19.2	-0.541	3.459	11.6	12.1

[a] *mean e.s.d. = 0.002 Å;* [b] *mean e.s.d. = 0.006 Å;* [c] *mean e.s.d. = 0.1° ;* [d] *mean e.s.d = 0.1°.*

Guest inclusion

Space-filling representations of the complex in Figures 20 (a)-(d) illustrate the position and orientation of the guest molecule within the TRIMEB cavity. The *O,O*-dimethyl phosphorothioate residue of the guest is deeply embedded and in contact with the 'roof' of the host cavity, formed by the primary methoxyl groups of glucose residues G1, G3 and G6. The nitro and methyl substituents of the phenyl group protrude from the secondary rim of the TRIMEB molecule.

The disordered guest model comprises two distinct molecules of fenitrothion (Figure 21), molecule A being the major component. The methyl nitro-phenyl ring planes are related by an approximate twofold rotation axis as well as a lateral shift. In fact, the aromatic ring planes are not coplanar but intersect at ~15°. Furthermore, as found for the fenitrothion molecule in TMEAFEN, the disordered components are distinct rotamers which include in the TRIMEB cavity in a similar fashion.

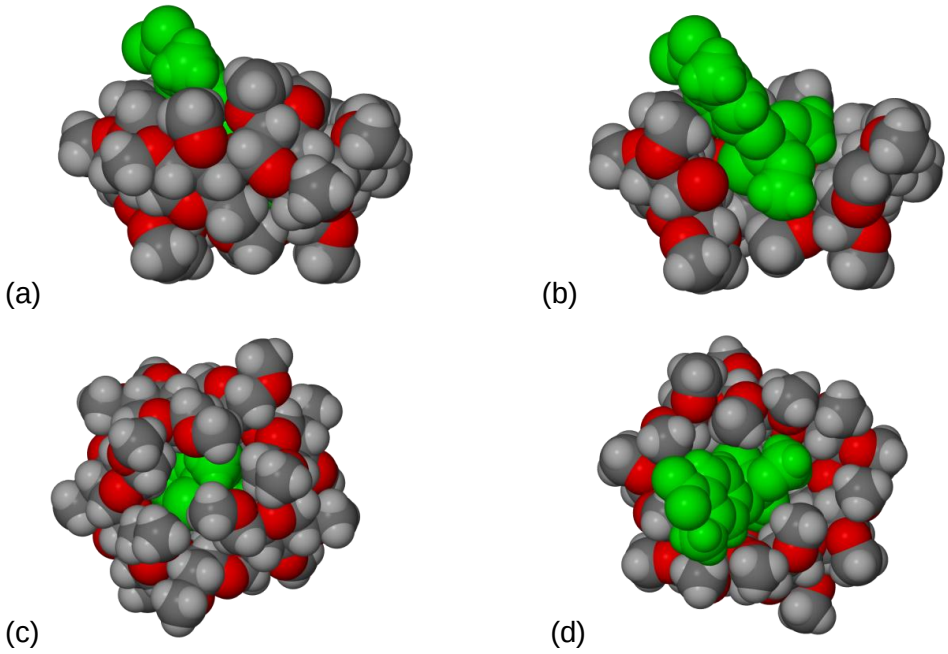

Figure 20. *(a) A side view, (b) a cross-sectional view, (c) a view from the primary rim and (d) a view from the secondary rim of the TMBFEN complex (Only the major disordered guest component has been shown for clarity).*

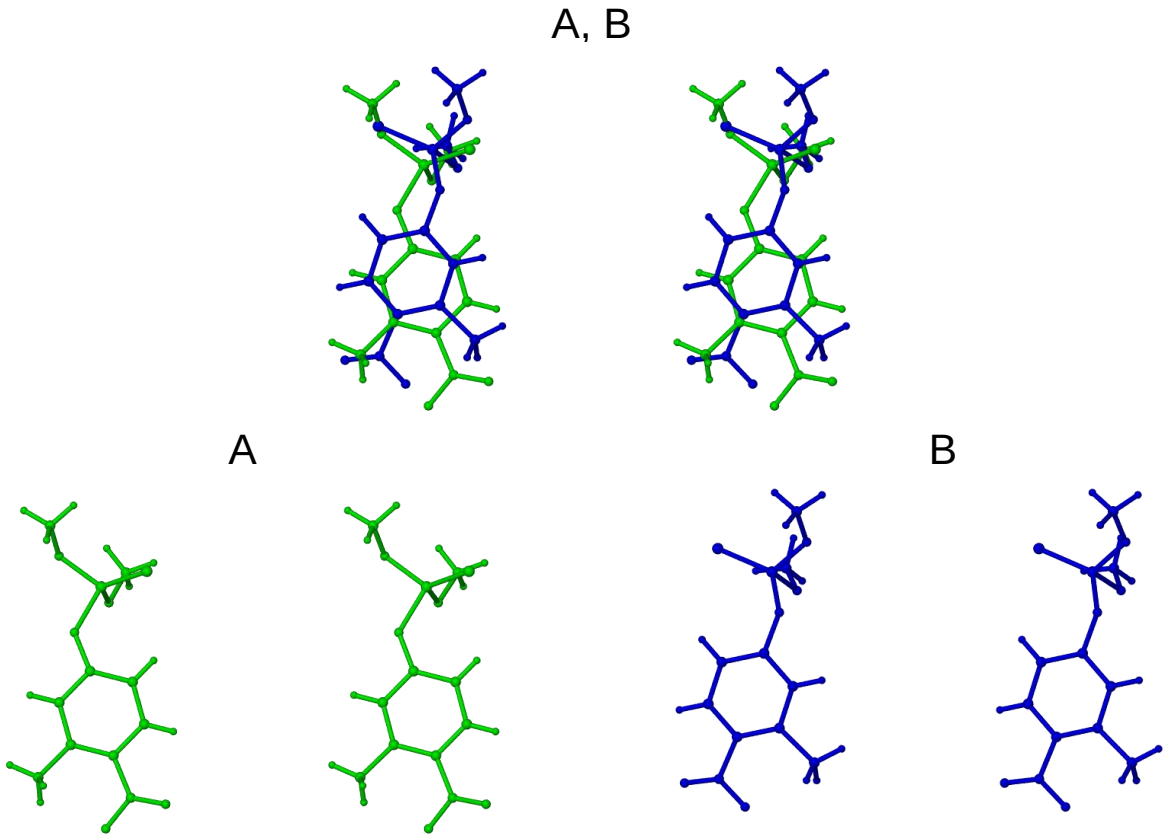

Figure 21. *Stereoviews of the disordered guests A/B of the TMBFEN complex and the deconvoluted disordered components A (green) and B (blue).*

Disordered component B is positioned slightly closer towards the primary rim of the CD cavity, with non-hydrogen atoms C14B, O13B and S17B all situated above the O4 mean plane while the major component A contains only one non-hydrogen atom (C16A) above the O4 mean plane (Figure 22).

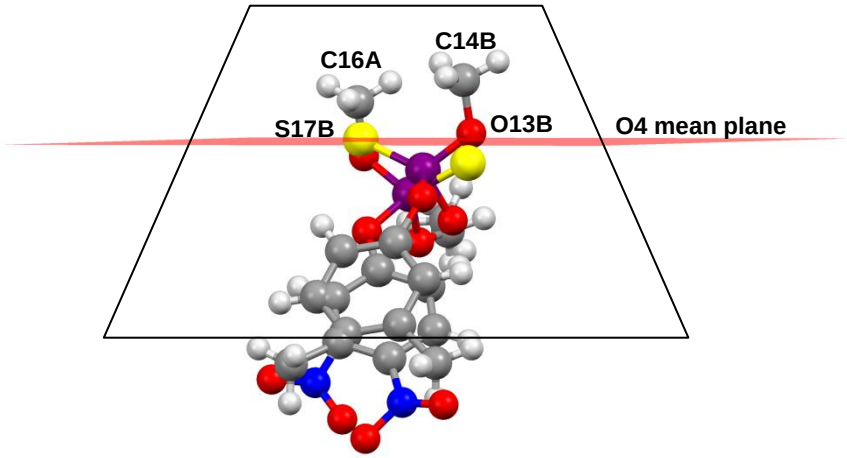

Figure 22. *Position of guest components relative to the O4 mean plane.*

Intra- and intermolecular interactions

The TMBFEN structure contains no hydroxyl groups or water molecules, resulting in primarily weak C–H•••O hydrogen bonds as the only source of crystal cohesion. The intramolecular interactions comprise two types; first, those between atoms O5 and C6(n-1) which occur at the primary rim and maintain the large tilt angles experienced by the methyl glucose units, and the intraglucose interactions between two methoxyl groups (involving atoms C7 and O3 or atoms C8 and O2) at the secondary rim of the CD cavity.

Table 14 lists five intermolecular host-host interactions as well as four host-guest interactions. Three of the four possible host-guest interactions occur at the primary rim of the TRIMEB molecule between the carbon atoms of the *O,O*-dimethyl phosphorothioate unit and particular host oxygen atoms. Only one host-guest interaction occurs at the secondary rim between the oxygen atom of the nitro-group and a twofold screw-related primary methoxyl group of a TRIMEB molecule. These hydrogen bonds are crucial in stabilising the overall crystal structure.

Table 14. *Host-host and host-guest hydrogen bonds for TMBFEN.*

Type	Interaction	D ••• A (Å)	D-H ••• A (°)	Symmetry operator*
Host-host	C2G2–H2G2•••O6G5	3.41(1)	151	*3/2-x, 1-y, 1/2-z*
	C2G3–H2G3•••O6G7	3.41(1)	160	*-1+x, y, z*
	C2G5–H2G5•••O6G2	3.38(1)	157	*3/2-x, 1-y, -1/2+z*
	C9G4–H9G9•••O3G6	3.08(1)	116	*-1+x, y, z*
	C9G5–H9GX•••O3G2	3.22(1)	126	*3/2-x, 1-y, -1/2+z*
Host-guest	C14A–H14B•••O4G6	3.48 (1)	136	*x, y, z*
	C14A–H14B•••O2G7	3.44(1)	131	*x, y, z*
	C14B–H14F•••O6G6	3.18 (1)	128	*x, y, z*
	C9G4–H9GZ•••O9A	3.45(1)	154	*1-x, 1/2 -y, 1/2-z*

*The symmetry operators refer to the O atoms.

Crystal packing

Crystal packing for TMBFEN is shown in Figure 23. Monomeric units of TMBFEN pack in screw-channel mode in a head-to-tail fashion. In this well-known packing arrangement, alternate host molecules in a particular column parallel to the *b*-axis are offset by several Ångstroms in the *x*-direction, resulting in an undulating host channel, as opposed to a linear one. The nitro group occupies an interstitial void created by surrounding host molecules.

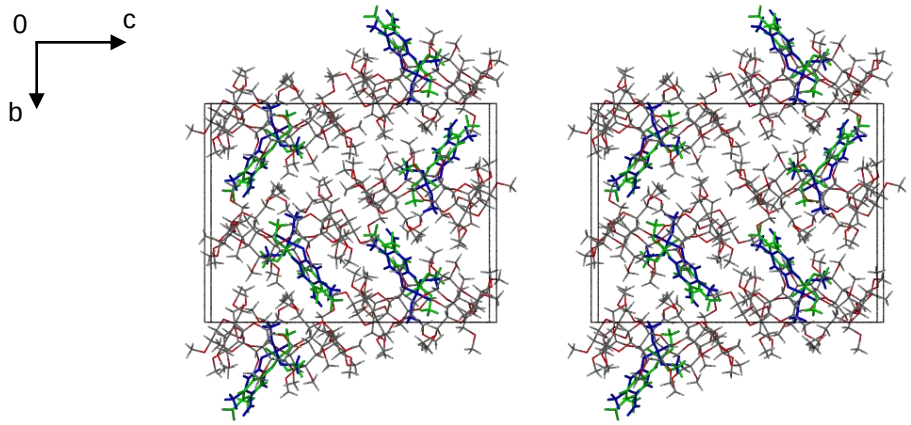

Figure 23. *Stereoview of the crystal packing for the TMBFEN complex viewed along [100]. Disordered guest molecules are shown in green and blue.*

Comparative PXRD

The computed pattern and experimental pattern show a close resemblance indicating that the single crystal is representative of the bulk sample (Figure 24). The shift of the calculated peaks to higher 2θ values is due to shrinkage of the single crystal on cooling to 173 K for the X-ray data collection. The experimental pattern was recorded at room temperature (294 K). This complex is isostructural with TMBCYC (Chapter 3) and therefore has a very similar PXRD pattern. The nature of the guest molecule does not seem to influence the PXRD pattern significantly as the packing arrangement of these particular TRIMEB inclusion complexes is governed mainly by the hydrogen bonds forming between the CD molecules.

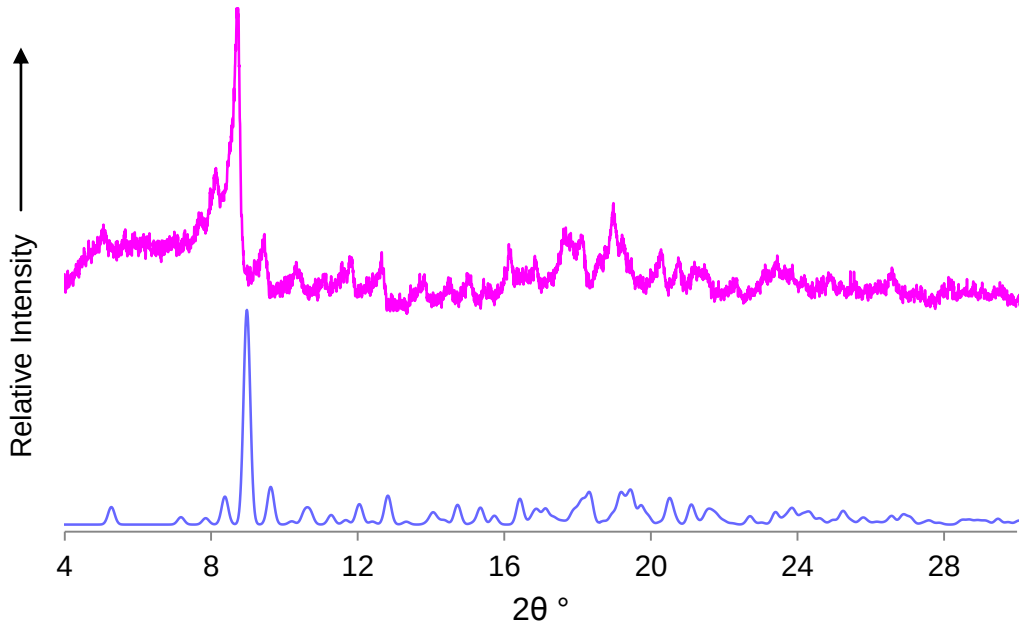

Figure 24. *Calculated (blue) and experimental (pink) PXRD traces of TMBFEN.*

DIMEB INCLUSION COMPLEX WITH FENITROTHION

Complex preparation

The DIMEB·fenitrothion complex (DMBFEN) was prepared in a similar manner to TMEAFEN. 20 mg of fenitrothion (~0.072 mmol) was added to a saturated aqueous solution of DIMEB (96 mg, 0.072 mmol) at 20 °C. Continuous stirring for 6 h, as well as several heating and cooling cycles between 20 and 60 °C led to a clear solution which was filtered into a clean vial, capped and placed in an oven at 60 °C. Colourless single crystals appeared over a 24 h period.

Confirmation of stoichiometry and integrity of fenitrothion

A 1:1 host-guest stoichiometry was established using ^{1}H NMR spectroscopy through integration of the respective host and guest signals (Table 15, see Appendices). There was evidence of a slight excess of the host. This can only be due to the presence of both DIMEB and DMBFEN crystals present in the sample submitted for ^{1}H NMR spectroscopy. TG analysis, however, was used in addition to ^{1}H NMR spectroscopy to confirm the 1:1 host-guest stoichiometry.

Table 15. *Integrals of the host and guest protons for DMBFEN used to confirm the stoichiometry.*

Proton (CD/G) – [Total no. of protons]	δ (ppm)	Integration of peaks	Experimental peak integral/ Theoretical proton no.
7 × H**1** (CD) – [7]	4.952	9.02	1.3
7 × H**2** (CD) – [7]	3.271	8.47	1.2
Ar-C$\underline{H}_3$ (G) – [3]	2.621	3.00*	1

* Reference integral.

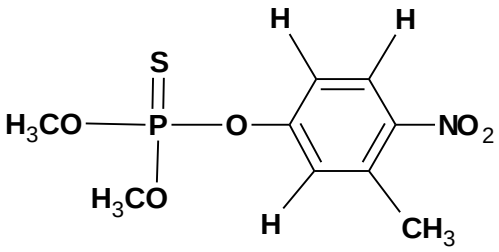

The structural integrity of the included fenitrothion molecule was confirmed with ^{31}P NMR spectroscopy which showed one signal at 65.460 ppm in $CDCl_3$. Uncomplexed fenitrothion in $CDCl_3$ has a single peak at 65.456 ppm (*cf*. pg. 166).

Thermal analysis

DMBFEN displays a complex DSC trace with three small, but notable, thermal events (Figure 25). At 132 °C there is a small endotherm which may be due to rearrangement of the complex structure to one that is more favourable for guest loss. The endotherm at 158 °C is attributed to guest loss while the broad exotherm at 234 °C can be attributed to the start of decomposition. The TG curve indicates a total mass loss of 17.9 ± 0.3 % (n = 2) between 100 and 242 °C. This results from the guest dissociating from the host (calcd. for 1:1 host-guest stoichiometry 17.2%). The slope of the TG curve changes considerably over the above-mentioned temperature range indicating that a more complicated process is involved. Host decomposition occurs beyond 300 °C.

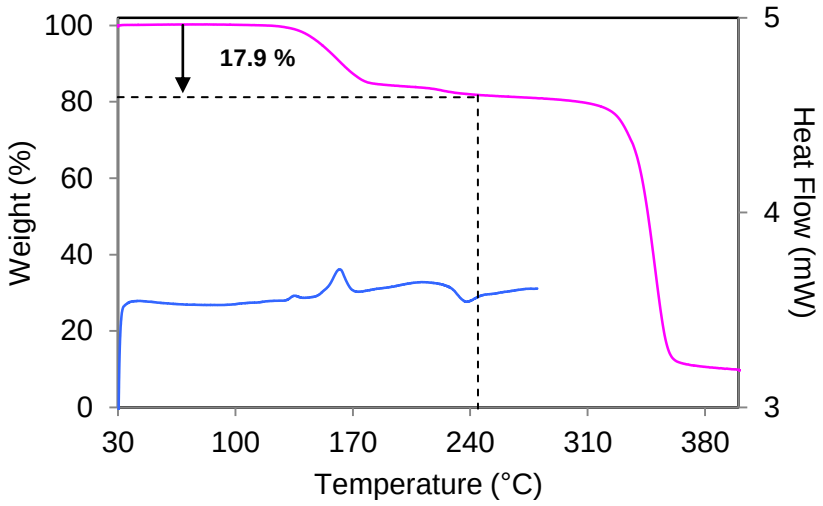

Figure 25. *Representative TG (pink) and DSC (blue) traces for DMBFEN.*

The HSM photographs (Figure 26) depict the nearly cubic colourless crystals of DMBFEN. The crystals become opaque at 160 °C and then start to decompose at 230 °C, which can be seen by the discolouration.

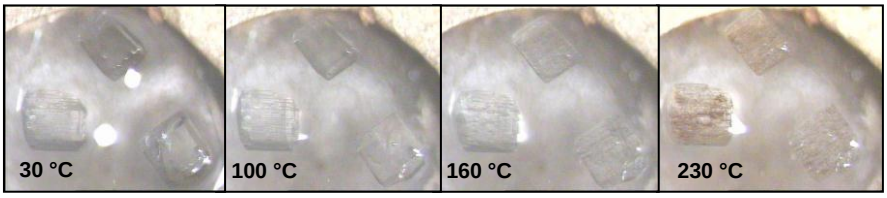

Figure 26. *HSM images of the DMBFEN crystals recorded at various temperatures.*

Crystal structure analysis

Data-collection and space group determination

Intensity data-collection for DMBFEN was performed on a Bruker KAPPA APEX II DUO diffractometer. Upon inspection of the reciprocal lattice layers with the program LAYER,[9] the X-ray diffraction pattern revealed Laue symmetry 2/*m*, corresponding to the monoclinic crystal system. The intensity-weighted reciprocal lattice also revealed alternation in intensity of the layer lines perpendicular to a*, from which it was deduced that the structure repeats itself at *x*, *y*, *z* and at approximately *x+1/2, y, z*. The space group $P2_1$ was identified based on the reflection conditions *hkl: none; h0l: none; 0k0: k = 2n* (the alternative space group $P2_1/m$ was eliminated due to its centrosymmetry, which is not compatible with the chiral host molecule). Space group $P2_1$ was later confirmed by the program X-PREP.[20] Due to the alternating strong and weak reflections it was possible to deduce the presence of two DIMEB molecules in the asymmetric unit.

Structure solution and refinement

The data-collection parameters and refinement parameters for the DMBFEN complex are reported in Table 16. As no isostructural DIMEB complex could be found in the literature, the program SHELXD was employed to solve the structure using *ab initio* methods.[17] The initial structure solution (correlation coefficient = 84.88) revealed most of the non-hydrogen host atoms for two DIMEB molecules and a partial guest molecule in one of the DIMEB host cavities. Before the first refinement in SHELXH-97[12] the carbon and oxygen atoms of the host were correctly assigned, as well as the atoms of the first guest molecule. The rest of the host atoms were located in the initial and subsequent difference Fourier maps. The methyl glucose moieties of two independent CD molecules in the asymmetric unit were labelled A1-A7 and B1-B7.

One primary methoxyl group per host molecule was disordered over two positions (on glucose residues B1 and A4). In the case of the primary methoxyl group on methyl glucose unit B1, all three atoms (C6, O6 and C8) were disordered and the major component refined with a s.o.f. of 0.53 while methyl glucose unit A4 contained only atom O6 that was disordered over two positions (s.o.f. = 0.69) while C8 was shared. All ordered host atoms were refined anisotropically except atoms C7A3, C7A7, C8B4 and C8B5 which had reasonable isotropic thermal parameters but unacceptable thermal ellipsoids when refined anisotropically.

Table 16. *Data-collection and refinement parameters for the DMBFEN complex.*

Chemical formula	$C_{56}H_{98}O_{35}\cdot C_9H_{12}O_5NPS$
Formula weight	1608.57
Crystal system	Monoclinic
Space group	$P2_1$
Unit cell constants	
a (Å)	19.626(2)
b (Å)	15.049(2)
c (Å)	26.854(3)
α (°)	90
β (°)	96.451(2)
γ (°)	90
Volume (Å^3)	7881.0(2)
Z	4
Density$_{calc}$ (g cm^{-3})	1.356
μ [MoKα] (mm^{-1})	0.156
F (000)	3432
Temperature of data collection (K)	173(2)
Crystal size (mm)	0.46 x 0.35 x 0.26
Range scanned θ (°)	2.04 - 28.39
Index ranges	h: -26, 26; k: -20, 19; l: -35, 35
ϕ and ω scan angle (°)	0.5
Total no. of frames	2494
Dx (mm)	50.00
Total no. of reflections collected	125785
No. of independent reflections	20368
No. of reflections with I > 2σ(I)	17090
No. of parameters	1636
R_{int}	0.0256
S	1.019
R_1 [I > 2σ(I)]	0.0770
No. of reflections omitted	34
wR_2	0.2129
Weighting scheme parameters	a = 0.144 and b = 7.338
$(\Delta / \sigma)_{mean}$	< 0.001
$\Delta\rho$ excursions (e Å^{-3})	1.30 and -0.98

The host hydrogen atoms were placed using a riding model and were refined isotropically with temperature factors 1.2 times those of their parent atoms. For the hydroxyl groups on each methyl glucose unit a hydrogen bond searching model (AFIX 83) was used to place the hydrogen atoms in sensible hydrogen bonding positions. However, this procedure was not suitable for all the hydroxyl groups and so distance restraints were applied between the hydrogen atom of the hydroxyl group and the hydrogen bond acceptor that was on the adjacent glucopyranose unit. This was necessary for hydroxyl groups on methyl glucose units A4, A5, A6, A7, B6 and B1.

Modelling of the fenitrothion guest

Once both host molecules had been located, the first guest molecule that resulted from the initial SHELXD solution was modelled, followed by a second in the other crystallographically independent DIMEB molecule. After refinement, the temperature factors of the guest in host molecule A were reasonable except those of the atoms belonging to the *O,O*-dimethyl phosphorothioate moiety. A similar type of disorder was found to that seen in the TMEAFEN complex where the two disordered guest molecules are essentially rotamers that result from rotation of substituents around the O11-P12 bond (Figure 27). Distance constraints were applied to atoms of the phosphorothioate moiety and an AFIX 66 instruction was applied to the phenyl group which constrained the ring as a rigid hexagon. The common atoms of the guest molecule were labelled A while the second sulphur and methoxy group were labelled D (Figure 27). The s.o.f.s of the two rotamers refined with an *x* value of 0.70 and are related by a 126° rotation around the O11-P12 bond. All the ordered atoms of guest molecule A were refined anisotropically, with the exception of atoms O9A, O10A and C17A.

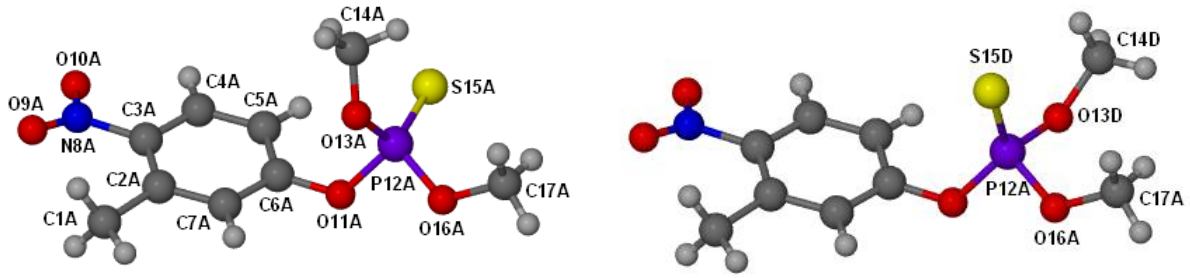

Figure 27. *Rotamers (disordered components A and D) of fenitrothion giving rise to twofold disorder.*

The first guest molecule modelled in host molecule B had many additional high electron density peaks surrounding it and the entire molecule had unacceptably high thermal parameters. There was an abnormally large peak situated close to the phenyl ring but it was not in the plane of the phenyl group. Two additional hexagonal rings were seen in the

difference Fourier map, suggesting two other guest molecule positions. After many attempts at modelling the various disordered components, three disordered components within host molecule B were evident. The relative population of each was unknown and required an analysis of the initial electron density peak heights for the phosphorus atoms of each component. Guest components B, C and E had initial phosphorus electron density peaks of 4.66, 3.07 and 2.86 e $Å^{-3}$, respectively, which resulted in fixed s.o.f. values of 0.44, 0.29 and 0.27 being applied to the three disordered components. Owing to the excessive disorder of the guests present in this particular structure, many distance restraints and three AFIX 66 commands were applied. Global temperature factors were assigned to each component and these refined to values of 0.10, 0.07 and 0.13 $Å^2$ for guest molecules B, C and E, respectively. The guest hydrogen atoms were placed and refined as described for all other fenitrothion complexes. The three disordered guest components in host molecule B are shown in Figure 28.

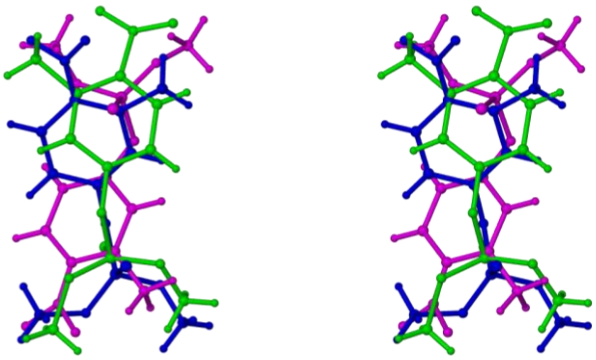

Figure 28. *Stereoview of the three disordered fenitrothion components in host molecule B [guest molecule B (green), guest molecule C (blue) and guest molecule E (pink)].*

Geometrical analysis of the DMBFEN structure

The crystallographic asymmetric unit of the DMBFEN complex comprises two DIMEB molecules each encapsulating a guest molecule. The asymmetric unit and numbering scheme employed for the glucose units are shown in Figure 29 (a) and (b) respectively.

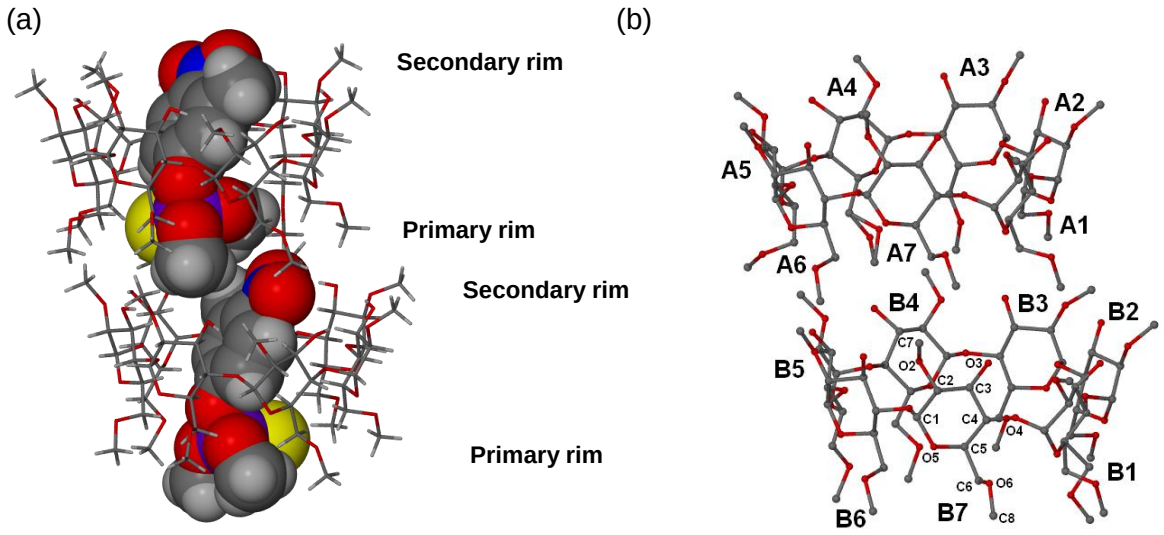

Figure 29. *(a) The asymmetric unit of the DMBFEN complex with only the two major guest components shown for clarity. (b) Macrocyclic structure and numbering scheme of the DIMEB glucose residues (hydrogen atoms have been omitted for clarity).*

Host conformation

All fourteen methyl glucose units of the two DIMEB molecules adopt the usual $^4C_1$ chair conformation. The primary torsion angle, ω (O5-C5-C6-O6), for the majority of the methoxyl groups is negative indicating the (-)-*gauche* conformation. Exceptions occur for methoxyl groups of methyl glucose units A3, A4 (both disordered components), B1 (minor component), B4 and B5, all of which have positive ω torsion angles and display a (+)-*gauche* conformation. The methoxyl groups are therefore mainly directed away from the CD cavity and do not block the primary rim of the CD cavity, as was observed for the TRIMEA and TRIMEB inclusion complexes.

Table 17 lists the geometric parameters of the O4-heptagon of the DMBFEN structure for the two independent DIMEB molecules. Other important features such as the deviation of the O4 atoms from the mean plane (α), the O2n•••O3(n-1) distance (associated with the intramolecular hydrogen bonds O2n•••H–O3(n-1)) and the tilt angles τ_1 and τ_2 are also listed. These parameters are defined in Chapter 1. The two host molecules adopt a similar

geometrical shape overall. The hosts both show slight ellipticity. The radii lengths from atom O4A1 and O4A4 to the centroid of the O4-heptagon (*l*) are larger than those for atoms O4A2 and O4A6 in the case of host molecule A. A similar situation can be seen for atoms O4B1, O4B4, O4B2 and O4B6 of host molecule B. If one were to construct a plane through the atoms of the phenyl rings for the two major guest components the planes would intersect close to atoms O4A1 and O4A4 of host molecule A (Figure 30) and similarly for atoms O4B1 and O4B4 of host molecule B. Therefore, the slightly larger range in parameters *l, D* and ϕ is due to the host accommodating the phenyl residue of the guest molecules.

Table 17. *Geometrical parameters for the host molecule of the DMBFEN complex.*

Residue	*l* (Å)	*D* (Å)	ϕ (°)	*d* (°)	α^a (Å)	$D_3{}^b$ (Å)	$\tau_1{}^c$ (°)	$\tau_2{}^d$ (°)
A1	5.18	4.35	123.6	-11.0	-0.240	2.864	18.5	18.1
A2	4.74	4.51	135.9	0.3	0.122	2.849	14.7	19.7
A3	5.09	4.32	125.2	7.8	0.169	3.049	6.1	6.6
A4	5.20	4.34	125.7	0.4	-0.171	2.831	19.8	19.1
A5	4.97	4.40	128.7	-13.5	-0.134	2.744	15.9	17.0
A6	4.80	4.37	132.3	9.5	0.268	2.715	8.8	12.6
A7	5.11	4.22	126.8	5.5	-0.014	2.954	11.3	12.3
B1	5.31	4.42	121.1	-6.5	-0.078	2.991	15.5	16.5
B2	4.65	4.56	137.7	4.7	0.147	2.925	14.5	17.0
B3	5.03	4.23	127.4	3.3	0.018	2.906	13.9	13.4
B4	5.33	4.32	123.1	-2.6	-0.137	2.841	17.4	17.5
B5	4.97	4.47	129.4	-6.8	0.009	2.796	10.1	11.5
B6	4.72	4.42	134.0	10.7	0.174	2.755	9.9	11.9
B7	5.18	4.16	126.5	-2.5	-0.132	2.887	2.0	4.1

[a] mean e.s.d. = 0.003 Å; [b] mean e.s.d. = 0.005 Å; [c] mean e.s.d. = 0.1° ; [d] mean e.s.d = 0.2°.

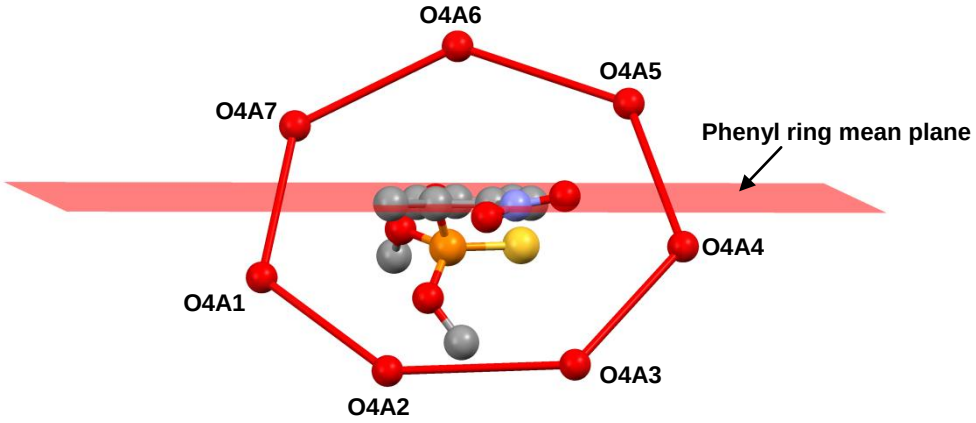

Figure 30. *The position of the phenyl ring of fenitrothion relative to the O4 atoms of host molecule A.*

The deviations of O4 atoms from the mean O4 plane and the ranges of values for the tilt angles are relatively small when compared to the trimethylated CDs. This can be attributed to the strong intramolecular hydrogen bonds (O2n•••H–O3(n-1)) that form between adjacent glucose units. The τ_1 and τ_2 tilt angles are all positive confirming the general inward trend of the methyl glucose units which gives rise to the toroidal CD shape. The O4 mean planes of the two independent DIMEB molecules are almost parallel to each other with a small angle of 2.65(2)° between them. They are slightly offset from one another (R_A = 1.67 Å and R_B = 2.10 Å) when viewed side-on; however, a projected view from the secondary or primary rim shows a large degree of similarity between the two independent host molecules.

Guest inclusion and conformation

As described earlier, host molecule A contains guest labelled A, with the minor component of the disordered *O,O*-dimethyl phosphorothioate rotamer labelled D. Host molecule B contains three disordered guest components with different orientations within the DIMEB cavity. Rotamers A and D and partial guest molecules B and C are positioned in the DIMEB cavity with their *O,O*-dimethyl phosphorothioate moieties situated at the primary rim of the DIMEB host molecules and the nitro phenyl groups at the secondary rim (Figure 29 (a)). Guest molecule E, which has a small s.o.f. value of 0.27, has the opposite orientation (Figure 28) with the phosphorothioate moiety situated at the wider secondary rim. This implies that the guest molecule can position itself in either orientation within the DIMEB cavity, but, as only a minor component adopts the latter mode of inclusion, the preferred orientation is that shown for guests A, B and C.

All guest molecules are fully encapsulated by the DIMEB molecules and there are no close contacts between the disordered guests and host molecules. Space-filling diagrams of guest molecules A and B as well as guest molecules A and E within their respective host molecules are shown in Figure 31 (a) and (b).

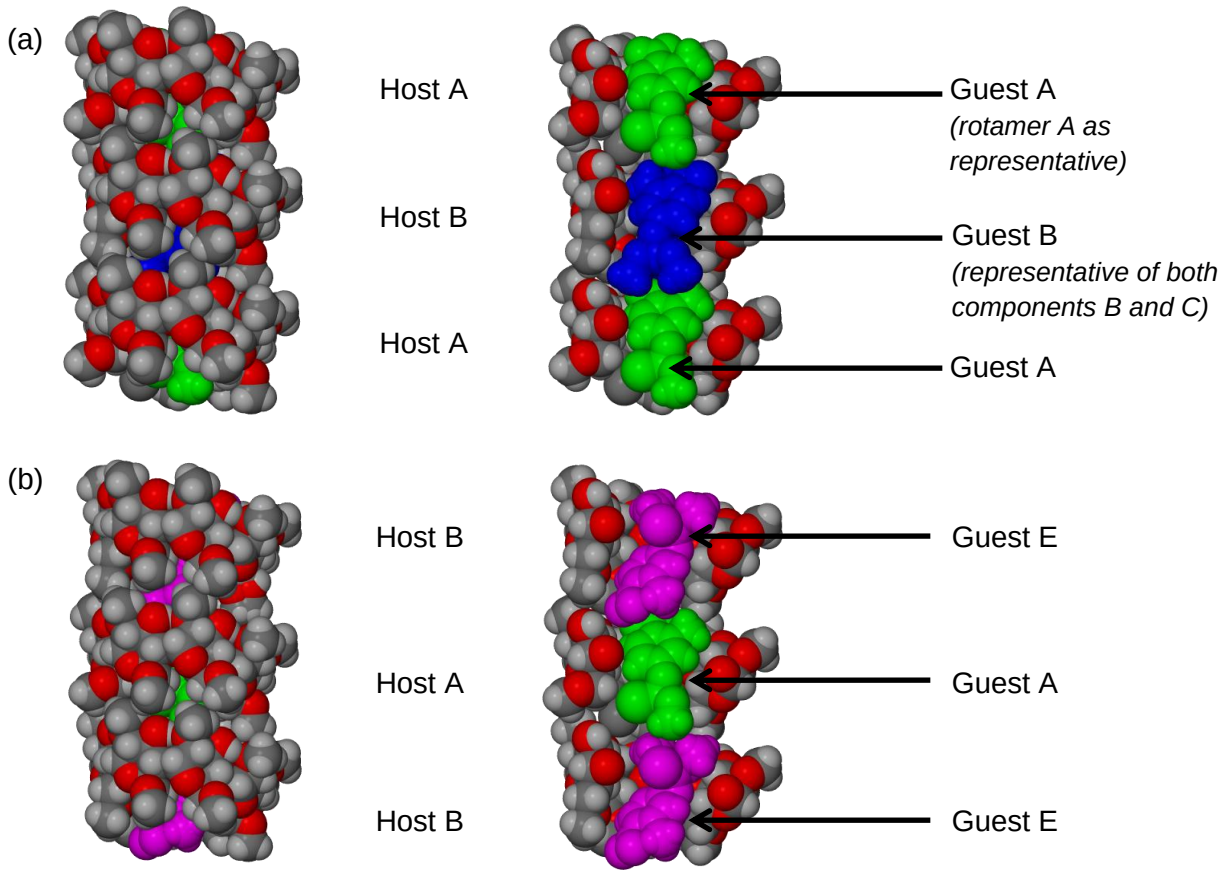

Figure 31. *Space-filling diagrams showing the relative orientations of guest molecules within the DIMEB cavity. Side view and cross-sectional views of guest molecules A and B (a) and guest molecules A and E (b) within host molecules A and B.*

Guest molecules A, B, C and E are tilted with respect to the O4 mean planes of host molecules A and B. The angles between the phenyl rings and their respective O4-heptagons are 34.6°, 25.0°, 6.0° and 30.9° for guests A, B, C and E, respectively. Even though the phenyl groups of the guests are not parallel to one another it is possible to relate the guests through approximate non-crystallographic symmetry operations (Figure 32). A rotation of approximately 180° around the O11-C6 bond of guest molecule A or B would result in very similar conformations of these guest molecules in their respective hosts (Figure 32 (b)). Guest molecules A and E are related through a pseudo-twofold rotation axis (Figure 32 (c)). A pseudo-inversion centre exists between guest molecules B and E (Figure 32 (d)); however, it would be more convincing if the two phenyl rings were aligned parallel to one another. It must be emphasised that due to the many disordered components the geometry of each guest is not ideal and the relationship described here between each guest component focuses on the rigid phenyl moiety and the relative positions of the nitro group, methyl group and the direction of the P=S bond.

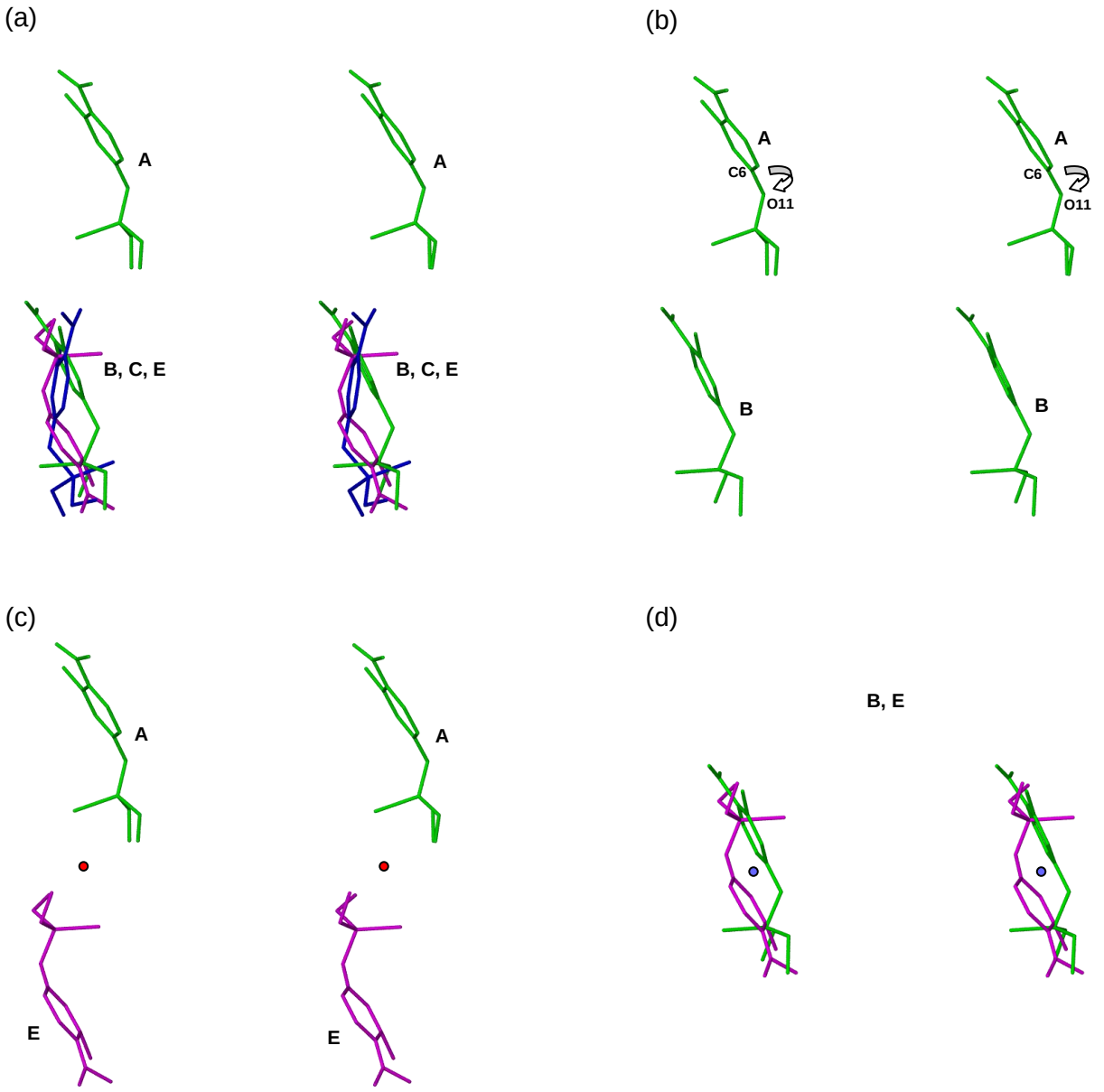

Figure 32. *Stereoview of guest molecules A, B, C and E (a). Stereoviews of guest molecules A, B (b), A, E (c) and B, E (d) illustrating approximate non-crystallographic symmetry elements and rotation operations that can be used to relate two guest components (~180° rotation, pseudo-twofold rotation [parallel to view direction], pseudo-inversion centre).*

An examination of the depth of inclusion for each guest molecule modelled in the DMBFEN structure was undertaken by measuring the normal distance from the O4 mean plane of the host to the phosphorus atom of each guest (Table 18). A negative value indicates that the phosphorus atom is positioned below the O4 mean plane close to the primary rim of the CD while a positive value implies that the phosphorus atom is closer to the secondary rim and above the O4 mean plane. From these distances it is evident that guests A, B and C are all

situated with the phosphorus atoms below the mean plane, with guest molecule C positioned the furthest away from the mean plane followed by guest molecules B and A. Guest molecule E has a completely different orientation, which is why the phosphorus atom is situated above the O4 mean plane (Figure 33).

Table 18. *Distances between the O4 mean planes of the host molecules and their respective P atoms.*

Guest molecule	Distance between O4 mean plane and P12 (Å)
A (and D)	-2.88
B	-3.93
C	-4.52
E	+0.66

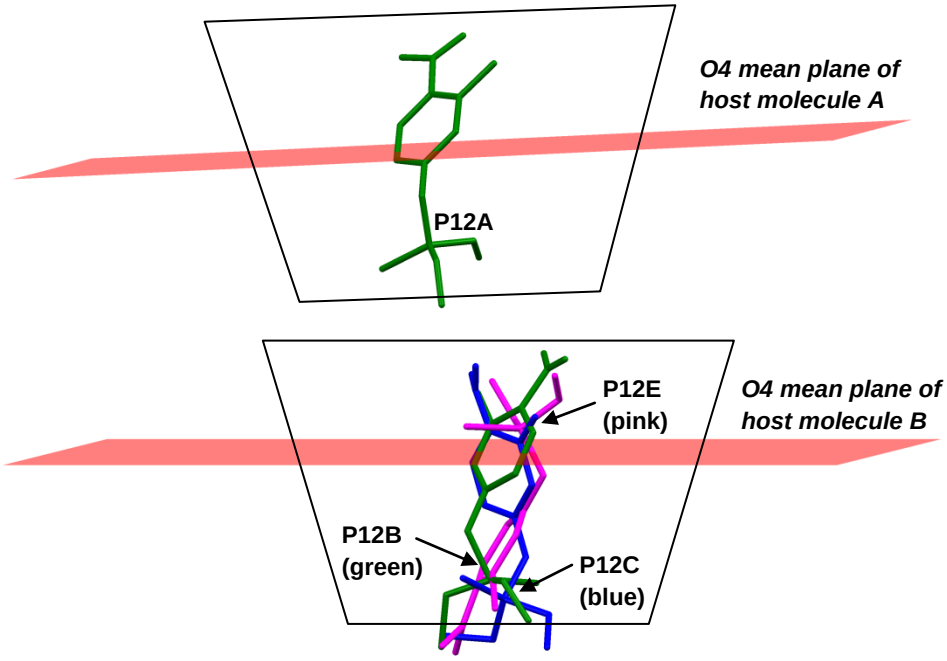

Figure 33. *Schematic representation of host molecules A and B and the relative guest positions with respect to the O4 mean plane [guest molecules A and B (green), guest molecule C (blue) and guest molecule E (pink)].*

Hydrogen bonding interactions

A total of fourteen strong intramolecular hydrogen bonds (O2n•••H–O3(n-1)) exist between glucopyranose units of the individual DIMEB molecules. The distances associated with these bonds have been tabulated above (Table 17, D_3) and the O•••H–O angles range from 145-170°. There are additional intramolecular hydrogen bonds of the type C6–H6•••O5′/O6′

and C7–H7•••O3′ which reduce the freedom associated with the methoxyl groups and contribute to the slight inward tilt of the methyl glucose units. Two host-guest interactions are present (Table 19). One occurs between the oxygen atom of the nitro group of guest A and a primary methoxyl group of a DIMEB molecule situated below the host in which guest A is included; the other host-guest interaction occurs between the phenyl group of guest E and host molecule B. Table 19 includes the host-host C–H•••O hydrogen bonds. As there are no water molecules, these weak C–H•••O hydrogen bonds are crucial in maintaining the host framework.

Table 19*: Host-guest and host-host hydrogen bonds for DMBFEN.*

Type	Interaction	D ••• A (Å)	D-H ••• A (°)	Symmetry operator*
Host-guest	C8B4–H8B8•••O10A	3.51(1)	171	*-1+x, y, z*
	C4E–H4E•••O4B	3.59(1)	161	x, y, z
Host-host	C2A1–H2A1•••O6A2	3.47(1)	150	1-*x*, -1/2+y, -*z*
	C2A2–H2A2•••O5A1	3.48(1)	160	1-*x*, 1/2+*y*, -*z*
	C7A2–H7A4•••O3B7	3.00(1)	124	1-*x*, 1/2+*y*, -*z*
	C2A3–H2A3•••O5A7	3.42(1)	148	*x*, 1+*y*, *z*
	C7A5–H7AC•••O6B6	3.42(1)	148	1-*x*, 1/2+*y*, -*z*
	C7A6–H7AF•••O5B5	3.43(1)	155	1-*x*, -1/2+*y*, 1-*z*
	C2B2–H2B2•••O5B1	3.39(1)	164	-*x*, 1/2+*y*, -*z*
	C1B5–H1B7•••O2A6	3.52(1)	156	1-*x*, 1/2+*y*, 1-*z*
	C2B7–H2B7•••O3B3	3.26(1)	128	*x*, -1+*y*, *z*
	C2B1–H2B1•••O6B2	3.40(1)	153	-*x*, -1/2+y, -*z*

*The symmetry operators refer to the O atoms.

Crystal packing

The DIMEB molecules pack head-to-tail in infinite columns along the *a*-axis (Figure 34). Owing to the twofold screw axis in the *y*-direction the adjacent columns are anti-parallel to one another. The slight ellipticity of the host molecules and the extension of the primary methoxyl groups into the interstitial sites assist in the close packing of these host molecules. Host molecule B is related to host molecule A by a lateral shift of ~ $a/_2$ (Figure 34 (b)).

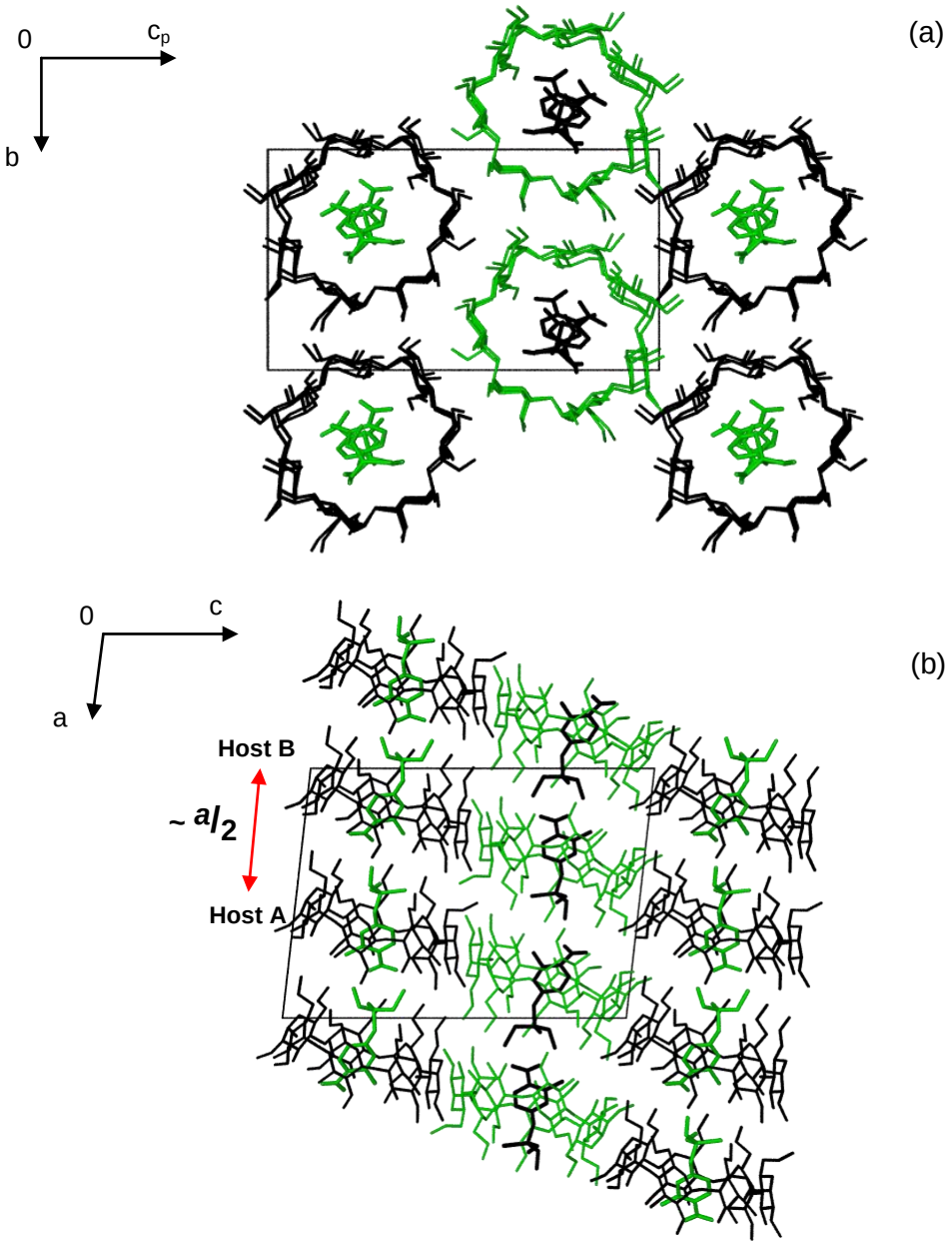

Figure 34. *Packing diagrams of the DMBFEN structure, viewed along (a) [100] and (b) [010]. The symmetry related molecules are distinguished by the reverse green and black host and guest molecules. Only guest molecules A and B are shown and the hydrogen atoms have been omitted for clarity.*

Comparative PXRD

It is possible to confirm the homogeneous nature of the sample prepared as the computed single crystal XRD pattern matches that of the experimental pattern of the bulk material (Figure 35). There is a slight shift in the peak positions to lower 2θ° values for the experimental trace. This is due to the different temperatures at which the data were collected.

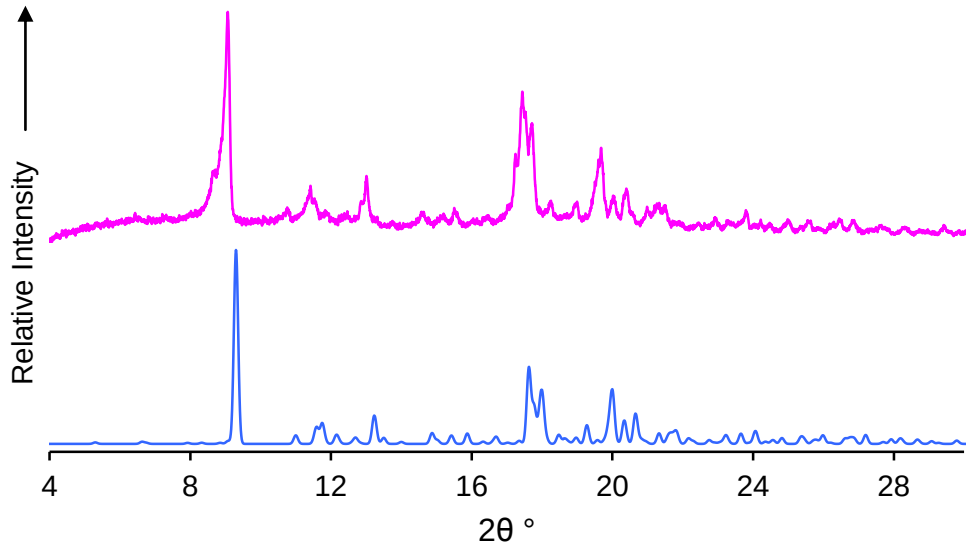

Figure 35. *Calculated (blue) and experimental (pink) PXRD traces of DMBFEN based on data collected at 173 and 294 K respectively.*

No other isostructural DIMEB complexes are known and most of the reported DIMEB complexes in the CSD are monomeric with a single DIMEB and guest molecule in the asymmetric unit. The DMBFEN complex thus represents a novel packing arrangement and the unusual feature of this structure, namely that complex units of host molecules A and B have significantly different guest contents, causes the subtle but significant differences in the two independent DIMEB host molecules.

SEMI-QUANTITATIVE SOLUBILITY STUDIES

A semi-quantitative investigation was carried out to determine whether or not the solubility of fenitrothion would increase when placed in aqueous CD solutions. The solubility tests were performed by weighing a sufficient amount of fenitrothion so as to ensure the solution prepared was always saturated with respect to this guest. Six different cyclodextrins were investigated, namely α-CD, β-CD, γ-CD, 2-hydroxypropyl-β-CD (HP-β-CD), DIMEB and TRIMEB. The concentration of all six CD solutions was 10 mM. A control experiment, in which the solubility of fenitrothion in the absence of CDs was determined, was necessary for comparison of the resulting data.

Fenitrothion was weighed directly into the volumetric flask from which the solution was due to be analysed. As fenitrothion is an oil, it was necessary to prevent the insoluble oil particles from interfering with the UV measurements. In order to achieve this ~0.1 g of silica gel (Kiesegel 60) was used to absorb the necessary fraction (oil particles) of fenitrothion that was insoluble. The CD solutions with fenitrothion were protected from light and placed in a mechanical shaker, thermostated to 25.0 ± 0.1 °C for 72 h. Before the UV-vis spectra of these solutions were measured they were filtered through a 0.2 µm nylon membrane.

The wavelength maximum for fenitrothion is 272 nm and it has an absorptivity coefficient of 6144 M^{-1} cm^{-1}. With this information it is possible to calculate the concentration of fenitrothion in each CD sample. The results obtained in this study, however, could not be evaluated accurately due to the substantially different UV-vis profiles obtained with each CD. The absorption maximum for each sample differed by up to 20 nm. This could be as a result of impurities present in the fenitrothion sample used or more likely because of different modes of inclusion in the various host molecules. Despite this, it was readily apparent that the native CDs do not increase the solubility of fenitrothion to as great an extent as the derivatised CDs. Dilutions were necessary for the solutions containing TRIMEB, DIMEB and HP-β-CD, indicating a higher concentration of fenitrothion present in these samples.

These experiments would need to be repeated using another technique such as high performance liquid chromatography in order to determine accurately the concentration of fenitrothion in the final solutions as well as determine whether any other products form during the 72 h periods.

DISCUSSION

Complex preparation

Complex preparation for all four solid-state inclusion compounds with fenitrothion discussed herein was not straightforward. Due to the labile nature of the agrochemical it was necessary to monitor the formation of its possible decomposition products that may have resulted during the host-guest crystallisation process. The insolubility of fenitrothion in water and the limited temperature range that could be used in preparation resulted in low yields of the BCDFEN complex which prevented us from quantifying the water content of the crystals and following its thermal behaviour using TG and DSC methods. The derivatised CDs increased the solubility of the guests quite considerably which resulted in larger yields of the complexes and their complete characterisation.

Complex stoichiometry and thermal analysis

The stoichiometries determined for the derivatised cyclodextrin complexes with fenitrothion are analogous to those seen in the cycluron series (Chapter 3). The β-CD complex, however, shows a 1:0.6 host-guest ratio. Two TRIMEA molecules encapsulate a single fenitrothion molecule and the wider seven-membered glucopyranose CDs (DIMEB and TRIMEB) form 1:1 host-guest complexes with fenitrothion. Techniques such as ^{1}H NMR spectroscopy, elemental analysis and TG were used to confirm these ratios.

The fenitrothion molecule was stable and remained associated with the derivatised CD molecules up to temperatures of 130, 140 and 120 °C for TMEAFEN, TMBFEN and DMBFEN, respectively. Thereafter, the guest was released in the case of the TMBFEN and DMBFEN complexes, followed by host decomposition. These events are comparable with what was recorded for the TMBCYC and DMBCYC complexes. The TMEAFEN complex shows gradual decomposition immediately after it melts at 210 °C. It was not possible to detect the formation of decomposition products of fenitrothion as either the DSC profiles were those typically seen for CD complexes and therefore masked all other events, or the DSC experiment was stopped after melting had occurred. The TG curves show decomposition for all complexes.

Conformations of the host and guest molecules

The parameters for the O4-polygons (*l*, *D*, ϕ and *d*), deviations of the O4 atoms from the O4 mean plane (α) and the τ_1 and τ_2 tilt angles listed for each complex fully describe the geometrical features associated with the different CD host molecules. The β-CD and DIMEB complexes contain hydroxyl groups that can form intramolecular hydrogen bonds. These

hydrogen bonds maintain the round, symmetrical structure of the β-CD and DIMEB host molecules. The O4 atoms of the DIMEB host molecule in the DMBFEN structure display slight deviations from a regular heptagon, but this is due to this host accommodating the phenyl residue of the fenitrothion molecule.

Methylation of the O2, O3 and O6 hydroxyl groups of α-CD and β-CD to yield the TRIMEA and TRIMEB host molecules respectively, precludes the possibility of formation of intramolecular hydrogen bonds (O–H•••O) between adjacent methyl glucose units, and causes steric hindrance which can only be relieved by the inward inclination of each methyl glucose unit towards the centre of the CD cavities. As a result, the O2n•••O3(n-1) distances at the secondary rim of the CD molecules increase from a mean value of 2.79 Å in the case of BCDFEN to a mean value of 3.42 Å for the TMBFEN complex. Both the TRIMEB and TRIMEA host molecules adopt a 'sealed' cup-like conformation as the primary methoxyl groups fold over their primary rims.

The asymmetric unit of the TMEAFEN complex contains two host molecules. The radii lengths (*l*) of the O4-hexagon in one of these host molecules display a wide range due to the significant strain induced by inclusion of the aromatic residue. The second O4-hexagon of the TRIMEA complex and the single heptagon of the TRIMEB complex, however, are more 'round' in comparison. This is due to both these host molecules including the more spherically shaped phosphorothioate unit of the fenitrothion molecule. With regard to the TMBFEN complex, the nitro and methyl substituents of the phenyl ring protrude from the host secondary rim, filling the interstitial sites between the host molecules. The DMBFEN complex shows considerable disorder of the guest molecules, featuring also alternative orientations of the guest molecule, situated with either the phosphorothioate group at the primary or secondary rim of the CD. The major components, however, are positioned with the phosphate ester group at the narrow primary rim. Considering only the major guest components of the DMBFEN complex and the ordered guests of the BCDFEN and TMBFEN complexes, their orientations within the respective host cavities are similar.

Intra- and intermolecular interactions

The BCDFEN complex contains 12 water molecules per CD molecule which results in many host-water, water-water and guest-water interactions which are all primarily strong O–H•••O hydrogen bonds. The derivatised CD complexes contain many weak C–H•••O hydrogen bonds ensuring close packing of the molecules, which is achieved without the incorporation of water molecules into the crystals. The host-guest intermolecular interactions occur mainly

between the nitro group, phenyl group or methoxyl group of the guest and either a C-H function or ethereal oxygen atom of a host methoxyl group.

Crystal packing

Two of the four fenitrothion complexes investigated are isostructural with other CD inclusion complexes. The host atomic coordinates, unit cell dimensions and space group symmetry of the TMBFEN complex correspond with those reported for the TMBCYC complex as well as the isostructural series termed BD3 by S. Lubhelwana.[21] The BCDFEN complex is isostructural with many other β-CD complexes which crystallise in an intermediate-type packing arrangement.

The TMEAFEN and DMBFEN complexes display novel packing arrangements. TMEAFEN is the first published TRIMEA complex in which the host molecules fully encapsulate the guest molecule in a head-to-head arrangement with a 2:1 host-guest ratio.[22] The only other known 2:1 TRIMEA complex is $(TRIMEA)_2 \cdot (S)$-metoprolol, but this complex packs in a head-to-tail 'channel-type' arrangement.[23] DMBFEN is one of the first DIMEB inclusion complexes found to crystallise in the monoclinic space group $P2_1$ with two independent DIMEB molecules in the asymmetric unit. This complex displays a channel-type packing arrangement with pseudo-halving of the *a*-axis. The extensive guest disorder within the two DIMEB molecules, gives rise to a unique arrangement of host molecules within the crystal.

The four fully elucidated fenitrothion inclusion complexes described herein demonstrate the affinity of fenitrothion for both native and derivatised CDs. Furthermore, these X-ray crystal structures yield the first accurate molecular parameters for the insecticide molecule, fenitrothion, revealing also the occurrence of various conformers.

PART 2: COMPLEXATION IN SOLUTION

THE REACTIVITY AND STABILITY OF FENITROTHION

Organophosphorus pesticides (OPs) such as fenitrothion and other analogues containing reactive phosphoric and thiophosphoric acid esters are important to study in aqueous media. Once OPs have been applied to their respective targets they can readily break down or transform into products, with higher toxicity levels and higher soil persistence levels than the original chemical, via processes such as adsorption, hydrolysis, oxidation and photochemical degradation.[24] It is important to understand these processes and be able to predict and assess the ultimate fate of OPs in the soil and develop methods or other formulations that will reduce the negative impact they have on the environment.

The photodegradation of fenitrothion has been studied extensively by Durand *et al,*[25] who confirmed the formation of many decomposition products including fenitrooxon, trimethyl phosphate, trimethyl phosphorothioate, the S-isomer of fenitrothion, denitrofenitrothion, parathion-methyl, 4-nitro-3-methylphenol and carbomethoxydenitrofenitrothion after 7 h of UV irradiation in a water-methanol solution (5:1). This illustrates how readily fenitrothion can decompose into ineffective byproducts under relatively mild conditions. The objective of the work presented here was to assess the rate of the hydrolysis of fenitrothion in the presence of various CD molecules, for comparison with the rate in their absence.

Compounds such as fenitrothion that contain both alkyl and aryl substituents are susceptible to nucleophilic attack by various chemical treatments. There are three possible degradation pathways that could occur (Figure 36) and these include nucleophilic attack at the central phosphorus atom resulting in P-OAr bond cleavage, nucleophilic attack at the aliphatic carbon with C-O bond cleavage, and nucleophilic attack at the aromatic moiety with Ar-O bond cleavage. It has been shown that with hard nucleophiles such as ^{-}OH and ^{-}OOH only P-OAr bond cleavage ($S_N2(P)$ reaction pathway) takes place while the reactions with NH_2OH and NH_2O^{-}, NH_2NH_2 and $BuNH_2$ involve two competing reactions occurring simultaneously, the P-OAr cleavage and the C-O bond cleavage ($S_N2(C)$ reaction pathway) at the aliphatic carbon.[26]

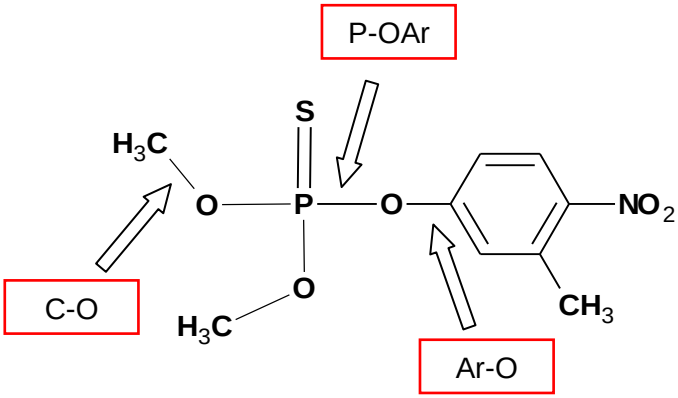

Figure 36. *Three possible degradation pathways of fenitrothion in the presence of nucleophiles.*

THE HYDROLYSIS OF FENITROTHION

The hydrolysis of fenitrothion (**1**) has previously been studied in the absence of cyclodextrins at varying concentrations of NaOH by Rougier *et al* [26] and Vico *et al*.[27] The rates of these reactions were determined by following the absorbance at 397 nm as a function of time due to the 3-methyl-4-nitrophenoxide (**2**) product that results from a reaction of fenitrothion with NaOH (Reaction 1). The UV-Vis spectrum of the product for these particular reactions matches that of **2** at the expected concentration thereby proving that the only reaction taking place is that of P-OAr bond fission, which has also previously been demonstrated by Greenhalgh *et al* above a pH of 8.[28] Rougier *et al* and Vico *et al* obtained second-order rate constants of (2.50 ± 0.08) × 10^{-3} M^{-1} s^{-1} and (2.0 ± 0.1) × 10^{-3} M^{-1} s^{-1}, respectively from the slope of a plot of k_{obs} versus NaOH concentration (Equation 1).[26,27] As the y-intercept was close to zero, the rate of reaction due to water was said to be negligible.

Reaction 1. *The alkaline hydrolysis reaction of fenitrothion in* 2% 1,4-dioxane/H_2O at 25 °C.

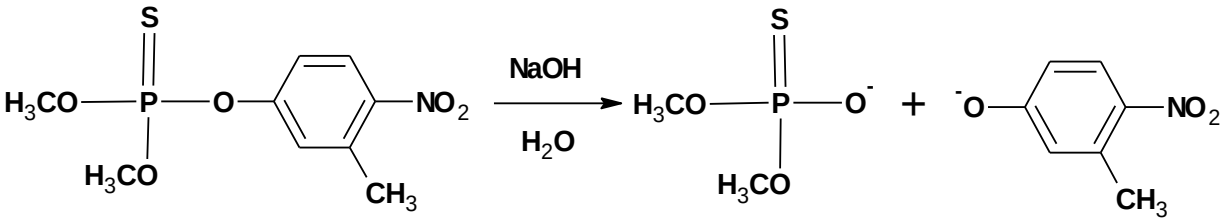

Fenitrothion (**1**)

3-methyl-4-nitrophenoxide (**2**)

$$k_{obs} = k_{OH}[HO^-] + k_{H_2O} \simeq k_{OH}[HO^-] \quad (1)$$

THE EFFECT OF CYCLODEXTRINS ON THE HYDROLYSIS OF FENITROTHION

In our study the rate of the hydrolysis reaction in the presence of CDs was investigated. The NaOH concentration was kept constant at 0.5 M and each CD concentration was varied from 2.5×10^{-4} M to 0.02 M or 0.01 M depending on which CD was being investigated. The hydrolysis reaction was studied in the presence of six different CDs, namely α-CD, β-CD, γ-CD, TRIMEB, TRIMEA and DIMEB. The native CDs contain hydroxyl groups that can be deprotonated by hydroxide ions in basic media. As a consequence it was necessary to consider the pK_a values of the native CDs, which are 12.3, 12.2 and 12.1 for α-, β-, and γ-CD, respectively,[29] when calculating the NaOH concentration required to prepare the solutions. DIMEB contains one hydroxyl group per glucose residue and as no documented pK_a value could be found, it was assumed that its pK_a value would be similar to that of β-CD.

Results and discussion

All the reactions were studied under pseudo-first order conditions as the concentration of fenitrothion (~5×10^{-5} M) was at least 50 times smaller than that of the cyclodextrin and many orders of magnitude smaller than that of the nucleophile. The kinetic profile obtained for one of the experiments with β-CD at a concentration of 0.02 M is displayed in Figure 37(a) with its corresponding UV-vis spectra in Figure 37 (b). Each k_{obs} value was obtained by fitting the first-order rate law in exponential form to the individual graphs of absorbance versus time.

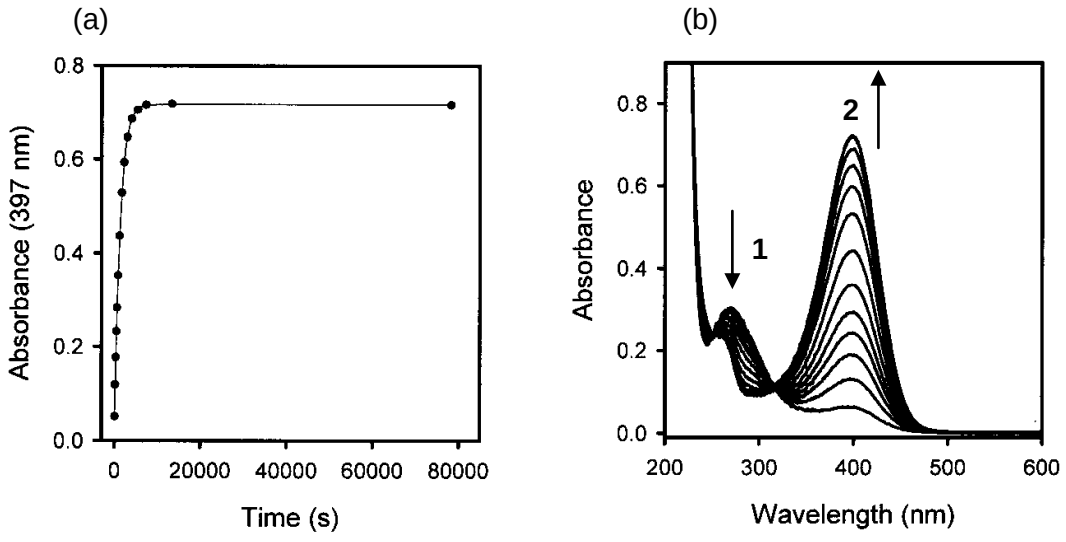

Figure 37. *The kinetic profile obtained for the hydrolysis of fenitrothion in the presence of β-CD (a) and the corresponding UV-Vis spectra (**1**: fenitrothion and **2**: 3-methyl-4-nitrophenol) (b). ($[NaOH]_{eff}$ = 0.50 M, $[\mathbf{1}]_o = 4.56 \times 10^{-5}$ M, [β-CD] = 0.02 M in 2% 1,4-dioxane/H_2O, ionic strength I = 1.0 M (NaCl) at 25 °C).*

The observed rate constants obtained for the reactions in the presence of α-CD, β-CD, γ-CD, TRIMEB, TRIMEA and DIMEB are presented in Table 20. Figure 38 (a)-(f) shows plots of the k_{obs} values as a function of the concentration of the various CDs. When comparing these graphs most of them display a similar inhibitory kinetic profile which is characteristic for 1:1 host-guest complex formation. For α-CD the inhibitory effect is not large while for its permethylated counterpart, TRIMEA, a sigmoidal curve is observed which can be attributed to a two-step complex process involving more than one CD molecule encapsulating the guest. TRIMEB and DIMEB show a stronger inhibitory effect than β- and γ-CD.

The observed rate constant in the absence of CDs was determined several times and as a result the average value $(1.23 \pm 0.02) \times 10^{-3}$ s^{-1} has been reported in Table 21. The highest concentration of CD that could be used to perform the kinetic experiments with TRIMEB, DIMEB and TRIMEA at a constant ionic strength of 1 M was 0.01 M, 0.005 M and 0.009 M, respectively. At a cyclodextrin concentration higher than these values precipitation of the CD occurred. This was confirmed by performing an experiment with DIMEB at a concentration of 0.01 M with an ionic strength of 1 M in an aqueous solution with 2% 1,4-dioxane. No substrate was added. A day later there was a solid precipitate at the bottom of the flask which was confirmed by ^{1}H NMR spectroscopy to be DIMEB.

Table 20. *Observed rate constants obtained at different CD concentrations for the hydrolysis of fenitrothion in 2% 1,4-dioxane/H_2O at 25 °C.*[a]

Cyclodextrin	Concentration, (mM)	k_{obs}, (s^{-1})
α-CD	0.00	$(1.23 \pm 0.02) \times 10^{-3}$
	0.50	$(1.20 \pm 0.02) \times 10^{-3}$
	2.50	$(1.20 \pm 0.02) \times 10^{-3}$
	5.00	$(1.13 \pm 0.03) \times 10^{-3}$
	10.00	$(1.06 \pm 0.02) \times 10^{-3}$
	15.00	$(1.01 \pm 0.02) \times 10^{-3}$
	20.00	$(9.6 \pm 0.1) \times 10^{-4}$
β-CD	0.00	$(1.23 \pm 0.02) \times 10^{-3}$
	0.50	$(1.13 \pm 0.02) \times 10^{-3}$
	1.00	$(1.15 \pm 0.03) \times 10^{-3}$
	5.00	$(8.6 \pm 0.3) \times 10^{-4}$
	10.00	$(8.5 \pm 0.2) \times 10^{-4}$
	15.00	$(7.96 \pm 0.09) \times 10^{-4}$
	20.00	$(7.77 \pm 0.02) \times 10^{-4}$
γ-CD	0.00	$(1.23 \pm 0.02) \times 10^{-3}$
	0.50	$(1.15 \pm 0.04) \times 10^{-3}$
	2.50	$(1.09 \pm 0.01) \times 10^{-3}$
	5.00	$(9.9 \pm 0.2) \times 10^{-4}$
	10.00	$(8.8 \pm 0.2) \times 10^{-4}$
	15.00	$(7.83 \pm 0.09) \times 10^{-4}$
	20.00	$(7.5 \pm 0.1) \times 10^{-4}$
TRIMEA	0.00	$(1.23 \pm 0.02) \times 10^{-3}$
	0.25	$(1.166 \pm 0.008) \times 10^{-3}$
	0.50	$(1.130 \pm 0.005) \times 10^{-3}$
	0.75	$(1.072 \pm 0.003) \times 10^{-3}$
	1.50	$(8.55 \pm 0.08) \times 10^{-4}$
	2.50	$(6.76 \pm 0.07) \times 10^{-4}$
	3.50	$(5.48 \pm 0.05) \times 10^{-4}$
	5.00	$(4.03 \pm 0.04) \times 10^{-4}$
	7.00	$(2.99 \pm 0.01) \times 10^{-4}$
	8.00	$(2.79 \pm 0.02) \times 10^{-4}$
	9.00	$(2.48 \pm 0.01) \times 10^{-4}$
TRIMEB	0.00	$(1.23 \pm 0.02) \times 10^{-3}$
	0.50	$(9.6 \pm 0.1) \times 10^{-4}$
	2.50	$(6.74 \pm 0.04) \times 10^{-4}$
	5.00	$(5.03 \pm 0.03) \times 10^{-4}$
	10.00	$(3.38 \pm 0.07) \times 10^{-4}$
	20.00[b]	$(2.20 \pm 0.05) \times 10^{-4}$
DIMEB	0.00	$(1.23 \pm 0.02) \times 10^{-3}$
	0.25	$(8.9 \pm 0.1) \times 10^{-4}$
	0.50	$(6.99 \pm 0.02) \times 10^{-4}$
	1.00	$(5.48 \pm 0.04) \times 10^{-4}$
	2.50	$(3.46 \pm 0.03) \times 10^{-4}$
	5.00	$(2.48 \pm 0.01) \times 10^{-4}$

[a] The effective concentration of NaOH in the reaction medium, $[NaOH]_{eff}$ = 0.50 M for α-CD, β-CD, γ-CD and DIMEB, $[\mathbf{1}]_o = (4.56 - 5.27) \times 10^{-5}$ M, ionic strength I = 1.0 M (NaCl). [b] The k_{obs} value was calculated using the linear function as a precipitate started to form after 90 min.

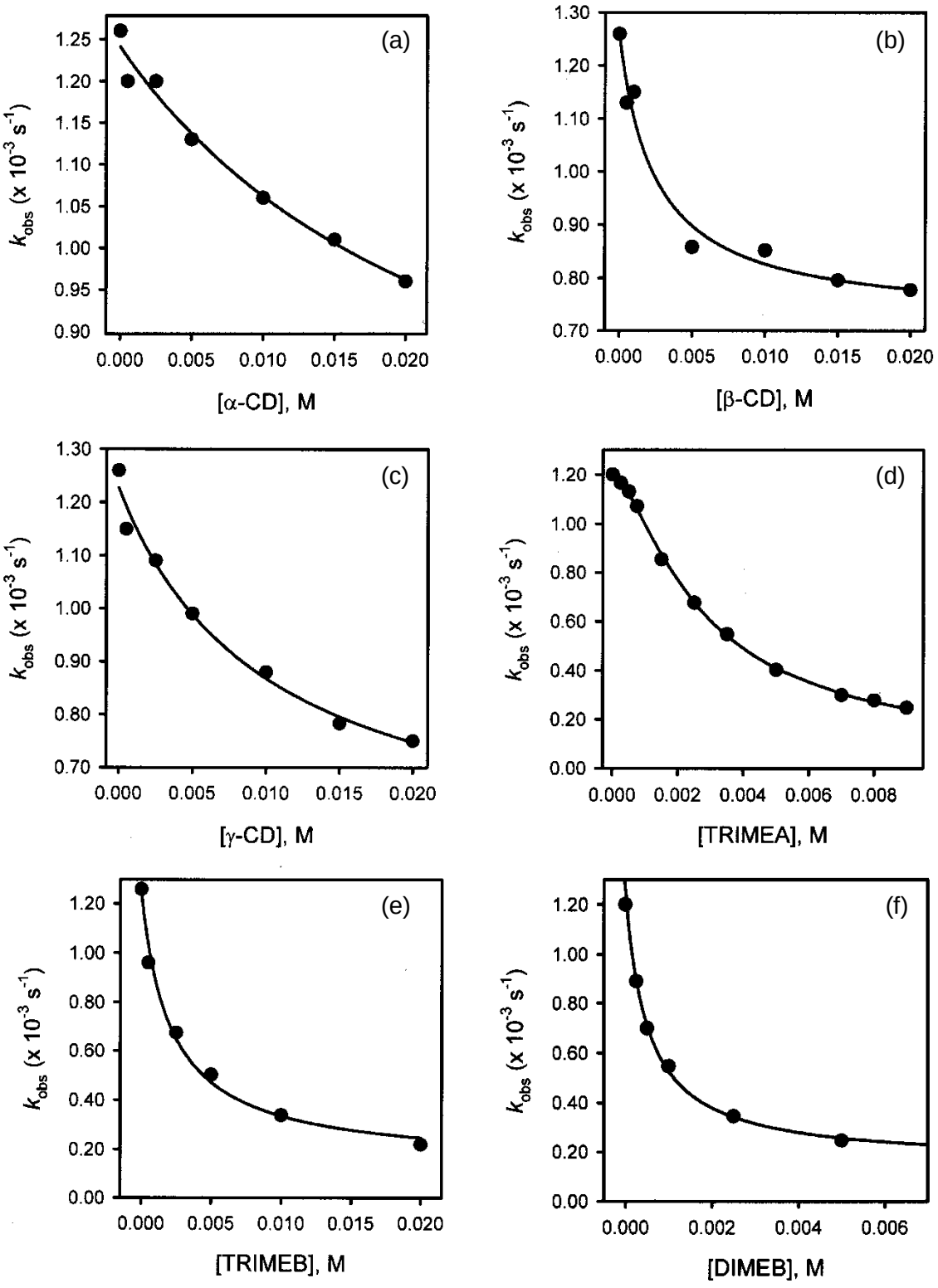

Figure 38. *The graphs of k_{obs} versus [CD] for the hydrolysis reaction of fenitrothion with (a) α-CD, (b) β-CD, (c) γ-CD, (d) TRIMEA, (e) TRIMEB and (f) DIMEB. (The k_{obs} values in the absence of the native CDs and TRIMEB were (1.26 ± 0.02) × 10^{-3} s^{-1} and (1.20 ± 0.02) × 10^{-3} s^{-1} in the absence of TRIMEA and DIMEB. In processing all of the kinetic data, a mean k_{obs} = (1.23 ± 0.02) × 10^{-3} s^{-1} was employed).*

Reaction 1 in the presence of ionisable CDs may take place as shown in Scheme 1, where k_0, k_1, and k_{CD} represent the reactions of the free substrate, the substrate complexed with the neutral CD (CDOH) and the reaction with ionised CD (CDO^-), respectively. k_2 represents the rate constant for the reaction of HO^- with fenitrothion included within the ionised CD (CDO^-) as was previously demonstrated by R. V. Vico *et al*.[27] It has also previously been shown that the main reaction pathway is that of $k_2^{Nu}[Nu^-]$ and the reaction pathway of k_{CD} is negligible.[27] The overall observed rate constant for Scheme 1 is shown in Equation 2, where *f* represents the fraction of ionised CD as defined in Equation 3 with $K_b = K_w/K_a$. The lengthy derivation of the expression for k_{obs} (Equation 2) was presented earlier,[30] and is not reproduced here. Considering the pK_a values of the CDs and a NaOH concentration of 0.50 M, f ≈ 1, Equation 2 simplifies to Equation 4.

Scheme 1. *Reaction pathways for the hydrolysis of fenitrothion in the presence of cyclodextrins with ionisable hydroxyl groups in basic media.*

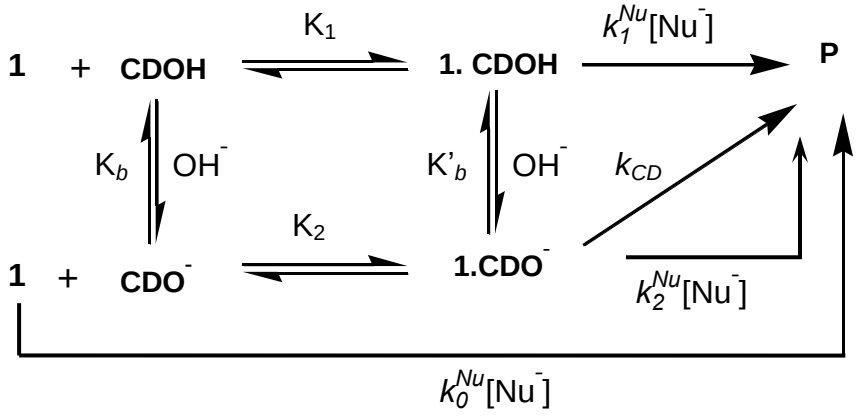

$$k_{obs} = \frac{k_0^{Nu}\,[Nu^-] + k_1^{Nu} K_1 [Nu^-]\,(1 - f)\,[CD] + (k_{CD} + k_2^{Nu}[Nu^-]) K_2 f\,[CD]}{1 + K_1(1 - f)\,[CD] + K_2\, f\,[CD]} \quad (2)$$

$$f = \frac{[HO^-]}{[HO^-] + K_b} \quad (3)$$

$$k_{obs} = \frac{k_0^{Nu}\,[Nu^-] + k_2^{Nu}\,[Nu^-]\,K_2\,[CD]}{1 + K_2\,[CD]} \quad (4)$$

The TRIMEB molecule is methylated at the 2, 3 and 6 positions, which simplifies Scheme 1 to Scheme 2 and k_{obs} for the hydrolysis of **1** in the presence of TRIMEB is given by Equation 5. One must take into account that Equation 4 and Equation 5 apply to a 1:1 host-guest relationship which is shown in the respective schemes. TRIMEA forms a 2:1 host-guest complex in the solid state and this is likely to occur in solution too, as can be seen by the unique sigmoidal curve (Figure 38 (d)). Scheme 3 represents the suggested reaction pathway for the hydrolysis of **1** in the presence of TRIMEA. Fenitrothion can either undergo nucleophilic attack by the hydroxide ion when uncomplexed, bound to one guest molecule, or included within two guest molecules. Equation 6 has been derived for this particular mechanism.

Scheme 2. *Reaction pathways for the hydrolysis of fenitrothion in the presence of TRIMEB.*

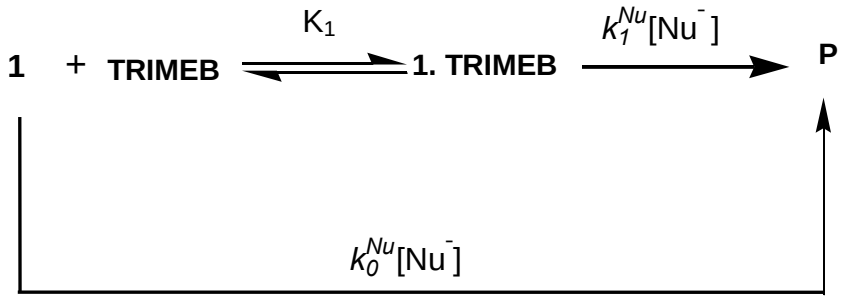

$$k_{obs} = \frac{k_0^{Nu}\,[Nu^-] + k_1^{Nu} K_1\,[CD]}{1 + K_1\,[CD]} \qquad (5)$$

Scheme 3. *Reaction pathways for the hydrolysis of fenitrothion in the presence of TRIMEA.*

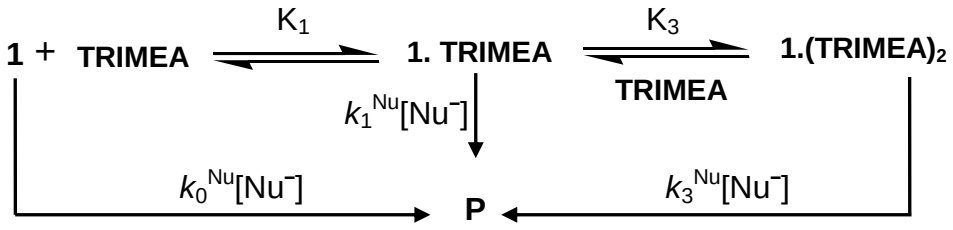

$$k_{obs} = \frac{k_0^{Nu}\,[Nu^-] + k_1^{Nu} K_1 [Nu^-][CD] + k_3^{Nu} K_1 K_3 [Nu^-][CD]^2}{1 + K_1\,[CD] + K_1 K_3 [CD]^2} \qquad (6)$$

For the native cyclodextrins, as well as TRIMEB and DIMEB, the observed rate constant versus concentration was fitted to an equation of the form of Equation 7, with **a** = k_0^{Nu}[Nu^-], **b** and **c** being adjustable parameters shown in Equations 8 to 11. Parameter **a** represents the rate of reaction of the free substrate, **b** is the product of the rate of reaction that occurs when fenitrothion is included in the cyclodextrin cavity and the association constant K_2, and parameter **c** considers only the equilibrium present in the system.

$$k_{obs} = \frac{\mathbf{a} + \mathbf{b}\,[CD]}{1 + \mathbf{c}\,[CD]} \tag{7}$$

$$\mathbf{b}_{Native/DIMEB} = k_2^{Nu} K_2 [Nu^-] \tag{8}$$

$$\mathbf{b}_{TRIMEB} = k_1^{Nu} K_1 [Nu^-] \tag{9}$$

$$\mathbf{c}_{Native/DIMEB} = K_2 \tag{10}$$

$$\mathbf{c}_{TRIMEB} = K_1 \tag{11}$$

The data obtained for parameters **a**, **b**, **c** and **b/c** for β-CD, γ-CD, TRIMEB and DIMEB are shown in Table 21. Parameter **b/c** is calculated so as to consider only the rate of reaction taking place within the CD cavity. The ratio k_{obs}^{CD}/k_{obs} has been calculated to determine the inhibitory effect of each CD at a particular concentration. The parameters were not calculated for α-CD as the association constant between α-CD and fenitrothion is small and equally the inhibitory effect (Δk_{obs} = 0.30 s^{-1}).

The kinetic data for the hydrolysis of fenitrothion in TRIMEA were fitted to Equation 12. The derivation of this equation can be found in Appendix D. This equation has four variable parameters with **b** being equivalent to that in Equations 7 and 9 and parameters **c**, **d** and **e** are defined in Equations 13 to 15. The data obtained for these parameters have been tabulated (Table 22). Parameter **c** represents the association constant for the reaction between one fenitrothion molecule and one TRIMEA molecule, **d** is the rate of the hydrolysis reaction when fenitrothion is included within two TRIMEA molecules multiplied by the association constants for the formation of both the 1:1 and 2:1 complexes formed, and parameter **e** is the product of the association constants K_1 and K_3.

$$k_{obs} = \frac{\mathbf{a} + \mathbf{b}\,[CD] + \mathbf{d}\,[CD]^2}{1 + \mathbf{c}\,[CD] + \mathbf{e}\,[CD]^2} \quad (12)$$

$$\mathbf{c}_{TRIMEA} = K_1 \quad (13)$$

$$\mathbf{d}_{TRIMEA} = k_3^{Nu} K_1 K_3 [Nu^-] \quad (14)$$

$$\mathbf{e}_{TRIMEA} = K_1\, K_3 \quad (15)$$

Table 21. *Parameters for the hydrolysis of fenitrothion in the presence of β-CD, γ-CD, TRIMEB and DIMEB.*

CD	**a** (s^{-1}) [a]	**b** (s^{-1})	**c**[b]	**b/c** (s^{-1})	f	k_{obs}^{CD}/k_{obs} [c]
β-CD	1.23×10^{-3}	$(3.01 \pm 0.08) \times 10^{-1}$	417 ± 118	7.2×10^{-4}	1	0.69
γ -CD	1.23×10^{-3}	$(5 \pm 3) \times 10^{-2}$	99 ± 36	5.0×10^{-4}	1	0.72
TRIMEB	1.23×10^{-3}	$(8 \pm 1) \times 10^{-2}$	511 ± 31	1.6×10^{-4}	-	0.27
DIMEB	1.23×10^{-3}	$(2.4 \pm 0.4) \times 10^{-1}$	1689 ± 93	1.4×10^{-4}	1	0.16[d]

[a] The averaged experimental value obtained in the absence of CD. [b] The 1:1 host-guest stoichiometries have been taken into account when calculating the association constants. The latter are dimensionless as the concentrations are expressed in mol dm^{-3} relative to the standard concentration of 1 mol dm^{-3}. [c] The values were determined at a cyclodextrin concentration of 10 mM for β-CD, γ-CD and TRIMEB. [d] Extrapolation of k_{obs} to a CD concentration of 10 mM using Equation 7.

Table 22. *Parameters for the hydrolysis of fenitrothion in the presence of TRIMEA.*

CD	**a** (s^{-1}) [a]	**b** (s^{-1})	**c** [b]	**d** [c]	**e** [b]	k_{obs}^{CD}/k_{obs} [d]
TRIMEA	1.23×10^{-3}	$(5.7 \pm 0.2) \times 10^{-1}$	527 ± 14	0	$(2.50 \pm 0.06) \times 10^{5}$	0.18

[a] The experimental value obtained in the absence of CDs. [b] The 2:1 host-guest stoichiometry was taken into account when calculating the association constant. The latter is dimensionless as the concentration is expressed in mol dm^{-3} relative to the standard concentration of 1 mol dm^{-3}. [c] Insignificant contribution (see text). [d] Extrapolation of k_{obs} to a CD concentration of 0.01 M using Equation 12.

The association constant determined for β-CD (Table 21) is in good agreement with the literature value of 417[31] as well as with the results published by Vico *et al* who obtained a value of 415 using a solvent system of 2% acetonitrile/H_2O.[27] Fenitrothion has a much weaker association with γ-CD which is expected as the cyclodextrin cavity is much larger and the intermolecular forces are weaker. γ-CD does, however, have a very similar inhibitory effect on the hydrolysis reaction of fenitrothion as β-CD, as is evident from the corresponding values of k_{obs}^{CD}/k_{obs} shown in Table 22. In the presence of β-CD and γ-CD the rate of the hydrolysis reaction is 31 % and 28% slower, respectively. So, even though the association constants are significantly different, the CD cavities protect the reactive phosphorothioate group to the same extent. The rates of reaction within the β-CD, γ-CD, TRIMEB and DIMEB cavities (**b**/**c**) are all one order of magnitude smaller than the rate of reaction taking place outside the CD cavities (**a**).

DIMEB has the highest association constant with fenitrothion and the rate of reaction within the CD cavity is very similar to that in the case of the TRIMEB cavity. The rates of hydrolysis with respect to the free substrate are 84 % and 73 % slower in the presence of DIMEB and TRIMEB respectively. The large difference in the inhibitory effect when compared to the native CDs may be due to the methyl groups present on DIMEB and TRIMEB which elongate the CD molecules and provide a slightly larger pocket in which the fenitrothion molecules can situate themselves. Furthermore, the methyl groups have the ability to block the entering hydroxide ions thereby preventing nucleophilic attack at the phosphorus atom. The DIMEB molecules in a highly basic medium, as applies here, are deprotonated. As a result the molecules are not as rigid as they would be in the protonated form due to the lack of intramolecular hydrogen bonds that form between the hydroxyl group on position 3 of one glucose unit and the *O*-methyl group of the adjacent glucose unit.

With regard to TRIMEA, if we divide **b** by **c** we obtain a value of 1.08×10^{-3} s^{-1}, which represents the rate of reaction occurring inside one TRIMEA molecule. This inhibitory effect has the same order of magnitude as that observed with increasing concentrations of the native α-CD. The advantage with TRIMEA is that it is able to form a 2:1 complex whereas for α-CD there is only a weak interaction between one CD molecule and the guest, and the phosphorothioate unit is not as protected as in the cage-like environment of the 2:1 TRIMEA complex. Parameter **d** contains $k_3^{Nu}[Nu^-]$ which represents the observed rate constant for the hydrolysis reaction of fenitrothion within *two* TRIMEA molecules. This value is insignificant in comparison to the other rate constants and can therefore be neglected. By dividing parameter **e** by **c** we can obtain the value of K_3, which is 474 and this is similar to the value

obtained for the 1:1 complex of TRIMEA and fenitrothion as well as the 1:1 complex of TRIMEB and fenitrothion.

Similar hydrolysis experiments have been performed by Kamiya *et al* [31] with fenitrothion and three cyclodextrins, namely β-CD, DIMEB and TRIMEB. The paper describing these studies does not, however, explicitly state at what CD concentration the first-order rate constants for the hydrolysis of fenitrothion in the presence of these CDs were determined. There is also no mention of co-solvents being used. Due to the very low solubility of fenitrothion, it is impossible to measure accurate rates of reactions and obtain reliable kinetic data without a small percentage of an organic co-solvent being present.

In order to broaden this investigation, one would need to perform further experiments with other possible nucleophiles that are found in soils that may react with a pesticide such as fenitrothion. A similar study to that performed by Durand *et al,*[25] focusing on the quantities and types of decomposition products of fenitrothion that form under UV irradiation, should be undertaken in the presence of CDs in order to understand the effect of these macrocyclic host molecules on the photodegradation rate of fenitrothion.

In conclusion, CDs show a significant inhibitory effect on the hydrolysis reaction of fenitrothion. Furthermore, the methylated CDs inhibit the hydrolysis reaction to a greater extent than the native CDs. Taking into account also the solid-state crystallographic structures of β-CD, TRIMEA, TRIMEB and DIMEB inclusion complexes, one can say that inclusion of fenitrothion within the various CDs occurs in a similar manner in both solution and in the solid state, with the exception that the host-guest ratio of the BCDFEN complex in the solid state is only 1:0.6. The BCDFEN, TMBFEN and DMBFEN crystal structures all feature the guest molecules positioned with their phosphorothioate groups directed towards the narrower, primary rim of the CD cavity and this group is therefore probably protected more effectively from nucleophilic attack than if it were positioned at the wider, secondary rim of the cyclodextrin.

INDUCED CIRCULAR DICHROISM

When an achiral chromophoric guest molecule interacts with an optically active molecule such as a cyclodextrin the achiral guest molecule becomes optically active and this effect is known as 'induced' circular dichroism (ICD).[32] The sign and magnitude of an ICD signal resulting from this interaction is unique and depends on the orientation of the guest chromophore in the host. It is necessary to know the directions and oscillator strength of the transition moments of the guest molecules to fully interpret the results obtained from an ICD spectrum.

Zhdanov *et al* have reviewed the subject of induced optical activities in cyclodextrin complexes, showing how chiroptical spectroscopic methods in combination with theoretical calculations and representations can be used to obtain information on the fine structure of CD complexes.[33] The application to CDs can be based on the Kirkwood-Tinoco theory of polarisabilities which has been cited by Connors[34] and states the following rule: if the transition dipole moment of the guest chromophore is aligned parallel to the axis of symmetry of the CD (that is, the axis of the CD cavity), then the sign of the ICD Cotton effect for that transition will be positive, whereas if the moment axis is aligned perpendicular to the cavity axis, the ICD sign will be negative. This rule applies to a chromophore that resides inside the cavity; if the chromophore is located outside the cavity the signs of the ICD are reversed. In this brief section the focus will be on the ICD spectra obtained when fenitrothion (an achiral molecule) interacts with each CD in solution and a comparison of the relative guest orientations within the various CDs will be presented based on the profiles of the ICD spectra. The solid-state structures of fenitrothion complexes with β-CD, TRIMEB, TRIMEA and DIMEB have been elucidated in this study, so some reference to the mode of inclusion in the solid state may assist with interpreting what is observed in solution.

Results and discussion

The circular dichroism spectra with their corresponding UV-visible absorption spectra for the complexes of fenitrothion with α-CD, β-CD, γ-CD, TRIMEA, TRIMEB and DIMEB are shown in Figure 39. It can be seen that the inclusion complexes of all the native CDs and DIMEB show a positive ICD signal followed by a negative signal as the wavelength increases, the positive signal being closely related to the absorption maxima in the UV-vis spectra (Table 23). The reverse is true for the complexation of TRIMEA and TRIMEB with fenitrothion in solution.

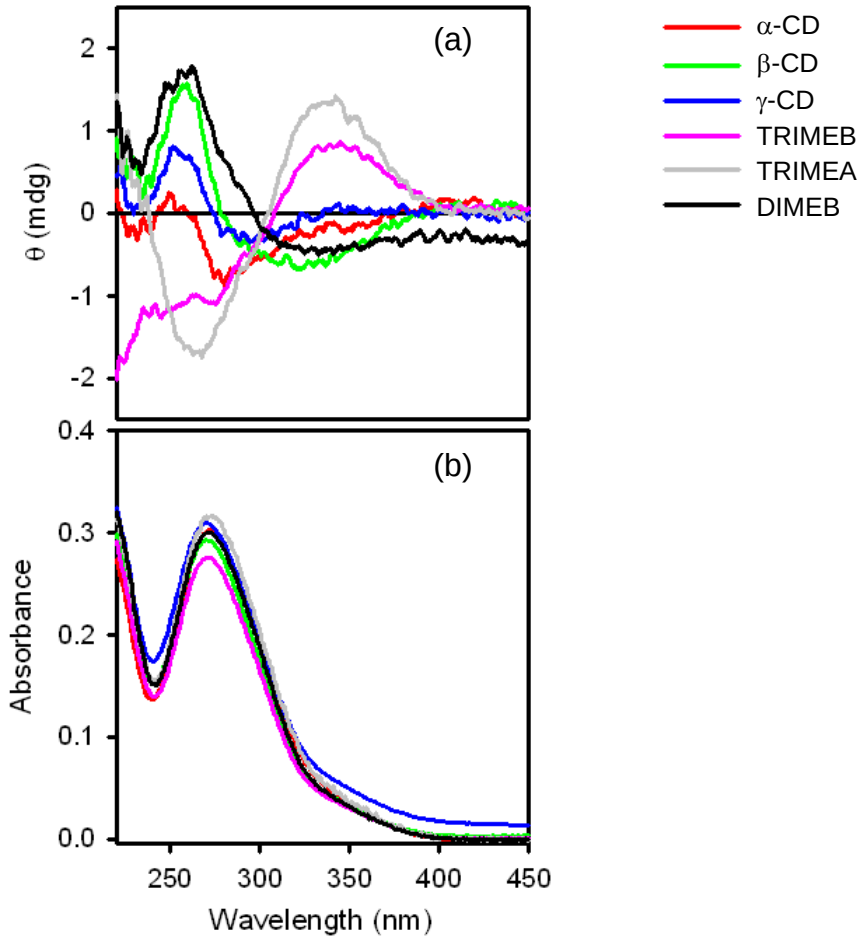

Figure 39. *ICD spectra (a) and UV-vis absorption spectra (b) for the complexation of fenitrothion with α-CD, β-CD, γ-CD, TRIMEB, TRIMEA and DIMEB in solution.*

Table 23: *Signs of the ellipticity signals and their corresponding wavelength maxima*

Cyclodextrin	λ^{ICD}, nm	Signal
α-CD	249	positive
	280	negative
β-CD	260	positive
	325	negative
γ-CD	252	positive
	294	negative
TRIMEB	230-275	negative
	345	positive
DIMEB	265	positive
	336	negative
TRIMEA	267	negative
	340	positive

The CD concentrations used for the ICD experiments were the same for α-CD, β-CD, γ-CD and TRIMEB (0.01 M). However, for TRIMEA and DIMEB the concentrations were 0.001 M and 0.0025 M respectively. The reason for the different CD concentrations was the limited quantity of TRIMEA available and the concern that DIMEB might precipitate from solution at higher concentrations.

The ICD signal for the complex with α-CD is very weak and within the noise level, indicating that there is very little interaction between the α-CD cavity and the fenitrothion molecule. For γ-CD the signal is somewhat larger than that of α-CD and the profile of the curve is the same. The orientation of the fenitrothion molecule in the α-CD and γ-CD cavities is thus likely to be the same, with fenitrothion having a greater interaction with γ -CD.

The β-CD and DIMEB complex circular dichroism spectra have a positive optical rotation signal at 260 nm and 265 nm respectively. DIMEB is present in a concentration four times smaller than that of β-CD. The intensity of a circular dichroism spectrum depends on the concentration of the complex; therefore, if the complex concentrations in solution were the same, the signal would be much greater for DIMEB than for β-CD. This implies that there is a very strong association between the DIMEB and fenitrothion molecules. This is in accordance with what was established from the kinetic studies, where the association constant for the complex between DIMEB and fenitrothion was calculated as 1689 but only 417 for the β-CD·fenitrothion complex.

The orientation of the fenitrothion molecule within the TRIMEA cavity is very different from that in DIMEB and the native CDs. The TRIMEA signal is also relatively large, especially when one takes into account the CD concentration which is 10 times lower than that of β-CD and 2.5 times lower than that of DIMEB. The reversal in optical rotation signals for TRIMEA leads to many possible modes of inclusion, or exclusion, in the absence of computed transition moments and other computational studies. In the solid state, TRIMEA forms a 2:1 host to guest complex with a cage-type structure so the phosphorothioate moiety and the aromatic moiety are both capable of interacting with a TRIMEA molecule. The TRIMEB solution complex displays a similar ICD spectral profile to what is seen for TRIMEA; this may indicate a protrusion of the chromophoric part of the guest molecule from the cavity, which was found to be the case in the solid-state crystallographic study.

Although association constants as well as further details of guest orientation within the host molecules can be deduced from ICD studies, their determination can be challenging. For this reason the technique was not pursued beyond what is reported here.

REFERENCES

1. *The Merck Index: An Encyclopedia of Chemicals, Drugs, and Biologicals*, eds. M. J. O'Neil, P. E. Heckelman, C. B. Koch, K. J. Roman, C. M. Kenny and M. R. D'Arecca, Merck & Co., Inc., Whitehouse Station, NJ, USA, 14th edn., **2006**.
2. Cambridge Structural Database and Cambridge Structural Database system, Version 5.32, Cambridge Crystallographic Data Centre, University Chemical Laboratory, Cambridge England, February **2011**.
3. R. Greenhalgh, B. Blackwell, C. Preston and W. Murray, *J. Agric. Food Chem.,* **1983**, 31, 710-713.
4. T. R. Fukuto, E. O. Hornig and R. L. Metcalf, *J. Agric. Food Chem.*, **1964**, 12, 169-171.
5. J. W. Miles, D. L. Mount, M. A. Staiger and W. R. Teeters, *J. Agric. Food Chem*., **1979**, 27, 421-425.
6. X. M. Han, V. K. Balakrishnan, G. W. van Loon and E. Buncel, *Langmuir*, **2006**, 22, 9009-9017.
7. M. R. Caira, *Roum. Chem. Quart. Rev*., **2000**, 8, 243-253.
8. F. Giordano, C. Novak and J. R. Moyano, *Thermochim. Acta*, **2001**, 380, 123-151.
9. L. J. Barbour, *J. Appl. Crystallogr*., **1999**, 32, 351-352.
10. G. M. Sheldrick, Program SADABS, Version 2.05, University of Göttingen, Germany, **2007**.
11. J. A. Hamilton and M. N. Sabesan, *Acta Crystallogr. Sect. B: Struct. Crystallogr. Cryst. Chem*., **1982**, 38, 3063-3069.
12. G. M. Sheldrick, SHELXH-97, *Acta Crystallogr*., **2008**, A64, 112-122.
13. V. Zabel, W. Saenger and S. A. Mason, *J. Am. Chem. Soc*., **1986**, 108, 3664-3673.
14. D. Mentzafos, I. M. Mavridis, G. Le Bas and G. Tsoucaris, *Acta Crystallogr*., **1991**, B47, 746-757.
15. W. Saenger, *J. Incl. Phenom*., **1984**, 2, 445-454.
16. Program SAINT, Version 7.60a, Bruker AXS Inc., Madison, WI, USA, **2006**.
17. G. M. Sheldrick, *Direct Methods for Solving Macromolecular Structures*, ed. S. Fortier, Dordrecht: Kluwer Academic Publishers, **1998**, 401-411.
18. M. R. Caira, S. A. Bourne, W. T. Mhlongo and P. M. Dean, *Chem. Commun.,* **2004**, 2216-2217.
19. M. R. Caira, V. J. Griffith, L. R. Nassimbeni, and B. van Oudtshoorn, *J. Incl. Phenom.,* **1995**, 20, 277-290.

20. XPREP, *Data Preparation and Reciprocal Space Exploration*, Version 5.1, © Bruker Analytical X-ray Systems*,* **1997***.*
21. S. Lubhelwana, MSc Dissertation, *Crystal Isostructurality and X-ray Diffraction studies of Cyclodextrin Inclusion Compounds*, University of Cape Town, South Africa, **2005**.
22. D. L. Cruickshank, N. M. Rougier, R. V. Vico, R. H. de Rossi, E. I. Buján, S. A. Bourne and M. R. Caira, *Carbohydr. Res*., **2010**, 345, 141-147.
23. M. R. Caira, W. T. Mhlongo and J. Li, *J. Optoelect. Adv. Mater*., **2008**, 10, 345, 141-147.
24. S. O. Pehkonen and Q. Zhang, *Crit. Rev. Env. Sci. Tec.*, **2002**, 32, 17-72.
25. G. Durand, M. Mansour and D. Barcelo, *Anal. Chim. Acta,* **1992**, 262, 167–178.
26. N. M. Rougier, R. V. Vico, R. H. de Rossi, E. I. Buján, *J. Org. Chem*., **2010**, 75, 3427-3436.
27. R. V. Vico, E. I. Buján and R. H. de Rossi, *J. Phys. Org. Chem*., **2002**, 15, 858-862.
28. R. Greenhalgh, K. L. Dhawan and P. Weinberger, *J. Agric. Food Chem*., **1980**, 28, 102-105.
29. J. Szejtli, *Chem. Rev*., **1998**, 98, 1743-1753.
30. R. V. Vico, Doctoral Thesis, Reactividad de compuestos fosforados con nucleófilos. Effecto de ciclodextrinas, Instituto de Investigaciones en Fisocoquímica de Córdoba (INFIQC), Departamento de Química Orgánica, Facultad de Ciencias Químicas, Universidad Nacional de Córdoba, Argentina, **2007**.
31. M. Kamiya and K. Nakamura, *Pestic. Sci*., **1994**, 41, 305-309.
32. D. Krois and U. H. Brinker, in *Cyclodextrins and their complexes*, ed. H. Dodziuk, Wiley-VCH Verlag GmbH & Co. KGaA, Weinheim, **2006**, ch. 10.4.
33. Y. A. Zhdanov, Y. E. Alekseev, E. V. Kompantseva and E. N. Vergeichik, *Russ. Chem. Revs*, **1992**, 61, 563.
34. K. A. Connors, *Chem. Rev*., **1997**, 97, 1325-1357.

Chapter 6: TRIMEB inclusion complexes and their reactivity in the solid state

Three isostructural TRIMEB inclusion complexes will be discussed followed by an analysis of the solid-state reaction kinetics of desolvation of each complex using isothermal and non-isothermal thermogravimetric methods.

THE GUESTS: FENITROTHION, FENTHION AND ACETOCHLOR

Fenitrothion, fenthion and acetochlor are oils at room temperature and were found to complex with TRIMEB in the solid state. The chemical structures of these three guests are shown in Figure 1. Fenitrothion and fenthion are close analogues and are classified as organophosphorus insecticides while acetochlor is a chloroacetanilide herbicide. The complex of fenitrothion and TRIMEB (TMBFEN) is discussed in Chapter 5 (pg. 190) and the X-ray crystal structure of the complex TRIMEB·fenthion has recently been elucidated by V. Maurel.[1] Following this introduction, an analysis of the solid-state inclusion complex of TRIMEB and acetochlor will be presented and the isostructurality among the three TRIMEB complexes will be confirmed with PXRD. The rates and mechanisms involved in loss of these agrochemicals from their TRIMEB inclusion complexes will be determined using isothermal and non-isothermal methods.

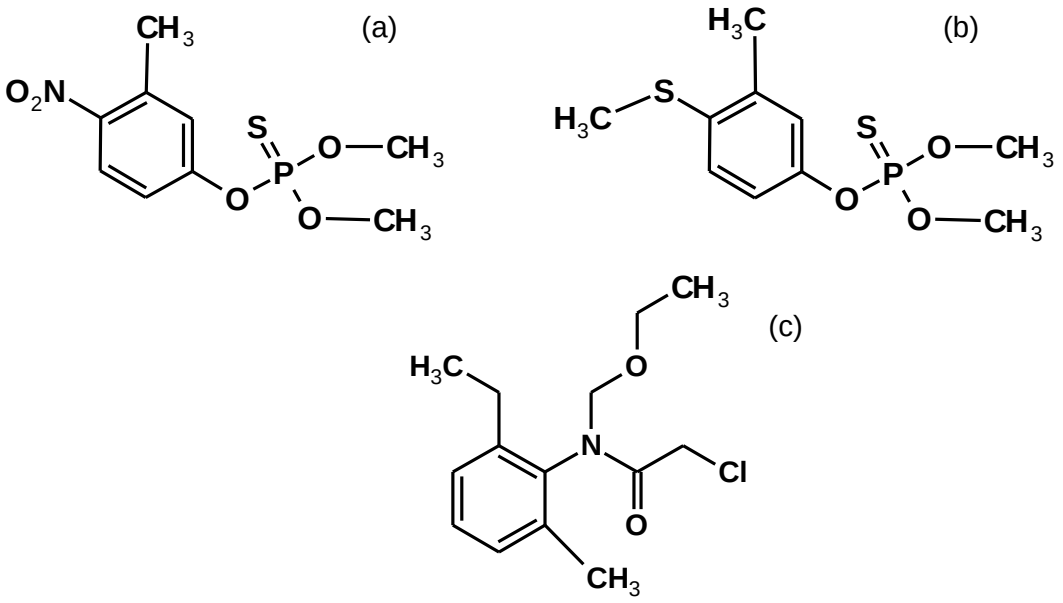

Figure 1. *The chemical structure of (a) fenitrothion, (b) fenthion and (c) acetochlor.*

TRIMEB·ACETOCHLOR INCLUSION COMPLEX

Complex preparation

The preparation of the TRIMEB·acetochlor inclusion complex (TMBACET) followed the conventional co-precipitation method for derivatised CDs. 106 mg (0.074 mmol) of the host was dissolved in water at room temperature, to which an equimolar quantity of acetochlor (20 mg, 0.074 mmol) was added. A total of 5 cm^3 of distilled water was used. The solution was stirred for several hours and then filtered into a clean vial and placed in an oven set at 60 °C. Single crystals appeared 12 h later.

Confirmation of stoichiometry and thermal analysis

The host-guest stoichiometry for TMBACET was established using thermogravimetry (Figure 2). The TG trace for the TMBACET complex displays a definite two-step mass loss in which the first mass loss of 16.0 ± 0.1 % (n = 2) corresponds to one guest molecule dissociating from the host (calcd. for 1:1 host-guest stoichiometry 15.9 %). This guest loss commenced at 125 °C and a plateau was reached at 236 °C before host decomposition started to occur. There was no mass loss prior to guest loss that could be attributed to dehydration of the complex. The DSC curve displayed one endothermic fusion peak at 136 °C. Fusion of the complex and guest loss therefore partially overlap.

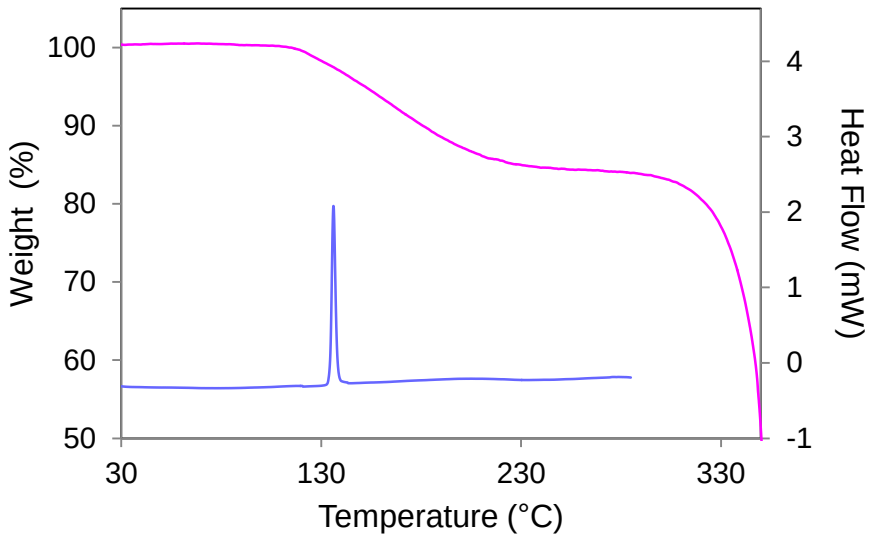

Figure 2. *Representative TG (pink) and DSC (blue) traces of TMBACET.*

Crystal structure analysis

Data-collection and space group determination

Single crystal X-ray diffraction data were collected on a Bruker KAPPA APEX II DUO diffractometer. The Laue system was found to be *mmm*, indicating the orthorhombic crystal system and the space group $P2_12_12_1$ was clearly identified from systematic absences. The asymmetric unit consists of one acetochlor molecule included within a TRIMEB molecule.

Structure solution and refinement

The crystal data and refinement parameters are reported in Table 1. Data were corrected for absorption by a numerical procedure using the program SADABS.[2] The TMBACET structure was solved by isomorphous replacement using only the host coordinates of an isostructural complex (TRIMEB·ethyl laurate hydrate).[3] All non-hydrogen atoms, except O6, C7, C8 and C9 of each methyl glucose unit, were used as the input fragment. The glucopyranose units were labelled G1-G7 with disordered moieties labelled A and B. The structure was refined with SHELXH-97, successive difference Fourier maps revealing the methoxyl groups.[4] Only one primary methoxyl group (on methylglucose unit G3) was disordered over two positions. The major component was assigned an s.o.f. of *x* and the minor component an s.o.f. of *1-x*. The final value of *x* refined to 0.65. All the non-hydrogen atoms of the hosts refined anisotropically except for the disordered atoms including C6A3, C6B3, O6A3, O6B3, C9A3 and C9B3, which were refined isotropically. All hydrogen atoms attached to the carbon atoms were placed in idealised positions using a riding model. The hydrogen atoms were assigned isotropic temperature factors 1.2 times those of their parent atoms except for the methyl hydrogen atoms, which were assigned isotropic temperature factors of 1.5 times those of their parent atoms. No water molecules were detected during X-ray analysis, in agreement with what was seen from the TG trace.

Table 1. *Data-collection and refinement parameters for the TMBACET complex.*

Chemical formula	$C_{63}H_{112}O_{35}\cdot C_{14}H_{20}ClNO_2$
Formula weight	1699.29
Crystal system	Orthorhombic
Space group	$P2_12_12_1$
Unit cell constants	
a (Å)	14.728(2)
b (Å)	21.542(3)
c (Å)	27.604(4)
$\alpha = \beta = \gamma$ (°)	90
Volume (Å^3)	8758(2)
Z	4
Density$_{calc}$ (g cm^{-3})	1.289
μ [MoKα] (mm^{-1})	0.131
F (000)	3656
Temperature of data collection (K)	100(2)
Crystal size (mm)	0.30 x 0.27 x 0.07
Range scanned θ (°)	1.8 - 25.9
Index ranges	h: -17, 15; k: -26, 22; l: -29, 33
ϕ and ω scan angle (°)	0.5
Total no. of frames	808
Dx (mm)	50.00
Total no. of reflections collected	55784
No. of independent reflections	9159
No. of reflections with I > 2σ(I)	6877
No. of parameters	1034
R_{int}	0.0696
S	1.027
R_1 [I > 2σ(I)]	0.0532
No. of reflections omitted	19
wR_2	0.1280
Weighting scheme parameters	a = 0.0755 and b = 5.8751
$(\Delta / \sigma)_{mean}$	< 0.001
$\Delta\rho$ excursions (e Å^{-3})	0.93 and -0.69

Modelling of the acetochlor guest

The guest molecule situated inside the TRIMEB cavity was relatively easy to model. The entire molecule could be assigned and modelled after a few successive difference Fourier refinement cycles. Atoms C17A and Cl18 were disordered over two positions (Figure 3). Both atoms were assigned a s.o.f. value of *x* while their counterparts (atoms C17B and Cl19) were assigned a s.o.f. value of *1-x*. The initial value of *x* was set to 0.5 but refined to a final value of 0.57. Distance restraints were required between atoms C6 and C7 and between C7 and C8. The majority of the guest atoms were refined anisotropically. Atoms C7, C8 and the four partial atoms (C17A, Cl18, C17B and Cl19) were refined isotropically. The guest hydrogen atoms were added in idealised positions in a riding model and refined with U_{iso} values 1.2-1.5 times the U_{iso} values of the atoms to which they were attached.

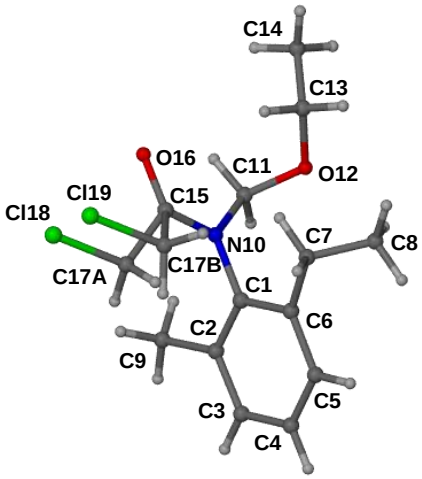

Figure 3. *The numbering scheme and disorder of the acetochlor guest molecule in the TMBACET complex.*

Geometrical analysis of the TMBACET structure

The asymmetric unit of the TMBACET complex consists of a single TRIMEB molecule and an included acetochlor molecule. The labelled TRIMEB host molecule is shown in Figure 4.

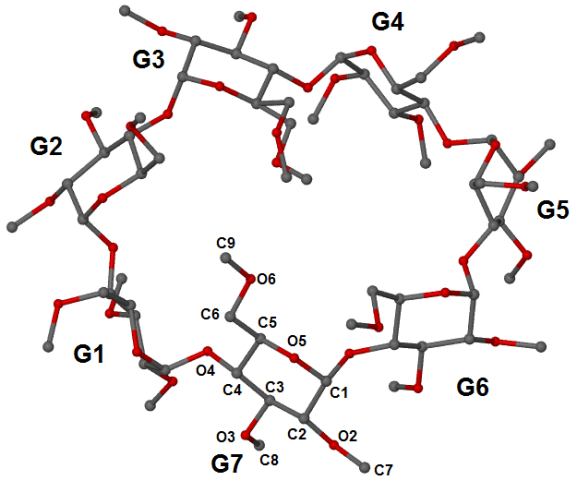

Figure 4. *Macrocyclic structure and numbering scheme of the TRIMEB glucose residues (hydrogen atoms have been omitted for clarity).*

Host conformation

All the glucose units are in the $^4C_1$ chair conformation. The primary hydroxyl torsion angles ω (O5-C5-C6-O6) are positive for methylglucose units G3 (both components) and G7 indicating a (+)-*gauche* conformation. All other methyl glucose units contain negative ω torsion angles and hence C6-O6 bonds are directed away from the CD cavity. The host geometrical parameters (Table 2) are similar to those of the TMBFEN complex (pg. 194) and the other isostructural TRIMEB complexes.[5] The large range of values seen for each parameter is due to the distorted saddle-like conformation the TRIMEB molecule adopts.

Table 2. *Geometrical parameters for the host molecule of the TMBACET complex.*

Residue	*l* (Å)	*D* (Å)	ϕ (°)	*d* (°)	α^a (Å)	$D_3{}^b$ (Å)	$\tau_1{}^c$ (°)	$\tau_2{}^d$ (°)
G1	5.56	4.39	114.8	26.9	-0.328	3.354	5.6	6.59
G2	5.07	4.44	122.1	-28.8	0.691	3.902	39.5	38.5
G3	4.31	4.58	145.0	-6.5	-0.121	3.466	46.3	53.7
G4	5.39	4.08	116.2	20.0	-0.558	3.653	4.2	6.59
G5	5.34	4.52	122.2	0.9	0.338	3.671	17.7	19.9
G6	4.58	4.42	134.7	-23.5	0.390	3.052	26.4	28.1
G7	4.74	4.34	134.3	1.6	-0.412	3.228	28.8	35.4

[a] mean e.s.d. = 0.002 Å; [b] mean e.s.d. = 0.006 Å; [c] mean e.s.d. = 0.1°; [d] mean e.s.d = 0.1°.

Guest inclusion

The position and orientation of the acetochlor molecule within the TRIMEB cavity are shown with space-filling representations in Figures 5 (a)-(d). The phenyl ring is situated within the cavity, close to the host primary rim. The methyl group is also situated in the TRIMEB cavity; however, the ethyl substituent and chloro-ethoxymethyl acetamide group protrude from the secondary rim of the TRIMEB cavity (Figure 5 (b)). The primary rim is 'sealed off' by the primary methoxyl groups which fold over giving the TRIMEB host molecule a cup-shape (Figure 5 (c)). Only one hydrogen atom of the guest molecule is situated below the O4 mean plane of the TMBACET molecule, demonstrating the relatively shallow mode of inclusion for this particular complex.

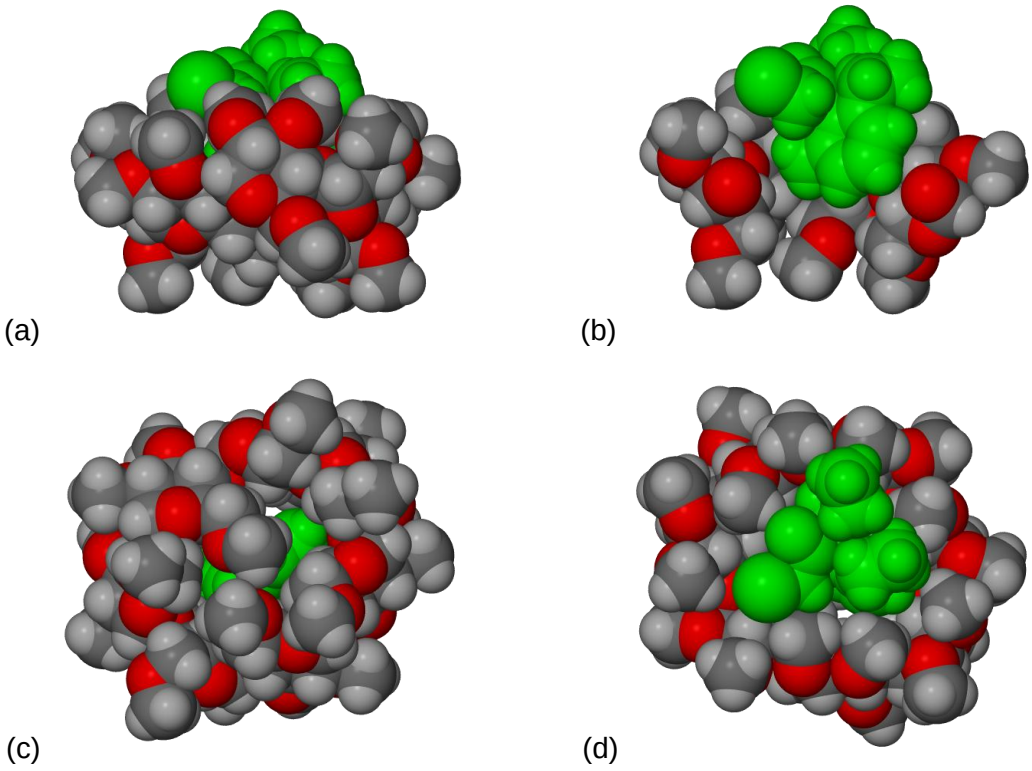

Figure 5. *(a) A side view, (b) a cross-sectional view, (c) a view from the primary rim and (d) a view from the secondary rim of the TMBACET complex (only the major host and guest components have been shown for clarity).*

Intra- and intermolecular interactions

The host conformation of the TMBACET complex is stabilised by several C-H•••O hydrogen bonds. There are a total of six intraglucose hydrogen bonds that occur at the secondary and primary rims of the TRIMEB cavity. Five of these interactions involve atoms C8 and O2, C8 and O4 or C7 and O2 at the secondary rim and only one occurs at the primary rim between atoms C9 and O5. These hydrogen bonds have an average bond length (C•••O) of 3.12 Å and C-H•••O angle of 120°. Seven intramolecular hydrogen bonds are present between adjacent methyl glucose units. All of these interactions occur at the secondary rim with a mean C•••O bond length of 3.11 Å and a mean bond angle of 129°. Table 3 lists the eight intermolecular host-host interactions which contribute to the overall stability of the crystal.

Table 3. *Intermolecular hydrogen bond interactions for the TMBACET complex.*

Interaction	D•••A (Å)	D-H•••A (°)	Symmetry operator*
C7G1–H7G3•••O2G4	3.54(1)	166	*-1+x, y, z*
C9G1–H9G1•••O6G5	3.40(1)	144	*3/2-x, 1-y, -1/2+z*
C2G2–H2G2•••O6G6	3.23(1)	160	*3/2-x, 1-y, -1/2+z*
C4G4–H4G4•••O3G7	3.32(1)	154	*1+x, y, z*
C7G5–H7GA•••O2G6	3.38(1)	152	*1/2+x, 1/2-y, 1-z*
C1G6–H1G6•••O6G1	3.42(1)	172	*3/2-x, 1-y, 1/2+z*
C2G6–H2G6•••O5G2	3.47(1)	148	*3/2-x, 1-y, 1/2+z*
C2G7–H2G7•••O6G4	3.43(1)	157	*-1+x, y, z*

* The symmetry operators refer to the O atoms.

Crystal packing

The crystal packing arrangement for the TMBACET complex is identical to that of the TMBCYC and TMBFEN complexes discussed previously (pg. 91 and 197 respectively). Figure 6 illustrates the packing arrangement for TMBACET. The complex units pack in a screw-channel mode and are arranged in a head-to-tail manner parallel to the *b*-axis. This diagram serves as a visual confirmation that the guest molecules are isolated from neighbouring host molecules.

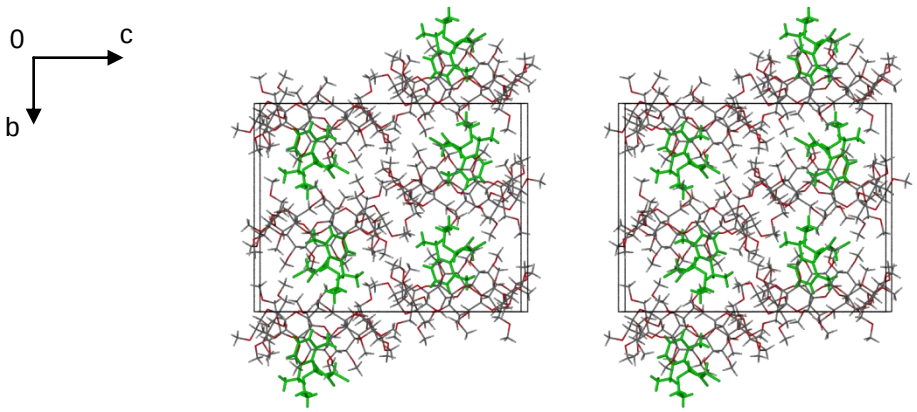

Figure 6. *Stereoview of the crystal packing for the TMBACET complex viewed along [100]. Guest molecules are shown in green.*

Comparative PXRD

The calculated and experimental PXRD traces are in good agreement for the TMBACET complex indicating that the single crystal selected for X-ray diffraction is representative of the bulk sample (Figure 7). The significant, general shift of the calculated pattern to higher 2θ values is a result of the relatively low temperature (100 K) of the single crystal X-ray data-collection.

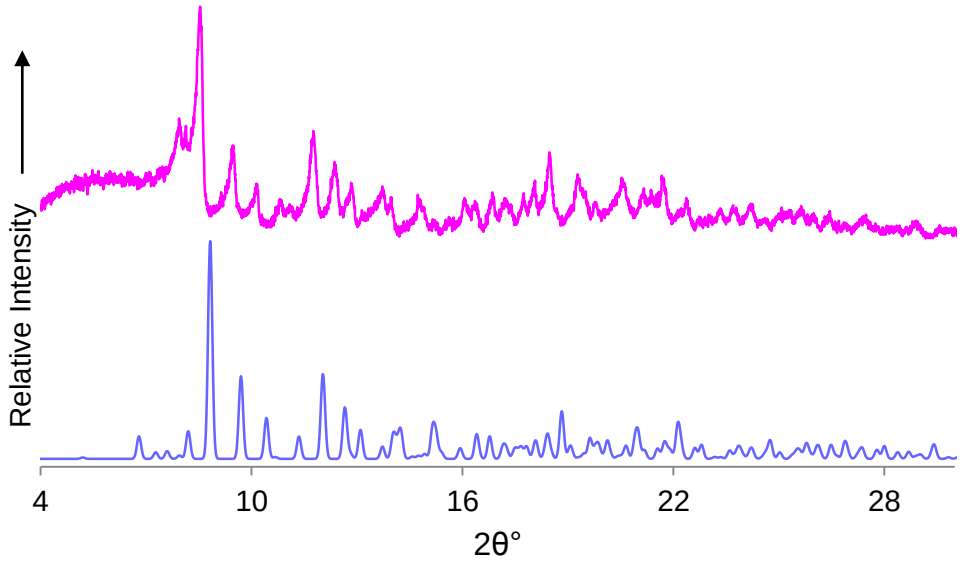

Figure 7. *Calculated (blue) and experimental (pink) PXRD traces of TMBACET.*

STUDY OF THE THERMAL STABILITY OF THREE ISOSTRUCTURAL SOLID-STATE TRIMEB INCLUSION COMPLEXES USING THERMOGRAVIMETRY

Complex preparation and isostructurality of the three complexes

The co-precipitation method did not result in sufficient yields of each complex for thermogravimetric studies to be conducted. Consequently, an alternative method was used, which involved kneading an equimolar quantity of both the guest and host with a mortar and pestle for 30 min in the absence of water (co-grinding). For all experiments, the mass of the guest was kept constant at 20 mg and the mass of TRIMEB varied depending on the molecular weight of each guest molecule. This method allowed at least 100 mg of each complex to be prepared, ensuring a sufficient quantity of material to perform all subsequent experiments with the same sample batch. Another important factor regarding sample preparation for kinetic studies using TGA is the uniformity of particle sizes of a particular sample. The reaction rate of solid-state processes tends to increase with decreasing particle size of the solid material.[6] The particle size distributions of the powdered samples in this study were measured using a Multisizer™ 3 Coulter Counter. The mechanical co-grinding method yielded samples with particle diameters in the range of 20 µm to 45 µm, having a mean particle size of *ca. 25* µm.

PXRD was used to confirm that complexation had occurred and that all three complexes were isostructural (Figure 8). The isostructurality of these complexes implies a common arrangement of the host molecules and thus the packing arrangements of the complex units are identical. Figure 9 illustrates the three inclusion complexes viewed from the primary rim of the CD cavities. Both organophosphorus complexes (TMBFEN and TMBFTN) have the phosphorothioate units situated closer to the primary rim with the phenyl moieties protruding from the secondary side of the CD cavity. The acetochlor molecule has the major part of the phenyl ring situated in the cavity with the two bulky substituents located outside the CD cavity.

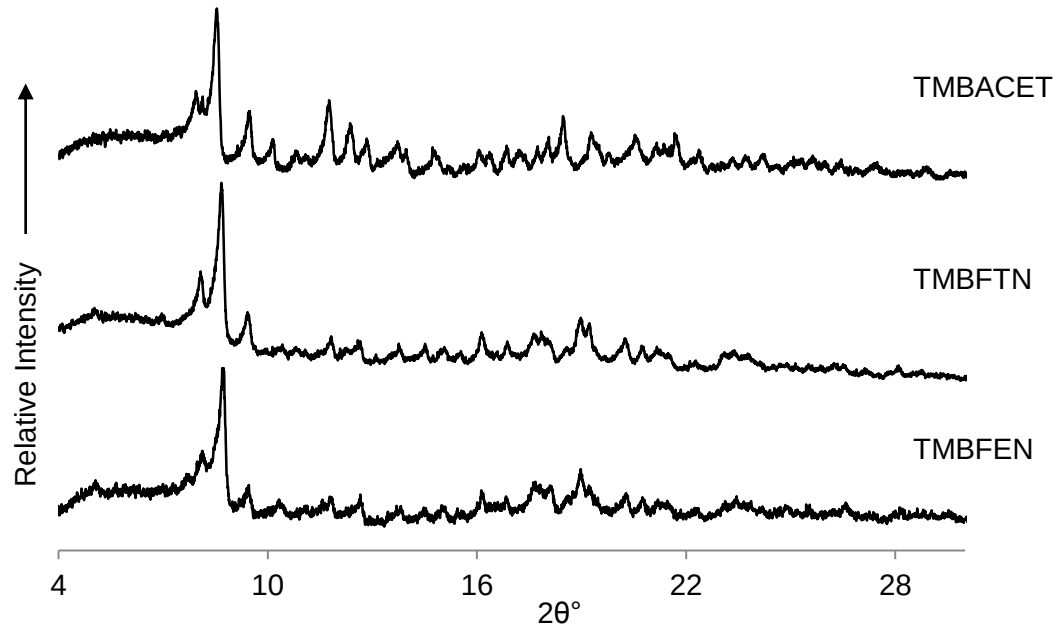

Figure 8. *PXRD traces of the three isostructural TRIMEB complexes formed using the mechanical co-grinding method.*

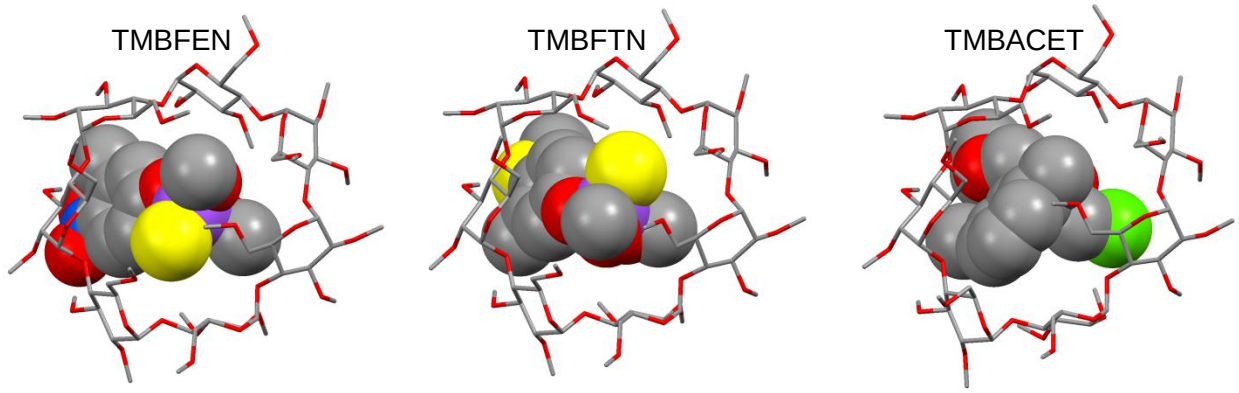

Figure 9. *View from the primary rim of the three isostructural TRIMEB inclusion complexes.*

Effect of particle size on thermal analysis

The TG traces for the three TRIMEB inclusion complexes all display two-step mass losses. The first is due to guest expulsion from the CD cavity and the second can be attributed to host decomposition (Figure 10). There was a significant difference in the onset temperatures of guest loss for the samples prepared by mechanical co-grinding of the host and guest molecules together, versus the samples prepared by the conventional method of co-precipitation, on which the crystal structure determination was based. These differences have been tabulated (Table 4) and are a result of the different particle sizes within each sample. The co-precipitation method produced large single crystals that were gently crushed

and blotted dry on filter paper before being placed in the TG instrument, whereas the kneaded material consisted of much smaller particle sizes and thus guest loss occurred at a lower temperature.

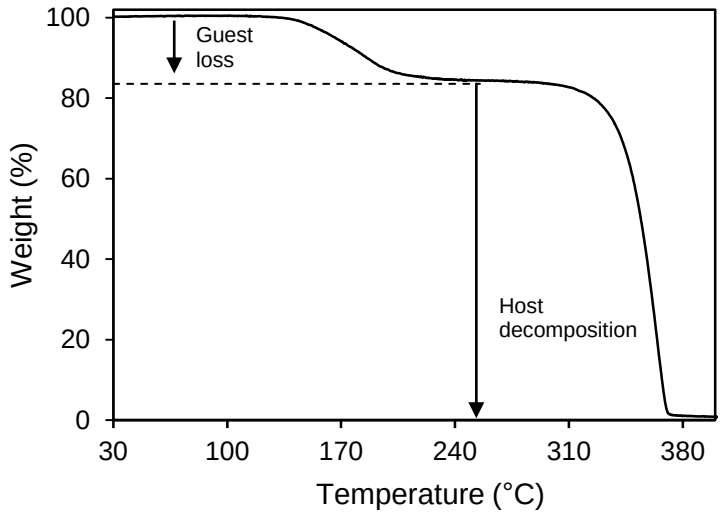

Figure 10. *(a) A schematic TG trace for the TRIMEB inclusion complexes with fenitrothion, fenthion and acetochlor.*

Table 4. *The onset temperatures of guest loss and the melting points of the three complexes prepared using two different methods.*

Complex	Onset temperature of guest loss as determined by TGA (°C)*		Temperature of complex fusion determined by DSC (°C)	
	Co-precipitation	Dry grinding	Co-precipitation	Dry grinding
TMBFEN	129	100	160	158
TMBFTN	135	93	153	152
TMBACET	109	83	136	133

* These temperatures were measured based on the standard 10 K min^{-1} heating rate.

The melting points of the complexes prepared by the two methods only differ by a maximum of 3 K and are also listed in Table 4. This minimal temperature difference confirms that the physical property of fusion is equivalent for the samples prepared by co-precipitation and co-grinding. Figure 11 illustrates the fusion endotherms for each of the complexes prepared using the method of co-grinding.

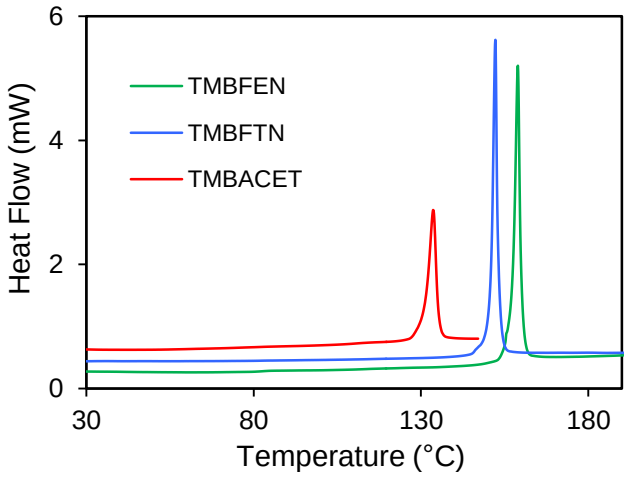

Figure 11. *The DSC curves illustrating the endothermic fusion peaks for each TRIMEB complex.*

Despite the early onset temperatures at which guest loss starts to occur for the complexes, the entire process of guest loss takes place over a wide temperature range (onset temp. to ~240 °C). Consequently, the processes of guest loss and fusion partially overlap, guest loss preceding fusion in each case. Following reaction rates of solid-state processes is normally a challenging task but it is further complicated when more than one process occurs at the same time. Nevertheless, these partially overlapping processes were studied using both isothermal and non-isothermal kinetic experiments.

The kinetics of heterogeneous reactions

There are two principal objectives when studying the reactions of solid-state chemical processes. The first is to be able to determine the rate equation that satisfactorily describes the extent of conversion of reactants or the formation of products with time as the reaction proceeds and the second objective is to understand the reaction mechanism.[7] With these data, the influence of temperature on the rate of reaction provides parameters such as the energy barrier associated with desolvation, guest loss and other decomposition processes.

The rate of a homogeneous reaction is measured by following the change in concentration of one of the reactants or products. For a heterogeneous reaction, concentration no longer has the same significance. Instead, the reaction depends on the chemical and physical changes occurring at a reaction interface. There are several methods based on thermogravimetric measurements that can be used to establish the kinetics of such reactions. The extent of a reaction (α, Equation 1) based on the mass loss of the sample can be measured as a function of time at a constant temperature ($d\alpha/dt$, isothermal kinetics) or α can be directly

related to a series of different, usually constant, heating rates (β = dT/dt) (dα/dt non-isothermal kinetics).

$$\alpha = \frac{m_o - m_t}{m_o - m_\infty} \quad (1)$$

Both isothermal and non-isothermal kinetic data can be fitted to a set of kinetic models based on certain mechanistic assumptions from which the activation energy (E_a) and frequency factor (A) can be calculated (model-fitting methods). On the other hand, model-free methods calculate E_a values without the mechanistic assumptions and this is achieved by grouping terms such as the frequency factor (A) and a kinetic function into the intercept of a linear equation and using the slope of the equation to calculate the activation energy.[8] In this work, the isothermal kinetic experiments were evaluated using the model-fitting method while the non-isothermal data were analysed using the model-free method.

Kinetic analysis of isothermal experiments

The sample size used for each isothermal TG run performed was ~1.8 mg. The material was evenly spread at the bottom of an open aluminium pan to ensure reproducibility and consistency for all experiments. The sample was heated to a desired temperature at 30 or 40 K min^{-1} and then maintained at that temperature until the guest had been released and the mass reached a constant value. These data were then used to generate weight percentage versus time curves and extent of reaction (α) versus time curves for analysis of the kinetics involved in guest loss (Figures 12 (a)-(c)). All curves display deceleratory behaviour.

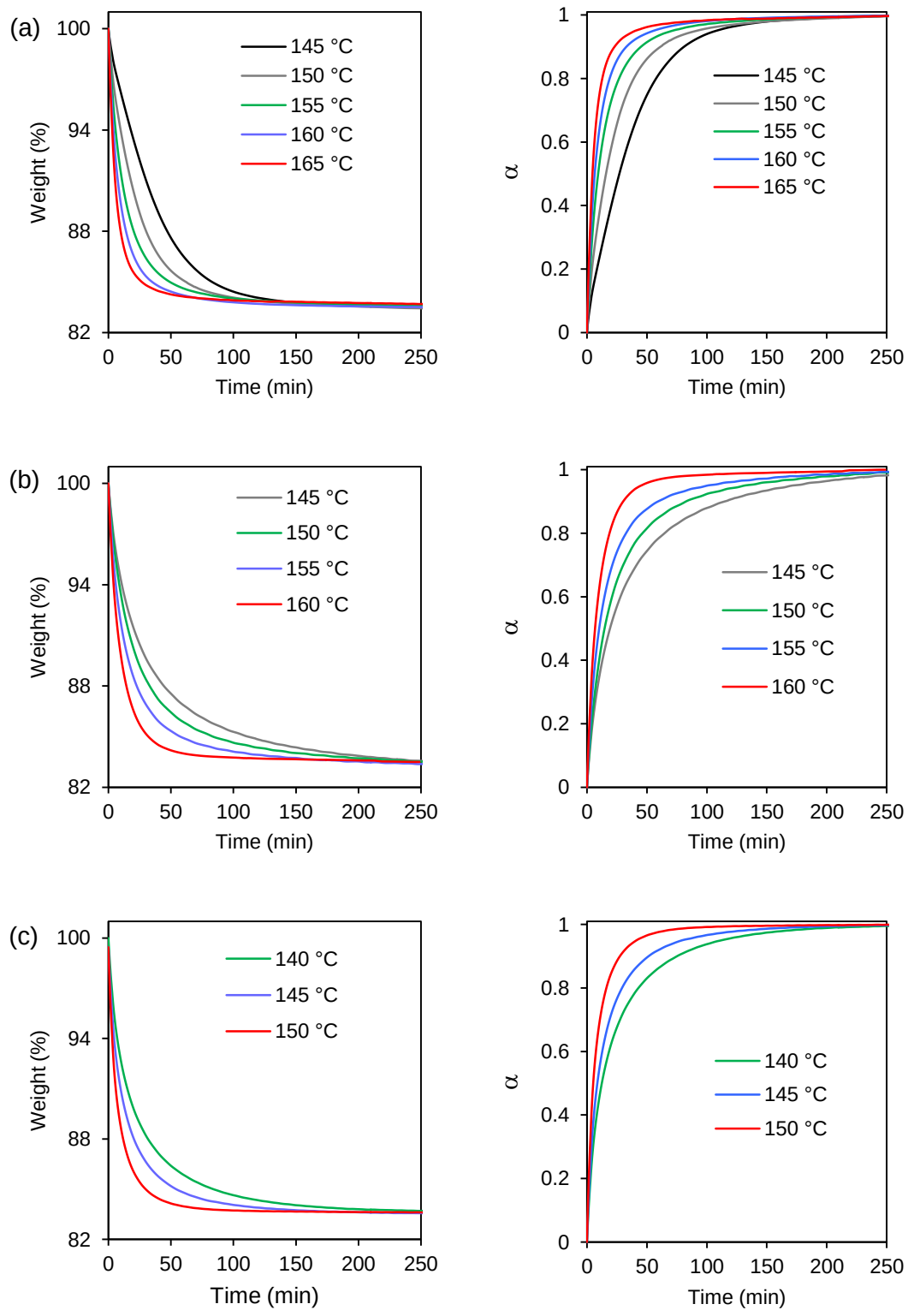

Figure 12. *The isothermal plots of weight loss percentage versus time (left-hand side) and α versus time (right-hand side) for (a) TMBFEN, (b) TMBFNT and (c) TMBACET.*

The α versus time curves were evaluated using various mathematical expressions derived from proposed mechanisms for a range of solid-state processes. For our results, the equation based on the first-order reaction model (F1) as well as the equation based on the 3-D diffusion model (3D) (Table 5),[7] showed a high degree of linearity and good correlation coefficients when fitted to the α versus time graphs over an α range of 0.0-0.8 for the F1 model and 0.1-0.9 for the 3D model.

Table 5. *The rate equations used to analyse the kinetic data obtained from the isothermal α versus time plots.*

Model	$g(\alpha) = kt$	$f(\alpha) = \frac{1}{k}\frac{d\alpha}{dt}$
Reaction order model: First order (F1)	$-\ln(1-\alpha)$	$1-\alpha$
Diffusion model: 3-D diffusion-Jander eqn. (3D)	$\left[1-(1-\alpha)^{\frac{1}{3}}\right]^2$	$3(1-\alpha)^{\frac{2}{3}} / 2\left[(1-\alpha)^{\frac{1}{3}}\right]$

Using both models we were able to obtain two sets of rate constants (*k*) at specific temperatures for each complex studied. An Arrhenius plot (ln*k* versus 1/T) provided a straight line, from which the activation energy associated with the composite process of guest loss and complex fusion could be determined. These plots are shown in Figures 13 (a)–(c) and the activation energies obtained for each complex with the two models have been listed in Table 6.

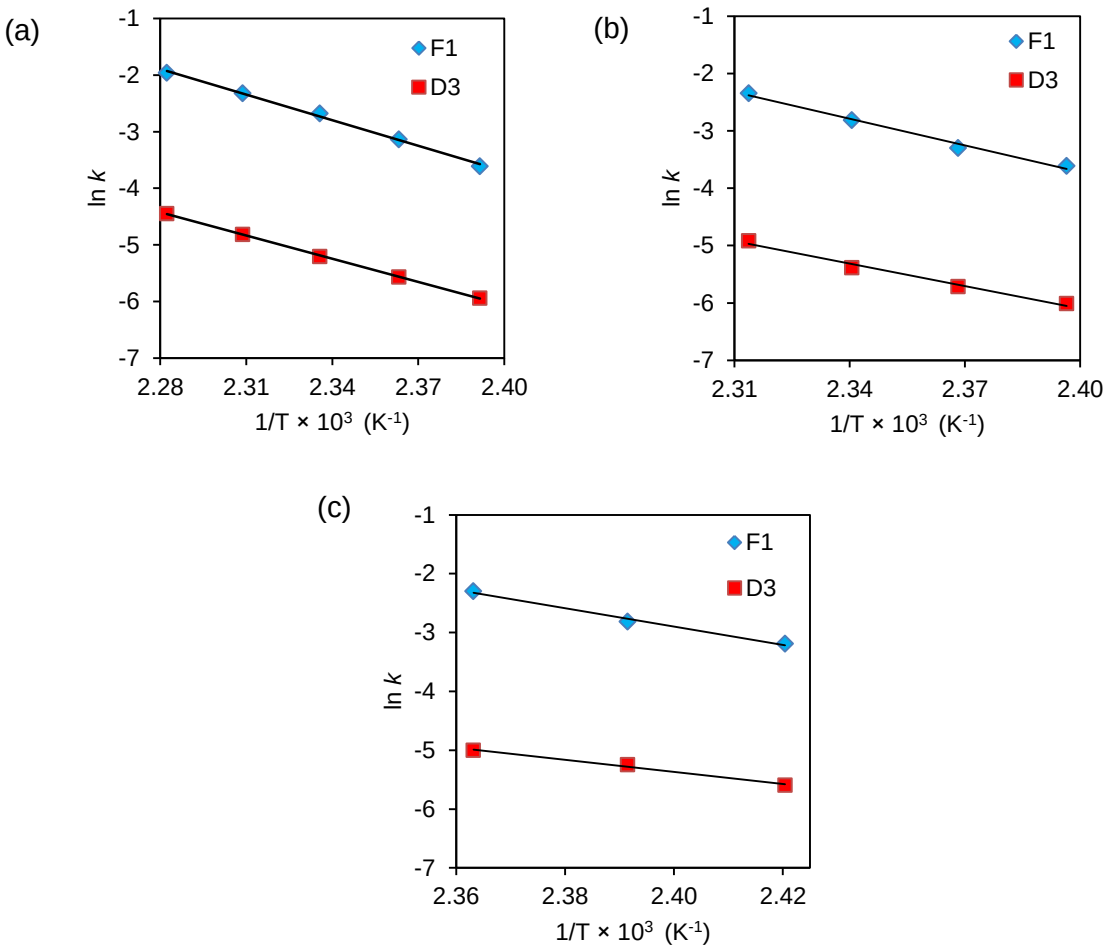

Figure 13. *The Arrhenius plots obtained from the isothermal kinetic data for the TMBFEN (a), TMBFTN (b) and TMBACET (c) complexes.*

Table 6. *Activation energies determined for each complex using the two best-fitting models.*

	TMBFEN		**TMBFTN**		**TMBACET**	
	F1	3D	F1	3D	F1	3D
E_a (kJ mol^{-1})	126±4	114±1	129 ± 10	109 ± 9	130 ± 13	86 ± 8
r^2	0.997	0.999	0.989	0.986	0.990	0.991

There are many instances in the literature where more than one solid-state mechanism can be used to describe a particular process.[9,10] The first-order reaction (F1) model is based on the apparent 'order' of reaction as seen for rate laws established in solution; however, it does not have the same significance for solid-state reactions. The mechanism of a first-order reaction involves random nucleation (either at a particle surface or at an imperfection)

and growth of these nucleation sites that does not advance beyond the individual crystallite nucleated.[7] For our study one can propose that the formation of fusion nuclei[11] is immediately followed by melting of the complex which, as seen by the similar activation energies calculated using this model, does not depend on the structure of the guest molecule being released.

The overall rate of the diffusion-limited reactions is controlled by diffusion of a product away from a reaction interface or reactant towards a reaction interface instead of nucleation or phase-boundary advancement.[12] The activation energies obtained from the 3D model (Table 6) are very similar once again but do display a decreasing trend. One can therefore propose that this particular model is dependent on the structure or physical properties of the guest molecule being expelled from the CD cavity.

It is possible that the above interpretation is somewhat flawed because the kinetic models are being applied to data collected over the majority of the α-range. As previously established, the complex melts midway during guest loss and is no longer in the solid form. The 3D model is therefore a reasonable model to be applied to the kinetics of the TRIMEB complexes as once the sample melts the guest can diffuse to the liquid-air interface without any directional restrictions. Prior to the complexes melting, the 3D model is consistent with the crystal packing arrangement of these complexes, as the guest molecules pack within the crystal such that they are isolated from one another. There are no continuous channels within the TRIMEB complex crystal structures along which the guest molecules are confined to diffuse.

Galwey *et al* have microscopic evidence that both melting and evolution of product gases appear for the thermal decomposition of various inorganic compounds.[13,14,15] These compounds, however, only show fusion spots on the crystal surfaces under high magnification but never undergo a complete melt. Nontheless they used variously derived solid-state rate equations to study these processes and stated that the quantitative analysis of their particular systems does not provide a direct measure of the extent of decomposition as there are two processes occurring together. A similar statement can be made with regard to the three TRIMEB inclusion complexes being studied.

Kinetic analysis of non-isothermal experiments

The sample size used for each non-isothermal TG run performed was kept small and relatively constant (1.77 - 1.94 mg) for each experiment. The material was evenly spread at the bottom of an aluminium pan before being placed in the TG instrument to ensure consistent and reproducible results. The samples were heated from 20 to 300 °C at different heating rates (1.0, 2.5, 5.0, 7.5 and 10.0 K min^{-1}) and the mass loss noted in each run was equivalent to one guest molecule being released for a 1:1 CD complex. Heating rates greater than 10.0 K min^{-1} were not used, as the process of guest loss and host decomposition began to overlap (i.e. there was no definite plateau between the two events). Figure 14 illustrates the thermogravimetric traces for the TMBFEN, TMBFTN and TMBACET complexes at the various heating rates and the remarkably lower onset temperatures of guest loss that were referred to in Table 4.

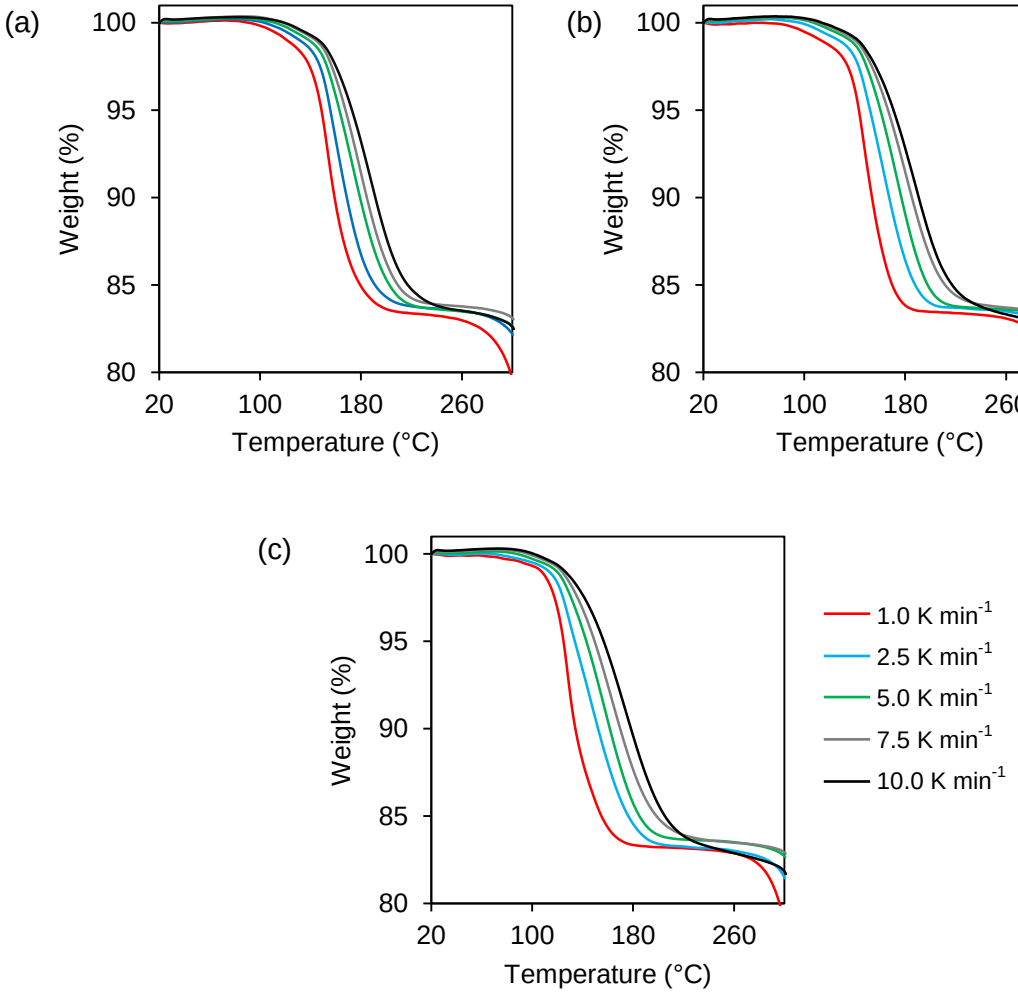

Figure 14. *Non-isothermal thermogravimetric traces for (a) TMBFEN, (b) TMBFTN and (c) TMBACET at the different heating rates.*

A model-free isoconversional method based on the Ozawa, Flynn and Wall (OFW) method[16,17] was used to determine the activation energy related to the results obtained from the non-isothermal experiments. This method relies on the use of more than one heating rate and the temperatures being recorded at specific conversion levels for each heating rate. The conversion levels are defined in terms of percentages based on the extent of the reaction (the term α is used which is analogous to that used for the isothermal experiments). Equation 2 allowed the determination of the activation energies at each conversion level, where β_α is the heating rate, A_α the frequency factor, $E_{a\alpha}$ is the activation energy, T_α is the temperature at each conversion level and $g(\alpha)$ refers to the kinetic model.

$$\log \beta_\alpha = \log \frac{A_\alpha E_{a\alpha}}{g(\alpha)R} - 2.315 - 0.457 \frac{E_{a\alpha}}{RT_\alpha} \qquad (2)$$

The conversion levels at which the activation energies were evaluated were 8, 12, 16 and 20 %. Table 8 lists the reciprocal temperature values for each complex at the various conversion levels for the different heating rates used. Figures 15 (a)-(c) show the linear plots of $\log \beta_\alpha$ versus the reciprocal temperature values from which the activation energies were calculated.

Table 8. *The reciprocal temperature values obtained at the various conversion levels for each heating rate for the three TRIMEB inclusion complexes investigated.*

			$1/T \times 10^3$ (K^{-1})			
Complex	Heating rate (β) (K min^{-1})	log β	8 %	12 %	16 %	20 %
TMBFEN	1.0	0.000	2.508	2.454	2.424	2.403
	2.5	0.398	2.458	2.406	2.378	2.362
	5.0	0.699	2.427	2.372	2.349	2.333
	7.5	0.875	2.398	2.354	2.331	2.313
	10.0	1.000	2.379	2.338	2.313	2.291
TMBFTN	1.0	0.000	2.543	2.479	2.447	2.429
	2.5	0.398	2.478	2.428	2.402	2.386
	5.0	0.699	2.438	2.392	2.370	2.351
	7.5	0.875	2.419	2.376	2.350	2.327
	10.0	1.000	2.403	2.362	2.332	2.307
TMBACET	1.0	0.000	2.599	2.571	2.551	2.537
	2.5	0.398	2.561	2.530	2.510	2.495
	5.0	0.699	2.530	2.499	2.475	2.453
	7.5	0.875	2.514	2.477	2.448	2.423
	10.0	1.000	2.501	2.453	2.417	2.388

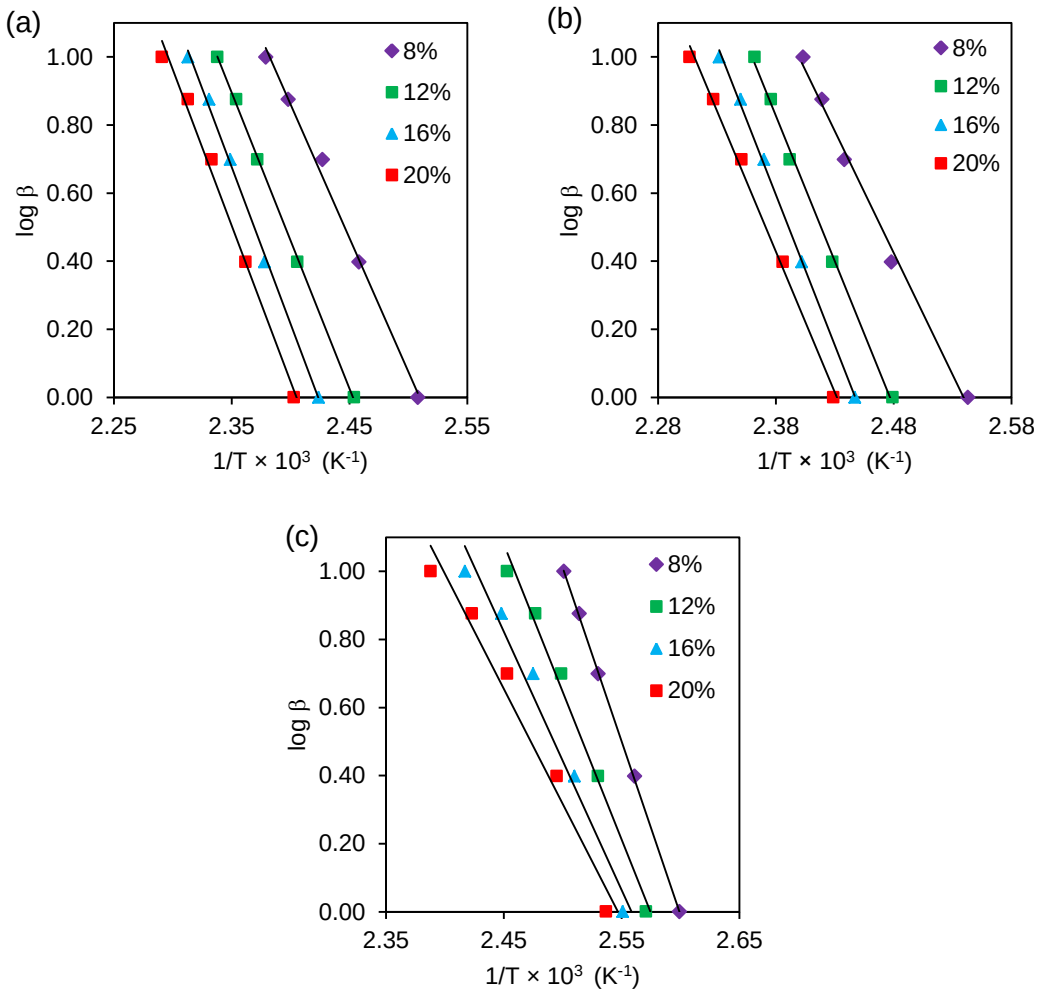

Figure 15. *Plots of logβ versus 1/T for (a) TMBFEN, (b) TMBFTN and (c) TMBACET.*

Figures 15 (a) and (b) illustrate fairly linear plots whereas Figure 15 (c) shows that the guest loss process is not uniform as the slope of the plots increases at lower conversion levels. The activation energies were calculated by equating the slope of the curves to $(-E_{a\alpha} \times 0.457) / R$ and solving for $E_{a\alpha}$ (refer to equation 2). These values are reported in Table 9 and have been averaged to establish the validity of the method for each sample.

Table 9. *Activation energies recorded at specific conversion levels for each CD inclusion complex.*

	$E_{a\alpha}$ (kJ mol^{-1})		
Conversion Level	**TMBFEN**	**TMBFTN**	**TMBACET**
8 %	142.9	130.1	185.5
12 %	158.2	155.3	157.8
16 %	167.7	160.6	138.0
20 %	166.8	150.4	123.0
Average	**158(12)**	**149(13)**	**151(27)**

The variation in E_a values obtained for the TMBFEN and TMBFTN complex is random with no trend occurring as the conversion level increases. The relative percentage errors for these activation energies are less than 10%, which is within the conventionally accepted range for isoconversional methods.[10] The TMBACET complex shows a decrease in the activation energy as a function of α.

The non-isothermal kinetic method is the preferred method to study the complicated systems presented by the three isostructural inclusion complexes. The activation energies calculated from these experiments depend mainly on the initial stages of guest loss. The conversion levels chosen were such that the vast majority of the temperatures recorded for the various heating rates at the specific conversion levels were lower than the respective melting points of the complexes. As the complex TMBACET has the lowest melting point (133 °C), one, two and three reciprocal temperature values recorded at the 12, 16 and 20 % conversion levels, respectively, were lower than the reciprocal fusion temperature of TMBACET. This may explain the decreasing trend seen for the activation energies in the case of the TMBACET complex at the various conversion levels. Finally, the activation energies determined using non-isothermal procedures provide a better representation of the energy required to remove only the guest molecule from the solid-state complex without the process of complex fusion interfering.

Discussion of isothermal and non-isothermal results

The results obtained using the isothermal and non-isothermal methods cannot be compared with one another due to the different ways in which the data were obtained (constant temperature versus constant heating-rate) and analysed (model-fitting versus model-free). Furthermore, the range over which the activation energy was determined was different for

the two methods. The partially overlapping processes of guest loss and fusion for each complex create complications in determining the activation energy associated with guest loss only. The two processes would need to be evaluated using a technique such as modulated differential scanning calorimetry which has the ability to separate reversible (melting) and non-reversible processes (guest loss) from one another.

This is a unique investigation as most solid-state kinetic studies deal with the desolvation, decomposition and polymorphic transformations of various materials. The process of guest loss from a trimethylated CD host molecule has never been considered before. However, there are several studies that have investigated the dissociation of a guest molecule from native CDs.[18,19,20] The activation energies reported for the thermal dissociation of benzyl alcohol and cinnamaldehyde from their β-CD inclusion complexes were reported as 158 and 160 kJ mol^{-1} respectively,[18,20] which are very similar to what was determined for the three TRIMEB inclusion complexes using the method of non-isothermal TGA. The process of guest loss for the β-CD complexes containing benzyl alcohol and cinnamaldehyde occur via a diffusion-based mechanism which is in agreement with what was found for the TRIMEB inclusion complexes. The dimensionalities of the diffusion-based models are obviously dependent on the packing arrangement of the complex units and are different for the β-CD and TRIMEB complexes discussed here.

It is of great importance to understand the thermal stability of CD inclusion complexes in the solid state. These studies show that a relatively high energy barrier is associated with guest loss from a TRIMEB molecule and that these solid-state complexes should remain intact during handling and storage of the material. Furthermore, the method of mechanical co-grinding used to produce these complexes could be used in industry to produce large quantities of the complex, thereby stabilising oil-based agrochemicals in a solid form.[21]

Solid-state kinetics is a complex area of research with many assumptions and mathematical manipulations but accompanied by visual techniques such as scanning electron microscopy one can obtain greater insight into the mechanisms associated with certain kinetic processes.

REFERENCES

1 V. Maurel, MSc Dissertation, *The Inclusion of Selected Bioactive Molecules in Cyclodextrins: A Physicochemical Study*, University of Cape Town, South Africa (in progress **2011**).

2. G. M. Sheldrick, Program SADABS, Version 2.05, University of Göttingen, Germany, **2007**.
3. D. Mentzafos, I. M. Mavridis and H. Schenk*, Carbohydr. Res*., **1994**, 253, 39-50.
4. G. M. Sheldrick, SHELXH-97, *Acta Crystallogr*., **2008**, A64, 112-122.
5. Cambridge Structural Database and Cambridge Structural Database system, Version 5.32, Cambridge Crystallographic Data Centre, University Chemical Laboratory, Cambridge England, February **2011**.
6. J. Pysiak, *J. Therm. Anal*., **1995**, 43, 9-19.
7. A. K. Galwey and M. E. Brown, in *Handbook of Thermal Analysis and Calorimetry, ed.* M. E. Brown, Elsevier Science, Amsterdam, The Netherlands, **1998**, vol. 1 ch. 3, 147-224.
8. A. Khawan and D. R. Flanagan, *J. Pharm. Sci.*, **2006**, 95, 472-498.
9. S. Vyazovkin and C. A. Wight, *J. Phys. Chem. A*, **1997**, 101, 8279-8284.
10. S. Vyazovkin and C. A. Wight, *Int. Rev. Phys. Chem*., **1998**, 17, 407-433.
11. A. K. Galwey, *Proceedings of the 7th International Conference on Thermal Analysis*, Wiley, New York, **1982**, 38-53.
12. *Solid State Chemistry of Drugs*, eds. S. R. Byrn, R. R. Pfeiffer and J. G. Stowell, SSCI, Inc., West Lafayette, Indiana, 2nd edn., **1999**, ch. 21, 443- 460.
13. N. J. Carr and A. K. Galwey, Proc. *R. Soc. London*, **1986**, A404, 101-126.
14. A. K. Galwey and G. M. Laverty, *Proc. R. Soc. London*, **1993**, A440, 77-93.
15. A. K. Galwey, L. Pöppl and S. Rajam, *J. Chem. Soc., Faraday Trans. I*, **1983**, 79, 2143-2151.
16. T. Ozawa, *Bull. Chem. Soc. Jpn.*, **1965**, 38, 1881-1886.
17. J. H. Flynn and L. A. Wall, *J. Polym. Sci. Part B: Polym. Lett*., **1966**, 4, 323-328.
18. J.-H. Li, N. Zhang, X.-T. Li, J.-Y.Wang and S.-J. Tian, *J. Therm. Anal*., **1997**, 49, 1527-1533.
19. T. L. Neoh, K. Yamauchi, H. Yoshii and T. Furuta, *J. Phys. Chem. B.*, **2008**, 112, 15914-15920.
20. N. Zhang, J.-H. Li, Q.-T. Cheng and M.-W. Zhu, *Thermochim. Acta*, **1994**, 235, 105-116.
21. J. Szejtli, *Starch*, **1985**, 37, 382-386.

CHAPTER 7: Conclusion

SUMMARY

The work discussed herein focuses on four pesticides (cycluron, endosulfan, fenitrothion and acetochlor) and their inclusion with various cyclodextrin molecules in solution and in the solid state. The results obtained with each pesticide are summarised here:

1. The herbicide, cycluron, was successfully complexed with β-CD, γ-CD, TRIMEA, TRIMEB and DIMEB in the solid state. Each of the complexes, except for the γ-CD complex, was fully characterised using X-ray diffraction and thermal analytical methods. Experiments conducted in solution showed complexation to occur between cycluron and each of the native CDs, with a 1:1 host-guest ratio. ^{1}H NMR spectroscopy allowed an evaluation of the association constants and stoichiometry only, while the more direct technique of isothermal titration calorimetry was used to determine the association constants, host-guest stoichiometries as well as the thermodynamic parameters associated with host-guest complexation.
2. The 7:3 isomeric sample of endosulfan formed inclusion complexes with β-CD, γ-CD and RAMEB in the solid state. These results were confirmed using powder X-ray diffraction. The single crystal X-ray structures of inclusion complexes of only the β-endosulfan isomer with β-CD and DIMEB were fully elucidated. The poor quality and low yields of the complexed material prevented adequate crystal structure analysis and characterisation of the α-endosulfan·β-CD complex. Solution-state studies were attempted; however, the low aqueous solubility of endosulfan prevented acquisition of measurable data.
3. Fenitrothion was comprehensively investigated both in solution and in the solid state. In the solid state, inclusion complexes were formed between the guest molecule and five CDs (β-CD, γ-CD, TRIMEA, TRIMEB and DIMEB). All of these complexes, except the γ-CD complex, were fully characterised using TG, DSC, HSM, PXRD and single crystal X-ray diffraction. Elemental analysis and ^{1}H NMR spectroscopy were also used to confirm the host-guest stoichiometries for the various complexes. In solution, the stoichiometries of the five CD-pesticide inclusion complexes were determined based on the results obtained from the kinetic data. The alkaline hydrolysis of fenitrothion in the presence of CDs allowed the stability of fenitrothion to be assessed and the binding strength of the CD-pesticide interactions to be quantified. In addition to the reaction kinetics followed in solution, the relative guest orientations within the same five CD molecules were examined using induced circular dichroism.

4. Acetochlor formed a crystalline inclusion complex with TRIMEB only. This particular complex was determined to be isostructural with two other TRIMEB complexes (TRIMEB·fenitrothion and TRIMEB·fenthion). The reactivity of these complexes in the solid state was investigated using isothermal and non-isothermal dynamic thermogravimetric methods. Studying the reactivity of these isostructural solid-state complexes was complicated due to the process of guest loss partially overlapping with complex fusion. Despite this, reliable activation energies for guest loss were determined and mechanistic models for this process were deduced.

CRYSTAL STRUCTURES

Since each of Chapters 3, 4 and 5 dealt with the inclusion of a specific pesticide with the various CD molecules, a different perspective based on a brief comparison of the solid-state structures formed between the various guests and each CD (β-CD, TRIMEA, TRIMEB and DIMEB) follows.

β-CD inclusion complexes

Single crystals of the BCDCYC, BCDFEN and BCD**B**END complexes were formed by the method of co-precipitation. All three complexes crystallised with a dimeric β-CD unit encapsulating the guest molecule/s. The compositions differed for the three complexes such that 1:1, 1:0.6 and 2:1 host-guest ratios were determined for BCDCYC, BCDFEN and BCD**B**END, respectively. Due to the low yield of the BCDFEN crystals, only hot stage microscopy was used to evaluate the thermal stability of this particular complex. Nevertheless, from these results it was evident that the thermal behaviour for all three complexes was similar, water being released between 30 and 100 °C and decomposition occurring above 200 °C. This is in agreement with data for many other β-CD complexes whose thermal analyses have been published.[1,2]

The cycluron and fenitrothion molecules of the host-guest complexes BCDCYC and BCDFEN were completely disordered over two positions in each CD cavity of the β-CD dimer. A different type of disorder was found within the BCD**B**END complex owing to the twofold rotation axis that is inherent in the space group *C*2, in which this complex crystallised. Only part of the endosulfan guest molecule was present in the asymmetric unit but through the twofold symmetry, the guest molecule was completed and a second guest component was generated. Both the BCDFEN and BCD**B**END complex structures were necessarily refined with many constraints and their final crystal structures are not of the

same standard as that of the BCDCYC complex; nonetheless, these crystal structures, with their accompanying analytical data, prove that the pesticide molecules investigated have an affinity for the interior cavity of a β-CD molecule.

Finally, upon evaluation of the crystal packing motifs for these three complexes there is one notable finding, namely that of the novel β-CD packing arrangement for the BCDCYC complex. This complex was described as having a channel-type packing arrangement even though there is a shift of ~3.0 Å between β-CD dimers of adjacent layers. This particular shift alters the packing arrangement of the β-CD dimers, which results in a new set of cell dimensions for a dimeric β-CD complex. The BCDFEN structure packs in an intermediate-type packing arrangement as the relative shift between consecutive dimers is as much as 6 Å. The known channel-type structures, of which the BCD**B**END complex is an example, have a maximum shift of 2.7 Å. Thus the BCDCYC complex falls in between these two well-classified packing arrangements.

TRIMEA inclusion complexes

Two solid-state inclusion complexes were formed with the host molecule TRIMEA. The guest molecules included were the urea herbicide cycluron and the organophosphorus insecticide fenitrothion. In the uncomplexed form these insecticides exist as a powder and an oil respectively. The two inclusion complexes, TMEACYC and TMEAFEN, have completely different thermal behaviours. The TMEACYC complex showed an interesting phase transition for a cyclodextrin complex that involved loss of the guest molecule (cycluron) with simultaneous melting of the complex. This was followed by recrystallisation of the host molecule, after which the resulting phase melted. These events were investigated with TGA, DSC and variable-temperature PXRD. In contrast, the TMEAFEN complex displayed two distinct slopes in the TG trace that could be reconciled with two endotherms in the DSC trace, corresponding to the start of guest loss followed by decomposition.

A 2:1 host-guest ratio was confirmed for the TMEACYC and TMEAFEN complexes using TGA and ^{1}H NMR spectroscopy respectively. For both complexes, one of the two TRIMEA molecules comprising the dimeric unit, which encapsulates the guest molecule, adopts an elliptical shape so as to accommodate the planar amide moeity in the case of the cycluron molecule, and the substituted phenyl ring in the case of the fenitrothion molecule. The elliptical shape of the TRIMEA molecule was more pronounced for the TMEAFEN complex than for the TMEACYC complex. TRIMEA forms an inclusion complex with cycluron and

fenitrothion in a capsule-type form (head-to-head dimer), which illustrates the ability of the TRIMEA host molecule to interact with both polar and non-polar portions of a guest molecule.

Both the TMEACYC complex and the TMEAFEN complex crystallise in the space group $P2_12_12_1$ but they have different unit cell dimensions and thus different packing arrangements. In both cases the guest molecules are isolated from one another and a modified dimeric herringbone packing arrangement is observed for each complex. There are water molecules present in the TMEACYC crystal structure that assist in the close packing and contribute to the overall stability of this structure. These are both novel packing arrangements and they demonstrate the ability of TRIMEA to form solid-state inclusion complexes with guest molecules larger than a di-substituted benzene ring.[3,4]

TRIMEB inclusion complexes

Three of the four selected pesticides formed inclusion complexes with TRIMEB. One other TRIMEB inclusion complex (TMBFTN, containing fenthion as a guest) was included in the solid-state kinetic experiments but the crystal structure analysis did not form part of this study. The three TRIMEB inclusion complexes with guest molecules cycluron, fenitrothion and acetochlor are isostructural and have very similar thermal behaviours. The slight differences in their thermal behaviours are due to the presence or absence of included water molecules in their crystal structures, as well as the chemical properties of the individual guest molecules.

The TMBCYC complex was the only one in which the guest molecule was not disordered. The entire fenitrothion guest molecule in the TMBFEN complex was disordered over two positions while only two atoms of the acetochlor molecule in the TMBACET complex were disordered over two positions. The conformations of the host molecules for the three complexes as well as the degree of tilting for each methylglucose unit of each complex were similar. For TMBCYC, TMBFEN and TMBACET a large portion of the included guest molecule is located close to the primary rim (‘roof’) of the TRIMEB cavities, while the ‘tail end’ protrudes from the secondary rims into the interstitial gaps. Owing to the isostructurality established for these complexes, the packing arrangements of their complex units are by definition identical.

DIMEB inclusion complexes

Three DIMEB inclusion complexes were prepared with the pesticides, cycluron, endosulfan and fenitrothion. The TG profiles for these complexes illustrated at least a two-step mass loss attributed to successive guest loss and host decomposition. The DMBCYC complex showed a three-step mass loss due to water being expelled prior to guest loss and host decomposition. Even though the DMB**B**END complex contained waters of crystallisation, the TG trace showed no evidence of water desolvation prior to the mass loss associated with guest expulsion. The guest molecule endosulfan was stabilised to a higher temperature (225 °C) than fenitrothion (120 °C) and cycluron (180 °C) when included in the DIMEB host molecule.

A 1:1 complex stoichiometry was determined for the three DIMEB complexes prepared. DMBCYC and DMB**B**END crystallised in the orthorhombic space groups $P2_12_12_1$ and $P2_12_12$ respectively, while the DMBFEN complex crystallised in the monoclinic space group $P2_1$. The asymmetric unit of the DMBCYC complex consists of a monomeric CD-guest unit. Both the DMB**B**END and DMBFEN complexes contain two independent DIMEB molecules in the asymmetric unit. The two DIMEB molecules in the DMBFEN complex are related to each other by a lateral shift of $a/2$, whereas for the DMB**B**END complex the two host molecules are entirely independent of one another. All three DIMEB complexes exhibit excessive guest disorder. The highest degree of guest disorder was observed for DMBFEN in which one DIMEB molecule contains three disordered guest components and the other contains two rotamers of fenitrothion. In all cases, satisfactory modelling of the various disordered guests was achieved.

These three crystal structures produced two unique packing arrangements for DIMEB complexes (DMB**B**END and DMBFEN), and one packing arrangement that differs only slightly from a known isostructural series of DIMEB complexes (DMBCYC). The DMBCYC, DMB**B**END, and DMBFEN complexes are characterised as having a channel-type packing arrangement with the host molecules aligned in a head-to-tail fashion. One of the major differences, however, is the angle of inclination between the O4 mean plane of the DIMEB units and the plane of the unit cell that is perpendicular to the channels formed by the DIMEB molecules. This particular angle is rather large for the DMBCYC and DMBFEN complexes and thus the guest molecules are isolated from one another, as the edge of the primary rim of one DIMEB molecule blocks the centre of the secondary rim of a DIMEB molecule situated below. The complex units of DMB**B**END form layers perpendicular to the

channels and as a result the guest molecules are able to link to one another by means of halogen bonds along the channels. These three novel inclusion complexes have increased the number of known packing arrangements for DIMEB species.

SIGNIFICANCE OF RESULTS OBTAINED IN SOLUTION

In several cases, the results that we obtained from solution-state experiments were in agreement with what was obtained in the solid state. This was particularly noticeable for the series of complexes formed with fenitrothion, where the host-guest ratios were found to be the same for four of the five complexes investigated in the two different phases. In addition to the stoichiometries, the orientations of the guest molecules established in the crystal structures correlated well with the kinetic data we obtained in solution. The work performed in solution provided quantitative estimates of the binding strengths between the cyclodextrins and pesticides as well as the thermodynamic parameters associated with complexation in solution.

In Chapter 1, we alluded to an association constant value of 10 000 as representing the upper limit for a CD-drug inclusion complex to be effective in the pharmaceutical industry.[5] The association constants (K) obtained for the cycluron and fenitrothion complexes investigated in solution have values much less than 10 000, except for the 2:1 TRIMEA·fenitrothion complex that had a cumulative association constant of 2.5×10^5. The 1:1 TRIMEA·fenitrothion complex in solution, however, had a much lower association constant of 527. For the cycluron series of solution-state investigations, β-CD had the highest association constant of 4753 as determined by ITC measurements. From these results it is possible to assume that CDs will not hinder the bioavailability of cycluron or fenitrothion in solution when present in a 1:1 host-guest stoichiometry.

The kinetic studies performed in solution with fenitrothion represented a simple investigation of how CDs can influence the chemical stability of organophosphorus insecticides. The methylated CDs inhibited the hydrolysis reaction of fenitrothion to a greater extent than the native CDs. More specifically, DIMEB had the greatest inhibitory effect on the degradation of fenitrothion and a reasonably high association constant (1689). DIMEB would therefore be the ideal CD to be used in formulations of fenitrothion, but due to its high cost RAMEB would probably be a better alternative.

FUTURE WORK

One of the main physical properties to be improved using CDs, addressed at the beginning of this thesis, was the aqueous solubility of the pesticides. The solubility studies performed in this investigation were semi-quantitative and measurements with a higher degree of accuracy should be obtained using techniques such as high performance liquid chromatography.

Since complexation has been confirmed between CDs and selected pesticides both in solution and in the solid state, the next step would be to test these complexes in the environment and compare the results to those obtained using the uncomplexed pesticide. Such investigations should include evaluating the soil mobility of the pesticide-inclusion complexes and the bioavailability of the guest when administered in the form of the cyclodextrin inclusion complex. If there is an increase in the bioavailability of a pesticide, its current formulations should be reassessed to determine whether or not the quantity of the toxic active ingredient (the pesticide) in such formulations can be reduced using CD technology. It would also be beneficial to determine the effectiveness of the complex at inhibiting its target pest versus the effectiveness of the uncomplexed guest.

FINAL COMMENTS

The work presented here is a fundamental study confirming that complexation between representative members of four different classes of pesticides and various CD molecules can occur in the solid state and in solution. The crystal structures yielded unequivocal proof that these pesticide molecules interact with the inner cavity of a CD molecule, while complexation in solution was confirmed by several methods, namely ^{1}H NMR spectroscopy, ITC, induced circular dichroism and through an evaluation of the kinetic rate constants (reduced guest hydrolysis rate in the presence of CDs). This study employed a wide range of experimental techniques and demonstrates the different ways in which cyclodextrin-pesticide complexes can be prepared and assessed in the solid state and in solution. The concept of forming these inclusion complexes is concerned with the safe, efficient and economical handling of pesticides from the time of manufacture to their final utilisation and disposal. All the data presented in this thesis are consequently of importance to any future development and applications of the pesticides investigated.

REFERENCES

1. M. R. Caira, *Roum. Chem. Quart. Rev.*, **2000**, 8, 243-253.
2. F. Giordano, C. Novak and J. R. Moyano, *Thermochim. Acta*, **2001**, 380, 123-151.
3. Cambridge Structural Database and Cambridge Structural Database system, Version 5.32, Cambridge Crystallographic Data Centre, University Chemical Laboratory, Cambridge England, February **2011**.
4. K. Harata, *Chem. Rev.*, **1998**, 1803-1827.
5. L. A. Miller, R. L. Carrier and I. Ahmed, *J. Pharm. Sci.*, **2007**, 96, 1691-1707.

Appendices

Four appendix folders can be found on the disk attached.

Appendix A includes the ^{1}H NMR spectra used to determine the host-guest stoichiometries of the solid-state inclusion complexes. These files are saved with their abbreviated complex names and have a .pdf file extension.

Appendix B contains the supplementary crystallographic information for each fully solved structure presented in this thesis. The files have been saved in a subfolder with their abbreviated complex names.

Appendix C lists the ^{1}H NMR chemical shifts recorded for the solution-state investigation between cycluron and the native CDs (Chapter 3, Part 2).

Appendix D contains the derivation of a kinetic expression for the hydrolytic decomposition of a guest, which includes the formation of a 2:1 host-guest complex (Chapter 5, Part 2).